UNIVERSITAT DE BARCELONA

FACULTAT DE FARMÀCIA I CIÈNCIES DE L'ALIMENTACIÓ

PROGRAMA DE DOCTORAT DE RECERCA, DESENVOLUPAMENT I CONTROL DE MEDICAMENTS

SKIN PERMEABILITY METHODOLOGIES FOR TOPICAL ABSORPTION PREDICTION

VICTOR CARRER VIVES

2018

UNIVERSITAT DE BARCELONA

FACULTAT DE FARMÀCIA I CIÈNCIES DE L'ALIMENTACIÓ

PROGRAMA DE DOCTORAT DE RECERCA, DESENVOLUPAMENT I CONTROL DE MEDICAMENTS

SKIN PERMEABILITY METHODOLOGIES FOR TOPICAL ABSORPTION PREDICTION

Memòria presentada per Victor Carrer Vives per optar al títol de doctor per la Universitat de Barcelona

Directora:
Lluisa Coderch Negra

Directora:
Cristina Alonso Merino

Doctorand:
Victor Carrer Vives

Tutora:
Ana Cristina Calpena Campmany

INDEX

INDEX

ABREVIATION LIST

ABBREVIATION LIST

ABS	Percutaneous absorption
ACN	Acetonitril
ATR	Attenuated total reflection
ATR-FTIR	Attenuated total reflection Fourier transform infrared
AUC	Area under the curve
Aze	Azelaic acid
Barr	Barratt equation
Bet	Betamethasone dipropionate
Bex	Bexarotene
CA	Concentration acceptor
Caf Aq	Caffeine aqueous solution
Caf	Caffeine
Caf Np	Caffeine nanoparticles
Cal	Calcipotriol monohydrate
CAS	Chemical abstracts service
CD	Concentration donor
Cli	Clindamycin
Clo	Clobetasol propionate
CLS	Classical least squares
CRM	Confocal Raman microscopy
CV	Cone voltage
D	Dermis
Dap	Dapsone
Dic	Diclofenac sodium
Dip	Diphenhydramine
DMSO	Dimethyl sulfoxide
E	Epidermis
EC	Colision energy
Efl	Eflornithine
FDA	Federal drug administration
Fin	Finasteride
Fo	Fluorouracil
Fra	Flurandrenolide
FTIR	Fourier transform infrared
GC	Glucocorticoids
Gly	Glycopyrrolate
HPLC-DAD	High performance liquid chromatography with diode array detector
ICH	*International Conference on Harmonisation*
Imi	Imiquimod
Jss	Steady-state flux of chemical across the skin
Ket	Ketoconazole
Kow	Octanol-water partition coefficient
Kp	Permeability constant
Lid	Lidocaine
Log D	Distribution coefficient logarithm
LPP	Long periodicity phase
MCR-ALS	Multivariate curve resolution-alternative least squares
Mi	Mitragotri equation
MP	Melting point
MV	Molecular volume

MW	Molecular weight
Nic	Nicotine
NT	Non treated
PC	Principal component
PCA	Principal component analysis
Pe	Effective permeability coefficients
PG	Propylene glycol
P-G	Potts and Guy equation
QSPR	Quantitative structure permeability relationship
Res	Resveratrol
RF	Receptor fluid
RS	Raman spectroscopy
Sal	Salicylic acid
SC	Stratum corneum
Skin-PAMPA	Skin parallel artificial membrane permeability assay
SPP	Short periodicity phase
t	Time
Tac	Tacrolimus monohydrate
Taz	Tazarotene
Ter	Terbinafine
TEWL	Transepidermal water loss
TFA	Trifluoroacetic acid
Tof	Tofacitinib
Tr	Retention time
UPLC-MS/MS	Ultra performance liquid chromatography - tandem mass spectrometer
W	Surface excess
WDS	Wool dry scouring
λ	Excitation wavelength
ν_{AS}	Symmetrical stretching
ν_{S}	Asymmetrical stretching
μFTIR	Synchrotron-Based Fourier transform infrared microspectroscopy

ACKNOWLEDGEMENTS & BACKGROUND

ACKNOWLEDGEMENTS

El meu profund agraïment a la meva directora de tesi Lluïsa Coderch. Sense les seves correccions, consells i recolzament aquesta tesi no s'hauria pogut completar. A la Cristina Alonso li dec només paraules amables no només per ser una gran mentora sinó també com a amiga, gràcies per la teva paciència.
Aquesta tesis és a més resultat de la feina d'una gran quantitat de persones amb les quals he treballat colze amb colze. Gràcies Mercè, Núria, Mª José, Bernat, Míriam, Sònia, Mònica i Anna per la vostra ajuda i esforços. Una part d'aquesta tesi també és vostra.

Voldria també agrair als meus companys i amics del IQAC Txell, Clara, Marc, Isabel, Vanesa, Bea, Ana, Marta, Jose i Ilaria així com la resta de gent que ha fet del meu pas pel IQAC una experiència més humana. A en Miguel i en Marc agrair-los-hi en especial la feina feta pel maquetatge i a la Marta per deixar-me utilitzar un obra seva com a portada. A les meves companyes de carrera i doctorat Mireia i Raquel només dir-los-hi que compto seguir compartint alegries i preocupacions per molts més anys. Hi ha un munt de companys i amics que no han intervingut directament en aquesta tesi, però si que han format part de la meva vida aquests anys, gràcies també a tots ells.

Part of this thesis has been written during my stay at the Center of Experimental and Applied Cutaneous Physiology in Berlin. Therefore, I would like to thank Prof Lademann and Dr Patzelt for giving me the opportunity of this priceless experience. Thanks also to Johannes and Maxime for their guidance and expert advice as well as Anja, Pin and Ceyda for their warm welcome. Un record també per la Miriam, per la teva gran ajuda i companyia durant la meva estada a Berlín.

Gràcies també als meus pares per ser un referent de sacrifici i dedicació i a la meva gran família pel seu amor incondicional. Finalment no voldria acabar sense agrair també a aquells que ja no hi són, us segueixo tenint amb mi.

Moltes gràcies a tots.

BACKGROUND

The results presented in this thesis were acquired in close collaboration with other national and international research entities. Retoderm technological platform included the IQAC-CSIC as well as two other companies from the dermatological field such as Almirall S.A and Draconis Pharma S.L. One of its main objectives was the study of skin absorption process with different *in silico* and *in vitro* methodologies to be used on the permeation prediction of new synthetized drugs. Moreover, collaboration with the Center of Experimental and Applied Cutaneous Physiology of Berlin was settled to exchange techniques and expertise on the drug skin penetration by confocal Raman microscopy. For such reason it is important to state that part of the presented results have been obtained using their infrastructure, expertise and assistance.

After a brief look on the skin structure and function, this thesis will present different methods to study the skin absorption. Then, these methods will be experimentally applied for better understanding of their respective advantages and limitations. Added at the end of this thesis (Annex) the publications and patents that arise from this dissertation are compiled.

INTRODUCTION

1. INTRODUCTION

Understanding of skin absorption processes is needed not only for assessment of the safety aspects of chemicals, other xenobiotics, or cosmetic formulations but also to determine drug release of substances to the different skin strata and further to systemic circulation.

In the field of pharmaceutical sciences, drug delivery to the skin is gaining more and more interest, owing to the high acceptance by patients. In this regard, two different cases have to be distinguished: local delivery to selected skin layers (e.g., antimycotics) and systemic delivery (e.g., hormones). In the context of bioavailability assessment, knowledge on the absorption behavior of the active compound is essential. For ethical reasons, fundamental skin absorption data can normally not be obtained by conducting *in vivo* studies. Therefore, other techniques must be used to obtain the desired information. One option to obtain these data is the use of *in vitro* penetration and permeation models[1–3].

1.1. Structure and Function of the Skin

The skin is a complex organ and a living membrane. This constitutes one of the largest interfaces between the body and the environment[4]. The function of the skin include from the one hand protection against chemical, physical and microbial injury. On the other hand it is involved in the regulation of body temperature and water loss, defense and repair. The functionality of the skin depends on its highly differentiated structure, with the main barrier function being located in the outermost skin layer, the Stratum Corneum[5].

1.1.1. Anatomical Structure of Human Skin

The multitude of different functions of the human skin can only be achieved by a unique anatomical structure of the different skin layers (Figure 1). These are as follows:

- *epidermis* consisting of
  - *Stratum Corneum* (outermost layer)
  - *Viable epidermis*
- *dermis*
- *subcutis or subcutaneous fatty tissue*

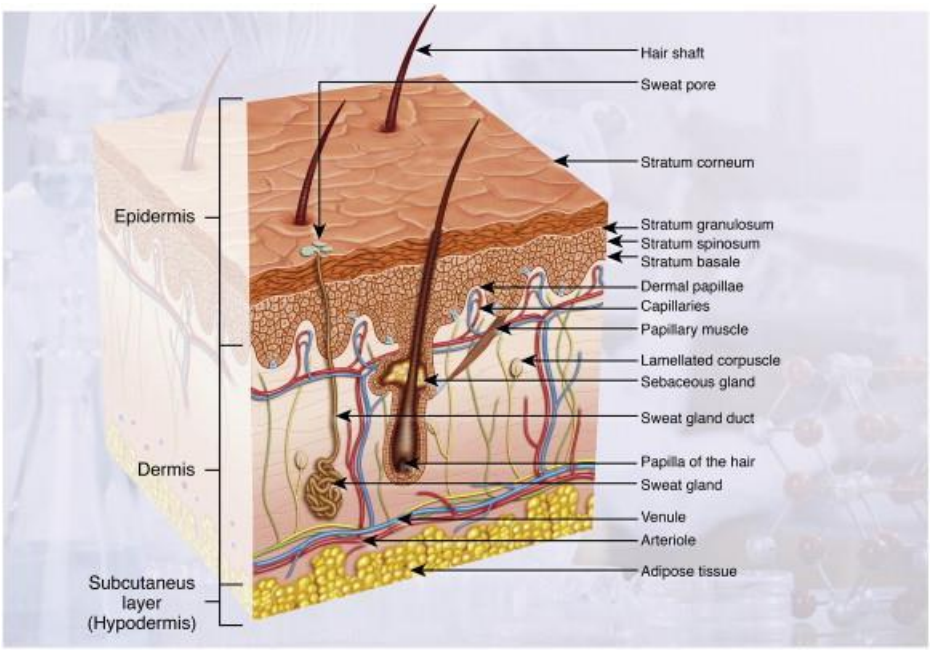

Figure 1 Schematic picture of the native sub-classified into three main compartments: epidermis, dermis and subcutis (hypodermis). Skin appendices like hair with sebaceous glands, sweat glands as well as blood vessels are embedded in the skin. Image taken from Mathes et al.[6]

1.1.1.1. Epidermis

Human epidermis comprises about 5% of full-thickness skin and is generally divided into two main layers: the Stratum Corneum and the viable epidermis.

The **Stratum Corneum** (SC) is the outermost cornified layer consisting of cells (corneocytes) that have lost their nucleus and all capacity for metabolic activity. Corneocytes are embedded in a lipid matrix or intercellular lipid lamellae. This structure is also known as the the brick (corneocytes) and mortar (lipids) structure (Figure 2). The SC is usually 10-25µm thick (excepting the soles of the feet and palms) and is crucial for the barrier function of the skin. Owing the relative impermeability of the cornified envelope to most compounds, the major route of penetration across the SC has been identified as the tortuous pathway between the corneocytes, implying that the lipid lamellae plays a key role in the skin barrier function. The hydrophobic lipids present in the intercellular spaces of the SC are 45-50% ceramides, 25% long chain free fatty acids (mostly chain lengths C22 and C24), and 5% of other lipids (cholesterol sulfate, cholesterol esters, ...) [7,8]. Some ceramide families are believed to play a different roles in skin properties[9]. Moreover, the free fatty acids cause the skin barrier to have a pH of 5.5, which affects the ionization state of the topically applied substances.

The intercellular lipids are arranged in layers (lamellae)(Figure 2) with two coexisting lamellar phases. These lamellar phases have a repeat distance of 6 nm (referred to as the SPP) or 13 nm (referred to as the LPP) [10–12]. There are three possible arrangements of the lipids: a very dense, ordered orthorhombic organization; a less dense, ordered hexagonal organization; and a disordered liquid organization. In healthy skin, lipids are mainly packed in an orthorhombic packing, while a small fraction of lipids adopts hexagonal packing [13–15]. In some inflammatory diseases, a higher fraction of the intercellular lipids assembles in a hexagonal packing, such as in atopic dermatitis[16]. This less dense lipid organization is associated with a reduced skin barrier function [17,18]. Also surfactants and organic solvents applied on the skin surface disrupt the barrier function of the skin an alter the lipid composition and organization [19].

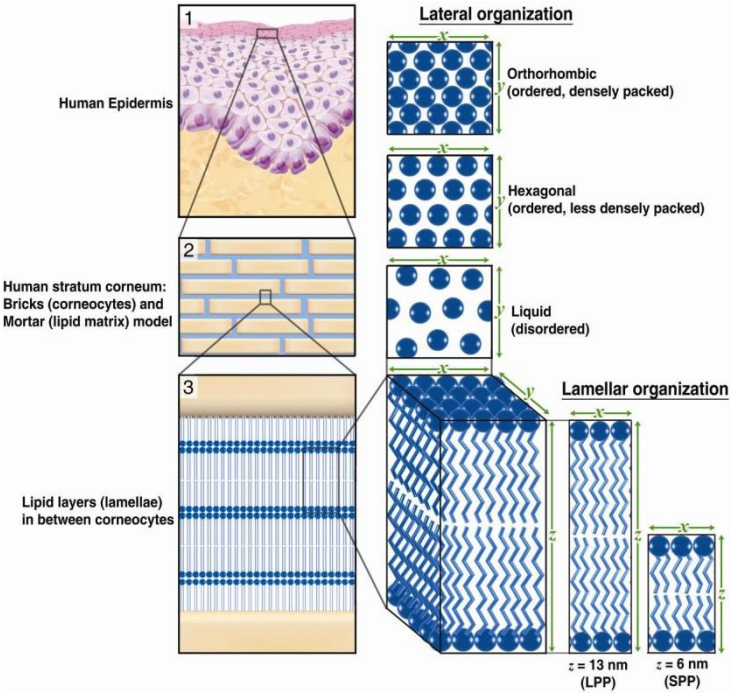

Figure 2 Lamellar and lateral organization in human Stratum Corneum. (1) Stratum Corneum containing corneocytes embeded in a lipid matrix. (2) Intercellular lipids arranged in layers (lamellae). (3) Coexisting lamellae phases. Image obtained from Janssens et al.[16]

The **viable epidermis** is made of several non-vascularized layers: the stratum germinativum (or basal layer), followed by the stratum spinosum, the stratum granulosum and the stratum lucidum which is only present at the sole of the food and the palm of the hand (Figure 1). Over a 28 days cycle, cells originated in the stratum

germinativum migrate to the skin surface undergoing different differentiation states. The cells in doing so discharge lipids into the intercellullar space (stratum granulosum) lose their nuclei and get flattened and cornified building up the SC brick and mortar structure. Furthermore, the viable epidermis contains melanocytes, which produce melanin for light protection and Langerhans cells responsible for the immune response.

1.1.1.2. Dermis

The dermis provides the nutritional support for the avascular epidermis (Figure 1). The dermis consists of a matrix of connective tissue composed of collagen, elastin and reticulin interspersed by skin appendages pilosebaceous units and hair follicles. The dermis is the locus of sensory nerves, blood vessels and lymphatics. It contains the inner segments of the sweat glands and pilosebaceous units. Both can be responsible for systemic drug absorption by acting as sinks and keeping the concentration in the dermis low.

1.1.1.3. Subcutis or subcutaneous fatty tissue

This layers acts mainly as a heat insulator, a mechanical cushion and stores high energy chemicals. It consists primarily of loose connective tissue and lobules of fat. It contains larger blood vessels and nerves than those found in the dermis.

1.1.2. Skin Absorption pathways

Skin absorption pathways (Figure 3) can be divided into the transport (a) **across the intact Stratum Corneum** and (b) along using **skin appendages**. The physicochemical properties of the compound, as well as the used formulation, are the main factors influencing the choice of pathway.

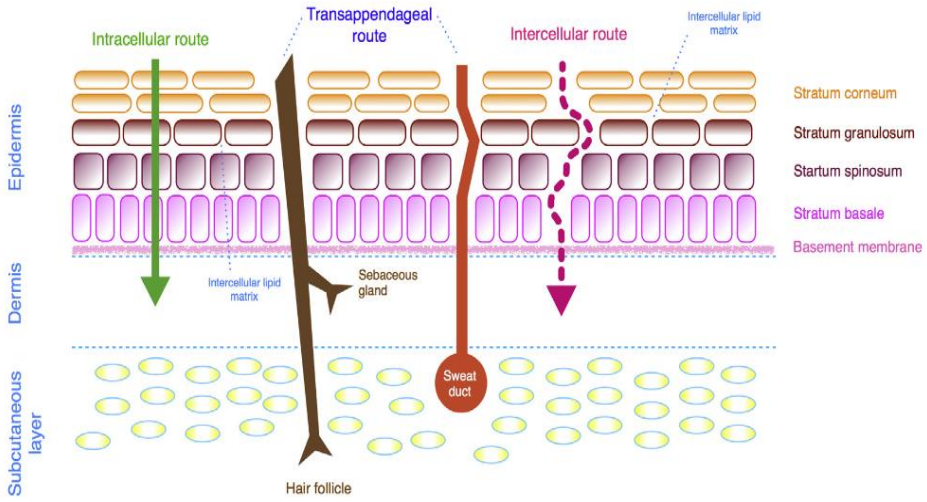

Figure 3 Skin absorption pathways from Filon et al.[20]

The Transappendageal Route

The transappendageal route consists of the glandular and the follicular pathways (Figure 3), with the latter one being the more important. The chemicals bypass the corneocytes, entering the shunts provided by the hair follicles, sweat glands, and sebaceous glands.

The follicular pathway is recently gaining importance. Anatomically, the hair follicle embodies an invagination of the epidermis resulting in an increased surface area available for absorption of drugs[21]. Moreover, these invaginations are surrounded by numerous blood capillaries that facilitate the systemic absorption[22]. The presence of antigen presenting cells in the hair follicles is of special interest with regard to immunological therapy. Furthermore, recent studies showed that the hair follicle can be a long-term drug reservoir for up to 10 days[23,24].

However, since appendages cover only 0.1% of the whole skin surface area, these pathways do not contribute significantly to dermal absorption during steady-state conditions of skin absorption. In contrast, in the initial stages of a skin absorption process and in the case of large hydrophilic compounds and ions, invasion through the appendages may play a considerable role. Recent studies also report that the appendages route may be involved in the absorption of liposomes, nanoparticles, and cyclodextrin-inclusion complexes[24,25].

Transport across the intact Stratum Corneum.

Generally, the SC is considered to be the rate limiting layer of the skin with regard to transdermal drug absorption. Drug permeation across the SC depends on the

interaction between the skin, the drug and the other components within the formulation.

Originating from the structure of the SC, two permeation pathways are possible: (a) **the intercellular route** and (b) the **intracellular route** (Figure 3).

In the **intracellular route**, the chemical is transferred through the keratine-packed corneocytes by partitioning into and out of the cell membrane. It is not considered as the preferred way of dermal invasion, the reason being the very low permeability through the corneocytes and the obligation to partition several times from the more hydrophilic corneocytes into the lipid intercellular layers in the SC and vice versa. The intracellular pathway can gain in importance when a penetration enhancer is used, which may modify the corneocytes protein structure and hence changing their permeability.

The **intercellular route** is the major route of penetration to most compounds, especially when steady-state conditions in the SC are reached. In this case the chemical is transferred around the corneocytes in the lipid-rich extracellular regions within the SC.

Permeation of a chemical through the SC is basically a diffusion process in which active transport plays no role. For many compounds, the lipophilic SC is the rate-limiting barrier. However, diffusion through epidermis and dermis can be rate limiting for very lipophilic materials and/or when the SC is damages or affected by disease.

Although this pathway is very tortuous and therefore much longer in distance than the overall thickness of the SC, the intercellular route is considered to yield much faster absorption due to the high diffusion coefficient of most drugs within the lipid bilayer. Resulting from the bilayer structure, the intercellular pathway provides hydrophilic and lipophilic regions, allowing more hydrophilic substances to use the hydrophilic and more lipophilic substances to use the lipophilic route. In addition, it is possible to influence this pathway by certain excipients in the formulation[26].

1.2. Skin absorption methodologies

Predicting human skin permeability of chemical actives efficiently and accurately is useful for developing dermatological medicines and cosmetics. The evaluation of percutaneous permeation of molecules is one of the main steps in the initial design and later evaluation of dermal or transdermal drug delivery. *In vivo* skin absorption studies are intrinsically rare, due to ethical, economical, and analytical concerns. Therefore, great efforts have been given to developing and validating alternative *in vitro* test methods[2,27,28]. A comprehensive compilation of literature data,

comparing the permeability of chemicals across animal and human skin *in vivo*, as well as *in vitro*, has been published by the European Centre for Ecotoxicology and Toxicology of Chemicals (ECETOC)[29]. The diversity of existing *in vitro* and *in vivo* techniques shows the difficulties of comparing results between different methods, species, ages, as well as healthy and diseased skin. Howes et al.[30] introduced a hierarchy of frequently applied *in vitro* methods for measuring percutaneous absorption which considers the resemblance to the *in vivo* situation (Figure 4). This knowledge can be very helpful when comparing different results of skin absorption studies.

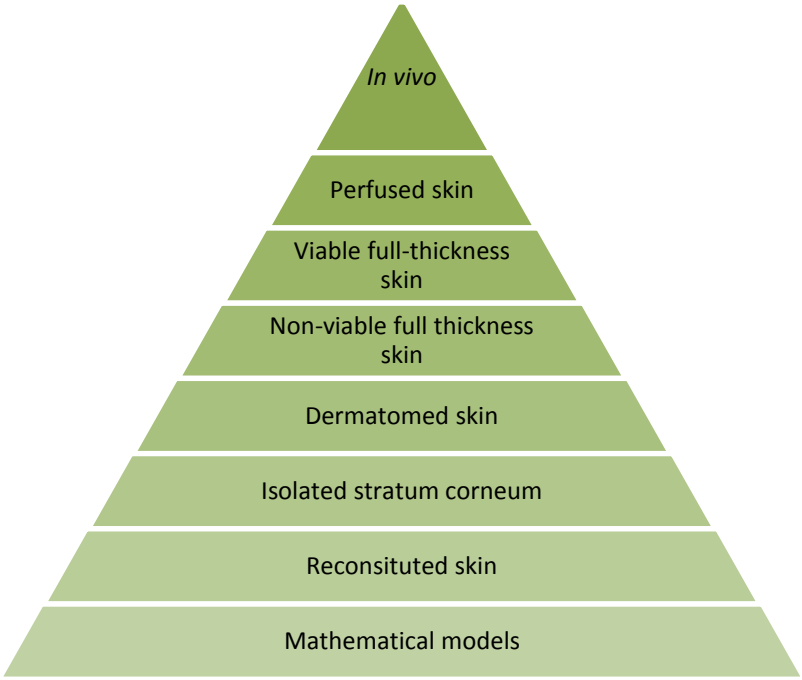

Figure 4 Hierarchy of commonly applied methods for studying percutaneous absorption considering their resemblance to the *in* vivo situation (adapted from Howes et al[30])

From the different scientific alternatives to investigate the percutaneous absorption phenomena it is now widely accepted that the transport processes of drugs in skin can be described by Fick's first law[31]. This equation assumes that diffusion occurs in favor of the concentration gradient, in other words, from higher to lower concentration. This principle is applied in recent mathematical models used to describe the dermal absorption through the SC[32].The permeability constant (K_p) is defined as the steady-state flux of chemical across the skin (J_{ss}) normalized by the concentration gradient (ΔC_v) and allows to compare results for different substances with reasonable accuracy (Equation 1).

Equation 1

$$K_p = \frac{J_{ss}}{\Delta C_v}$$

For such reason the assessment of the permeability constant (K_p) has been the main focus of permeation models.

An introduction of the scientific knowledge of the different methods experimentally assayed in this doctoral thesis are presented as follows.

1.2.1. *In silico* approaches/Mathematical models (QSPR)

Quantitative structure permeability relationship (QSPR) models try to find a relationship between the logarithm of the permeability coefficient ($\log K_p$) and molecular features (descriptors). Many data sets for skin permeability models employ the collection of the logarithms of permeability coefficients by Flynn[33] or subsets thereof. Despite that its reliability has been repeatedly questioned, the Flynn data set is still the most important source for developing QSPR models.

A number of empirical models were proposed to relate the experimental permeability data, the octanol-water partition coefficient and the molecular weight of molecules[34–36]. Potts and Guy[37] took advantage of the Flynn's large compilation to generate a widely cited equation (P-G)(Table II), in which K_{ow} accounts for solute octanol-water partition coefficient, MW for molecular weight and K_p for skin permeability coefficient.

Other models predict the skin permeability by directly taking into account the diffusion pathway. Significant progress was made only very recently when Mitragotri (Mi)[38] presented a scaled particle theory on solute partition and diffusion across lipid bilayers. Relating the solute molecular radius to the molecular weight, Lian et al.[39] established that the equation formulated by Mitragotri can also be read as the Mi equation from Table II in section 4.1.

The Potts and Guy and the Mitragotri models have been widely reported in the literature; nonetheless, the Barratt model [40] was also selected because diverse physico-chemical properties were considered. Other attempts have been made to re-model the permeability data by dividing them into smaller subsets. Following the removal of distinct classes, steroids were identified as outliers to QSPR models for permeability[40]. Further parameters were included to describe effects such as hydrogen bonding[41] and melting point[40]. The selected Barratt equation (Bar) is presented in Table II, and this equation represented the behavior of the largest

number of molecules in their current dataset (which included 60 non-hydrocortisone molecules)[40].

Finally, it has to be considered that transdermal penetration prediction through mathematical models based on structure-permeability of many compounds generally indicate their reliability for small subsets[39]. Therefore, these models predict the permeability of low molecular weight compounds and a mean lipophilicity. This is not the case for high hydrophilic compounds (particularly charged molecules) or for high lipophilic compounds[42].

1.2.2. *In vitro* approaches

Percutaneous penetration in man warrants *in vivo* experiments in humans. These experiments are often morally undesirable, expensive and time consuming. Additionally, high inter- and intra-individual variability is found in the data. Therefore, alternatives to *in vivo* studies in humans are sought. The suitability of the different *in vitro* permeability models using excised skin (human or animal) to mimic the *in vivo* studies has been widely reviewed[43,44], but obtaining a sufficient supply of excised human and animal skin is often a challenge and tends to be costly.

There have also been attempts to create synthetic membranes that may be used as human skin models to investigate the transdermal diffusion properties of pharmaceutical and cosmetic compounds and formulations. The FDA has encouraged the use of porous synthetic membranes to evaluate the performance of topical products because they act as a support without posing a rate-limiting barrier[45]. Unlike skin, these membranes are inert and do not introduce biological variations. Moreover, the variability subjected to the anatomical site, age, race of the skin donor and skin-biopsy preparation and storage can be overtaken.

In vitro skin permeation studies have been used for many years for the assessment of skin penetration drugs from topical or from transdermal products. Following the *in vitro* methodologies used in this thesis are described.

1.2.2.1. Franz diffusion cells with skin biopsies or synthetic membranes

The Franz diffusion cell is one of the most widely used systems for *in vitro* skin permeation studies[46]. With this methodology, any type or determinate amount of formulation (within the capacity of the donor chamber) may be applied to the skin or to synthetic membranes. Then the amount of drug that diffuses across the skin or membrane can be determined. Franz-type diffusion cell systems are relatively simple in design (Figure 5), with static diffusion cells that consist of the following two main parts: a receptor and a donor chamber. The membrane/skin is inserted between these

two compartments. The dose of the tested agent is applied into the donor chamber on the epidermal skin surface. An agent that permeates through the skin is accumulated in the receptor chamber (under the dermal skin surface), which is filled with the appropriate solution (receptor fluid in our case). After the exposure time, the skin sample can be processed to obtain the different skin layers. In that way, the distribution of the study compound can be determined.

Because of its simplicity and cost-effectiveness, in this thesis Franz diffusion cells will be employed to study the drugs diffusion in a variety of membranes but also in pig skin in which the drug disposition in different skin layers could be studied.

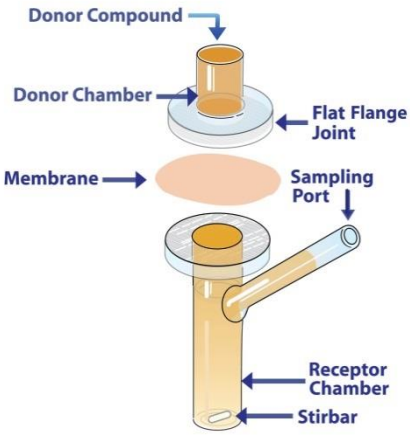

Figure 5 Details of Franz diffusion cell. Extracted from Ses-GMBH.

Ex vivo porcine skin

A wide range of animal models has been used as alternatives to human skin to evaluate percutaneous permeation of substances. These include pig, mouse, rat, guinea pig, and snake models.

Porcine skin is histologically similar to human skin[47,48] with a comparable SC thickness of 21–26 µm[23,49] and when studying their Raman and infrared spectra they are found to be highly similar[50–52]. In addition, the average hair-follicle density in porcine ear skin is 20/cm^2 compared to 14–32/cm^2 in human forehead skin[23]. As well as being similar to human skin, porcine ear skin is also convenient to obtain and has been widely used in skin-permeation studies[53]. In a range of studies using both lipophilic[54,55] and hydrophilic[56] permeants, the permeability of pig skin was found to be similar to that of human skin, but to differ to a greater extent from dog or rodent skin. Sato et al.[56] attributed the similarity in permeability to the similar SC lipids, barrier thickness, and morphological aspects of pig and human skin.

The dermatomization technique may be used for harvesting skin, as well as for reduction of the dermal thickness. The recommended thickness is 400-700µm for pig skin[43] and normally is from the dorsal area. Samples comprise epidermis including SC, as well as part of the dermis (Figure 6). Although the dermatome will cut through hair follicle, the holes will readily close during incubation in aqueous media, due to swelling of the tissue. For such reason when the absorption through the hair follicle wants to be studied, non dermatomed skin (normally ear skin) should be employed.

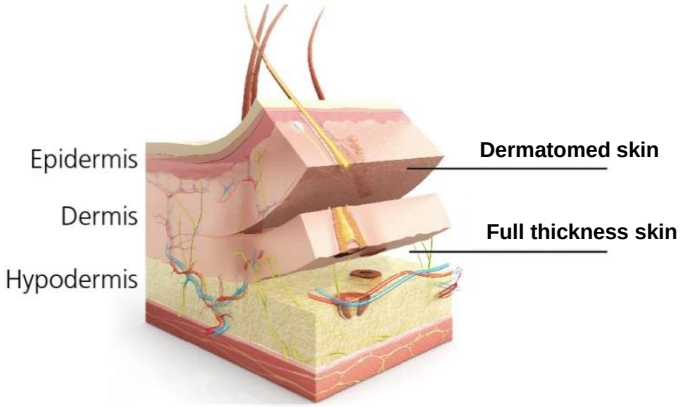

Figure 6 Scheme of different skin thickness used for dermal aborption studies

Polymeric synthetic membranes

Polymeric synthetic membranes are composed of a thin sheet of polymeric macromolecules that can control the passage of components through them. They may be composed of synthetic polymers (e.g., polysulfone and polycarbonate) or semi-synthetic cellulose polymers (e.g., cellulose acetate and cellulose nitrate). These membranes can contain different structures and polymers that attempts to mimic the skin structure (Figure 7). Such membranes are then used in diffusion cells as skin surrogates. Despite their high reproducibility and simplicity, one of their restraints is the weaker barrier function compared to the skin, especially because of the difficulty to mimic the SC lipidic structure[19].

The first efforts to study synthetic membranes and compare to skin absorption were carried out by Landmann in 1984[57]. More recently, Anwar and colleagues[58] developed a simplified model that should serve to a bridge gap between the more realistic but complex model systems and the simple models. The challenge here is to develop models that lend themselves to both molecular-level experiments and simulations.

In this thesis, a new approach based on the polymeric synthetic membranes is proposed to create better skin surrogates. In a similar strategy than in skin-PAMPA in which ceramides and cholesterol are employed (section 1.2.2.2) lipidic components can be added to polymeric synthetic membranes to emulate the lipidic matrix. Due to the similarity with the SC composition, lanolin was selected and the obtained lanolin-models were then evaluated.

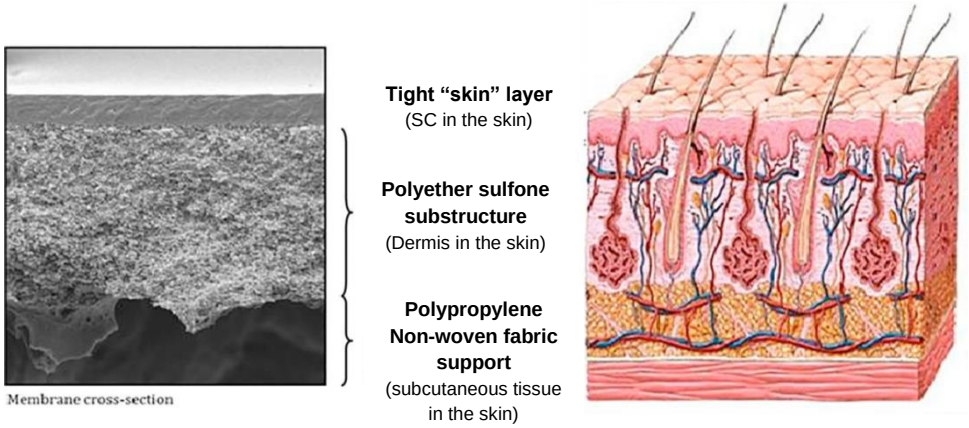

Figure 7 Cross section of a synthetic membrane (Strat-M®) and diagram of human skin. The Strat-M emulates in its structure three different layers of human skin. Image is extracted from Haq et al.[59]

1.2.2.2. Skin Parallel Artificial Membrane Permeability Assay

The Skin Parallel Artificial Membrane Permeability Assay (Skin-PAMPA) is an *in vitro* assay for skin penetration measurements. The skin-PAMPA membrane (Figure 8) was created by using cholesterol, free fatty acid and a ceramide along-analog compound that mimics the features of ceramides in the lipid matrix. The ceramide-analogue compound has been extensively used and its properties have been found to be suitable for PAMPA membrane.

Based on a 96-well microtiter plate format, this system allows to screen compounds and to effectively predict their permeability by calculating the effective permeability coefficients (P_e). Testing compounds are applied in the donor solution to diffuse to the acceptor solution through the PAMPA membrane for a period of time (t) (Figure 8). Calculus are performed when concentrations in the acceptor well (C_A) and the donor well (C_D) are determined[60].

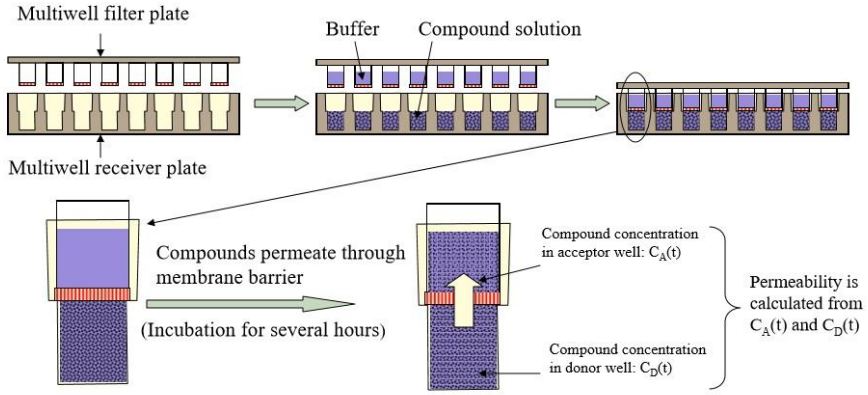

Figure 8 Skin-PAMPA methodology overview. Image taken from Discovery Analytical Consulting©.

This assay can predict transdermal penetration, establishing good correlation with human skin penetration[61,62] and hence allows a high throughput screening of a large number of drugs and pre-formulations at low cost.

1.2.3. *In vivo* tape stripping technique

In this technique SC is sequentialy substracted with adhesive tape strips (Figure 9). The skin-stripping approach was based on the concept that time profiles of the drug concentration in the outermost part of the epidermis, the SC, could characterize drug absorption (uptake) into the SC and drug elimination out of the SC into the deeper layers of the epidermis and dermis below, where clearance by the capillary loops of the circulatory system would occur[63]. The relevance of sampling the SC as a general way to evaluate topical bioequivalence was that differences in the rate and extent of the active moiety at nearby sites of action deeper in the epidermis or dermis were assumed to arise from differences in drug concentration profiles in the SC[64]. There is substantial evidence that supports this assumption. For example several studies with different products containing betamethasone dipropionate, betamethasone valerate, or triamcinolone acetonide[65–68] found a good correlation between the drug concentrations in the SC and the pharmacodynamic vasoconstriction (skin blanching) response produced by these glucocorticoids within the dermis, where the dermal vasculature resides.

Taken collectively, there are several strengths of skin stripping as a pharmacokinetics-based approach to evaluate the bioequivalence of topical dermatological drug products. Sampling of the SC by skin stripping is based on fundamental principles that

are rational and analogous to principles that are accepted for traditional pharmacokinetics-based bioequivalence assessments for systemically delivered drugs.

In conclusion, tape stripping of the SC, is another commonly used technique that is minimally invasive so it can yield the concentration profiles of topically applied compounds *in vivo* after the tape strips quantification analysis.

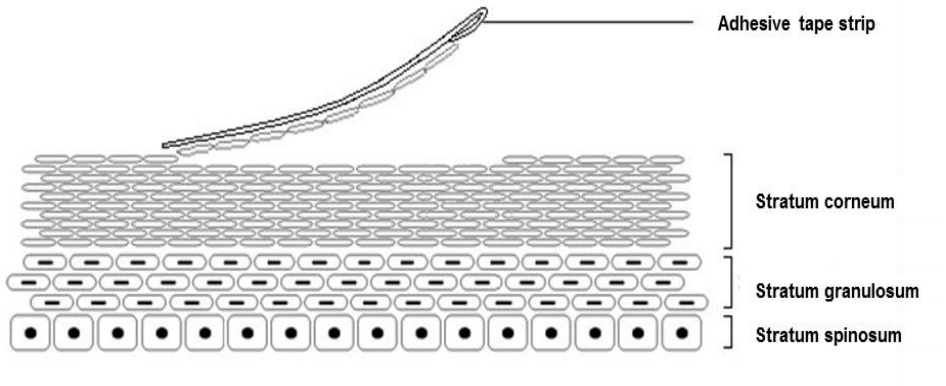

Figure 9 Removal of a layer of Stratum Corneum with an adhesive tape strip. Extracted from Au et al.[68]

1.2.4. Spectroscopic techniques

Over the last years, there has been an exponential increase in the use of Raman (RS) and Fourier transform infrared (FTIR) spectroscopic techniques in skin science and dermatology. Both provide a wealth of information on the cellular and molecular level from solid and liquid specimens without using external agents such as dyes, stains or radioactive labels [24-28]. These techniques are gaining more importance as valuable tools for the drug delivery, diagnose or clinical applications[69–71]. Both techniques detect molecular vibrations that depend on the composition and structure of the samples

FTIR is a form of vibrational spectroscopy (Figure 10) that relies on the absorbance, transmittance or reflectance of infrared light. FTIR measures how much light is absorbed by the bonds of a vibrating molecule; that is, the remaining energy from the original light source after being passed through the substance. In comparison, Raman spectroscopy is based on Raman scattering, which is described as inelastic scattering of incident light from a sample and frequency shift by energy of its characteristic molecular vibrations (50–3500 cm^{-1} range) (Figure 10). The variation of energy during scattering is attributed to the interactions between chemical bonds involved in the

samples and the photon. The specific peaks originate from particular chemical bonds, allowing the application of RS technique in the semi-quantitative analysis.

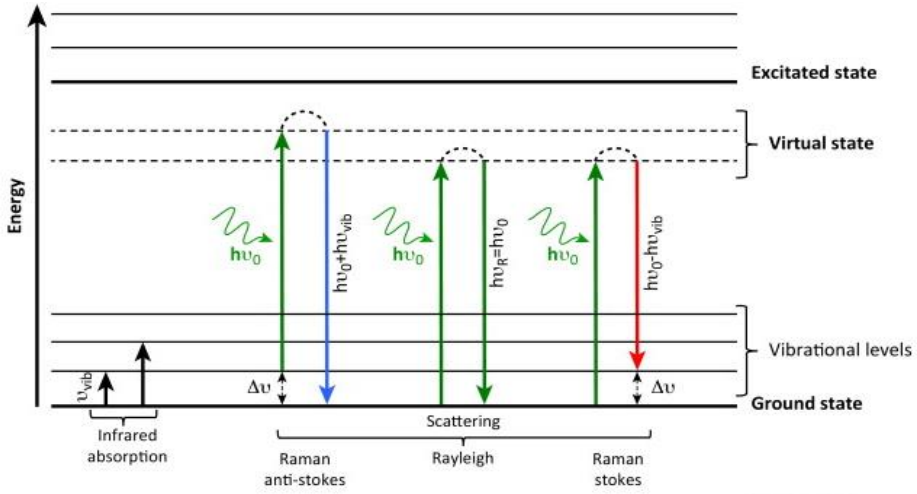

Figure 10 Diagram showing transitions occurring between energy levels during infrared absorption and Raman scattering phenomena. Extracted from Sulé-suso et al.[72]

RS and FTIR differ in some key fundamental ways. RS depends on a change in polarizability of a molecule, whereas IR spectroscopy depends on a change in the dipole moment. RS measures relative frequencies at which a sample scatters radiation, unlike FTIR spectroscopy which measures absolute frequencies at which a sample absorbs radiation. In spite of the weak intensity of Raman phenomena, it has two major advantages. Firstly, water, commonly present in biological samples, shows only slight Raman scattering and very strong FTIR absorption. Secondly, since in Raman and FTIR spectra the same vibrational states are assessed, Raman spectra are composed of narrower bands than FTIR spectra. Overall, despite their differences, both techniques serve the purpose of identifying unknown substances. Molecules that cannot be detected with the one method can be easily detected with the other, and that leads researchers to use them both in a complementary way.

In this doctoral thesis different techniques based on FTIR and RS are employed: confocal Raman microscopy, attenuated total reflection Fourier transform infrared spectroscopy and Synchrotron-Based Fourier Transform Infrared microspectroscopy.

In confocal Raman microscopy (CRM) a confocal microscope is added to a Raman spectrometer allowing the acquisition of spectra with high spatial resolution in the z dimension (depth line), in x-z dimension (depth slice) and also in x, y and z dimensions (tridimensional data). Then 2D or 3D images of the relative abundance of biomolecules can be determined based in the intensity of Raman bands or in powerful spectroscopic

analysis. The technique bears tremendous potential for diverse skin applications ranging from the analysis of physiological component distribution in skin tissue and the diagnosis of pathological states up to biopharmaceutical investigations such as drug penetration kinetics within the different tissue layers[73].

Attenuated total reflection Fourier transform infrared (ATR-FTIR) offers another way in FTIR to record spectra from non-transparent biomedical samples. At the interface between an ATR crystal of high refractive index and the sample of lower refraction index, an evanescent wave penetrates a few micrometers into the sample. The spectrum collected represents then the average signal from the area of the sample that the light passed through.

Synchrotron-Based Fourier Transform Infrared microspectroscopy (μFTIR) is a conventional infrared spectrometer with very little modifications to be adapted to the synchrotron infrared source and to a microscope. These modifications represent a significant enhancement over the conventional IR. Through a 10-μm pinhole, the brightness of a synchrotron source is 100–1000 times higher than a conventional thermal (globar) source. Accordingly, the improvement in spatial resolution and in spectral quality to the diffraction limit has led to a plethora of applications that is just being realized. Some authors studied simultaneously skin composition, structure and molecule penetration[74]. Others have been used μFTIR to study the effect of penetration enhancers on SC lipidic structure and to follow exogenous molecule penetration[75].

The spectral analysis is a crucial step to extract conclusions of the experiments in RS but also in FTIR. To extract information of the spectra many mathematical calculus can be performed: baseline, normalization, second derivative, principal component analysis, etc.

Moreover when the spectral contribution of a substance wants to be determined other methods arise. In this thesis peak fitting, classical least squares (CLS) and multivariate curve resolution-alternative least squares (MCR-ALS) analysis will be performed.

Peaks and spectral bands are usually studied with peak fitting method. Experimentally measured bands or peaks are fitted with theoretical models that create individual peaks from a spectrum that, when added together, match the original data. Then, the peak parameters like amplitude, intensity or the peak position can be easily determined and subsequently studied in detail.

To apply the classical least squares regression (CLS)[76] to the spectral data, the pure compound spectrum of each constituent (loadings) is required. Then the contribution

(scores) of each loading in the dataset can be calculated. These scores are used to create a map showing the distribution of each reference spectrum.

Multivariate Curve Resolution-Alternating Least Squares (MCR-ALS)[77] has been widely used for different applications of Raman-based hyperspectral imaging[78] and determination of skin penetration of substances[79]. Similarly to CLS, MCR-ALS can recover the concentration and pure spectra of analytes of interest and can additionally estimate the spectra of possible interferences. This method has proved to be particularly useful in cases, where spectra of the pure substances were not available[80–83]. However, with this method, known reference spectra can be also used as a starting point for the calculation. Similar to CLS, the algorithm will calculate the scores and loadings of each component to create a 2D image.

In the present thesis CRM, ATR-FTIR and µFTIR techniques will be used not only to study the molecular disposition and penetration within the skin, but also to study the absorption of substances and the molecular changes that the actives or the vehicles may promote in the different skin layers.

AIMS

2. AIMS

The main aim of this work is to evaluate different *in silico*, *in vitro* and *in vivo* methods to asses skin permeability of active molecules, to select in the future the appropriate ones to be included in screening cascades of novel drugs. To this end a group of topical molecules for different indication and with diverse physico-chemical properties were selected. Correlation of methodologies was sought also to increase understanding of active penetration through the skin.

This main aim can be split into the following specific objectives:

- To seek for correlation on permeability behavior of *in silico* Quantitative structure permeability relationship (QSPR) models and *in vitro* skin-PAMPA and Franz diffusion cells with synthetic membranes and pig skin respectively.

- To determine the effect of vehicles on skin permeation using Franz diffusion cells with pig skin to be related with their physicochemical properties and clinical efficacy.

- To demonstrate the enhancer effect of propylene glycol based on skin modification.

- To design and obtain new synthetic membranes containing lanolin with improved membrane barrier to better emulate mammal skin on *in vitro* permeation models.

- To validate the Franz diffusion cells with pig skin with *in vivo* stripping results.

- To improve the confocal Raman spectroscopy methodology to achieve quantitative analyses to be correlated with Franz diffusion cell results.

- To demonstrate the suitability of confocal Raman microscopy to study structural skin layer modifications and the follicular penetration of actives.

MATERIALS

3. MATERIALS

3.1. Porcine skin

In accordance with an approved Institutional Animal Care and Use Committee protocol, unboiled porcine skin was obtained from the dorsal area (dermatomed skin) or the ear (non-dermatomed skin) of weanling female white/Landrace pigs weighing 30-40 kg. The skin was provided by the Clinic Hospital of Barcelona. Following euthanasia of the pigs, the bristlers were removed carefully with an animal clipper and were subsequently gently washed with water.

If dermatomed skin was needed, the hair-clipped skin was dermatomed with a Dermatome GA630 (Aesculap, Germany) to a thickness ranging from 500±50 µm, cut in appropriate pieces (2.5 cm inner diameter) and then sealed and stored under vacuum at -20ºC until their use.

3.2. Synthetic membranes

The Skin-PAMPA™ sandwiches were purchased from Pion INC (precoated permeability plates; P/N 120691) and were used after an overnight hydration with hydration solution (Pion P/N 120706). The full set up process is described in section 4.2.

Two different polymeric membranes were employed as surrogates for creating a new synthetic membranes containing lanolin: StratM® (Merck Milipore, Germany) and Nuclepore® (Sigma-Aldrich, USA).

3.3. Actives

A vast number of topical actives were employed in this thesis to study and compare the different permeation models. Table I contains a list of the actives as well as some other characteristics to show the high diversity of the subset.

Table I Compound (abbreviation), CAS number, manufacturer, main indication and ionization state of the selected substances.

Compound (Abbreviation)	CAS Number	Manufacturer	Indicaction	Ioniz. State
Azelaic acid (Az)	123-99-9	Sigma	Acne	Acid
Betamethasone dipropionate (Bet)	5593-20-4	Sigma	Inflammation	Neutral
Bexarotene (Bex)	153559-49-0	Selleck	Lymphoma	Acid
Caffeine (Caf)	58-08-2	Merck, USA	Anticellulite and antioxidant	Basic
Calcipotriol monohydrate (Cal)	147657-22-5	MatTek	Psoriasis	Neutral
Clindamycin (Cli)	18323-44-9	Axon Medchem	Antibacterial acne	Basic
Clobetasol propionate (Clo)	25122-46-7	AK Scientific	Inflammation	Neutral
Dapsone (Dap)	80-08-0	Fluka	Antibacterial	Neutral
Diclofenac sodium (Dic)	15307-79-6	Sigma	Actinic keratosis	Acid
Diphenhydramine (Dip)	58-73-1	Pacific	Pruritus	Basic
Eflornithine (Efl)	70052-12-9	Chem-Impex International	Facial hirsutism	Zwitterion
Finasteride (Fin)	98319-26-7	Fluka	Alopecia	Neutral
Fluorouracil (Fo)	51-21-8	Sigma	Actinic keratosis	Neutral
Flurandrenolide (Fra)	1524-88-5	Sigma	Eczema, psoriasis	Acid
Glycopyrrolate (Gly)	596-51-0	Spectrum Chemical	Hyperhidrosis	Quaternary salt
Imiquimod (Imi)	99011-02-6	Ak Scientific	Actinic keratosis	Neutral
Ketoconazole (Ket)	65277-42-1	Intex Quimica	Fungal infection	Neutral
Lidocaine (Lid)	137-58-6	Sigma	Pain	Basic
Nicotine (Nic)	22083-74-5	Tocris, UK	Smoking addiction	Basic
Resveratrol (Res)	501-36-0	Sigma , USA	Antioxidant	Neutral
Salicylic acid (Sal)	69-72-7	Sigma	Acne , psoriasis	Acid
Tacrolimus monohydrate (Tac)	109581-93-3	LC Laboratories	Atopic dermatitis	Neutral
Tazarotene (Taz)	118292-40-3	Sigma	Psoriasis Acne	Neutral
Terbinafine (Ter)	91161-71-6	Selleck	Onychomicosis	Basic
Tofacitinib (Tof)	477600-75-2	MedChem Express	Psoriasis	Neutral

METHODS

4. METHODS

4.1. *In silico* skin permeability models: QSPR

Three mathematical models were used to predict the skin permeability coefficient (K_p in cm/s) or the facility of the compound to permeate across the skin (Table II). The Potts and Guy equation (P-G) and the Mitragotri equation (Mi) take into account the molecular weight (MW) and the solute octanol-water partition coefficient (K_{ow}). The third mathematical model was the Barratt equation (Barr), which, in addition to the octanol-water partition coefficient, takes into account MV as the molecular volume and MP for the melting point.

Table II Mathematical Models for Predicting Skin Permeability; Mitragotri (Mi), Potts and Guy (P-G) and Barratt (Bar) models

Model	Equation
P-G Equation[37]	$log\ K_p = 0.71\ log\ K_{ow} - 0.0061MW - 6.3$
Mi Equation[38,39]	$logK_p = 0.7\ log\ K_{ow} - 0.0722\ MW^{\frac{2}{3}} - 5.2518$
Bar Equation[40]	$log\ K_p = 0.82\ log\ K_{ow} - 0.0093\ MV - 0.039MP - 2.36$

The three models consider the substance lipophilicity, an important parameter that affects skin permeation. To study the permeability in our subset of compounds, the calculus for $\log K_p$ was performed with the distribution coefficient ($\log D$) at pH 5.5 (skin surface pH) where the molecules can be ionized.

Two different software platforms, ChemAxon algorythm (Chemaxon, Hungary) and BIOVIA PipelinePilot (Accelrys, USA) were employed to obtain the distribution coefficient at pH=5.5 ($\log D$ pH 5.5) and the molecular weight (MW). The molecular volume was obtained from the BIOVIA PipelinePilot application software.

The melting points (MP) of pure compounds were measured in a Büchi B-540 in Almirall R&D Centre. The melting point was calculated with the medium value obtained between the temperature in which a visual modification of the solid form was observed and the final temperature in which the transition was completed. The increment of the temperature was approximately 1ºC/min.

4.2. Skin Parallel Artificial Membrane Permeability Assay (skin-PAMPA)

Skin-PAMPA is a high throughput screening *in vitro* assay used to study the transcellular permeation of compounds. Active permeabilities were studied when they were solved in a solution at the physiological skin surface pH (5.5) and in propylene glycol (PG) which is a commonly employed cosolvent-enhancer. Assays were performed in Almirall R&D Centre. Each active was diluted in propylene glycol (Sigma Aldrich, USA) or a buffer solution (Pion, No. P/N 110151 50 mL) at 20 µM. In both cases, a 2% v/v of dimethyl sulfoxide (DMSO) (Sigma-Aldrich, USA) was employed.

Before forming the sandwich (Figure 8), the bottom (donor) plate was filled with 200 µL of the previously described solution. The acceptor plate was filled with 200 µL of fresh Prisma HT Buffer at pH 7.4 and containing 2% v/v DMSO. The resultant sandwich was incubated for 5 h at room temperature. After the permeation time, the PAMPA sandwich was separated, and 100 µL of both the donor and acceptor compartments was transferred to UPLC plates. The analytical procedure followed for their analysis is detailed in section 4.6.2.

4.3. Permeation studies with Franz diffusion cells

The absorption penetration profile was studied with the Franz cell assay. Such assay was widely employed in this thesis and allows not only the study of absorption through membranes or through skin biopsies. Moreover when working with skin, the amounts of substance can be determined in different layers.

Static Franz diffusion cells (Lara-Spiral, Courtenon, France) with a nominal surface area of 1.86 cm^2, and the receiver compartment capacity with approximately 3 mL were employed. The OECD Guidelines[84] and the published opinions of the Scientific Committee on Cosmetic Products and Non-Food Products[85] were closely adhered to during this study. Additionally, several other classical and updated principles of percutaneous absorption were considered[86].

The employed membrane/skin was thawed and mounted with the top/SC side facing the donor compartment. The receptor chamber was filled with receptor fluid (RF), Dulbecco phosphate-buffered saline at pH 7.4 (Sigma, St. Louis MO, USA) in MiliQ water with the addition of 0.04% (w/v) and gentamicin sulfate salt (Sigma, USA). Nevertheless in the case of poorly hydrophilic substances its solubility within the receptor fluid can be an impediment for its diffusion. To overtake this impediment, a 5% (w/v) of bovine serum albumin (Sigma, USA) was also added following the recommendations of OECD2010 to increase the uptake of lipophillic compounds[87].

Air bubbles were carefully removed between the skin and the RF. The RF was agitated with a magnetic stirring bar.

The assembled Franz-type cell was placed in a thermostatically controlled water bath maintained at 37ºC containing a magnetic stirring device, and the skin surface temperature was maintained at approximately 32ºC. To eliminate the damaged skin, the transepidermal water loss value (TEWL) was measured with a Tewameter TM210 (Courage & Khazaka, Cologne, Germany) at the moment of the formula application, considering correct TEWL values under 15 $g/m^2/h$.

At this point, 20 µL of each formulation was applied to the top of the membrane/skin delimited by the upper cell. At 24 h, receptor fluid was collected and extracted) was transferred to a 5-mL volumetric flask and stored at -20ºC until analysis.

In the case of skin, the different skin layers were separated as follows. Skin surface was washed and wiped with a cotton bud to remove any remaining formulation. Then, 8 strippings were carried out on the surface horny layers of the SC with strips of adhesive tape (D-Squame, Cuderm Corporation, Dallas, USA) applied under controlled pressure. Lastly, the epidermis was separated from the dermis after heating the skin at 80ºC for several seconds.

The extractor employed solvents were different depending on whether the analysis was carried out by UPLC-MS/MS (section 4.6.2) or HPLC-DAD (section 4.6.1). The wash and the cotton bud were extracted into 10 mL of solvent (W). The strips were extracted into 2 mL. The Stratum Corneum value (SC), epidermis (E) and dermis (D) were appropriately extracted into 1 mL extractor solvent. The different skin samples were extracted appropriately in 1 mL of extractor solvent.

4.4. Design new lanolin synthetic membranes

The addition of lanolin is proposed as a strategy to emulate the lipidic matrix and therefore increase the permeation similarity between normal skin and synthetic membranes to be applied to *in vitro* permeation methodologies previously described.

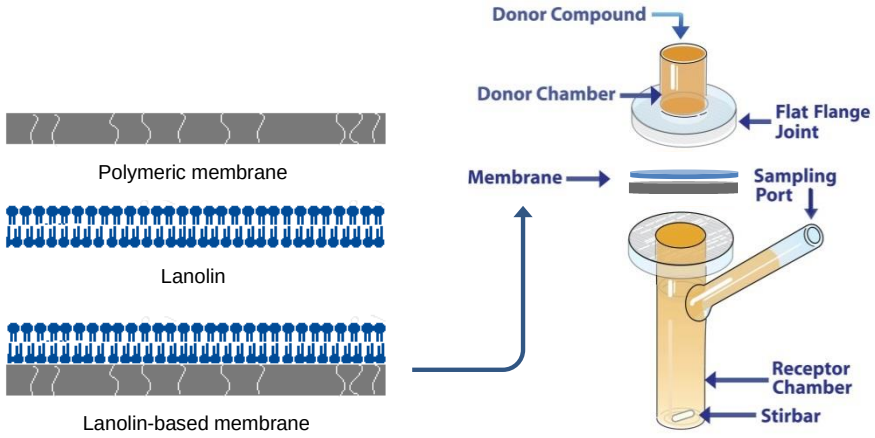

Figure 11 Lanolin addition to polymeric synthetic membranes and Franz-cell assembly

Lanolin was extracted from Spanish merino sheep's using the WDS process which is detailed in the LIFE 11 ENV/ES/588 project[88]. In brief, the wool was scured with hexane, to remove dust impurities the hexane solution was centrifuged and lanolin's recovered from the hexane with distillation at 35ºC. Finally lanolin was desiccated to remove the residual water.

Addition of lanolin was performed to the Strat-M and Nuclepore membranes (Figure 11). In Strat-M membranes, 100 µL of lanolin 5% in hexane:ethanol 96% (2:1) solution was applied three times on the top of the membranes under N_2 flow. Next, these Strat-M-lanolin membranes were stored at 85°C for 10 minutes to fix the lipids and dry the membrane. Lanolin was also added to the Nuclepore membranes following the more complex procedure for lipid fixation previously detailed by Pullmannová et al.[89], wherein the membranes were hydrated in hexane:ethanol 96% (2:1) and then dried at room temperature. Under N_2, 100 µL of lanolin 5% in hexane:ethanol 96% (2:1) was applied on the top. The membranes were stored at 2-6°C in a vacuum desiccator for 24 h. Finally, the membranes were placed at 85°C for 10 minutes and, after 3 h at room temperature, the membranes were ready to use.

Each studied membrane was mounted in a Franz-type cell following the method of section 4.3. TEWL, as an indicator of the membrane integrity/barrier function, was acquired after system stabilization and nine replicates for every model were evaluated during 24h. Once the results were obtained, the Kruskal-Wallis test was performed to detect significant differences between the pig skin and the different models. So then, the barrier function improvement and similarity against porcine skin after the lanolin addition could be discussed.

4.5. *In vivo* tape stripping methodology

Six volunteers (all women) with no history of dermatological disease participated in this study, which was approved by the Ethics Committee (IQAC-CSIC, Barcelona, Spain). Specific information of the study was given to the participants, and their written consents were obtained. The median age of the volunteers was 33 years, ranging between 25 and 42 years, and phototypes II, III and IV were included[90]. The treated sites (2 × 1 cm) were the non-hairy areas of the ventral forearm surface. The administration involved application of 10 µL/cm^2 of active solution, according to reported guidelines[84]. This amount represents 500 µg of the total amount of active per area (cm^2). The application was non-occlusive.

The active permeation profile across the SC was determined with the widely detailed [91,92] stripping method. After an application time of 24 h, a sequential removal of the outer skin layers from each volunteer was carried out by tape stripping (D-Squame™ tapes, ø = 22 mm, CuDerm, Dallas, USA). Each tape was fixed to the skin surface using a specific device that exerted a constant pressure of 80 g/cm^2 for 5s, and the tape was removed from the test area with a gentle movement. For each repeated strip, the tear-off direction was varied to obtain homogeneous removal of the SC cell layers. A total of ten tape strips were used on all the treated sites.

4.6. Extraction and analysis

The quantification of the actives in the different samples was done with two different devices: HPLC-DAD and UPLC-MS/MS. Actives were quantified and extracted accordingly with the different experiments. The extractor solvent for compounds analysed with HPLC-DAD are detailed on Table III (section 4.6.1) while ACN-TFA was the extractor solvent of all compounds analyzed with UPLC-MS/MS (section 4.6.2).

In both cases after the analysis, the results were presented as normalized amounts (%) of permeated substance with their standard deviation. The permeated amounts (ABS) in the case of skin was considered the sum of the epidermis, dermis and receptor fluid. For the rest of the membranes, the amounts were found to be equivalent to those in the receptor fluid.

4.6.1. High performance liquid chromatography (HPLC-DAD)

Before the HPLC analysis, all the extracts were sonicated 15minutes and filtered with a 0.45µm Nylon filter (Cameo, USA). The amount of active in the samples was determined by HPLC methodology validated according to ICH Q2 (R1) guidelines in terms of linearity, accuracy and precision[93]. The HPLC system consisted of a WVR-Hitachi HPLC with a CM5430 DAD detector, L-2130 Pump, L-2200 Autosampler, and an

Interfase. The flow rate was 1 mL/min under isocratic conditions, and the injection volume was 20 µL. The columns, wavelengths and mobile phases as well as calibration curve for every active are compiled in Table III.

Table III HPLC analytical conditions for lidocaine (Lid), diclofenac sodium (Dic), betamethasone dipropionate (Bet), caffeine (Caf) and Resveratrol (Res). Employed abbreviations: Excitation wavelength (λ) in nanometers; Retention time (Tr) in minutes; 0.5% of trifluoroacetic acid in acetonitrile (ACN-TFA)

Active	Extractor Solvent	Column	λ(nm)	Tr (min)	Mobil phase	Linear regression equation (R^2)
Lid	ACN-TFA 0.5%	LiChrocart® 125-4 Lichrosphere® 100RP-18 5µm	205	14	70% buffer phosphate pH 7 30% ACN	$A = 414046[Lid] - 68532$ (0.9999)
Dic	Methanol	LiChrocart® 250-4 Lichrosphere® 100RP-18 5µm	254	18	66% methanol 34% phosphoric acid 0.7%	$A = 80050[Dic] - 2484$ (0.9997)
Bet	Methanol	LiChrocart® 250-4 Lichrosphere® 100RP-18 5µm	239	11	73% methanol 27% water	$A = 1811416[Bet] + 47781$ (0.9999)
Caf	Phosphate saline buffer pH 7.6	LiChrocart® 125-4 Lichrosphere® 100RP-18 5µm	271	13	75% water 25% methanol	$A = 17608[Caf] - 1048.8$ (0.9999)
Res	Methanol	LiChrocart® 250-4 Lichrosphere® 100RP-18 5µm	303	4.5	52% methanol 5% acetic 48% water	$A = 52321[Res] - 21132$ (0.9998)

4.6.2. Ultra performance liquid chromatography-tandem mass spectrometer (UPLC-MS/MS)

Wash, D-Squame tapes, epidermis and dermis samples were extracted with acetonitrile (Sigma, USA) with 0.5% of trifluoroacetic acid (Sigma, USA) (ACN-TFA 0.5%) and diluted with water 1:3 (v/v) before the analysis by UPLC-MS/MS. Receptor fluid sample levels were determined by UPLC-MS/MS after protein precipitation with ACN-TFA 0.5%, centrifugation at 4000 rpm for 10 min (4ºC) and dilution of the supernatant with water 1:3 (v/v).

All the UPLC-MS/MS analysis were performed in Almirall R&D center. The MS detector used was Waters XEVO TQS. The column used was a Waters Acquity UPLCTM BEH C18

(1.7 µm, 2.1x50 mm), and it was maintained at 40ºC. The autosampler temperature was 8ºC. The mobile phase A contained 0.05% HCOOH+2.5 mM of NH3 (pH 3), and the mobile phase B was acetonitrile (ACN). The flow remained stable at 0.400 µL/min for all the compounds. The analytical conditions for the actives are detailed in Table IV.

Table IV Analytical UPLC conditions. Employed abbreviations: Time 0 (i); Cone voltage (CV) in V; Collision energy in eV (EC); Excitation wavelength (λ) in nanometers; Retention time (Tr) in minutes

Active	Precursor ion (m/z)	Product ion (m/z)	CV (V)	EC (eV)	% Phase A (time)	λ (nm)	Tr (min)
Aze	187.10	125.0	25	20	85 *(i)*- 55 (1 min)- 5 (1.10 min)- 85 (1.70 min)	NA*	1.15-1.2
Bet	505.25	279.1	20	20	55 *(i)*- 5 (1 min)- 55 (1.70 min)	254	1.05
Bex	347.21	186.0	50	-	20 *(i)*- 5 (1 min)- 20 (1.70 min)	258	0.99
Cal	395.1	105	15	35	85 *(i)*- 5 (2 min)- 85 (2.20 min)	265	1.85
Cli	425.18	126.0	45	25	85 *(i)*- 55 (1 min)- 5 (1.10 min)- 85 (1.70 min)	200-400	1.04
Clo	467.19	278.0	50	25	20 *(i)*- 5 (1 min)- 1.70 (20 min)	246	1.07
Dap	249.06	92.0	30	20	85 *(i)*- 60 (1 min)- 5 (1.10 min)- 85 (1.70 min)	295	1.10
Dic	296.02	215.1	20	20	65 *(i)*- 5 (1 min)- 65 (1.70 min)	277	1.08
Dip	255.16	167.1	30	20	85 *(i)*-35 (1min)- 5 (1.10 min)-85 (1.70 min)	220	1.08
Efl	183	120	20	30	5 *(i)*- 95 (3 min)- 5 (3.10 min)	NS**	1.82
Fin	373.28	57	45	40	65 *(i)*- 20 (1 min)- 5 (1.10 min)- 65 (1.70 min)	204	1.0
Fo	129	86	35	15	5 *(i)*- 95 (3 min)- 5 (3.20 min)	266	0.4
Fra	437.3	361	5	15	62(i)- 45 (0.70 min)- 5 (1.10 min)- 62 (1.20 min)	NS**	0.6
Gly	319.21	116.1	40	25	20 *(i)*- 5 (1 min)- 20 (1.70min)	237	1.14
Imi	241.14	185.1	50	20	85 *(i)*- 55 (1min)- 5 (1.10 min)- 85 (1.70 min)	245	1.14
Ket	531.15	82	40	25	75 *(i)*- 40 (1 min)- 5 (1.10 min)-75 (1.70 min)	243	1.07
Lid	235.17	86.1	40	20	95 *(i)*- 60 (1 min)- 5 (1.10 min)- 95 (1.70 min)	277	1.08
Nic	163	132	30	20	85 *(i)*- 35 (4.10 min)- 5 (4.20 min)	260	1.10
Sal	137	93	45	20	95 *(i)*- 44 (3 min)- 10 (3.10 min)- 95 (3.20 min)	301	1.86
Tac	804.48	768.0	35	20	45 *(i)*- 5 (1 min)- 45 (1.70 min)	200-400	1.23
Taz	352.3	324.1	50	25	71 (i)- 88 (0.70 min)- 95 (0.80)- 71 (1.20 min)	NS**	0.60
Ter	292.2	141	30	20	65 *(i)*- 5 (1 min)- 65 (1.70 min)	284	0.98
Tof	313.3	149	45	25	95 (i)- 75 (1 min)- 5 (1.10 min)- 95 (1.70 min)	290	1.21

*NA: not applicable **NS: no signal

4.7. Confocal Raman microscopy

Two different measurements were employed in this doctoral thesis with confocal Raman microscopy. From one side, in the depth profiling (Figure 12A), the Raman

spectra were obtained measuring the treated skin in the z-axis (depth). From the other side in the imaging the Raman spectra were acquired in the x-y axis in a skin cross-section so an image of the spectral information can be obtained (Figure 12B).

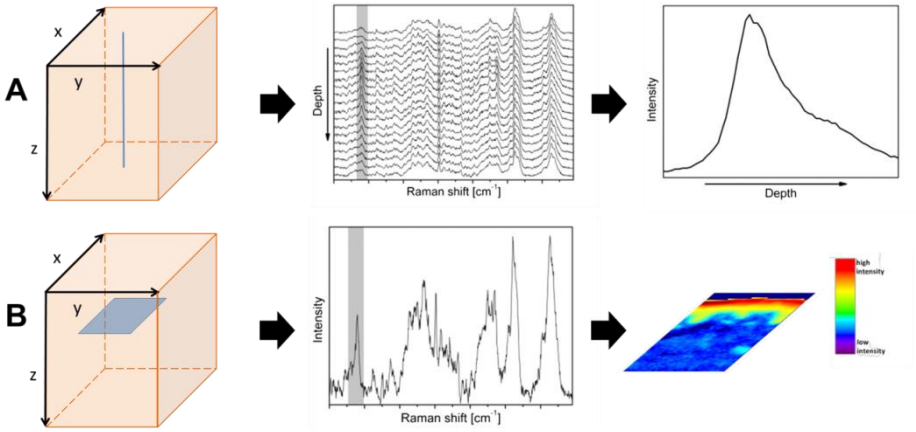

Figure 12 A. Depth profiling: Raman spectra are recorded along a z-directed line, peak intensities are depicted as intensity profiles against depth. B. Imaging: Raman spectra are acquired in the x–y direction; intensities are represented by color in a two dimentional picture Figure is adapted from Franzen et al. [94]

4.7.1. Depth profiling of substances into the skin

Confocal Raman microscopy (CRM) allows the study of the diffusion through the skin of substances by studying the skin spectral changes when going in depth (z-axis) into a sample, especially with substances with bands that are not overlapped with the skin spectra. This semi-quantitative technique has been optimized to achieve a quantitative assay, both methodologies are described below.

Raman spectra acquisition

Raman spectra were acquired using a Renishaw (Gloucestershire, UK) Model inVia confocal Raman microscope in Almirall R&D Centre. Excitation (approximately 100 mW at the sample) was provided by a 532 nm diode laser. The exciting laser radiation was coupled to the microscope through a wavelength-specific mode optical fiber. The incident laser beam was collimated via a lens and passed through a holographic band pass filter before it was focused onto the sample through the objective of the microscope. A Leica 50x/0.75 NA objective was used in this study. Spectra were

acquired using a 1 s exposure time, 3 accumulations and an 1800 line/mm grating. The spectral resolution was approximately 1 cm^{-1}, and the spectral window ranged from 190 to 1950 cm^{-1}.

Quantitative detection

For the quantitative detection with CRM, different biopsies of tissue were incubated at different active concentrations and then analyzed with Raman. Therefore, when a specific band of the substance is observed, its intensity can be related to the solution concentration. Finally when analyzing the sample at different depths, the obtained intensities can be correlated with the different concentrations.

The active was solved in phosphate buffered saline solution at pH 7.6 (Sigma-Aldrich, St. Louis, MO, USA) to reach solutions containing a wide range of concentrations (see results of caffeine in section 5.4.1).

For incubation experiments, epidermis (Ep) was separated from the dermis after heat dry treatment at 80ºC for few seconds. Each Ep sample was weighted previous immersion in a specific solution. The mean of weight of Ep samples was 10.84 ± 1.57 mg. Ep samples were completely immersed in 3 mL of each solution by triplicate, during 20h. Afterwards, the Ep was removed and dried between two filter papers under controlled pressure (80g/cm² for 10 seconds). The content of active from Ep was analysed by confocal Raman microscopy (CRM) (detailed above) and quantified by HPLC-DAD (section 4.6.1).

4.7.2. Imaging of transfollicular penetration of caffeine with Confocal Raman microscopy

Confocal Raman microscopy (CRM) was here used to image the follicular penetration of caffeine vehiculized in nanoparticles (Caf-NP) and aqueous solution (Caf-Aq). Cryosections of porcine skin applied with each formulation are analyzed with CRM. The obtained spectra are analyzed with different spectroscopic methods to create 2D images of caffeine distribution.

All the different processes described in this section were performed in the Center of Experimental and Applied Cutaneous Physiology (CCP) placed in Berlin.

Skin sample preparation

A test area of 2×3 cm were marked on non dermatomed porcine ear skin (section 3.1) using window color (Marabu GmbH & Co KG, Tamm, Germany) for every formulation and one for non-treated skin (NT). 10 µL/cm^2 of caffeine formulation were applied on the surface of the test area. In order to simulate the *in vivo* situation, the selected areas were massaged 2 min using a massage applicator (Minivibrator RFM, Rehaforum

Medical GmbH, Elmshorn, Germany) after topical application of the formulation. The formulations were allowed to penetrate for 30 min.

After 30 min of penetration time, biopsies of the treated and the non-treated areas were taken using a scalpel. Cryospray (Cryo-Spray, SLEE medical GmbH, Mainz, Germany) was applied to facilitate separation of the skin samples from the underlying tissue. The biopsies were flattened between two glass slides, again fixed with cryospray and finally placed in liquid nitrogen and subsequently stored in a freezer at -20 °C until further use. The cross-sectional tissue samples of the biopsies were prepared using a cryomicrotome (Cryostat Microm HM 560, Microm International GmbH, Walldorf, Germany).

Each biopsy was embedded in Tissue freezing medium (Leica Biosystems Nussloch GmbH, Germany) on a metal sample holder inside the cryomicrotome at -30°C. The embedded skin was sectioned into 30 µm slices by microtome blades before being placed onto Superfrost glass slides (Carl Roth GmbH + Co KG, Karlsruhe, Germany) and for later analysis stored at -20 °C. For the subsequent measurements, the sections on hair follicles were selected.

CRM mapping acquisition

Measurements of cross-sections were performed using a Labram HR800 Evolution CRM (Horiba Jobin Yvon, France) in the fingerprint region (400–2500 cm^{-1}) with excitation at 473 nm and 6.1 mW optical power on the sample surface and a spectral resolution of <4 cm^{-1}. The following settings were employed: grating of 600 g/mm, 100× objective, spot of 0.85 µm and 5 s of exposure time per spectrum. The microscopic images of the hair follicles were collected with a 10× objective.

The Autofocus reflection mode integrated in the Labspec software (Horiba Jobin Yvon, France) was employed for the detections of the sample surface for every position. The autofocus setup was established individually for both hair follicles according to the following procedure: by visually focusing on the sample, a z-value of 0 µm was assigned to the lowest point of the sample (glass cover-slide), then the z-value of the highest point of the sample was obtained (normally placed on the hair). Thereby, the setup range for the autofocus was established, which was scanned in 1 µm steps for the surface determination in both mappings.

Reference components spectra

The CLS and MCR-ALS methods (briefly explained in section 1.2.4) use reference spectra of pure substances to determine the distribution of the compound in the hair follicle. The non-treated cryosections were employed to obtain reference spectra of Stratum Corneum (SC), epidermis, dermis, glass substrate, Cryospray drops and

caffeine, which proved to result in high sensitivity. Franzen *et al.*[95] used reference spectra of Sebum, Epidermis, Dermis and hair. The reference spectrum of the active was obtained by measurements of the pure compound.

Except for the five times increased accumulation time, all the reference measurements were performed on the same settings, as employed for the mapping acquisition.

Data Analysis

All spectra were pre-processed using the Labspec software. After cosmic spike removal, a polynomial fit was used to subtract the fluorescence background. In order to evaluate the distribution of caffeine in the hair follicle, the following methods were employed.

The peak fitting module is integrated in the Labspec software. The caffeine-based Raman peak at 555 cm^{-1} was approximated using non-linear regression of a Gaussian function. This peak was chosen for analysis due to its prominence in caffeine and the minor overlapping with the main skin Raman bands. For each measured position, the peak amplitude at 555 cm^{-1} was plotted as a false color intensity image overlaid on the microscopic image.

The CLS fitting section of the Labspec software was used to perform multivariate CLS regression on the multidimensional array of spectra using a set of reference component spectra (caffeine, Stratum Corneum, epidermis, dermis, hair, glass and cryospray). The scores and the reference spectra were normalized and restricted to non-negativity. Finally, all scores of the different component were plotted in false color intensity images, overlain on the microscopic images. As each Raman spectrum is a fingerprint of the chemical composition of the sample, the distribution of different substances can be analyzed. Using the reference spectra of the substances, the relative contribution of the reference spectra at each measurement point is calculated. By assigning the spectrum of each chemical substance to a color, the distribution of all the reference spectra within the examined section can be indicated giving a color coded image of the scanned area.

The recorded spectra were also analyzed using the MCR-ALS algorithm. This was implemented in self programmed software based on Matlab R2016a (the MathWorks, Inc., Natick, MA, USA) and incorporated the graphical user interface MCR-ALS GUI 2.0 developed by Tauler *et al*.[96] Reference spectra of seven different components were applied to the analyses as initial estimates (caffeine, Startum Corneum, epidermis, dermis, glass and cryospray). The only constraint applied for the optimization process was non-negativity of the resolved scores and loadings. Semi-quantitative parameters were calculated from the scores by dividing the caffeine score by the sum of all scores

for every measured position, according to Vajna *et al*. [97] The final scores for caffeine were plotted superimposed in red to the microscopic image.

4.8. Infrared spectroscopy

Two techniques based on the Fourier transform infrared (FTIR) spectroscopy (Figure 13) are used in this doctoral thesis. From one side, attenuated total reflection in conjuction with a FTIR (ATR-FTIR) was used to evaluate the lipidic conformation. On the other side, a synchrotron-based Fourier transform infrared microspectroscope was used in a similar way than CRM in section 4.7.2 to acquire FTIR spectra in the x-y axis in a skin cross section.

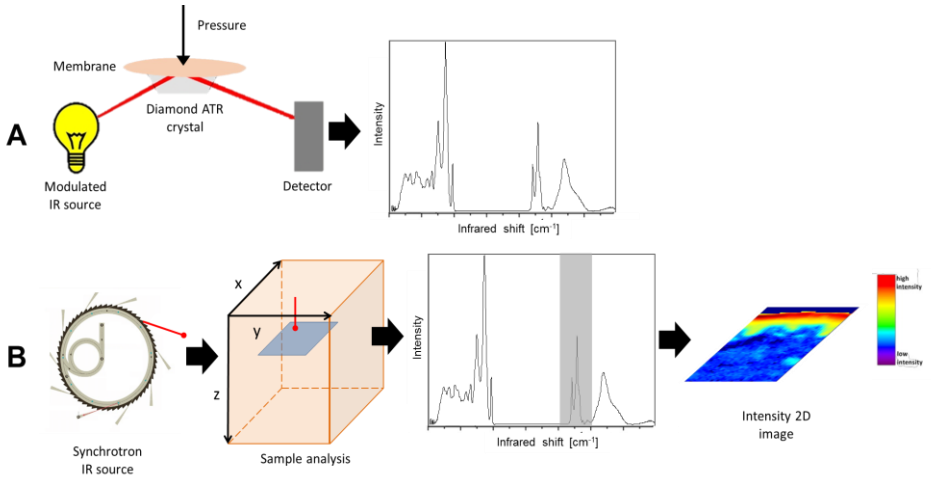

Figure 13 A. Spectra acquisition in ATR-FTIR. B. Scheme of the μFTIR: synchrotron light (red line) irradiates the sample (in blue); each analyzed position means one spectra; combining the spectral information with the spatial information, 2D images can be created. Figure is adapted from Franzen et al. [94]

4.8.1. Evaluation of the lipidic conformation of lanolin synthetic membranes by ATR-FTIR

Lipidic conformation can be studied with ATR-FTIR (Figure 13A). The infrared spectra were obtained using the 360-FTIR spectrophotometer Nicolet Avatar (Nicolet Instruments, Inc., Madison, WI) equipped with an attenuated total reflection (ATR) accessory that used a diamond with an angle of incidence of 45° in a horizontal orientation.

Before analysis, the samples were placed with the SC/lanolin side facing the ATR diamond. To ensure reproducible contact between the sample and crystal, a pressure

of 10 kPa was applied to the samples. All analyzed spectra represented an average of 32 scans obtained with a resolution of 4 cm^{-1}, and the wavenumber range used was 4000–700 cm^{-1}. The peak positions were determined with the aid of OMNIC software version 7.3 (Nicolet, Madison, WI) using a Gaussian-Lorentzian peak fitting and baselined spectra. Two different peaks were studied: 2850 cm^{-1} and 2920 cm^{-1}, which are assigned to the CH2 symmetric and asymmetric stretching vibration, respectively. Analysis of every sample was made in triplicate.

4.8.2. Imaging of skin cross-sections with Synchrotron-Based Fourier Transform Infrared microspectroscopy

Synchrotron-Based Fourier Transform Infrared microspectroscopy (µFTIR) can be used to map skin cryosections (Figure 13B). When a sample area is analyzed, many measurements in each map position are performed. Each position means one spectrum. By combining the spatial information with the spectral information 2D images can be created.

µFTIR sample preparation

The same day of slaughter, 10µL/cm^2 of substance were applied and gently spread over the skin surface (treated skin section)(section 3.1). The incubation of the skin was performed at room temperature (20-25ºC) on a Petri plate with wet paper filter to avoid drying of the skin. After 30min of exposure, a biopsy from the treated area covered with aluminum foil to avoid interferences was embedded in CRYO-M-BED (Bright, UK), frozen in nitrogen liquid and stored at -30ºC. For the preparation of the non-treated samples (Blank skin section), a biopsy of skin was taken and then treated as explained for the PG sample. The day before the FTIR analysis, the skin blocks were cut at 6µm thickness and mounted in a CaF_2 window.

µFTIR experiments

Synchrotron-Based Fourier Transform Infrared microspectroscopy was performed at the MIRAS beamline at ALBA synchrotron (Cerdanyola del Vallès, Spain)[98]. CaF2 windows containing the cross-sections were placed in a Hyperion 3000 microscope (Bruker, USA) coupled to Vertex 70 spectrometer (Bruker, USA). The employed detector was a 50 µm HgCdTe (MCT) Detector (10000-600 cm^{-1}).

The infrared spectra were acquired at room temperature in transmission mode. The data were recorded using an aperture size of 10 µm x 10 µm. Spectra were collected in the 4000–800 cm^{-1} mid-infrared range at a spectral resolution of 4 cm^{-1} with 128 co-added scans per spectrum.

µFTIR data treatment and statistical analysis

To extract spectral information, the OPUS software (Bruker, USA) was used. The obtained data was processed as follows: the spectra with higher intensities than 1.5 cm^{-1} were excluded for the calculations due to the lack of spectral quality and the presence of saturated regions. Then each spectra was manually grouped considering in which layer was acquired (epidermis or dermis) and if it was untreated (NT) or treated with propylene glycol (PG).

The peak positions were determined with the aid of OMNIC software version 7.3 (Nicolet, Madison, WI) using a Gaussian-Lorentzian peak fitting after baseline and normalization. Analysis of every spectrum was made and the average and the standard deviations calculated in every sample.

To compare the different spectra groups the principal component analysis (PCA) was performed using the Unscrambler® (CAMO software, Norway).

RESULTS AND DISCUSSION

5. RESULTS AND DISCUSSION

5.1. Comparative study between *in silico* and *in vitro* models for prediction the permeability of topical actives

In this section, the permeability of topical active agents with very different physico-chemical properties was investigated with different methodologies. Three *in silico* models (Potts and Guy, Mitragotri and Barratt) and two *in vitro* models (skin-PAMPA and Franz cells) were applied to determine percutaneous absorption profiles. Permeability in Franz cells was determined for compounds formulated in propylene glycol and for some of the compounds in the commercial formulas to evaluate the fundamental vehicle effect.

As it can be seen on Figure 14 the selected set of actives comprises a wide chemical diversity, including: 1 quaternary salt, 1 zwitterion, 5 acids, 5 bases and 11 neutral compounds. Following the results of the different applied methodologies are discussed.

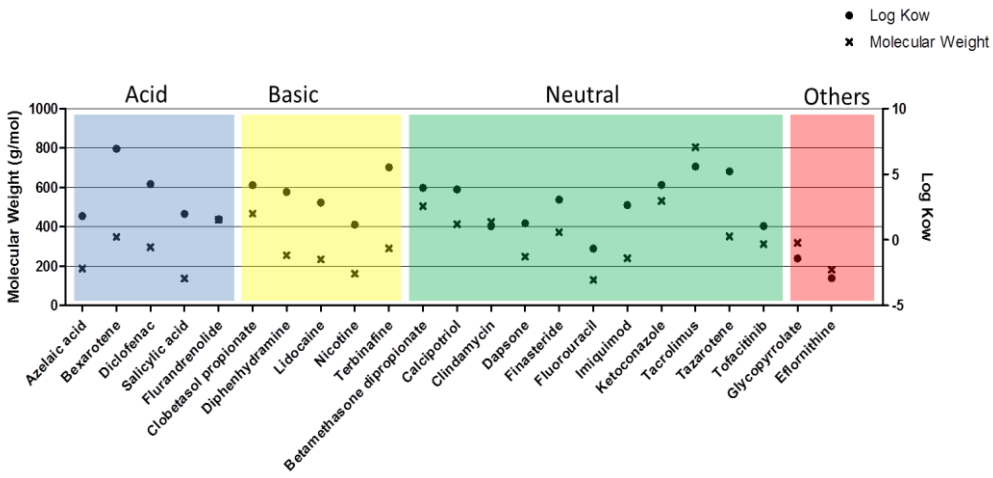

Figure 14 Selected topical actives with their molecular weight and lipophillicity ranked according their chemical nature

5.1.1. *In silico* skin permeability models (QSPR)

The physico-chemical properties of the actives were determined to be applied to the three selected *in silico* models from Table II (section 4.1).

The obtained physicochemical properties are compiled in Table V. All three models take into account the lipophilicity as the main parameter of the active. It must be kept in mind that the lipophilicity of a substance can be influenced by the pH of the environment. For this reason, the octanol-water distribution coefficients ($\log D$) were determined at pH 5.5 (pH of Stratum Corneum from skin). The different models also take into account other properties of the actives, such as molecular weight, molecular volume and melting point.

Table V Theoretical physico-chemical properties. Molecular weight (MW), Molecular volume (MV), Melting point (MP), Octanol-water distribution coefficients ($\log D$) at pH 5.5.

Name	MW	MV	MP (ºC)	$\log D$ pH 5.5
Azelaci acid (Aze)	188.22	162.92	110	-0.16
Betamethasone dipropionate (Bet)	504.59	411.59	187	3.96
Bexarotene (Bex)	348.48	307.32	225	5.5
Calcipotriol monohydrate (Cal)	412.61	372.49	114	3.84
Clindamycin phosphate (Cli)	424.98	350.54	108	-1
Clobetasol propionate (Clo)	466.97	367.35	199	4.18
Dapsone (Dap)	248.3	180.41	173	1.27
Diclofenac sodium (Dic)	296.15	212.31	276	2.75
Diphenidramine (Dip)	255.36	225	171	0.52
Eflornithine (Efl)	182.17	140.97	241	-4.66
Finasteride (Fin)	372.54	327.9	258	3.07
Fluorouracil (Fo)	130.08	84.37	285	-0.66
Flurandrenolide (Fra)	436.51	355.69	215.5	1.56
Glycopirrolate (Gly)	318.43	274.74	194	-1.41
Imiquimod (Imi)	240.3	203.05	301	2.4
Ketoconazole (Ket)	531.43	405.76	151	3.65
Lidocaine (Lid)	234.34	214.37	69	0.61
Nicotine (Nic)	162.23	143.03	91	-1.96
Salicylic acid (Sal)	138.12	100.49	161	-0.67
Tacrolimus (Tac)	804.02	692.51	129	5.59
Tazarotene (Taz)	351.46	290.17	104	5.22
Terbinafine (Ter)	291.43	269.25	42	2.36
Tofacitinib (Tof)	312.37	252.79	113.7	-0.25

These physico-chemical properties showed that the selected actives cover a wide range of molecular weight between 130.08 g/mol for fluorouracil and 804.02 g/mol for tacrolimus. As the molecular volume value is closely related to the molecular weight, a wide range of molecular volumes was also obtained. Additionally, a wide spectrum of melting points was observed. The range of the melting points fluctuates between 42ºC (terbinafine) and 301ºC (imiquimod).

Additionally, a vast range of lipophilicities was obtained. The lower distribution coefficients are the ones for eflornithine, indicating the most hydrophilic compound, whereas the maximum values for the distribution coefficients are for bexarotene and tacrolimus, as the most hydrophobic compounds.

Mathematical models that consider different physico-chemical properties are able to predict the skin permeability constant ($\log K_p$). Values of the different properties of the chosen topical actives were obtained. Then, the three selected models (Potts and Guy, Mitragotri and Barratt) were applied, and three permeability constants per active were obtained (Table VI). It should be kept in mind that the skin surface pH is approximately 5.5; for this reason, the $\log D$ at this pH was employed in the three models.

The mathematical equations of the three models are quite similar, especially between the Mitragotri and the Potts and Guy models. The first terms of the three equations have a linear relationship between them. The lipophilicity is multiplied for a factor from 0.7-0.82 in all equations. The second terms of the three equations refer to the "molecular size" effect represented as the molecular weight (Mitragotri and Potts and Guy) or the molecular volume (Barratt). Even though their values are different, the second terms for the three models have a strong linear correlation in our subset of actives. However, the Barratt equation includes the melting point value, which is responsible for the main differences between models.

Table VI *in silico* Log K_p (cm/s) predictions using Mitragotri (Mi), Potts and Guy (P-G) and Barratt (Bar) models applying $\log D$ at pH 5.5. *In vitro* log P_e values using Skin-PAMPA in buffer (pH 5.5) and in PG.

	in silico QSPR models		
	Log K_p (cm/s) Mi	Log K_p (cm/s) P-G	Log K_p (cm/s) Bar
Azelaci acid (Aze)	-7.74	-7.56	-8.31
Betamethasone dipropionate (Bet)	-7.05	-6.56	-10.23
Bexarotene (Bex)	-4.98	-4.52	-9.47
Calcipotriol monohydrate (Cal)	-6.56	-6.09	-7.13
Clindamycin phosphate (Cli)	-10.03	-9.60	-10.67
Clobetasol propionate (Clo)	-6.67	-6.18	-10.11
Dapsone (Dap)	-7.22	-6.91	-9.74
Diclofenac sodium (Dic)	-6.54	-6.16	-12.85
Diphenidramine (Dip)	-7.79	-7.49	-10.69
Eflornithine (Efl)	-10.83	-10.72	-16.90
Finasteride (Fin)	-6.84	-6.39	-12.93
Fluorouracil (Fo)	-7.57	-7.56	-14.82
Flurandrenolide (Fra)	-8.31	-7.85	-12.79
Glycopirrolate (Gly)	-9.60	-9.24	-13.64
Imiquimod (Imi)	-6.36	-6.06	-14.02
Ketoconazole (Ket)	-7.43	-6.95	-9.04
Lidocaine (Lid)	-7.57	-7.30	-6.53
Nicotine (Nic)	-8.77	-8.68	-8.86
Salicylic acid (Sal)	-7.65	-7.62	-10.14
Tacrolimus (Tac)	-7.58	-7.23	-9.26
Tazarotene (Taz)	-5.19	-4.74	-4.85
Terbinafine (Ter)	-6.78	-6.40	-4.58
Tofacitinib (Tof)	-8.75	-8.38	-9.35

In general, lower Kp values were obtained in the Barratt model, whereas the Potts and Guy and Mitragotri models present very similar values. Log Kp values obtained with the different models of the different compounds are represented in Figure 15.

A linear relationship occurs between the Potts and Guy and Mitragotri models, as expected (r^2=0.99). Both models have the same underlying assumption that the

tortuous lipid matrix is the pathway for transdermal permeation and predict skin permeability from the lipophilicity and the molecular weight. Even though the relationship between the Barratt values and the Potts and Guy values has a slope close to 1, the values are very dispersed, obtaining a regression factor of only 0.213. Much higher permeability was obtained for lidocaine and terbinafine with low melting points and lower permeability for diclofenac, eflornithine, finasteride, fluorouracil, flurandrenolide and imiquimod, all with melting points higher than 240ºC. On the other hand, all the models predicted the highest permeability for tazarotene and the poorest permeability for eflornithine. Their degrees of permeability are mainly due to their lipophilic properties.

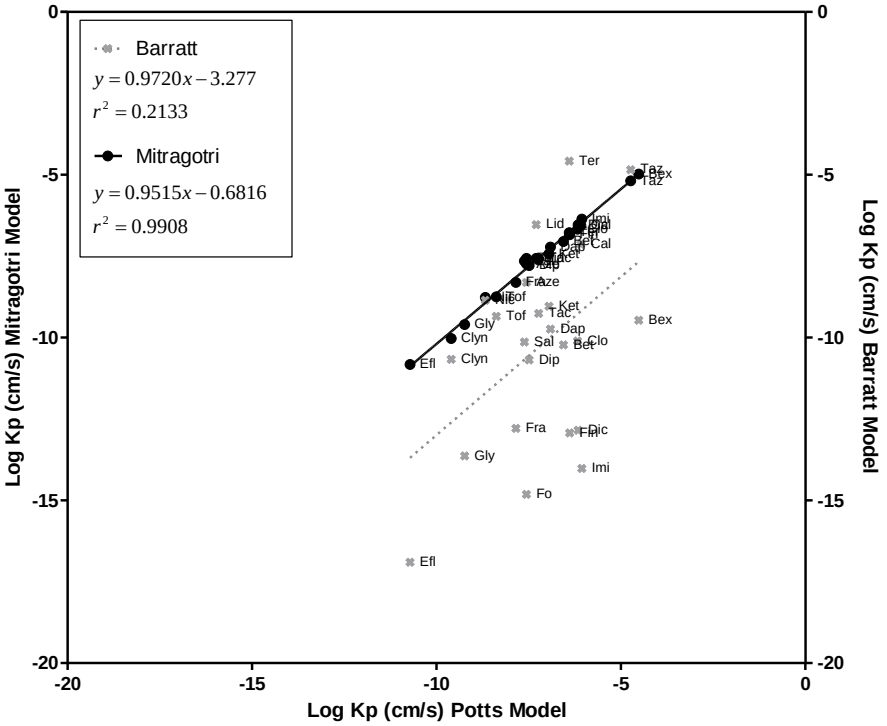

Figure 15 Linear correlation of LogKp obtained with Potts and Guy against Mitragotri's (black dots and solid line) and Barratt's (gray cross and discontinuous line) permeability constants.

5.1.2. *In vitro* skin permeability models

Two *in vitro* skin permeability models have been applied in the present work using synthetic membranes (skin-PAMPA, detailed in section 4.2) or pig excised skin (section 3.1) mounted in Franz cells (detailed in section 4.3)

5.1.2.1. Permeabilities of topical actives studied with skin-PAMPA

The actives selected with the QSPR models (Table V) were also studied with the skin-PAMPA methodologies. Actives were all formulated in propylene glycol and in a buffer solution at pH 5.5 (section 4.2). Permeation assay was performed following the amounts in each compartment were obtained with UPLC-MS/MS (section 4.6.2), the P_e was calculated following the procedure detailed by Ottaviani et al. [60].

The P_e gives us information about the intrinsic facility of each compound for diffusing across the PAMPA membrane. The results in both experiments (PG and buffer 5.5) are compiled in n Table VII.

Table VII Skin-PAMPA log P_e values (cm/s) for buffer and PG

	Skin-PAMPA (Buffer pH5.5) log P_e (cm/s)	Skin-PAMPA (PG) log P_e (cm/s)
Azelaci acid (Aze)	-7.28	-6.7
Betamethasone dipropionate (Bet)	-5.98	-7.7
Bexarotene (Bex)	-5.4	-7.7
Calcipotriol monohydrate (Cal)	-5.6	-8.8
Clindamycin phosphate (Cli)	-9.07	-7.6
Clobetasol propionate (Clo)	-5.64	-7.6
Dapsone (Dap)	-6.5	-8.9
Diclofenac sodium (Dic)	-4.39	-7.3
Diphenidramine (Dip)	-8.07	-7.2
Eflornithine (Efl)	-7.09	-6.9
Finasteride (Fin)	-6.17	-7.3
Fluorouracil (Fo)	-6.73	-5.2
Flurandrenolide (Fra)	-6.2	-7.4
Glycopirrolate (Gly)	-9.29	-8.2
Imiquimod (Imi)	-9.34	-8.1
Ketoconazole (Ket)	-6.24	-9.3
Lidocaine (Lid)	-6.07	-6.3
Nicotine (Nic)	-7.02	-7.5
Salicylic acid (Sal)	-6.5	-7.2
Tacrolimus (Tac)	-9.71	-8.9
Tazarotene (Taz)	-8.63	-9.3
Terbinafine (Ter)	-6.93	-9.1
Tofacitinib (Tof)	-7.3	-7.4

The results showed the high influence of the vehicle on the distribution across the PAMPA membrane. In Figure 16, the different actives are labelled considering their log P_e: high permeability in green (log P_e <-6), medium permeability in yellow (log P_e between -6 and -8) and low permeability in red (log P_e >-8). When the buffer at pH 5.5 was employed, our set of actives showed a high rank of permeability constants (-10 to -5) (solid pattern in Figure 16). In contrast, when the substances were vehiculazed in propylene glycol, the permeability constants ranged from -9 to -7 (dotted pattern in Figure 16). The substances with a high permeability in the buffer solution reduced their

permeability when the propylene glycol was employed, whereas the opposite effect was observed in the actives with lower permeability constants in the buffer. This effect could be due to the influence of the propylene glycol by diminishing the barrier properties of the membrane which may modulate the active permeabilities. The influence of propylene glycol on the skin structure will be studied in depth on section 5.1.5.

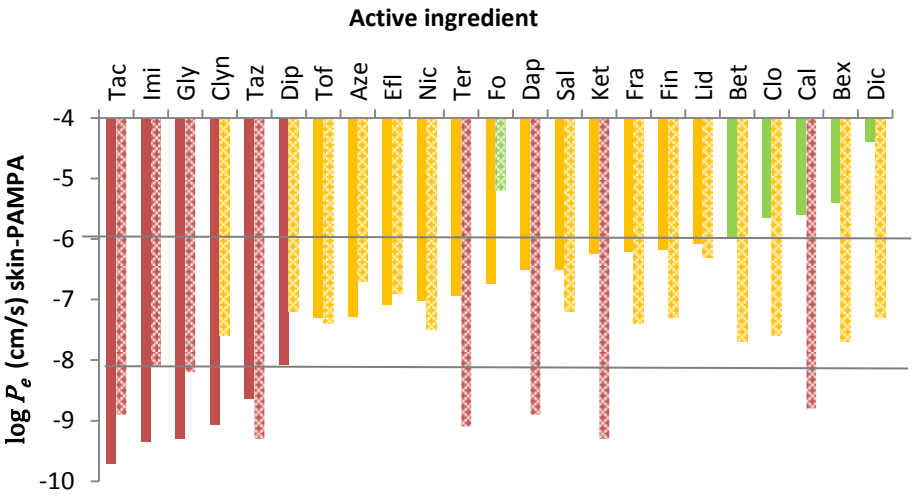

Figure 16 Skin-PAMPA log P_e (cm/s) values in buffer solution at pH 5.5 (solid pattern) and in propylene glycol solution (dotted pattern). Actives are classified in high (green), medium (yellow) and low (red) permeability and ordered from lowest to highest log P_e in buffer.

5.1.2.2. Permeability and skin absorption of topical actives by Franz diffusion cells

Then, another *in vitro* assay was performed to study the prediction helpfulness of the *in silico* models. Franz diffusion cell (section 1.2.2.1) with dermatomed porcine skin was employed following the corresponding method described in section 4.3 for percutaneous absorption determination.

The use of Franz diffusion cells makes possible to determine the actual amount of drug that diffuses across the skin. The distribution in the various skin compartments and in the receptor fluid, mimicking the systemic compartment of the selected compounds was determined by UPLC-MS/MS (section 4.6.2). Moreover, the effect of the commercial vehicle comparing the penetration profiles in propylene glycol versus the respective commercial cream will be discussed.

Therefore, this *in vitro* system has been used to compare the skin penetration profiles of each compound in different formulations, PG solutions, and some of their corresponding commercial creams (Table VIII).

Table VIII Formulations, concentration, manufacturer and abbreviation used in the Franz cell assays.

	Formulation	Concentration	Formulation manufacturer	Abreviation
Bet	Betamethasone dipropionate PG Sol.	0.5 mg/g	Self-prepared	Bet-PG
	Diproderm® cream	0.5 mg/g	MSD	Bet-cre
Clo	Clobetasol PG Sol.	0.5 mg/g	Self-prepared	Clo-PG
	Clovate® cream	0.5 mg/g	IFC	Clo-cre
Fo	Fluorouracil PG Sol.	50 mg/g	Self-prepared	Fo-PG
	Efudix® cream	50 mg/g	Meda Pharmaceuticals Ltd.	Fo-cre
Fra	Flurandrenolide PG Sol.	0.5 mg/g	Self-prepared	Fra-PG
Gly	Glycopirrolate PG Sol.	5 mg/g	Self-prepared	Gly-PG
Ket	Ketoconazole PG Sol.	20 mg/g	Self-prepared	Ket-PG
	Fungarest® crema	20 mg/g	Janssen, Belgium	Ket-cre
Lid	Lidocaine PG Sol.	20 mg/g	Self-prepared	Lid-PG
	Dermovagisil® cream	20 mg/g	Laleham health, UK	Lid-cre
Tac	Tacrolimus PG Sol.	1 mg/g	Self-prepared	Tac-PG
Taz	Tazarotene PG Sol.	1 mg/g	Self-prepared	Taz-PG
Tof	Tofacitinib PG Sol.	10 mg/g	Self-prepared	Tof-PG

The retention of the actives in the skin was first evaluated from solution in a pure solvent, such as propylene glycol, with the objective to keep the formulation as simple

as possible, having in mind that PG is a solvent used in many topic formulations, and that it is able to solubilize most compounds. Moreover, to avoid permeability differences caused by concentration, the propylene glycol solutions were formulated at the same concentration as the corresponding commercial formulation for most of the employed actives. This, however, implies in some cases that different amounts of different actives were applied; moreover, the important drag effect caused by the active saturation degree in each formulation was not considered. It is also important to remark that the receptor fluid was chosen to be the same for all actives (section 4.3) even though the great differences in lipophillicity for all actives. Despite the addition of bovine serum albumin, the capacity of the receptor fluid to solve lipophillic compounds may play an important role to explain permeability differences between the tested actives.

The resulting recovery was acceptable (100±25%) for all the tested formulas. The compounds were recovered from the skin surface (W), Stratum Corneum (SC), epidermis (E), dermis (D) and receptor fluid (RF)(Table IX). The concentrations retained by the SC were not absorbed by the skin and did not contribute to the systemic dose. However, the concentrations found in the epidermis and dermis could be absorbed and reach the systemic level[46]. Therefore, the amount of percutaneous absorption (ABS) is normally assumed to be the sum of the concentrations in the epidermis, dermis and receptor fluid. Moreover for many of the selected actives their receptors are located in the epidermis and the dermis tissue (E+D), so the amounts founded in such layers are important to know. The amounts of actives in every layer are represented in Table IX and Figure 17 for the actives formulated in propylene glycol (PG) and in Table X and Figure 18 for the commercial creams. To better compare the different formulations, the absorbed amounts are compiled in Table XI.

Table IX Distribution of compounds in pig skin expressed as % of substance for each sample: surface excess (W), Stratum Corneum (SC), epidermis (E), dermis (D) receptor fluid (RF), percutaneous absorption (ABS).

	Conc. (mg/g)	W (%)	SC (%)	E (%)	D (%)	RF (%)	D+E (%)	ABS (%)
Bet- PG	0.5	88.36±3.90	5.24±1.87	3.87±1.34	0.56±0.43	1.96±1.38	**4.43**	**6.39**
Clo-PG	0.5	88.12±1.75	5.00±2.75	3.79±1.60	2.39±1.81	0.71±0.41	**6.18**	**6.89**
Fo-PG	50	83.73±3.08	10.41±2.81	4.22±1.82	0.78±0.47	0.86±0.75	**5.00**	**5.86**
Ket-PG	20	91.66±2.15	3.25±1.74	3.32±1.23	0.63±0.39	0.50±0.13	**3.95**	**4.45**
Lid-PG	20	32.36±10.79	4.28±1.04	1.01±0.57	2.32±0.45	60.02±10.64	**3.33**	**63.35**
Fra-PG	0.5	89.99±4.06	4.25±2.14	1.94±0.61	1.33±1.85	1.64±2.31	**3.27**	**4.91**
Gly-PG	5	77.12±3.59	7.51±3.79	7.27±2.12	2.04±2.12	4.56±2.45	**9.31**	**13.87**
Tac- PG	1	77.51±5.51	13.40±1.57	6.37±1.56	1.76±0.56	0.96±0.40	**8.13**	**9.09**
Taz-PG	1	94.85±1.20	2.48±0.84	1.37±0.86	0.99±0.59	0.31±0.12	**2.36**	**2.67**
Tof-PG	10	71.00±6.00	19.2±4.3	7.2±2.8	2.1±0.81	0.25±0.32	**9.3**	**9.55**

Percutaneous absorption of the 10 evaluated actives in PG shows a similar behavior, the active is distributed following the order W>SC>E>D. To sum up our data from the PG solutions, a relation between a high retention in W and less permeation was found for most of the actives. The compounds were found to have a reduced distribution when going in depth through the skin.

As it can be seen, Taz is highly found in the W and partially retained in the SC; therefore, it is the lowest absorbed compound (Table XI). Although the absorption behavior of Taz differs from the skin permeation predicted by its physical-chemical properties, others authors demonstrated its limitation of percutaneous absorption when Taz was topically applied [99].

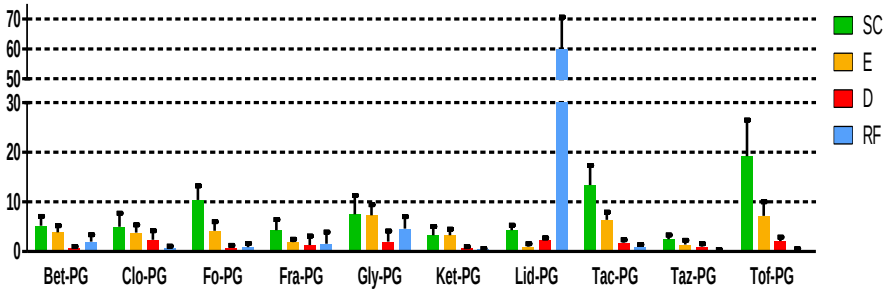

Figure 17 Cumulative amounts (%) found in the Stratum Corneum (SC), epidermis (E), dermis (D) and receptor fluid (RF).

Bet, Clo, Fo, Ket and Fra are compounds with medium permeabilities (from 4.45% to 6.89%) when they are formulated in PG. The results also show that low amounts of substance are found in the W for Gly, Tac and Tof, but at the same time, they show high retention in the SC. These three substances are also more retained in the subsequent skin layer (E) than the rest of the compounds. As a consequence, Gly, Tac and Tof have high percutaneous absorption (Table X).

Surprisingly, Lid presents a different profile. The compound is scarcely retained in the W and SC, but that it is mainly detected in the receptor fluid (60%). Moreover, when the E and D layers are observed, more lidocaine is found in D than in E, whereas in all the other PG solutions, the amounts obtained in E are always higher than those in D. Lidocaine is a basic molecule with a hydrophilic value at pH 5.5 but this changes to lipophilic at pH 7 due to its pKa[100]. The pH gradient at the SC depth and the change of hydrophilic to lipophilic property of Lid may influence its high diffusion.

Commercial creams of 5 of these actives were also evaluated with the Franz cell assay. In general, most of the other creams maintain the compound distribution explained before for PG solutions (W>SC>E>D) (Figure 18). The obtained order of the percutaneous absorption was Li>Clo>Ket ≅ Bet>Fo (Table XI).

Table X Distribution of compounds in pig skin expressed as % of substance for each sample: surface excess (W), Stratum Corneum (SC), epidermis (E), dermis (D) receptor fluid (RF), percutaneous absorption (ABS)

	Conc. (mg/g)	W (%)	SC (%)	E (%)	D (%)	RF (%)	D+E (%)	ABS (%)
Bet- cre	**0.5**	97.32±0.75	1.35±0.76	0.85±0.28	0.35±0.22	0.14±0.12	**1.2**	**1.34**
Clo-cre	**0.5**	95.91±4.62	0.99±1.64	0.86±0.91	1.17±1.78	0.07±0.02	**2.03**	**2.1**
Fo-cre	**50**	97.09±0.13	1.42±1.11	0.61±0.21	0.13±0.06	0.04±0.03	**0.74**	**0.78**
Ket-cre	**20**	94.89±2.26	2.33±2.56	0.62±0.28	0.17±0.06	0.83±0.18	**0.79**	**1.62**
Lid-cre	**20**	90.55±3.83	3.10±0.38	0.29±0.11	0.66±0.24	5.40±3.67	**0.95**	**6.35**

Lidocaine showed a similar distribution when it was applied as a cream. As previously detailed, Lid-PG was mainly found in the RF, and in contrast to the other formulations, the amounts in D are greater than those in E. Such a situation is also repeated in Lid-cre; high absorption and dermis accumulation of the compound was detected. However, it should be noted that the great diminution of penetration of lidocaine in all skin strata is due to an important percutaneous absorption of 6.3%; that is, however, ten times lower than the same active in PG.

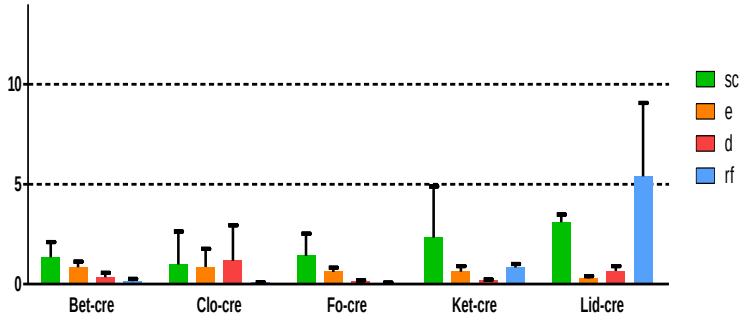

Figure 18 Cumulative amounts (%) found in the Stratum Corneum (SC), epidermis (E), dermis (D) and receptor fluid (RF).

The vehicle effect on the compound skin distribution can be compared, considering that the PG solutions are formulated at the same concentration as the commercial formulations. A common feature for the PG solutions is that in every skin layer (SC, E and D), the different actives are much more retained than in creams. This leads to the higher absorption observed for PG solutions than creams since the absorbed averages are the sum of E, D and RF (Table XI).

Table XI Absorbed amounts (%) calculated from the sum of epidermis, dermis and receptor fluid normalized amounts.

Active (concentration)	PG solutions	Creams
Betamethasone dipropionate (0.5 mg/g)	6.39	1.34
Clobetasol propionate (0.5 mg/g)	6.89	2.1
Fluorouracil (50 mg/g)	5.86	0.78
Ketoconazole (20 mg/g)	4.45	1.62
Lidocaine (20 mg/g)	63.35	6.35
Flurandrenolida (0.5 mg/g)	4.91	-
Glycopyrrolate (5 mg/g)	13.87	-
Tacrolimus (1 mg/g)	9.09	-
Tazarotene (1 mg/g)	2.67	-
Tofacitinib (10 mg/g)	9.55	-

Summarizing the effect of the vehicles studied , it can be concluded that PG solutions show, in general, the highest amounts in all the different layers of the skin (SC, E, D), and that the observed compound distribution (W>SC>E>D) is generally maintained in PG and cream formulations. The observed enhancer effect of PG in the skin has been widely described [101]. In this thesis an additional study based on the effect of PG on the skin lipids by IR has been performed (section 5.1.5). It must be noted that our study does not consider the effect of the compound saturation degree in its formulation and that the steady state of the system cannot be assumed after 24 h of exposition in all the formulations.

5.1.3. Correlations between models

In silico *vs skin-PAMPA*

One of the objectives of this work was to study the relationship between the different predictive assays of topical exposure. Log Pe by skin-PAMPA of all compounds at pH 5.5 and in PG were related to the Log Kp obtained with the three models applying $\log D$ at pH 5.5. Linear correlations between the two Pampa lists of values and the three *in silico* models were very low. The best correlation was found between Potts and Guy and Mitragotri models with skin-PAMPA values at pH 5.5 with slopes of approximately 0.4 and correlation coefficients of approximately 0.1 (Figure 19). Therefore, a very poor linear correlation was found between this *in vitro* model with the three *in silico* models for the actives studied.

Most of the studies carried out to obtain the *in vitro* models present a $\log K_p$ deducted from more than 50 actives, and the linear regression is obtained from bulk data in

which the individual actives do not always match[102]. In the present work, only 23 actives were studied, and in Figure 19, it is clear that several compounds give different results using the *in silico* methodology rather than the skin-PAMPA. In particular, compounds with marked hydrophobic character, such as bexarotene, imiquimod, tacrolimus, and specially, tazarotene, present a lower permeation than the one expected by the *in silico* models. In contrast, eflornithine, the most hydrophilic compound assayed, presents higher permeation than expected by the models.

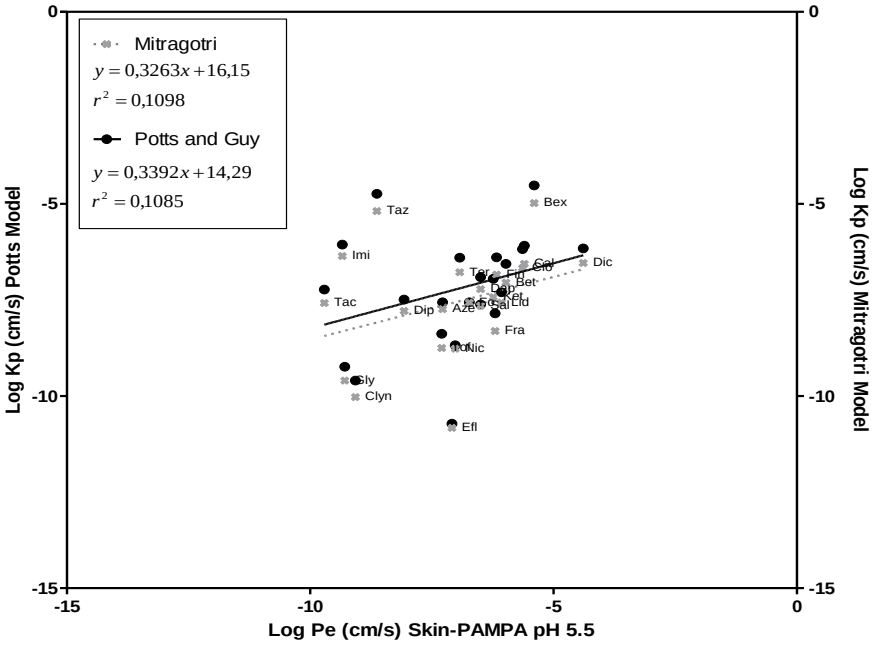

Figure 19 Linear correlation of log Pe (cm/s) from the skin-PAMPA assay at pH 5.5 against $\log K_p$ (cm/s) obtained by the Potts and Guy and Mitragotri model.

Skin-PAMPA vs Franz diffusion cells

The Franz data were also correlated with the ones obtained by skin-PAMPA. It is important to have in mind that results obtained for the Franz cells account only for 10 actives when formulated in PG and 5 actives in creams. When the Franz cell data are compared against the skin-PAMPA also low correlations are obtained in our set of actives. However, the permeability constant from the PAMPA assay at pH 5.5 was better compared with the percutaneous absorption obtained with Franz cell assays of the actives in creams (Figure 20). Even though a low correlation coefficient is observed when related to percutaneous absorption, it increases when correlated with E+D amount. Lid shows a high absorption due to its high amounts found in the RF.

Therefore, when the log Pe skin-PAMPA pH 5.5 is compared with E+D without RF, the correlation factor increases.

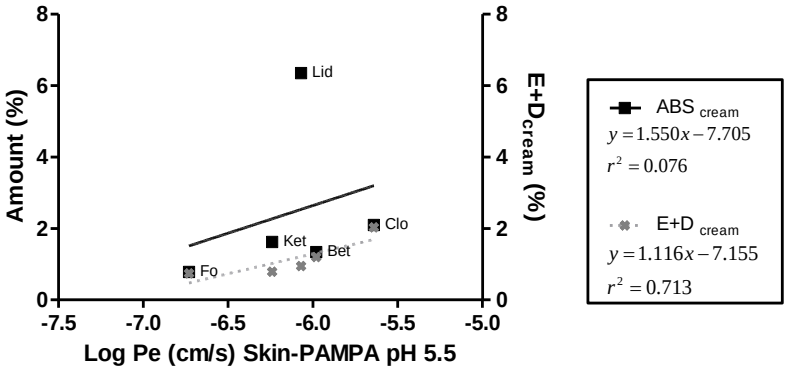

Figure 20 Linear correlation of log P_e (cm/s) from the skin-PAMPA assay at pH 5.5 against log K_p (cm/s) obtained by the Potts and Guy and Mitragotri model.

The results obtained in this work underline the role of the formulation in skin penetration and retention of compounds. It was found that skin uptake of a drug is strictly related to solvent uptake, suggesting the relevance of the solvent drag effect in skin delivery for the tested actives. Then, the effect of vehicles on skin penetration has been studied in more detail in the next section 5.1.4.

Sumarizing sections 5.1.1, 5.1.2 and 5.1.3. A comparative study of percutaneous absorption with Franz diffusion cells with propylene glycol solutions and some of their commercial creams was presented. Higher absorption rates were observed in the propylene glycol solutions compared with the cream formulas, due to the widely reported enhancer effect of propylene glycol. The fundamental effect of the vehicle in the permeability of topical actives is apparent.

The results of the skin-PAMPA assay at pH 5.5 and the amount of the compound in the epidermis and dermis of the Franz cell data of the cream formulations were better correlated. This correlation indicates the effectiveness of the two *in vitro* assays at assessing the formulation and the detrimental effect of PG on the skin or on the membrane with lipids from skin. Mathematical models and *in vitro* models are good prediction methodologies to determine permeation for some but not all topical actives. Franz cell diffusion permeation is important not only to determine total permeation but also to settle the amounts of actives in each skin layer, which is fundamental for topical skin treatments.

A research paper entitled "Comparative study between in silico and in vitro models for predicting the permeability of topical actives" based on the results of sections 5.1.1, 5.1.2 and 5.1.3 is at the moment under preparation

5.1.4. Effect of vehicle on skin penetration

Glucocorticoids (GCs) are actives widely used in the treatment of skin diseases. The efficacies of topical GCs are linked to their availability to reach their receptors. The affinity between the receptor and the steroid as well as its cellular uptake and residence time, determines the clinical effect[103–105]. All these processes are highly influenced by the physicochemical properties of the drug as well as the vehicle[65,106–109]. Moreover steroids potency can also differ depending on the vehicle in which they are formulated. Hence, to modulate their effects they are available in a wide range of preparations including gels, creams, ointments, foams, lotions, oils and sprays[110].

The aim of this section is to study the relationship between the skin absorption, the substance lipophilicity and the effect of the vehicle of glucocorticoids. Therefore, a study is presented using the static diffusion cells of betamethasone dipropionate (Bet), clobetasol propionate (Clo) and flurandrenolide (Fra). Three different vehicles are assayed including commercial creams, their respective ointments and propylene glycol solutions (Table XII). The three compounds are all formulated at the same concentration as in their commercial formulations.

Table XII Formulations, concentration, manufacturer and abbreviation used in the Franz cells assay

	Formulation	Conc. (mg/g)	Formulation manufacturer	Abreviation
Bet	Betamethasone dipropionate PG Sol.	0.5	Self-prepared	Bet-PG
	Diproderm® cream	0.5	MSD	Bet-cre
	Diproderm® ointment	0.5	MSD	Bet-oin
Clo	Clobetasol PG Sol.	0.5	Self-prepared	Clo-PG
	Clovate® cream	0.5	IFC	Clo-cre
	Declobán® ointment	0.5	Teofarma	Clo-oin
Fra	Flurandrenolide PG	0.5	Self-prepared	Fra-PG
	Cordran® SP Cream	0.5	Oclassen Pharmaceuticals Inc	Fra-cre
	Cordran® SP ointment	0.5	Oclassen Pharmaceuticals Inc	Fra-oin

It should be noted that although each formulation has the same concentration of the active ingredient, each formulation will have a different degree of saturation in each vehicle, which highly influences the absorption of substances through the skin[111].

One of the important parameters that influences the high affinity of a GC for its receptor (and therefore its glucocorticoid effect) is the lipophilicity of the molecule which are compiled in Table V for the three actives. Fra is the least potent of the selected drugs, which is in accordance with its low $\log D$ value. In the cases of Bet and Clo, it has to be considered that betamethasone dipropionate is a prodrug of the free form, betamethasone. After topical administration, the drug is hydrolysed by esterase enzymes primarily in the skin. Then, after the hydrolysis of the molecule, the lipophilicity and $\log D$ values are much lower. Therefore, the most potent substance (Clo) has the highest $\log D$ value.

Besides the affinity of a substance for its receptor, the efficacy of a topically applied substance is linked to its availability to contact the target/receptor. Glucocorticoid receptors are known to be located in epidermal and dermal cells[103,112]. Therefore, in Table XIII, in addition to the compound distribution in the different layers, the amount of compound in E+D and the percutaneous absorption (E+D+RF) are also described.

In general, the three compounds in all of the formulations have a common penetration profile, in which the amount of substance found in each layer decreased when increasing in depth (SC>E>D). Only Clo-oin and Clo-cre have similar amounts in all three skin strata. The amount found in the receptor fluid is clearly dependent not only on the substance but also on the vehicle.

Table XIII Distribution of compounds in pig skin expressed in µg and % for each sample: surface excess (W), Stratum Corneum (SC), epidermis (E), dermis (D), receptor fluid (RF), and the total amount in µg

		W (%)	SC (%)	E (%)	D (%)	RF (%)	D+E (%)	ABS (%)
Bet	**Bet- PG**	88.85 ± 3.90	5.21 ± 1.87	3.78 ± 1.34	0.48 ± 0.43	1.75 ± 1.38	**4.26**	**6.01**
	Bet-cre	97.30 ± 0.75	1.43 ± 0.76	0.87 ± 0.28	0.33 ± 0.22	0.13 ± 0.12	**1.2**	**1.33**
	Bet-oin	96.32 ± 0.70	2.06 ± 0.32	0.95 ± 0.39	0.49 ± 0.12	0.18 ± 0.13	**1.43**	**1.61**
Clo	**Clo-PG**	88.12 ± 1.75	4.94 ± 2.75	3.84 ± 1.60	2.39 ± 1.81	0.71 ± 0.41	**6.21**	**6.91**
	Clo-cre	95.91 ± 4.62	0.99 ± 1.64	0.86 ± 0.91	1.17 ± 1.78	0.07 ± 0.02	**2.03**	**2.1**
	Clo-oin	89.72 ± 3.40	2.53 ± 3.10	2.12 ± 0.91	2.65 ± 1.53	3.03 ± 2.08	**4.77**	**7.8**
Fra	**Fra-PG**	89.99 ± 4.06	4.25 ± 2.14	1.94 ± 0.61	1.33 ± 1.85	1.64 ± 2.31	**3.27**	**4.91**
	Fra-cre	90.98 ± 0.40	1.77 ± 0.02	0.77 ± 0.02	0.69 ± 0.02	5.79 ± 0.22	**1.46**	**7.25**
	Fra-oin	93.08 ± 3.06	1.69 ± 2.16	1.45 ± 0.84	0.80 ± 0.65	1.28 ± 0.17	**2.25**	**3.53**

*ABS is the absorbed amount and represents the sum of E+D+RF

For Bet, when it is applied in PG solution, the amount found in the receptor fluid is quite significant, whereas in the cream and ointment, the amount decreases. This is probably due to the enhancement effect of PG. Therefore, higher amounts of both E+D and E+D+RF for Bet are obtained for the PG formulation.

Clo has a similar lipophilicity to that of Bet but a lower MW, and it is the most retained compound in the E and D as well as in the E+D+RF in all of the employed formulations. This higher accumulation of the substance agrees with the higher potency of Clo compared to Fra and Bet. The glucocorticoid receptors are located in the E and D, and hence, high amounts of Clo in both tissues can lead to a higher efficacy of this corticoid.

Fra is the most hydrophilic compound and showed less affinity for the E and D. For example, the three formulations of Fra show higher amounts of the substance in the RF than in the upper layer, the D. This is clearly more marked for Fra-cre. This special behaviour is consistent in the three formulations and can be explained by the presence of the acetonide group in the D ring, which enhances the penetrability and the percutaneous absorption of this type of corticoid[113]. In summary, in Clo, Bet and Fra, the retention in the tissue (E+D) is always greater when PG is employed. Fra-cre contains a high amount of analyte in the RF, which leads to high absorption (E+D+RF) with higher systemic exposure.

Therefore, comparing the drug penetration profiles and their physico-chemical properties, it can be concluded that the more hydrophobic compounds (Clo and Bet)

are present in higher amounts in the E+D, while the hydrophilic compound (Fra) is mostly present in the receptor fluid, which leads to higher percutaneous absorption.

Additionally, it is important to note the effect of the vehicle. The main components of the commercial formulations are water, cetostearyl alcohol and other oily components for creams[114–116]and paraffin along with waxes without any water content for ointments[117]. Besides, it is important to note that Clo-cre, Clo-oin and Fra-cre also contain PG.

The three compounds showed great differences when they were applied in the different formulations, proving that the vehicle is critical in regards to percutaneous absorption (Figure 21). Higher amounts of the substance are obtained in the epidermis and dermis when ointments are employed compared to creams. This is consistent with the general rule that the highest glucocorticoid efficacy is fulfilled with ointments compared to creams[118]. This fact is also related to the absence of water content and the presence of the waxes and petrolatum of ointments, which is believed to enhance the penetration of the substance due to the occlusive effect[119]. In view that oily formulations enhance the GC effect/penetration, ointments are mostly used in cases of severe dermal diseases and/or on areas with a large SC (such as the palms of the hands or soles of the feet).

On the other hand the enhancement effect of propylene glycol can be discerned. For the three PG solutions, the distribution patterns are similar. The SC retains the highest amount of substance (about 5%); moreover, the amounts found in the E were also higher than with the other vehicles. This is not so clear for the amount in the dermis. It could be noted that the PG solutions show the highest amounts of corticoid in the E+D when compared with creams and ointments, mainly due to the important amount in the E. However, the influence that the degree of saturation may induce in the percutaneous absorption of the different vehicles, which has not been considered in this work, should be investigated.

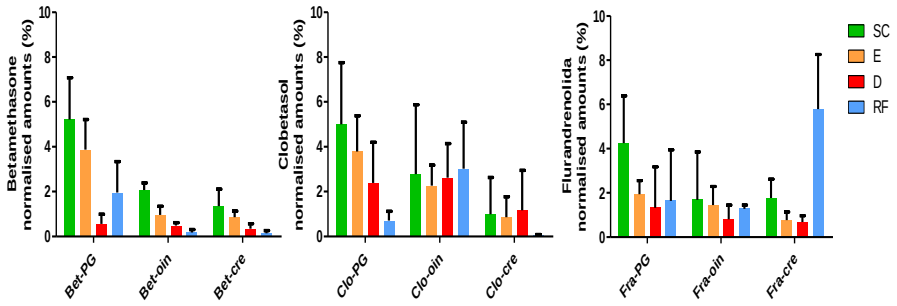

Figure 21 Normalized amounts of betamethasone (Bet), clobetasol (Clo), flurandrenolide (Fra) applied in different formulations: propylene glycol solutions (PG), ointments (oin) and creams (cre).

Results obtained in sections 5.1.2, 5.1.3 and 5.1.4 indicated the effect of PG acting as an enhancer of skin permeation. In the next section the effect of propylene glycol on skin modification is studied by ATR-IR to understand this fact.

Summarizing, the influence of PG on the maximum amounts of the analyte in the SC and E and similar amounts of the analyte in the D for PG and ointments, with level being much lower for creams, should be pointed out. The penetration enhancement for Clo-oin and for Fra-cre in the receptor fluid is also observed. This could be due to the presence of PG in these vehicles.

Since the aim of these glucocorticoids is to act at the E and D, this study confirms the higher corticoid efficacy of Clo due to its higher presence in these skin layers. Additionally, propylene glycol and the ointments applied induced a higher penetration into these layers than the corresponding creams.

The results compiled in section 5.1.4 are part of a work published in "Drug Testing and Analysis" entitled "In vitro penetration through the skin layers of topically applied glucocorticoids" (Annex 1)

5.1.5. µFTIR study of skin propylene glycol disrruption.

Propylene glycol (PG) has been used as a common solvent for many drugs in this thesis. PG acts changing the solubility of the compound in the formulation, but it may also act as a fluidizer of the intercellular lipid matrix, acting as skin enhancer.

Non treated skin and skin treated with PG with synchrotron-Based Fourier Transform Infrared microspectroscopy (µFTIR)(section 4.8.2) with the aim to study the skin alterations when submitted to propylene glycol. Non dermatomed porcine skin was cross sectioned and analysed with µFTIR after PG exposure as detailed in section 4.8.2.

Skin spectrum is displayed in Figure 22. The two strong absorption bands at around 1650 cm^{-1} (amide I) and 1550 cm^{-1} (amide II) are typical protein bands which arise mainly from C-O stretching and N–H bending vibrations, respectively, of amide groups of the peptide backbone in proteins[120]. The absorption bands from 3000 to 2800 cm^{-1} are due to the C–H stretching motions of the alkyl groups present in both proteins and lipids. The signal linked to proteins is a broad band, rather weak compared to the lipids absorption which exhibits four fine peaks at around 2850 cm^{-1} (CH_2 symmetrical stretching), 2920 cm^{-1} (CH_2 asymmetrical stretching), 2870 cm^{-1} (CH_3 symmetrical stretching) and 2955 cm^{-1} (CH_3 asymmetrical stretching)[121]. A prominent band at 1745 cm^{-1} related to the C-O stretching band of phospholipids, esters and glycerides[122] has been also detected.

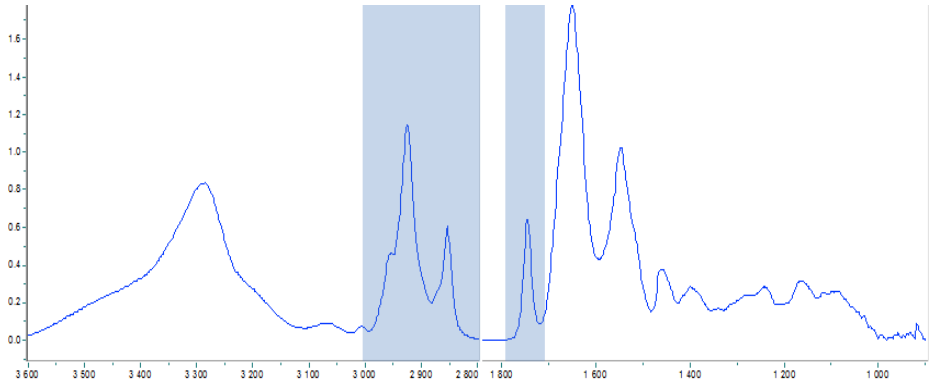

Figure 22 Baselined FTIR spectrum of skin. Lipidic region (3000-2800 cm^{-1}) and the C-O stretching band (1745 cm^{-1}) are shaded.

Study of the 2800-3000 region

The **Area under the curves** (AUCs) were calculated in the 2800-3000 cm^{-1} region in all the spectra to study how lipids are distributed in both cryosections (NT and PG). Combining the AUC values with the spatial information, the 2D images of the AUC distribution were reconstructed (Figure 23).

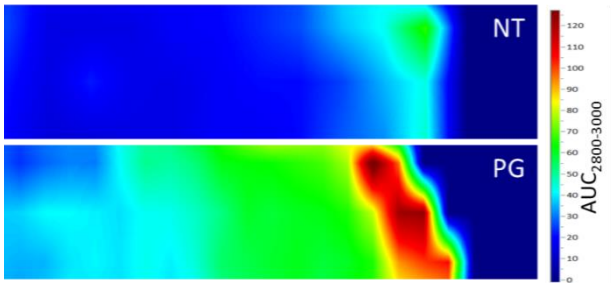

Figure 23 Spatial distibution of area under the curve between ($AUC_{2800-3000}$) in non-treated (NT) and treated with propylene glycol (PG) skin cross sections

Our data shows that for NT and PG, the AUCs are higher in the right part of the images which corresponds to the outermost part of the skin. This agrees with the described higher presence of lipids in the Stratum Corneum. Comparison of the NT images are compared against the PGs indicates that the treatment of propylene glycol in the skin increased the AUCs not only in the outermost region but also in the deeper layers.

Moreover, the position and the band width of the lipid stretching bands at 2850 and 2920 are sensitive markers of their chain conformational order (see section 1.1.1.1): the increased rotational motion of the alkyl chains during the orthorhombic–hexagonal transition and the introduction of *gauche* defects in the chains during the hexagonal–liquid transition lead to broadening of the band and its shift to higher wavenumbers. To study the position shifts within our samples different studies were performed.

The spatial information taken with this µFTIR was used to create images of the position shifts in the NT and PG samples. With this purpose in mind, the **peak fitting method** (section 1.2.4) was applied at 2850 ($\nu_S(CH_2)$) and at 2920 ($\nu_{AS}(CH_2)$) positions for all the spectral data to detect the respective position shifts.

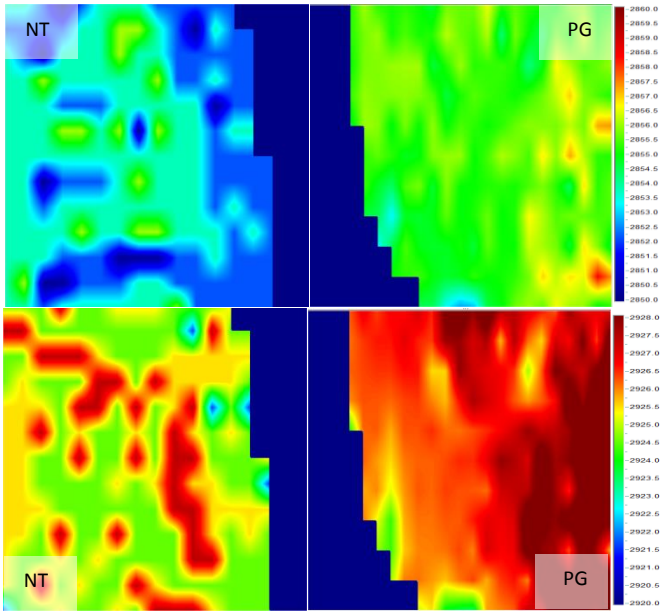

Figure 24 Upper images contain 2850 cm^{-1} position variations for blank and PG mapped areas. Lower images contain 2920 cm^{-1} position variation for blank and PG mapped areas

In Figure 24, the increasing position shift at 2850 cm^{-1} and 2920 cm^{-1} after propylene glycol treatment can be observed. The NT position values fluctuate between 2850 (predominant in the outermost region) until 2855 (in the deeper regions) which is in accordance with the increasing lipid disorder in the dermis described in other works. When PG is applied the position values are mainly at 2855 and in some regions raise upon 2858. Moreover after PG treatment no progression of lipid disorder can be so clearly observed when going in depth into the skin. Similar information can be extracted regarding the position shift at 2920 in both samples. In the Blank values between 2923 are predominant in the image and smaller regions with values of 2926 are observed. The PG treatment clearly increases the position shift to higher values, being values between 2926 and 2928 predominant in all the mapped area.

To specifically study the position shifts in the SC, E and D, the **CLS method** (section 1.2.4) was applied. Taking under consideration the microscopic image, one spectrum for each skin layer were taken as a reference spectrum and loaded for the CLS score calculations.

The obtained scores, with values from 0 to 100, indicate the similarity between each sample spectrum against the three loaded reference spectra. Plotting these scores as

an image and overlying it with the microscopic image the distribution of each skin layer can be distinguished (Figure 25).

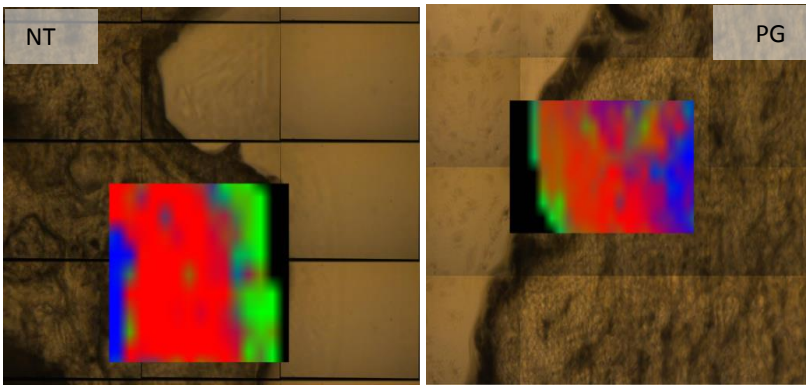

Figure 25 CLS scores ploted in green (Stratum Corneum), red (epidermis) and blue (dermis) for the non treated (NT) and propylene glycol treated (PG) samples.

In green, the Stratum Corneum is distributed in a narrow area on the outermost part of the skin. Epidermis (in red) meant a wider region under the Stratum Corneum. Finally, a small portion of the dermis was recognized in both cases (blank and PG) in the deepest region of the analyzed area. Both samples seemed to present the three layers reasonably distributed if considering the microscopic image.

Hence, in view that the reference spectra were correctly assigned, the loaded reference spectra were analyzed to see their differences and to relate them with increased lipid fluidity caused by propylene glycol.

The position shifts at 2920 and 2850 for all the 6 spectra: Stratum Corneum, epidermis and dermis for blank and PG samples; were analyzed using the peak fitting (Figure 26).

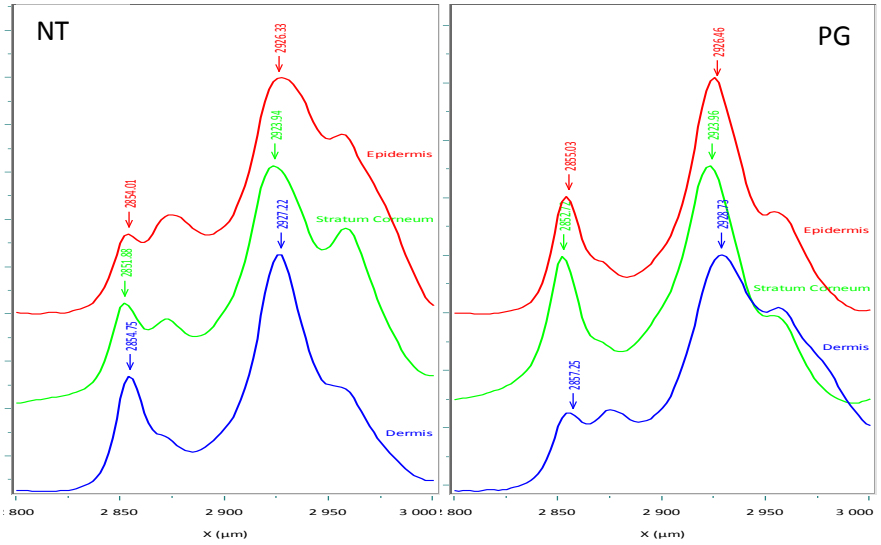

Figure 26 Classical least squares (CLS) loaded spectra of stratum corneum (green), epidermis (red) and dermis (blue) and the positions at 2850 and 2920.

The results confirmed the shifts to higher values after PG treatment. Both positions were sensitive to the PG treatment and also were different between the different skin layers. In the three skin layers, when comparing PG against Blank, positions at 2850 and 2920 increased. Moreover the increasing shifts are observed within each sample when going in depth: SC values are lower than E and D. Nevertheless, it is important to state that even that the different components were correctly assigned, to have more robustness in our results, more spectra should be studied.

Hence, the spectra of the mapped areas were manually assigned to E or D comparing with the microscopic image. After elimination of the spectra with low quality, 69 spectra were assigned to dermis treated with PG, 95 to epidermis with PG, 72 dermis non-treated and 101 to epidermis non-treated. Peak positions at 2850 and 2920 were obtained using a gaussian-lorentzian peak fitting in every spectrum. Then, averages and standard deviations of every sample were calculated and compiled in Table XIV. It is important to remark the increasing frequencies for the two bands at 2850 ($\nu_S(CH_2)$) and at 2920 ($\nu_{AS}(CH_2)$) indicating and increasing disorder of the lipids not only in the epidermis, but also more remarked in the dermis when the skin is treated with PG.

Table XIV Peak position at CH_2 symmetrical stretching ($\nu_S(CH_2)$) and CH_2 asymmetrical stretching ($\nu_{AS}(CH_2)$) and standard deviations of epidermis and dermis in treated with propylene glycol (PG) and non-treated (blank) samples.

	Epidermis		Dermis	
	$\nu_S(CH_2)$	$\nu_{AS}(CH_2)$	$\nu_S(CH_2)$	$\nu_{AS}(CH_2)$
Blank	2852.35 ±2.74	2924.44 ±2.96	2852.58 ±3.53	2924.63 ±2.33
PG	2853.31 ±2.54	2925.36 ±2.28	2854.33 ±2.13	2925.36 ±1.08

We confirmed here the results observed in Figure 26. Increasing frequencies at both positions indicate increasing disorder of lipids not only in epidermis but also in the dermis after PG treatment.

C-O stretching band at 1745 cm^{-1}

The peak analyzed at 1745 cm^{-1} corresponding to C-O stretching of lipids seemed to be predominant after the PG treatment in dermis and in epidermis. Not much information was found in this particular band and the effect that PG may cause. Therefore further analysis was performed.

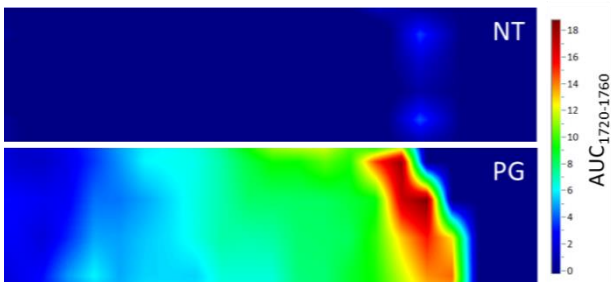

Figure 27 Spatial distibution of area under the curve between 1780-1700 ($AUC_{1780-17000}$) in non treated (NT) and treated with propylene glycol (PG) skin cross sections

The region between 1780-1700cm^{-1} was baselined and normalized (section 4.8.2). AUC for this band are calculated and plotted in Figure 27. Similar distributions than in Figure 23 were observed. As this specific band is related with the lipid content and the PG exposure, in both cases (NT and PG) the outermost region of the skin contains the highest AUC values. NT compared with PG showed that after PG treatment all the AUC values increased in all the skin depth.

This dataset was also handled by principal component analysis (PCA) for epidermis (Figure 28a) and dermis (Figure 28b). This technique is commonly used for data classification. It reduces the dimension of the data and extracts only the relevant information. The resulting principal components (PCs) represent the variance in the data set with decreasing order (PC1 means larger variance than PC2 and so on). The scores represent the original data in the new dimensional space spanned by the PCs. Hence, when plotting PC-1 against PC-2 the each spectrum is displayed as a score which carries information about the sample.

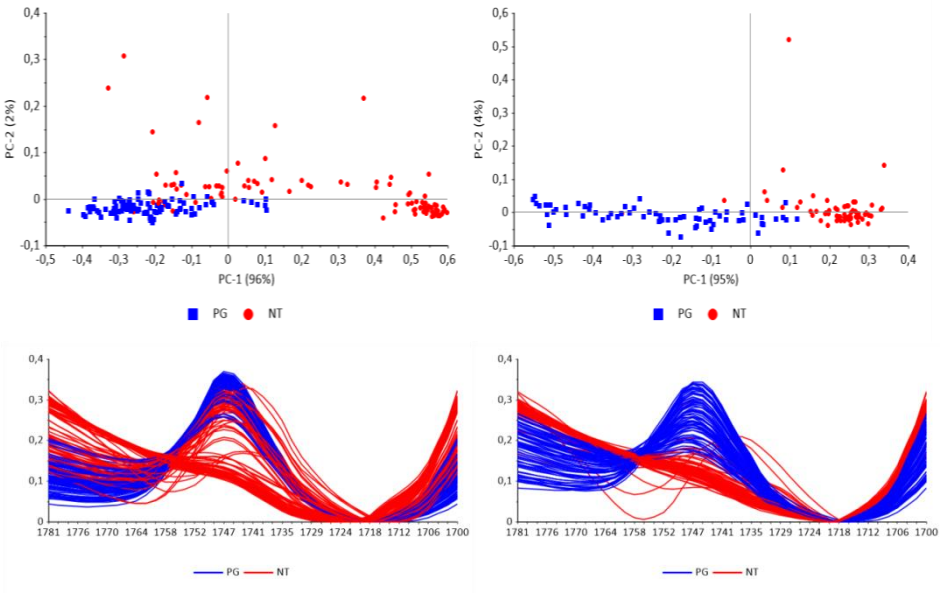

Figure 28 Principal component analysis of epidermis (a) and dermis (b) at 1745 cm^{-1}. Spectra are colored in red (non treated) and blue (PG). Upper part contains the representation of PC-1 against PC-2 of all the spectra. The spectra used for the PCA calculation are also displayed in the lower part.

In our case, the PC-1 explained more than the 95% of the variation of our data in both cases. When representing the PC-1 against the PC-2, in epidermis and dermis it could be observed that the treated (blue) and the non-treated (red) groups were clearly sorted using the PC-1. This means than in this region we can clearly distinguish differences when skin is treated with propylene glycol. This fact can be also observed when the spectra of PG and NT samples are displayed together. We could observe that the 1745cm^{-1} band was more present after propylene glycol treatment and allowed

the differentiation of most of the treated or the non-treated in the epidermis (a) and moreover in the dermis (b) spectra.

To sum up the alteration of the barrier function of propylene glycol includes affecting bilayer structure of the intercellular lipids. Based on numerous experiments[123], the action of solvents such as PG was attributed to a pure cosolvent effect. Maximizing the thermodynamic activity of a drug in the vehicle PG contributes to increased drug uptake into the skin [124]. However it is unlikely that only one mechanism is responsible for the enhancement of drug penetration, particularly for small molecules. The present study indicates not only an increase in disorder of lipid in epidermis and dermis after treatment with propylene glycol but modification of the C-O band attributed to phospholipids, glycerides and esthers in the upper regions of the skin but also in depth.

The work carried in the synchrotron ALBA was possible thanks to a grant from the Consortium for the Construction, Equipping and Exploitation of the Synchrotron Light Sources (CELLS).

5.2. Design of new lanolin synthetic membranes for *in vitro* methodologies

Results obtained in section 5.1.3 demonstrate a very poor correlation between penetration of actives with different *in silico* and *in vitro* models. The key of these methodologies is the membrane used to obtain the permeation parameters. Therefore, membranes with permeability properties similar to the skin are seek.

The structure of lanolin, which mimics the lipidic matrix of the SC by having a similar chemical composition, may offer a suitable strategy to achieve accurate modeling of the skin barrier properties by combination with synthetic membranes. It has been demonstrated that lanolin shares some lipidic compounds with the human SC such as cholesterol and its derivatives or some free fatty acids[125,126]. The presence of ceramides in lanolin fractions was reported[127]. Moreover, other physical properties are common such as the presence of lipids in the solid and liquid state at physiological temperature[128]. It is important to note that, with the WDS process[88], the resulting lanolin has more polar lipids with much human resemblance[129].

The main aim of this section is to obtain lanolin-based synthetic membranes to be used in skin permeation studies as models of mammalian skin. Lipid structural IR evaluation

and water permeation and penetration assays of three topical actives will be performed to determine the effect of lanolin on the membrane skin models.

Lanolin synthetic membranes were formed with Strat-M and Nuclepore membranes with lanolin deposition as described in section 4.4. Permeation assays were performed to be compared against the original synthetic membranes (Strat-M and Nuclepore) and to the skin.

5.2.1. Membrane structural properties and permeability to water

The lipidic conformation for pure lanolin, porcine skin, Nuclepore-lanolin and Strat-M-lanolin was studied using **ATR-FTIR spectroscopy** (section 4.8.1). This technique is a non-invasive technique with a depth penetration of 1 µm that makes it suitable to investigate lanolin or SC without isolation from other layers. For this study, of particular interest are the bands associated with the alkyl chain of the lipids. Information about the conformational order-disorder of the skin lipids can be extracted by the analysis of the 2920 and 2850 cm^{-1} stretching bands. In the case of symmetric CH_2 stretching, vibrations of 2849 cm^{-1}, 2850 cm^{-1} and 2852 cm^{-1} indicate orthorhombic, hexagonal and liquid crystalline, respectively. An increase in the vibrational frequency generally indicates an increase in the disorder. A similar behavior was observed for the asymmetric CH_2 stretching at 2920 cm^{-1}, although the symmetric stretching is more sensitive to the conformation changes.

In our case, the peak position in all the replicates was determined, and their average and standard deviation were calculated (Table XV).

Table XV ATR-FTIR of CH2 symmetric and asymmetric stretching modes of pure lanolin, Nuclepore-lanolin, Strat-M-lanolin and pig skin.

	Lanolin	Nuclepore-lanolin	Strat-M-lanolin	Pig skin
λCH_2 St. Sym (cm^{-1})	2848.5±0.01	2848.5±0.10	2848.5±0.03	2849.4±0.03
λCH_2 St.Asym (cm^{-1})	2917.9±0.07	2917.9±0.19	2916.3±0.03	2916.9±0.08

All the analyzed samples have a vibrational frequency of approximately 2849 or less corresponding in all cases to orthorhombic conformations. Low standard deviations were obtained in all the samples. These values agree with the ones corresponding to the natural lipidic packaging of pig healthy skin. Therefore, the two proposed synthetic models present a highly ordered lipidic structure that could emulate the lipidic package of the SC.

The **transepidermal water loss (TEWL)** is commonly used to measure membrane/skin barrier function permeability and integrity. The loss of water across the membrane is a

valuable clue to determine whether a membrane is suitable to test the skin absorption (section 4.3). In this work, the TEWL values and their respective standard deviation have been calculated for each membrane (n=9) before the formula application (Figure 29).

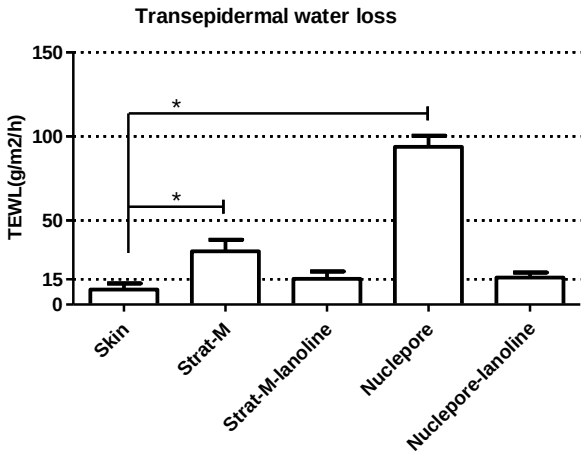

Figure 29 Transepidermal water loss (TEWL) measured on skin, Strat-M, Strat-M-lanolin, Nuclepore and Nuclepore-lanolin. (*) indicates a P value ≤ 0.001 from the Kruskal Wallis test

A low standard deviation was obtained in all the different membranes, including the skin. This is an important detail considering that it may imply homogeneity and stability not only on the skin biopsy but also on the commercial membranes (Strat-M and Nuclepore) and the presented lanolin-containing membranes from this work (Strat-M-lanolin and Nuclepore-lanolin).

The skin biopsies are considered appropriate to be tested on Franz cell diffusion studies when values are equal to or below 15 $g/m^2/h$ [130]. Observing the values obtained from the commercial models, the TEWL values for Strat-M are lower than those for Nuclepore, indicating a better barrier function for Strat-M. However, their permeability is far away from the maximum accepted for the OECD guidelines. The TEWL results of Strat-M-lanolin and Nuclepore-lanolin indicate that the addition of lanolin brings an important reduction of the TEWL values, making the values comparable to those from the skin. Then, by adding lanolin to the original synthetic membrane, a significant reduction is observed, implying an increase in barrier function.

5.2.2. *In vitro* diffusion with Franz cell assembly of membranes

In order to study the potential of the membranes to mimic the skin absorption, permeabilities of StratM, Nuclepore, Strat-M-lanolin and Nuclepore-lanolin and porcine skin are determined for three actives: Lidocaine, diclofenac sodium and betamethasone 17,21-dipropionate using the *in vitro* Franz cell diffusion methodology (section 4.3).

These three actives were employed considering that they are commonly used in topical formulations as they were stated in section 5.1. Moreover, they have a different chemical nature (basic, acid and neutral respectively) and a different lipophilicity. The distribution coefficient ($\log D$) at pH 7.4 and 5.5, as well as their molecular weight, were calculated *in silico* using the Pipeline Pilot software (Table XVI).

Table XVI Molecular weight (MW) and octanol water distribution coefficients ($\log D$) at pH 5.5 and 7.4 obtained from the Pipeline Pilot software

Active (acidic nature)	$\log D$ at pH 5.5	$\log D$ at pH 7.4	MW (g/mol)
Lidocaine (basic)	0.61	2.33	234.34
Diclofenac sodium (acid)	2.75	1.10	318.14
Betamethasone 17,21-dipropionate (neutral)	3.96	3.96	504.59

$\mathrm{Log}\,D$ was determined at pH 5.5 because it is the pH of the skin surface, and $\log D$ was determined at pH 7.4 because it is the pH of the receptor fluid and blood. As shown in Table XVI, betamethasone dipropionate, as a neutral active, showed no changes in $\log D$ at the different pH values. By contrast, lidocaine (base) and diclofenac sodium (acid) showed opposite behaviors. At lower pH, the increase in the ionized form of the lidocaine caused a decrease in $\log D$, resulting in higher hydrophilicity. In the opposite case, the $\log D$at pH 5.5 for diclofenac sodium was higher than that at pH 7.4 because the non-ionized form is predominant at acidic pH. This implies that, at pH 5.5, the $\log D$ range is, from highest to lowest is betamethasone dipropionate> diclofenac sodium> lidocaine, with lidocaine the most hydrophilic compound. However, at pH 7.4, the $\log D$ range is betamethasone dipropionate> lidocaine> diclofenac sodium, with diclofenac sodium the most hydrophilic compound. This could be important to predict or explain permeation of these actives through the different membranes.

The three actives were formulated in propylene glycol at 2%, 0.5% and 1%. The passive diffusion of these three formulations was studied in Franz-cells systems onto pig skin biopsies, lanolin-free synthetic membranes (Strat-M and Nuclepore) and lanolin synthetic membranes (Strat-M-lanolin and Nuclepore-lanolin). Table XVII contains normalised amounts after the HPLC analysis (4.6.1).

When pig skin biopsies were used, the amount of actives was evaluated in the Stratum Corneum (SC), epidermis (E), dermis (D) and receptor fluid (RF). Skin permeation (ABS) is considered the summed amounts from the epidermis, dermis and receptor fluid (Table XVII).

When the actives were applied on the skin, lidocaine shows the highest permeation rates followed by diclofenac sodium. Betamethasone dipropionate was the less absorbed compound. As explained previously, $\log D$ is an important parameter when studying diffusion across membranes. In the case of skin, $\log D$ at pH 5.5 must be considered because this is the physiological pH in this tissue. When observing the $\log D$ at pH 5.5 and molecular weight for the three actives, the absorption through the skin seems to be promoted by low molecular weights and low $\log D$ values. Lidocaine (highly absorbed) is small and the most hydrophilic compound, followed by diclofenac sodium with a medium value of $\log D$ and molecular weight. Betamethasone dipropionate is a lipophilic and heavy molecule poorly absorbed across the skin (Table XVII and Figure 30).

Table XVII Normalized amounts (%) found in the Stratum Corneum (SC), epidermis (E) dermis (D) and receptor fluid (RF). In the case of artificial membranes, ABS belong to the amounts found in the receptor fluid.

Normalized amounts (%)		Lidocaine 2%	Diclofenac sodium 0.5%	Betamethasone dipropionate 1%
Skin	SC	5.02±4.56	9.70±4.25	13.60±3.37
	E	4.61±3.63	7.34±2.22	4.30±1.58
	D	2.94±0.96	1.84±1.53	0.00±0.01
	RF	50.02±10.05	11.68±6.17	0.00±0.00
	ABS	57.58±7.63	20.86±9.24	4.30±1.57
Strat-M	ABS	26.48±8.14	49.19±4.23	0.78±1.36
Strat-M-lanolin	ABS	68.40±6.50	45.22±9.36	4.03±0.59
Nuclepore	ABS	98.37±2.10	94.56±0.45	8.69±2.16
Nuclepore-lanolin	ABS	90.81±2.84	29.58±9.78	10.54±0.99

*ABS: the absorbed amount through the skin is considered to be the sum of epidermis, dermis and receptor fluid

The permeation obtained using the commercial membranes confirms the deductions made when observing the TEWL values. We observed higher values of TEWL on

Nuclepore than in Strat-M that could imply higher permeation on Nuclepore. Hence, the three different actives were more permeated in Nuclepore rather than in Strat-M. These differences were hardly seen on betamethasone dipropionate because the lack of solubility in the acceptor fluid limits its diffusion through the membrane (Figure 30).

When observing the actives absorption rank in Strat-M, unlike on skin, diclofenac sodium was more permeated than lidocaine. Similar results can be deduced for Nuclepore, but its low barrier (demonstrated observing the TEWL values) does not allow the differentiation between lidocaine and diclofenac sodium. These permeability changes between diclofenac sodium and lidocaine can be explained observing their respective $\log D$. As discussed previously, the pH at the skin is 5.5, whereas the pH at the commercial membranes is that of the receptor fluid, pH 7.4. Observing their respective $\log D$, diclofenac sodium was demonstrated to be more hydrophilic than lidocaine at pH 7.4. Therefore, the same deduction observed when the actives were applied on the skin can be extracted: the most hydrophilic compound, which, in this case is diclofenac sodium, is more permeated than lidocaine. Betamethasone dipropionate with the highest $\log D$ remains the less permeated compound.

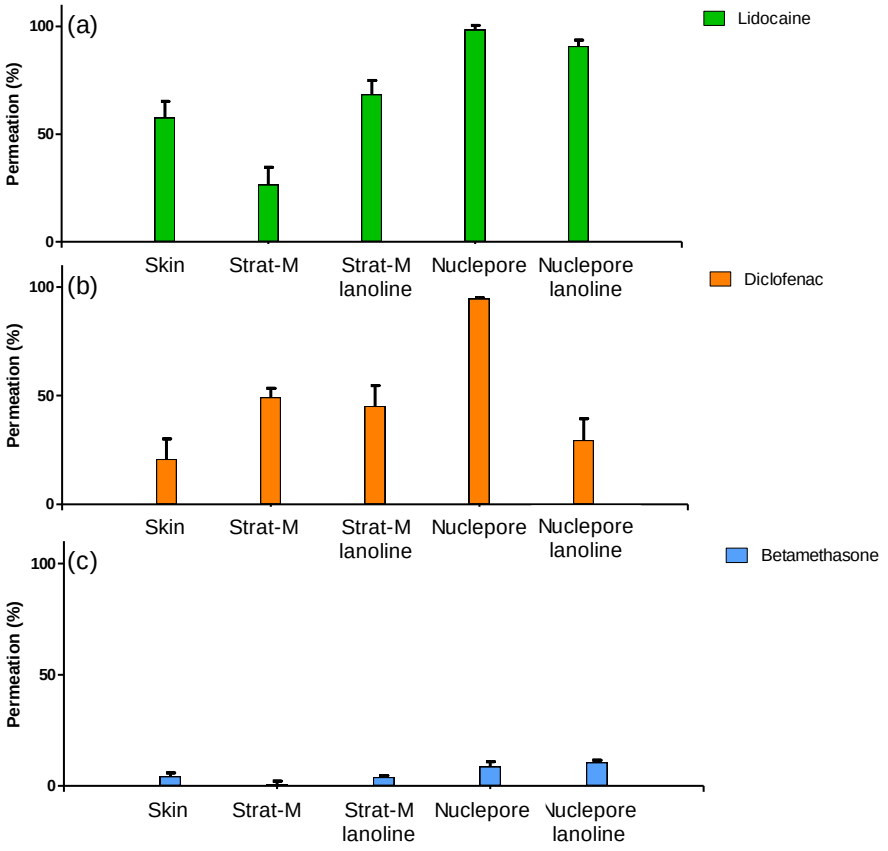

Figure 30 Normalized absorbed amounts (%) in skin, Strat-M, Strat-M-lanolin, Nuclepore, Nuclepore-lanolin for lidocaine(a), diclofenac sodium (b) and betamethasone dipropionate (c)

In summary, the lanolin layer was added to Strat-M and Nuclepore synthetic membranes. Comparing their TEWL values against those from the lanolin-containing membranes, an increment of the barrier function as a result for the lanolin addition was observed. The permeation results obtained for the three actives showed this barrier enhancement. The addition of lanolin promotes the reduction in the absorption of the three substances.

Lanolin addition to the artificial membranes caused a reduction of TEWL and a modulation of permeation of the three different compounds, leading to results much

similar those obtained with the skin. Lanolin previously demonstrated its ability to reinforce SC lipids, leading to improved skin barrier function in *in vivo* topical studies[129]. This work confirms its suitability regarding its use as an artificial membrane for permeation or percutaneous absorption models.

Part of the studies to prove similarity between the lipid matrix and lanolin wich are published in "Skin Pharmacology and Physiology" entitled as "Solvent-Extracted Wool Wax Thermotropic Properties and Skin Efficacy" (Annex 2)

The results from section 5.2 have been published as a research paper called "Lanolin-Based Synthetic Membranes as Percutaneous Absorption Models for Transdermal Drug Delivery" in Pharmaceutics-MDPI (Annex 3).

Besides these membranes and results have been protected with a Patent (Annex 4)

5.3. Comparison of *in vivo* stripping, *in vitro* permeation study and confocal Raman spectroscopy of resveratrol

The objective of the present work is to examine and compare the skin penetration of an antioxidant such as resveratrol (Res) using *in vivo* and in vitro methodologies and applying also a spectroscopic technique such as confocal Raman microscopy with the same purpose.

In a previous work, the *in vitro* percutaneous penetration using Franz diffusion cells was evaluated to assess compound delivery into the different layers of the skin (SC, epidermis and dermis) as well as into the receptor fluid when the compound applied topically on porcine skin[131]. Then, two other methodologies are presented in this doctoral thesis to study permeability of Res; An *in vivo* assay minimally invasive in which the SC in sequentially substracted with adhesive strips (section 1.2.3) and a confocal Raman microscopy (CRM) (section 4.7.1). These techniques were used to determine the penetration profile of resveratrol to be compared with the results of an ex vivo dermatomed porcine skin mounted in a Franz diffusion cell for 20h (section 4.3).

5.3.1. Percutaneous penetration of resveratrol by *in vivo* stripping

In this work, the percutaneous penetration of resveratrol was determined *in vivo* on human skin. For these experiments, an aqueous-ethanolic solution (70:30) was selected as the simple application vehicle to dissolve the resveratrol to be used at the

5% (w/v) concentration. The *in vivo* penetration of resveratrol into the human skin was obtained using the stripping methodology (section 1.2.3), based on the successive extraction of the SC layers by consecutive stripping with adhesive tapes[132] described in section 4.5.

The content of Res removed with the tape strips was quantified by triplicate with HPLC measurements (section 4.6.1) after methanol extraction of the combined groups of strips from 1–5 and 6–10 strips. The concentration of resveratrol obtained in the combined tapes, as a function of the strip number, is shown in Figure 31(expressed in percentage) and Table XVII (expressed in µg/cm^2), along with the mean values.

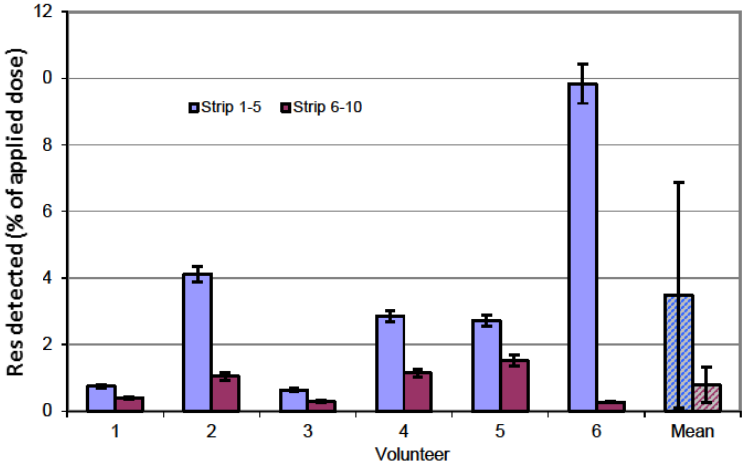

Figure 31 Concentration profiles of resveratrol (Res) from strips 1 to 5 and 6 to 10 in the SC *in vivo*, expressed as a percentage of the applied dose detected

Table XVIII Amount of resveratrol detected in the combined tapes for each volunteer, expressed in µg/cm^2

Volunteer	1	2	3	4	5	6	Mean ± SD
Strips 1–5	3.99	12.17	1.89	8.61	8.24	19.72	9.10 ± 6.35
Strips 6–10	1.06	3.11	0.83	3.45	3.63	0.83	2.15 ± 1.38
Total amount (µg/cm^2)	5.05	15.28	2.72	12.06	11.86	20.55	11.25 ± 6.56

Taking into account the differences observed among the volunteers from Figure 31, the mean resveratrol recovery was 4.27 ± 3.35% (11.25±6.56 µg/cm^2), and the majority was present on strips 1–5.

The amount of SC extracted by the adhesive tape strips was dependent on a variety of factors [92], such as the anatomical site, subject age, and time of year. The quantity of

cells in the layers[133] and the thickness of the SC[134] change with the anatomical zone, corresponding to the changes in the composition and amount of lipids. External factors can also influence the quantity of the SC extracted by the stripping method. The mode of extraction from the skin, the pressure time on the forearm skin and the presence of topically applied substances are external factors[135] to take into account. In this work, efforts were made to control the intrinsic variability by carrying out the assays during the same time of year (over 2 days) for the group of volunteers and by using only the same area of the arm (the volar forearm). To take the external factors into consideration, the adhesive strips were attached to the skin surface with constant pressure and all the assays were carried out by the same technician. Despite considering the above factors, the amount of Res obtained showed a high variability.

Moreover, the major amount (77%) of the penetrated resveratrol was localized to the upper layer of the SC (strips 1–5), and the compound detection decreased with the SC-depth because smaller amounts of resveratrol were extracted and less SC tissue were removed by the tape strips from the deeper layers.

5.3.2. *In vivo* stripping and *in vitro* Franz diffusion cells correlation results

In vivo studies are essential assays for a more realistic evaluation of the skin permeation of topical applications. However, the usage of skin biopsies with *in vitro* Franz diffusion cells is an alternative to *in vivo* methods. This *in vitro* method has been fully described in the previous sections (1.2.2.1). In a previous study[131], a specific *in vitro* percutaneous absorption was carried out to obtain the percutaneous profile of Res in the porcine skin. Figure 32 shows the comparison of the mean values from the *in vivo* study with the percutaneous absorption *in vitro*, expressed as a percentage of the applied amount recovered (%).

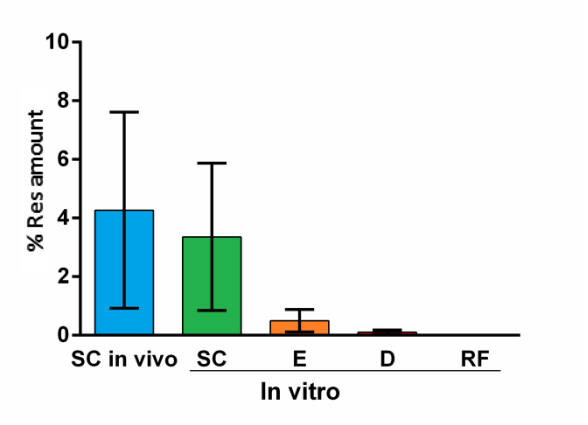

Figure 32 Percutaneous absorption of resveratrol *in vitro* expressed as a percentage of the amount detected in the different skin layers [Stratum Corneum (SC), epidermis (E), dermis (D)] and the receptor fluid (RF). The results were compared to the mean value obtained from the SC layer by the stripping method

The results indicated that Res was located mainly in the SC layer and the viable epidermal layer. Resveratrol is immediately metabolized in the body[136]; thus, a topical administration could be an efficient option for its application to benefit the skin while avoiding the systemic presence of the compound. Other authors had established the permeation data of Res using different topical formulations[137]. The results obtained also indicated higher amounts of the compound in the skin than are observed from delivery at the systemic level. Therefore, the low capacity of percutaneous penetration observed for Res (0.6% skin absorbed[131]) may confirm its use as an ingredient in cosmetic products.

The results obtained *in vivo* demonstrate that Res penetrates the SC layers, corroborating the results obtained *in vitro*. The percentage of Res obtained in the SC layer from the *in vivo* permeation (4.27 ± 3.35% of the applied dose) was similar to (not significantly different) that *in vitro* (3.36 ± 2.51% of the applied dose).

5.3.3. Percutaneous penetration of resveratrol by CRM

The CRM (section 4.7.1) technique was applied to obtain the spectra of Res and the non-treated porcine skin. Both spectra are compiled in Figure 33 and were obtained in the 100–3200 cm^{-1} region.

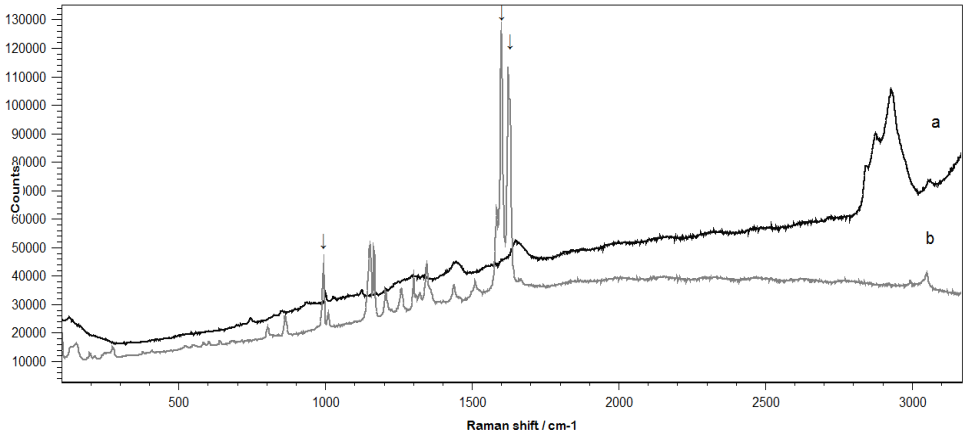

Figure 33 Raman spectra (100–3200 cm^{-1}) of untreated pig skin acquired at the skin surface (a) and Res (b)

The spectrum of the porcine membrane shows different bands that are distinctive for the lipids and proteins of SC layer, for example, the ring-breathing mode in Phe is shown at 1004 cm^{-1}, amide I at 1650 cm^{-1}, lipids at 2820 cm^{-1} and protein (keratin) at 2940 cm^{-1}. In Figure 35, the band at 995 cm^{-1}, and the overlapped 1610/1640 cm^{-1} pair detected in the spectrum of Res, can be used to follow Res permeation into the skin. The other peaks from Res, such as the ones in the 1003 cm^{-1} region, are as a result of the aromatic ring-breathing mode, and the ones in the 1610 cm^{-1} region are due to conjugated C=C bonds and ring-stretching modes.

Res was topically applied to dermatomed pig skin mounted in a Franz-type cell (section 4.3). After 24 h of exposure five tape strips were used to remove the excess compound from the skin surface. Afterwards, successive confocal Raman spectra from the applied skin were obtained every 7 µm to a final depth of 49 µm in the 600–2300 cm^{-1} region. The spectral series are shown in Figure 34.

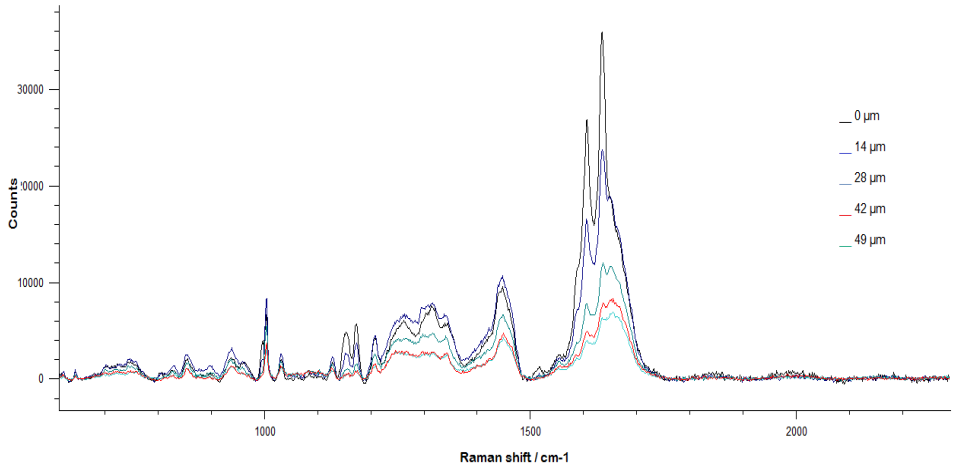

Figure 34 Illustration of spectral changes obtained from the pig skin following the application of Res, at different depths. The top spectrum was collected at the surface of the skin, while the bottom one was collected 49 µm below the surface

The spectral signals from both the skin and the applied Res compound are shown. The perception of the peaks in the 1610/1640 cm^{-1} region from the SC surface to a depth of ~49 µm demonstrated the penetration of Res to 49 µm into the skin. Modifications in the C=C peak regions and amplitudes are noted with the depth, as shown in Figure 34. The results show the presence of Res in the SC compartment and in the viable epidermis. Relative Res concentrations were obtained from the Raman profiles, following the method described by Caspers et al. [138]. To rectify the variability of the absolute Raman intensity, which diminishes at the deeper levels of the skin, the corresponding coefficients were normalized to the Raman keratin signal (~2940 cm^{-1}). Normalization to the Raman Phe ring peak from the SC layer (~1004 cm^{-1}) was not considered because the intensity of this band increases due to the contribution of the vibration of Res at 995 cm^{-1} giving a signal that is superimposed with the skin Phe ring breathing[139]. The normalization approach revealed the amount of Res in the SC and viable epidermis relative to the amount of keratin. The depth concentration profiles of Res are presented in Figure 35. The highest concentration of the compound was obtained near the skin surface. The concentration decreased at a depth of approximately 20 µm. It can be observed that Res concentration was constant between the depths of 20–49 µm, corresponding to the viable epidermis.

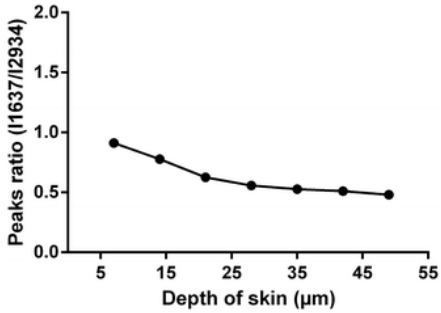

Figure 35 Representative distribution profiles of Res in the porcine skin from 7 to 49 µm

In this section 5.3, different *in vitro* and *in vivo* methodologies were used to assess the skin permeation of the antioxidant resveratrol after topical application. A depth concentration profile of resveratrol was obtained by CRM. The presence of bands in the 1610 cm−1 zone indicated that resveratrol permeated to a minimum of 50 µm. The results demonstrated that the percentage of resveratrol obtained from the *in vivo* permeation assay was similar to that obtained *in vitro* using the Franz cell system.

The findings reported in the present study indicate the suitability of Raman microscopy and *in vitro*/*in vivo* percutaneous absorption procedures for the evaluation of resveratrol skin permeation. The active compound retained within the skin, especially in the SC, after topical administration may be an effective treatment for the mitigation of free radical exposure.

This work is part of a research publication published in the Archives of Dermatological Research entitled "Skin permeation and antioxidant efficacy of topically applied resveratrol" (Annex 5)

5.4. Confocal Raman spectroscopy of caffeine penetration on skin

The combination of Raman spectroscopy with confocal microscopy (confocal Raman microscopy) is an optical technique to provide qualitative information about the biochemical composition of the skin, such as the lipid and water contents and the effects of moisturising factors [22, 23] . Moreover, the permeation profile of an active through the skin layers and its possible interactions with endogenous skin components can be studied with this technique (section 1.2.4).

Following, two CRM studies are described to obtain a quantitative evaluation of caffeine in SC and epidermis (section 5.4.1) and to evaluate the distribution of caffeine in the hair follicles using different mapping methodologies (section 5.4.2). Caffeine was chosen because it is one of the standard models commonly used as a hydrophilic tracer to evaluate skin absorption and penetration via traditional *in vitro* and *in vivo* methods[140,141] as well as in CRM studies[142].

5.4.1. Percutaneous penetration of caffeine by CRM

The present study seeks to optimize a methodology for completely quantitative measurement of the amount of caffeine (Caf) at different depths. A semi-quantitative depth profile was obtained with normalization of the Raman intensities. These ratios of Raman intensities were correlated with the caffeine concentration using an external calibration curve. The calibration curve was carried out with porcine skin incubated in different concentrations of caffeine; afterwards, each skin sample was analyzed by CRM and HPLC-DAD to determine the relation between the Raman signal intensity and the caffeine concentration per skin mass and to create a depth profile. These correlation curves allow full quantification of the caffeine in skin from Raman intensity ratios at different depths. Raman data acquisition and quantitative detection of caffeine are described in section 4.7.1.

5.4.1.1. Quantitative CRM methodology optimization

The porcine skin was incubated with different caffeine solutions and the skin samples were analyzed by CRM. Then skin samples were extracted and analyzed by HPLC to obtain correlation between the two techniques.

Analysis of caffeine in epidermis by HPLC

Caffeine (Caf) was extracted from epidermis (Ep) samples after 20 hours of incubation in solutions at different Caf concentrations. The extracted samples were analysed by HPLC-DAD (section 4.6.1) and the results are shown in Table XIX. As it can be seen, the percentage of absorbed caffeine per tissue mass is very similar in all the samples. The mean percentage of Caf recovery per mass of Ep (mg) was 0.100 ± 0.009%/mg Ep, demonstrating the low variability in caffeine absorption due to its similar penetration into tissues from different donors.

Table XIX Amounts of caffeine absorbed in the extraction of Ep after 20h incubation into caffeine solutions (expressed as µg Caf/mg Ep) and percentage of caffeine absorbed

Solution of Caf **concentration (µg/mL)**	**µg** Caf**/ mg** Ep	**%** Caf **absorbed per mg** Ep
10.2	12.648	0.083
5.0	7.711	0.104
3.1	4.481	0.104
1.7	2.497	0.105
0.71	1.025	0.098
Mean ± SD		**0.100 ± 0.009**

Analysis of caffeine in epidermis by CRM

To monitor a compound by CRM analysis, it is necessary to identify the Raman bands of the exogenous compound in the matrix correctly. Skin is a complex tissue containing multiple components that present Raman signals. Porcine skin was used in this CRM work as a substitute tissue for human skin because of similar permeability. Raman studies demonstrated the same band assignments in both types of skin, indicating the similar spectra of porcine and human skin[50,142]. The endogenous Raman peaks of skin can interfere with detection of the tested compound. The caffeine molecule presents defined Raman bands that permit its differentiation from skin components. Figure 36 presents the Raman spectra of caffeine (Caf), Ep incubated in caffeine solution (Ep+Caf) and untreated porcine Ep.

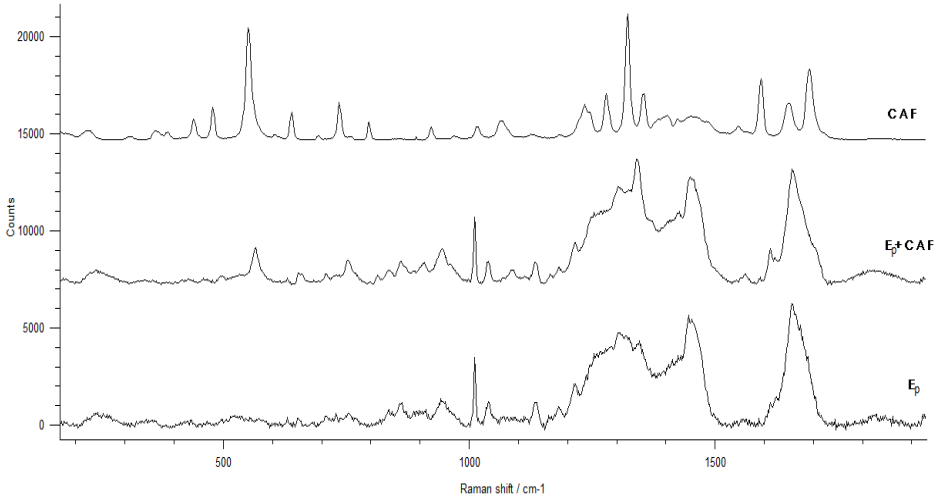

Figure 36 Raman spectra of caffeine (Caf), Ep incubated in caffeine solution (Ep+Caf) and untreated porcine Ep.

The Ep spectrum shows various bands that are specific to skin, for example, the C–C vibration mode of aromatic amino acids (AA) at 1004 cm^{-1} and the N–C=O deformation in amide I (AI) at 1660 cm^{-1}[142]. The caffeine band at 555 cm^{-1}, assigned to the O=C–N deformation mode, was selected as a marker because it has enough intensity and does not overlap with other bands from skin components. The spectrum of Ep with caffeine confirms the detection of the compound in the skin due to the clear identification of the Raman peak. The caffeine band at 1331 cm^{-1} was dismissed because of its overlap with the Raman bands of skin, as shown in the Ep+Caf sample (Figure 36).

The variability in Raman spectra was estimated in the different Ep donors (data not shown). Despite the inter-individual variability in the intensity of the Caf peak in the spectra, the results did not indicate any significant differences between donors, as in previously investigations[143]. The absolute intensity of Raman bands decreases at the deeper levels of skin because of the lower resolution inside the sample. To rectify this Raman variability, the selected band of a compound can be normalised to a skin peak as an internal reference. Skin presents different peaks that can be used as a reference[138,142]. In this study, the caffeine peak of Ep samples (555 cm^{-1}) was correlated to the aromatic amino acids and the amide I peaks (1004 cm^{-1} and 1650 cm^{-1}, respectively). Normalisation of the Caf peak to the Raman band of skin at 1290-1311 cm^{-1} was not considered because the intensity of this skin band is compromised by the contribution of the caffeine vibration at 1305 cm^{-1}. The variability of the normalised data from Raman signals was analysed along the depth. Figure 42 shows the ratio of the peak of caffeine (555 cm^{-1}) with the two skin reference peaks (AA and AI) acquired at different depths.

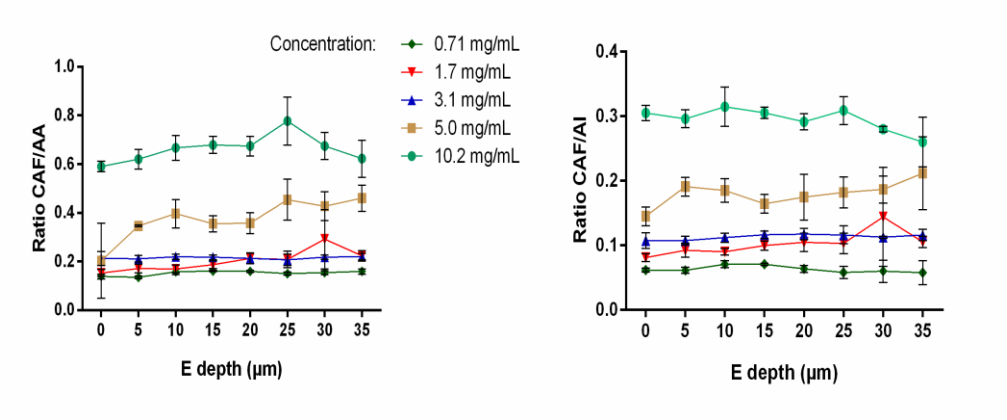

Figure 37 Ratio peaks of caffeine (CAF) with the two internal references: aromatic amino acids (AA) at 1004 cm^{-1} and amide I (AI) at 1660 cm^{-1} at different skin depths

The Ep surface position in spectral data was selected considering the aromatic amino acid peak at 1004 cm^{-1}, which had the maximum intensity[144]. The Raman peak ratios of Caf vs aromatic amino acids and amide I remained constant at various Ep depths for each concentration of caffeine. This horizontal correlation demonstrated that the peak ratio is independent of the Ep depth, counteracting the attenuation in the Raman intensity. Low variability was associated with the normalised data of CAF/AA and CAF/AI ratios at each depth for all concentrations, as shown in Figure 37.

Correlation of caffeine from HPLC/CRM analysis

The ratio intensities (CAF/AA and CAF/AI) could be related to the concentration of Caf quantified by HPLC. The relation between both experimental data values permits a correlation between the CRM data and the quantitative amount of the compound. To establish a correlation between the normalised ratios and the caffeine concentration, Raman ratios were plotted versus the amount of caffeine (µg Caf/mg Ep) determined by HPLC analysis. The correlation is shown in Figure 38 for both cases.

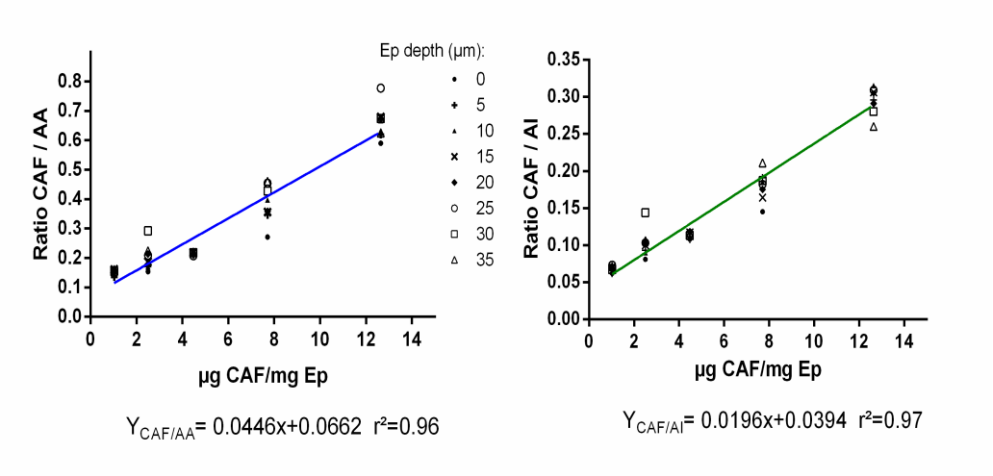

Figure 38 Correlation between the Raman peak ratios obtained by CRM versus caffeine amount per mass of E determined by HPLC in different E depths

Despite the dispersion in the plotted results due to the intrinsic variability of the skin samples, a mean linear correlation was obtained for both ratios. Linear regression equations for the experimental data were obtained with a good correlation, demonstrating that the relation for both signals was independent of Ep depth.

Linear regression between the normalised ratios of caffeine and the amount of compound (µg Caf) contained in the Ep samples at different caffeine concentration enables quantification of the compound with skin profile data. Our study analysed caffeine in the SC and viable epidermis at depths up to 35 µm. These results corroborate the findings of Franzen et al.[143], even though those authors detected the compound only in an isolated SC. The obtained linear regression results were used to evaluate the penetration profile of Caf in an *in vitro* percutaneous study.

5.4.1.2. Percutaneous penetration of caffeine determined by CRM

For *in vitro* percutaneous penetration experiments, 20 µL of aqueous-ethanolic solution containing 5 % caffeine was applied to dermatomed porcine skin deposited in a Franz static diffusion cell. After 20 hours, the excess compound on the skin surface was removed with gently pressing of a tape strip. Afterwards, successive confocal Raman spectra were obtained every 5 µm to a final depth of 35 µm. The spectral series is shown in Figure 39. As in the Ep sample, the skin surface was considered the point at which the signal intensity of aromatic amino acids at 1004 cm^{-1} was maximal.

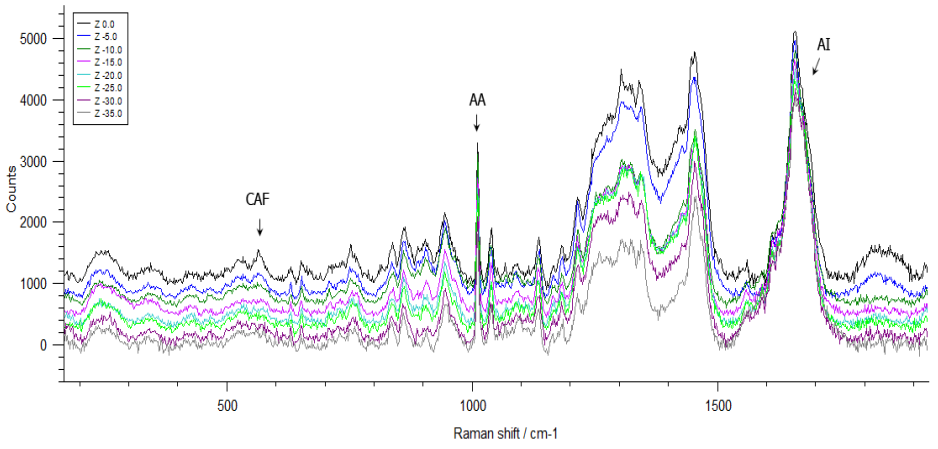

Figure 39 Illustration of spectra obtained of pigskin following the application of caffeine solution, at different depths (0 to 35µm). The top spectrum was collected at the surface of the skin, while the bottom one was collected 35 µm below the surface of the skin

The presence of the peak at 555 cm^{-1} corresponding to caffeine demonstrated the penetration of this compound. The results show the presence of caffeine in the SC and in the viable epidermis. Relative caffeine concentrations were determined from Raman data using the aromatic amino acid and amide I bands of skin. The relative concentrations as a function of the skin depth represent the qualitative penetration profile of caffeine in skin. The semi-quantitative penetration profile of caffeine is plotted in Figure 40.

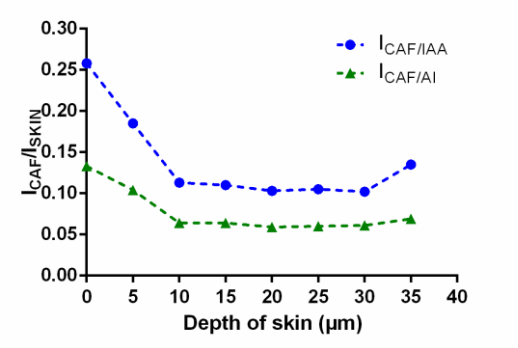

Figure 40 Semi-quantitative penetration profiles of caffeine into the pig skin determined by CRM. Profiles were obtained for each internal skin reference

As can be seen, the highest concentration of compound was detected close to the skin surface. The concentration appeared to level off at a depth of approximately 10 µm. The results showed that the caffeine concentration was constant between 10 and 35

µm, which are the depths corresponding to the viable epidermis. The two semi-quantitative profiles obtained from the two internal skin references are qualitatively similar, but have different peak ratio levels due to the variability in the Raman band intensities of caffeine and skin components.

The use of CRM for quantitative measurements requires a correlation between the Raman signal and the concentration of caffeine to convert the semi-quantitative data to quantitative data. In the previous experiment, we established a linear correlation between caffeine detected by CRM and the caffeine concentration quantified by HPLC. The semi-quantitative data of caffeine can be transformed to a quantitative penetration profile by applying the linear correlations for the Raman ratios and Caf concentration shown in Figure 38. The use of the CAF/AA and CAF/AI ratios in each linear regression equation provides the absolute value of caffeine at the different depths. Figure 41 presents the profiles for the absolute amount of caffeine in pig skin considering both internal skin references in the Raman data. As can be seen, the quantitative profile obtained from the CAF/AA ratio is close to the profile from the CAF/AI ratio, equalising the effect of the Raman signal.

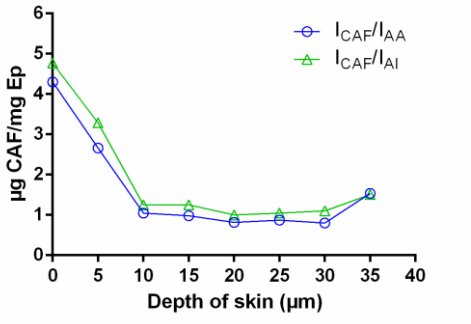

Figure 41 Quantitative penetration profiles of caffeine obtained from semi-quantitative data and linear correlation Raman-Caf concentration

Until now, most studies carried out using the CRM technique presented semi-quantitative results. Active compounds of dermo-pharmaceutical formulations applied *in vivo* can be analysed by CRM, a non-invasive method. Quantitative determination of compounds could be envisaged after *in vivo* evaluation following the CRM protocol presented in this work. More investigations are necessary with a wide range of compounds and experimental conditions in order to establish the correct and specific protocol for each case.

Summarizing, an experiment has been carried out to validate the use of confocal Raman microscopy to obtain a quantitative profile of the skin penetration of caffeine. A linear correlation between Raman signal ratios (I_{CAF}/I_{SKIN}) and the Caf concentration (µg Caf/mg Ep) obtained by HPLC was determined. Next, a semi-quantitative and even a quantitative depth profile of the Caf penetration in porcine skin was obtained by this technique. The transformation to quantitative data permits equalisation of the fluctuation of Raman data, providing a representative absorption profile.

The presented procedure relates the Raman data and the caffeine concentration per skin mass. The findings provide further support for the application of CRM to the study of the drug disposition in skin via this non-invasive technique for direct quantification of a drug in skin.

The results from section 5.4.1 are now under revision in the Archives of Dermatological Research entitled as "Caffeine delivery in porcine skin: a confocal Raman study"

5.4.2. Imaging of follicular penetration of caffeine

The trans follicular route for drug administration into the skin has gained attention mainly driven by the advent of nanoparticle-based delivery systems that facilitates the absorption into the hair follicle. Nevertheless, the study of the follicular penetration is challenging as it requires high spatial resolution and molecular sensitivity to the applied drugs. A suitable technique to fulfill this need is confocal Raman microscopy (CRM), which can combine the spectral and the spatial information in order to be used for hyperspectral imaging. Besides the spectroscopic analysis of the individual chemical composition, CRM offers the possibility of imaging by scanning the sample, thus, facilitating the visualization of spatially resolved component distribution.

Comparison of the usefulness of Gaussian-peak fitting, classical least-squares (CLS) and Multivariate Curve Resolution-Alternating Least Squares (MCR-ALS) models to provide semi-quantitative and spatially resolved information about the distribution of caffeine into the hair follicle is presented. Moreover, the differentiation of different constituents existing in the cryosections is achieved.

Caffeine is applied to the non-dermatomed ear skin in two different formulations: 5% w/v in water: ethanol solution (50:50) (Caf-Aq) and 1.4mg/mL of caffeine nanoparticles coated with PVP in water (Caf-NP). Cross-sections containing a hair follicle of Caf-NP and Caf-Aq treated skin as well as a non-treated were studied. The followed procedure is detailed in section 4.7.2.

5.4.2.1. Reference component spectra

Several components are observed in the mapped cryosections. First, their spectra were acquired. Figure 42 and Figure 43 show the pre-processed spectra of the reference components such as intrinsic and extrinsic skin components.

Noticeable differences between the different tissue spectra (SC, hair, epidermis and dermis) can be observed. A major difference recognized in the hair spectrum is the Sulphur content, which is indicated by the relatively higher intensities of the S–S-related band around 510–530 cm^{-1}. This higher amount of sulfur is due to the higher amounts of sulfur-containing amino acids (cysteine) from the hair's hard keratins. In the hair, 7–8% of the amino acids are cysteine, whereas in the SC (another highly keratinized tissue) it represents only the 0.5%[145]. The higher content of keratin in the hair is also disclosed by the higher amide I band at 1650 cm^{-1} compared to the other spectra.

The SC shows some particularities compared to the hair, not only on the lower intensities of the bands related to the sulfur content previously detected (505 and 1650 cm^{-1}), but also for the presence of a prominent bank at 1064 cm^{-1} related to the skeletal C–C stretch of lipids[146]

The dermis spectrum can be differentiated from that of the epidermis by the two double bands in the 815-850 and 920-940 cm^{-1} range. This pattern is representative for collagen[147], which is localized in the dermis in significantly higher quantities than in other tissue regions[148]. On the other hand, the amide I band associated to keratin (1650 cm^{-1}) is higher for the epidermis than for the dermis, probably because of the higher keratinization of the tissue.

The selected caffeine labelling band as in the previous section (5.4.1) is 555 cm^{-1} which is assigned to the δ C=O–N deformation modes[149](Figure 43). Regrettably, this band is slightly overlaid with one prominent band at 550 cm^{-1} attributed to Si-O-Si bending vibrations from the microscope slide glass. This band overlapping may cause difficulties to assign the spectral differences in this region to the presence of caffeine or glass if no further spectral analysis is performed.

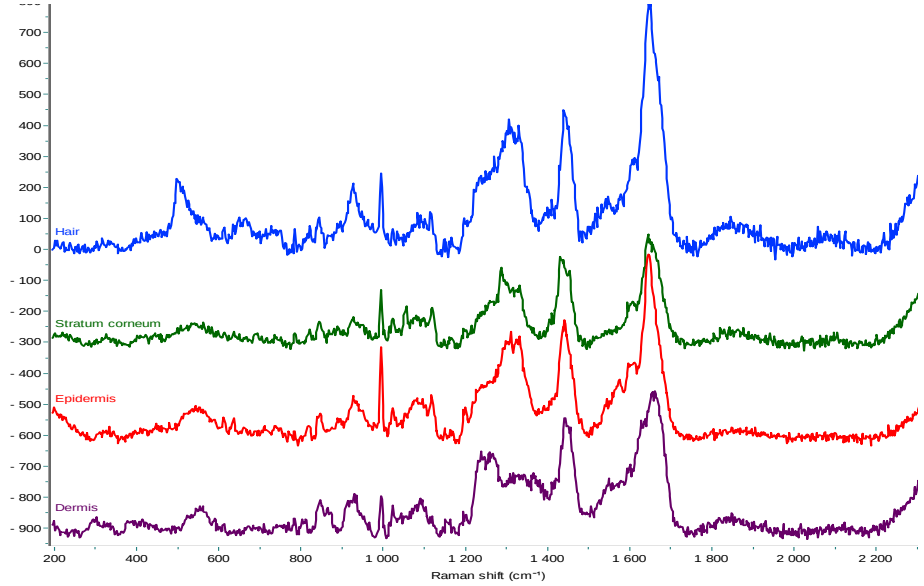

Figure 42 Collected reference spectra of hair (blue), SC (green), epidermis (red) and dermis (purple)

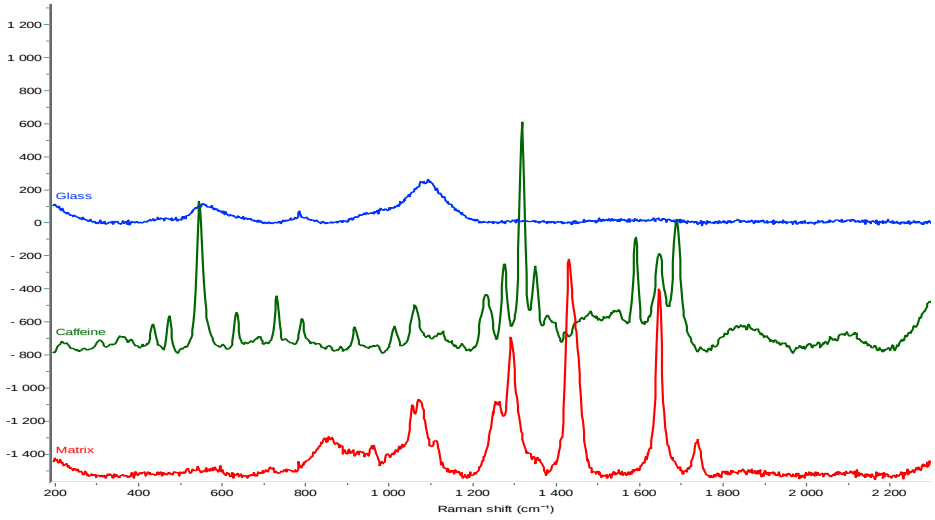

Figure 43. Collected reference spectra of caffeine (green), glass cover slide (blue) and cryospray (red)

5.4.2.2. Mapping methodologies for caffeine distribution

After the discussion of the spectral differences from the different cross-section components, Peak fitting, CLS and MCR-ALS spectral analysis are studied to follow the caffeine distribution within the mapped area.

Peak fitting methodology

The peak fitting methodology was used in the 555 cm^{-1} position to study the caffeine distribution in both hair follicles. Combining the amplitude values with the spatial information, images of the amplitudes within the sample are obtained. No trace of caffeine were apparently detected in in Caf-Aq (Figure 44) or treated with Caf-NP (Figure 45) hair follicles. Large and uniform regions with high values of amplitude are detected in both hair follicles. When comparing with the microscopic images, these bands are easily be attributed to the glass. The peak fitting in this region seems to be useless to detect caffeine's distribution. Caffeine's band at 555 cm^{-1} is partially overlapped with glass wider band at 550 cm^{-1}, therefore the peak amplitudes of glass interfere caffeine's detection with this method.

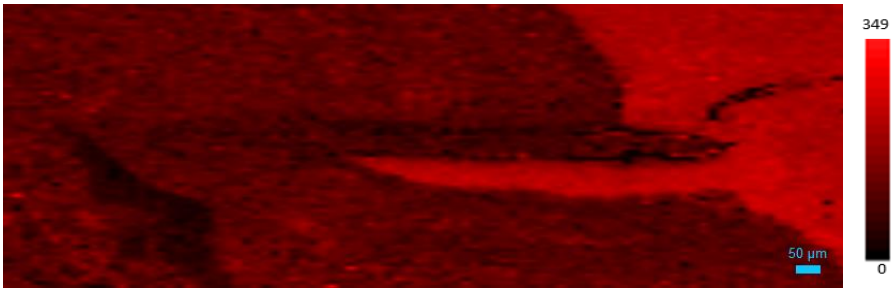

Figure 44. Peak amplitude labelling at 555 cm^{-1} for the Caf-Aq treated hair follicle

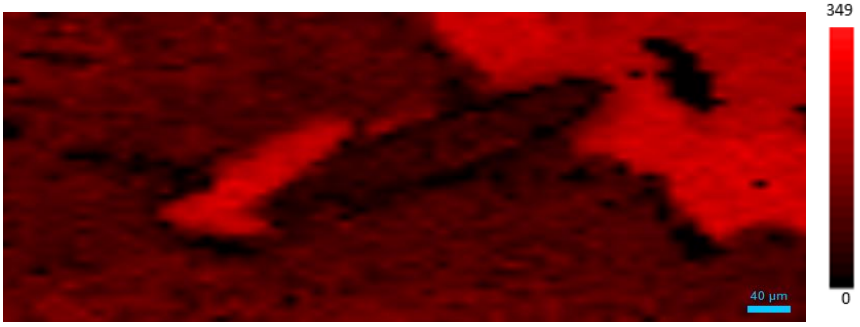

Figure 45. Peak amplitude labelling at 555cm^{-1} for the Caf-NP treated hair follicle

Classical least-squares regression methodology (CLS)

After processing the spectral data with CLS to identify the component distribution, a false color Raman image is obtained, allocating each pixel with a color representing the contribution of the reference Raman spectra. For both of the analyzed hair follicles all spots with spectra representing the dermis are shown in red, epidermis in yellow, hair in brown, SC in green, cover-slide glass in navy blue, caffeine in pink and cryospray drops in light blue.

The loaded reference spectra were pre-processed as described in section 4.7.2. This approach displays differences in intensity scores and allows the spatial association of multiple components simultaneously in one pixel. Therefore this procedure facilitates a more detailed depiction of the distribution of the different components.

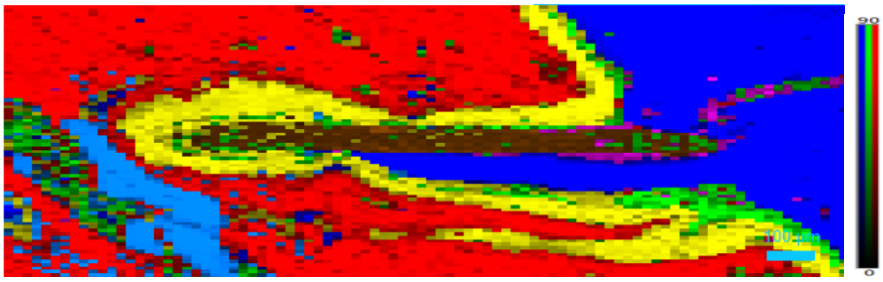

Figure 46 CLS scores for the Caf-Aq treated hair follicle. Scores are plotted in: (red), epidermis (yellow), hair (brown), SC (green), cover-slide glass (navy blue), caffeine (pink) and cryospray drops (light blue)

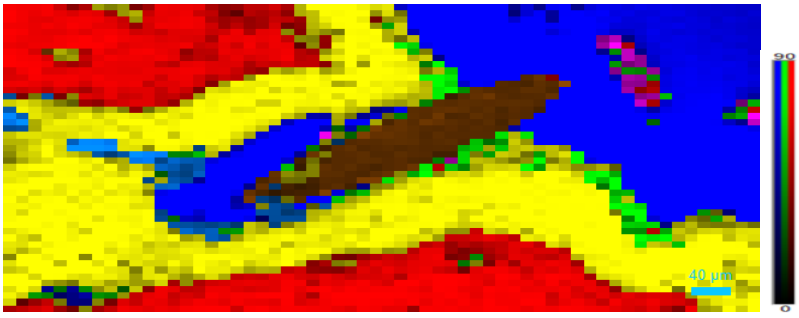

Figure 47. CLS scores for the Caf-NP treated hair follicle. Scores are plotted in: (red), epidermis (yellow), hair (brown), SC (green), cover-slide glass (navy blue), caffeine (pink) and cryospray drops (light blue)

Comparing Figure 46 and Figure 47 with Figure 48 and Figure 49, respectively, the hair is correctly assigned in both cryosections. The epidermis and the dermis can be clearly differentiated in two different layers. The distributions of the three compounds (hair,

epidermis and dermis) fit the distribution in the microscopic image when compared side by side.

The CLS analysis has more difficulties to correctly map the distribution of the SC. In Figure 46, the obtained scores are distributed not only on the skin surface, but also scattered on the hair and on the deepest region of the hair follicle (left side in Figure 46). The SC is correctly marked in the infundibulum and external SC. After the infundibulum, the scores of the SC are rather discontinuous and less intense in both cryosections. One possible explanation could be that whereas in the upper infundibulum the epitelious is covered by intact SC, the barrier of the lower infundibulum is interrupted as the differential patter switches from epidermal to tricholemmal differentiation[22]. Therefore, the collected spectra in these regions are gradually changing to more “epidermis-like” features. The SC scores are also plotted broadly nearby the cryospray drops, in the deeper area of the mapped area. It should be remarked, that in this area also other components are not well allocated. The scores of hair, SC and glass are mapped in this region but none of these components are observed nearby in the microscopic image. Therefore, it seems that the cryospray drops may interfere the measurements, clogging up the correct component identification in this area. The caffeine is observed mainly surrounding the upper part of the hair in the image but also accumulated in the SC of the outer part of the follicle. It should be noted that the hair follicle was applied with a caffeine solution in water. Hereby, the absence of permeation enhancer in the formulation would suggest that caffeine will have strong difficulties to go through the skin or the hair follicle. Therefore no significant amounts of caffeine are expected in the deeper layers of the skin.

On the other hand, in the Caf-NP treated hair follicle Figure 47 the epidermis and dermis are well assigned. The SC is also distributed near the infundibulum and the skin surface. Nevertheless, some areas are difficult to interpret, especially on the upper-left side of the image. No considerable amounts of caffeine are detected surrounding the hair, the main caffeine contributions are located in the formulation drop on the right side of the image.

Multivariate Curve Resolution-Alternating Least Squares (MCR-ALS)

The same areas analyzed by CLS are also analyzed with MCR-ALS. The resulting caffeine scores are plotted in red superimposed to their respective acquired microscopic images (Figure 48 and Figure 49). The spectrums of glass, dermis, epidermis, SC, hair, caffeine and cryospray drops were employed as starting estimates for the calculations.

When the caffeine scores of the Figure 48 are examined, similar conclusions concerning the caffeine distribution are observed comparing to the CLS scores. The caffeine scores for the MCR-ALS analysis show that the caffeine is mostly allocated surrounding the outer part of the hair. Also the caffeine is distributed near the upper infundibulum and the outermost SC from the skin surface. Moreover the diffusion of caffeine from the SC to the deeper layers of the dermis can be observed. In regards to the caffeine scores nearby the cryospray drops this area showed previous misidentification therefore they can be considered as artifacts.

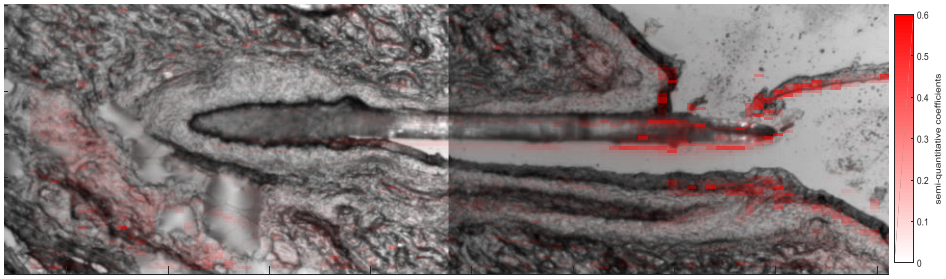

Figure 48. MCR-ALS scores for caffeine (red) in the Caf-Aq treated hair follicle, overlaid on 2 subsequently recorded stitched microscopic images with 10× magnification.

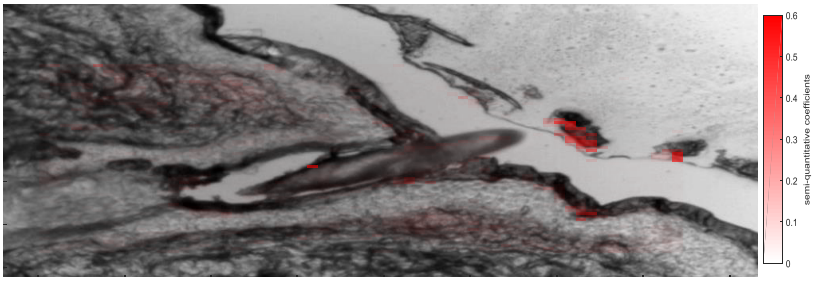

Figure 49. MCR-ALS scores for caffeine (red) in the Caf-NP treated hair follicle

Relating to Figure 49, the higher values of MCR-ALS caffeine scores are distributed in the formulation drop and in one thinly area from the stratum corneum. These caffeine scores distribution is also coincident with the scores obtained in the CLS analysis.

To sum up, different spectroscopic analysis to study caffeine's distribution into the hair follicle when vehiculized in two different formulations were applied. Cross sections of the tissue were mapped and analyzed with CRM. CLS and MCR-ALS analysis give to a similar distribution of caffeine into the hair follicle with much better resolution than peak fitting. Both methodologies seemed to be useful when the active and the skin bands are overlapped. Nevertheless, the spectroscopic analysis should be further studied to ensure that the resulting distribution is linked only to the active and not to areas with noise or higher fluorescence.

The work from section 5.4.2 was carried out during a 8 month stay in the "Center of Experimental and Applied Cutaneous Physiology" leaded by Prof. Jürgen Lademann in the Universitätsmedizin of Berlin

One publication related with confocal Raman microscopy entitled "Surface determination of 3D confocal Raman microscopy imaging of the skin" was published in the Laser Physics Letters (Annex 8)

CONCLUSIONS

6. CONCLUSIONS

- The selected ***in silico* methods** (Potts and Guy, Mitragotri and Barratt) predicted the permeability constant ($\log K_p$) of the substances, taking into account their respective physico-chemical properties. In general, lower Kp values were obtained using the Barrat model for the compounds with higher melting points. However, all the models agreed that tazarotene had the highest permeability and that eflornithine had the poorest permeability mainly based on their lipophilic properties

- The *in vitro* assay **Skin-PAMPA** with artificial membranes was performed with 23 actives using aqueous buffer at pH 5.5 or propylene glycol. When the buffer was employed, the actives showed a high range of permeability constant (from -10 to -5), which diminishes (from -9 to -7) when the substances are vehiculated in propylene glycol. This solvent, which is well known as a skin enhancer, modulates permeability by increasing the permeability of compounds with poor permeability and diminishing the permeability of actives with high permeability.

- Percutaneous absorption with **pig skin on Franz diffusion cells** was performed on 10 actives and the commercial creams of five of them. The active amounts in the different skin strata (Stratum Corneum, epidermis and dermis) and the receptor fluid were determined. Distribution of compounds was in general found to decrease when going in depth through the skin.

- The five **creams** evaluated tend to decrease the **permeability**, with lower amounts of active in all the skin layers (SC, E and D), but maintaining the compound distribution in the different strata. Results indicate that, in general, creams have lower permeation rates than PG solutions alone.

- The **role of the formulation** in skin penetration and retention of compounds was studied in depth with three corticoids formulated in propylene glycol, and commercial creams and ointments. The influence of PG on the maximum amounts of analyte in the SC and E and similar amounts in the D for PG and ointments with a much lower level of creams was found. This suggests the relevance of the solvent drag effect in skin delivery for the tested actives.

- **Correlations between permeation models** indicate very poor results. Linear correlations between the two Pampa lists of values and the three *in silico* models were very low. However, the results of the skin-PAMPA assay at pH 5.5 and the amount of the compound in the epidermis and dermis of the Franz cell data of the cream formulations were better correlated. This correlation indicates the

effectiveness of the two *in vitro* assays at assessing the formulation and the detrimental effect of propylene glycol.

— Structural lipid modification due to **propylene glycol** used on formulations was performed by **ATR-IR.** Epidermis and dermis were found to be modified not only altering the lipidic order of the bilayer structure but also changing the C-O band attributed to phospholipids, glycerides and esthers. This could be one of the reasons of the poor correlation between permeation methodologies when actives are formulated with PG.

— **Lanolin** was added to **synthetic membranes** to mimic the lipids from the skin for permeation studies. Their highly lipidic order as an orthorhombic structure significantly reduces the TEWL values, similar to the porcine skin levels. Besides a modulation of the permeation of three different compounds, were similar to those obtained with the skin. In conclusion, combining synthetic membranes with lanolin may be a useful approach to mimic the absorption of topical actives.

— Percutaneous penetration of resveratrol was also determined by ***in vivo* stripping**, based on the successive extraction of the SC layers by consecutive stripping with adhesive tapes. A good correlation was obtained with the use of pig skin with Franz diffusion cells.

— **Confocal Raman Spectroscopy** was optimized to determine the skin penetration of Caffeine. A quantitative analyses was achieved until 35µm depth at the epidermis. Moreover the mapping methodologies for caffeine distribution shows the allocation of the active surrounding the outer part of the hair with much better map distribution using MCR-ALS and CLS calculations. Nevertheless further studies should be carried out to optimize caffeine detection and avoid interferences.

Summarizing, the *in silico* models gives only a rough idea about actives penetration. The Skin-PAMPA needs an improvement of the lipidic membrane, therefore an approach was suggested with the use of lanolines. The influence of vehicles on skin penetration was determined with Franz diffusion cells with pig skin and the lipid skin modification of propylene glycol was demonstrated with µFTIR. Results of all these methodologies were combined with a poor correlation between them. However, the *in vivo* stripping approach was successfully correlated with the Franz diffusion cells one. Quantitative permeation determination and mapping resolution obtained by CRM provides further confidence to study drug disposition directly on the skin.

BIBLIOGRAPHY

7. BIBLIOGRAPHY

1. Narishetty, S. T. K.; Panchagnula, R. Transdermal delivery of zidovudine: Effect of terpenes and their mechanism of action. *J. Control. Release* **2004**, *95*, 367–379, doi:10.1016/j.jconrel.2003.11.022.

2. Moody, R. P.; Nadeau, B.; Chu, I. In vitro dermal absorption of pesticides: VI. In vivo and in vitro comparison of the organochlorine insecticide DDT in rat, guinea pig, pig, human and tissue-cultured skin. *Toxicol. In Vitro* **1994**, *8*, 1225–1232.

3. Scott, R. C.; Batten, P. L.; Clowes, H. M.; Jones, B. K.; Ramsey, J. D. Further validation of an in Vitro method to reduce the need for in Vivo studies for measuring the absorption of chemicals through rat skin. *Toxicol. Sci.* **1992**, *19*, 484–492, doi:10.1093/toxsci/19.4.484.

4. Wong, R.; Geyer, S.; Weninger, W.; Guimberteau, J. C.; Wong, J. K. The dynamic anatomy and patterning of skin. *Exp. Dermatol.* **2016**, *25*, 92–98, doi:10.1111/exd.12832.

5. Trommer, H.; Neubert, R. H. H. Overcoming the stratum corneum: the modulation of skin penetration. A review. *Skin Pharmacol. Physiol.* **2006**, *19*, 106–21, doi:10.1159/000091978.

6. Mathes, S. H.; Ruffner, H.; Graf-Hausner, U. The use of skin models in drug development. *Adv. Drug Deliv. Rev.* 2014, *69–70*, 81–102.

7. Law, S.; Wertz, P. W.; Swartzendruber, D. C.; Squier, C. A. Regional variation in content, composition and organization of porcine epithelial barrier lipids revealed by thin-layer chromatography and transmission electron microscopy. *Arch. Oral Biol.* **1995**, *40*, 1085–1091, doi:10.1016/0003-9969(95)00091-7.

8. Madison, K. C. Barrier Function of the Skin: ‘"La Raison d”Etre" of the Epidermis. *J. Invest. Dermatol.* **2003**, *121*, 231–241, doi:10.1046/j.1523-1747.2003.12359.x.

9. Kessner, D.; Ruettinger, A.; Kiselev, M. A.; Wartewig, S.; Neubert, R. H. H. Properties of ceramides and their impact on the stratum corneum structure: A review - Part 2: Stratum corneum lipid model systems. *Skin Pharmacol. Physiol.* 2008, *21*, 58–74.

10. Bouwstra, J.; Pilgram, G.; Gooris, G.; Koerten, H.; Ponec, M. New aspects of the skin barrier organization. *Skin Pharmacol. Appl. Skin Physiol.* **2001**, *14 Suppl 1*, 52–62, doi:10.1159/000056391.

11. Madison, K. C.; Swartzendruber, D. C.; Wertz, P. W.; Downing, D. T. Presence of Intact Intercellular Lipid Lamellae in the Upper Layers of the Stratum Corneum. *J. Invest. Dermatol.* **1987**, *88*, 714–718, doi:10.1111/1523-1747.ep12470386.

12. Groen, D.; Gooris, G. S.; Bouwstra, J. A. New insights into the stratum corneum lipid organization by X-ray diffraction analysis. *Biophys. J.* **2009**, *97*, 2242–2249, doi:10.1016/j.bpj.2009.07.040.

13. Damien, F.; Boncheva, M. The extent of orthorhombic lipid phases in the stratum corneum determines the barrier efficiency of human skin in vivo. *J. Invest. Dermatol.* 2010, *130*, 611–614.

14. Pilgram, G. S. K.; Engelsma-Van Pelt, A. M.; Bouwstra, J. A.; Koerten, H. K. Electron diffraction provides new information on human stratum corneum lipid organization studied in relation to depth and temperature. *J. Invest. Dermatol.* **1999**, *113*, 403–409, doi:10.1046/j.1523-1747.1999.00706.x.

15. de Jager, M. .; Gooris, G. .; Dolbnya, I. .; Bras, W.; Ponec, M.; Bouwstra, J. . The phase behaviour of skin lipid mixtures based on synthetic ceramides. *Chem. Phys. Lipids* **2003**, *124*, 123–134, doi:10.1016/S0009-3084(03)00050-1.

16. Janssens, M.; van Smeden, J.; Gooris, G. S.; Bras, W.; Portale, G.; Caspers, P. J.; Vreeken, R. J.; Hankemeier, T.; Kezic, S.; Wolterbeek, R.; Lavrijsen, A. P.; Bouwstra, J. A. Increase in short-chain ceramides correlates with an altered lipid organization and decreased barrier function in atopic eczema patients. *J. Lipid Res.* **2012**, *53*, 2755–2766, doi:10.1194/jlr.P030338.

17. van Smeden, J.; Janssens, M.; Kaye, E. C.; Caspers, P. J.; Lavrijsen, A. P.; Vreeken, R. J.; Bouwstra, J. A. The importance of free fatty acid chain length for the skin barrier function in atopic eczema patients. *Exp.Dermatol.* **2014**, *23*, 45–52.

18. Ishikawa, J.; Narita, H.; Kondo, N.; Hotta, M.; Takagi, Y.; Masukawa, Y.; Kitahara, T.; Takema, Y.; Koyano, S.; Yamazaki, S.; Hatamochi, A. Changes in the ceramide profile of atopic dermatitis patients. *J. Invest. Dermatol.* 2010, *130*, 2511–2514.

19. Yang, L.; Mao-Qiang, M.; Taljebini, M.; Elias, P. M.; Feingold, K. R. Topical stratum corneum lipids accelerate barrier repair after tape stripping, solvent treatment and some but not all types of detergent treatment. *Br. J. Dermatol.* **1995**, *133*, 679–85, doi:10.1111/j.1365-2133.1995.tb02738.x.

20. Larese Filon, F.; Mauro, M.; Adami, G.; Bovenzi, M.; Crosera, M. Nanoparticles skin absorption: New aspects for a safety profile evaluation. *Regul. Toxicol. Pharmacol.* 2015, *72*, 310–322.

21. Lademann, J.; Knorr, F.; Richter, H.; Blume-Peytavi, U.; Vogt, A.; Antoniou, C.; Sterry, W.; Patzelt, A. Hair follicles--an efficient storage and penetration pathway for topically applied substances. Summary of recent results obtained at the Center of Experimental and Applied Cutaneous Physiology, Charite -Universitatsmedizin Berlin, Germany. *Skin Pharmacol. Physiol.* **2008**, *21*, 150–155, doi:10.1159/000131079.

22. Blume-Peytavi, U.; Vogt, A. Human hair follicle: Reservoir function and selective targeting. *Br. J. Dermatol.* 2011, *165*, 13–17.

23. Jacobi, U.; Kaiser, M.; Toll, R.; Mangelsdorf, S.; Audring, H.; Otberg, N.; Sterry, W.; Lademann, J. Porcine ear skin: an in vitro model for human skin. *Ski. Res Technol* **2007**, *13*, 19–24, doi:10.1111/j.1600-0846.2006.00179.x.

24. Lademann, J.; Richter, H.; Schaefer, U. F.; Blume-Peytavi, U.; Teichmann, A.; Otberg, N.; Sterry, W. Hair follicles - A long-term reservoir for drug delivery. *Skin Pharmacol. Physiol.* **2006**, *19*, 232–236, doi:10.1159/000093119.

25. Alvarez-Román, R.; Naik, A.; Kalia, Y. N.; Guy, R. H.; Fessi, H. Skin penetration and distribution of polymeric nanoparticles. *J. Control. Release* **2004**, *99*, 53–62, doi:10.1016/j.jconrel.2004.06.015.

26. Samaras, E. G.; Riviere, J. E.; Ghafourian, T. The effect of formulations and experimental conditions on in vitro human skin permeation - Data from updated EDETOX database. *Int. J. Pharm.* 2012, *434*, 280–291.

27. Narishetty, S. T. K.; Panchagnula, R. Transdermal delivery system for zidovudine: in vitro, ex vivo and in vivo evaluation. *Biopharm. Drug Dispos.* **2004**, *25*, 9–20, doi:10.1002/bdd.381.

28. Yu, X. Z.; Jin, X. P.; Yin, L.; Shen, G. Z.; Lin, H. F.; Wang, Y. L. Influence of in vitro methods, receptor fluids on percutaneous absorption and validation of a novel in vitro method. *Biomed. Environ. Sci.* **1994**, *7*, 248–258.

29. Carmichael, N. European Centre for Ecotoxicology and Toxicology of Chemicals. In *Encyclopedia of Toxicology: Third Edition*; 2014; pp. 547–548 ISBN 9780123864543.

30. Howes, D.; Guy, R.; Hadgraft, J.; Heylings, J.; Hoeck, U.; Kemper, F.; Maibach, H.; Marty, J. P.; Merk, H.; Parra, J.; Rekkas, D.; Rondelli, I.; Schaefer, H.; Täuber, U.; Verbiese, N. Methods for Assessing

Percutaneous Absorption the Report and Recommendations of ECVAM Workshop 13. In *ATLA Alternatives to Laboratory Animals*; 1996; Vol. 24, pp. 81–106.

31. Maibach, H. Dermatological formulations: Percutaneous absorption. By Brian W. Barry. Marcel Dekker, 270 Madison Avenue, New York, NY 10016. 1983. 479 pp. 16 × 23.5 cm. Price $55.00 (2070 higher outside the US. and Canada). *J. Pharm. Sci.* **1984**, *73*, 573–573, doi:10.1002/jps.2600730442.

32. Fitzpatrick, D.; Corish, J.; Hayes, B. Modelling skin permeability in risk assessment--the future. *Chemosphere* **2004**, *55*, 1309–14, doi:10.1016/j.chemosphere.2003.11.051.

33. Flynn *Principles of Route-toRoute Extrapolation for Risk Assessment*; Elsevier B.V.: Amsterdam, 1990;

34. Wilschut, A.; ten Berge, W. F.; Robinson, P. J.; McKone, T. E. Estimating skin permeation. The validation of five mathematical skin permeation models. *Chemosphere* **1995**, *30*, 1275–1296.

35. Abraham, M. H.; Martins, F.; Mitchell, R. C. Algorithms for skin permeability using hydrogen bond descriptors: the problem of steroids. *J. Pharm. Pharmacol.* **1997**, *49*, 858–865.

36. Anderson, B. D.; Higuchi, W. I.; Raykar, P. V Herterogeneity Effects of permeability-partition coefficient relationships in human stratum corneum. *Pharm. Res.* **1988**, 566.

37. Potts, R. O.; Guy, R. H. Predicting skin permeability. *Pharm Res* **1992**, *9*, 663–669.

38. Mitragotri, S. A theoretical analysis of permeation of small hydrophobic solutes across the stratum corneum based on Scaled Particle Theory. *J Pharm Sci* **2002**, *91*, 744–752.

39. Lian, G.; Chen, L.; Han, L. An evaluation of mathematical models for predicting skin permeability. *J Pharm Sci* **2008**, *97*, 584–598, doi:10.1002/jps.21074.

40. Barratt, M. D. Quantitative structure-activity relationships for skin permeability. *Toxicol Vitr.* **1995**, *9*, 27–37.

41. Potts, R. O.; Guy, R. H. A predictive algorithm for skin permeability: the effects of molecular size and hydrogen bond activity. *Pharm. Res.* **1995**, *12*, 1628–1633.

42. Toropov, A. A.; Toropova, A. P.; Cappellini, L.; Benfenati, E.; Davoli, E. QSPR analysis of threshold of odor for the large number of heterogenic chemicals. *Mol. Divers.* **2017**, doi:10.1007/s11030-017-9800-5.

43. Abd, E.; Yousef, S. A.; Pastore, M. N.; Telaprolu, K.; Mohammed, Y. H.; Namjoshi, S.; Grice, J. E.; Roberts, M. S. Skin models for the testing of transdermal drugs. *Clin. Pharmacol. Adv. Appl.* 2016, *8*, 163–176.

44. Waters, L. J. Recent developments in skin mimic systems to predict transdermal permeation. *Curr. Pharm. Des.* **2015**, *21*, 2725–2732, doi:10.2174/1381612821666150428124733.

45. CDER Semisolid Dosage Forms Scale-Up and Postapproval Changes: Chemistry, Manufacturing, and Controls; In Vitro Release Testing and In Vivo Bioequivalence Documentation Available online: https://www.fda.gov/downloads/drugs/guidances/ucm070930.pdf.

46. Epa Dermal Exposure Assessment : Principles and applications. **1992**, 1–388.

47. Gray, G. M.; Yardley, H. J. Lipid compositions of cells isolated from pig, human, and rat epidermis. *J. Lipid Res.* **1975**, *16*, 434–440.

48. Wester, R. C.; Melendres, J.; Sedik, L.; Maibach, H.; Riviere, J. E. Percutaneous absorption of salicylic acid, theophylline, 2, 4-dimethylamine, diethyl hexyl phthalic acid, and p-aminobenzoic acid in the isolated perfused porcine skin flap compared to man in vivo. *Toxicol Appl Pharmacol* **1998**, *151*, 159–165, doi:10.1006/taap.1998.8434.

49. Wester, R. C.; Maibach, H. I. In vivo methods for percutaneous absorption measurements. *J. Toxicol. - Cutan. Ocul. Toxicol.* 2001, *20*, 411–422.

50. Choe, C.; Lademann, J.; Darvin, M. E. Analysis of Human and Porcine Skin in vivo/ex vivo for Penetration of Selected Oils by Confocal Raman Microscopy. *Skin Pharmacol. Physiol.* **2015**, *28*, 318–330, doi:10.1159/000439407.

51. Kong, R.; Bhargava, R. Characterization of porcine skin as a model for human skin studies using infrared spectroscopic imaging. *Analyst* **2011**, *136*, 2359, doi:10.1039/c1an15111h.

52. Zhu, Y.; Choe, C.-S.; Ahlberg, S.; Meinke, M. C.; Alexiev, U.; Lademann, J.; Darvin, M. E. Penetration of silver nanoparticles into porcine skin ex vivo using fluorescence lifetime imaging microscopy, Raman microscopy, and surface-enhanced Raman scattering microscopy. *J. Biomed. Opt.* **2015**, *20*, 51006-1–8, doi:10.1117/1.JBO.20.5.051006.

53. Lademann, J.; Richter, H.; Meinke, M.; Sterry, W.; Patzelt, A. Which skin model is the most appropriate for the investigation of topically applied substances into the hair follicles? *Skin Pharmacol. Physiol.* 2010, *23*, 47–52.

54. Dick, I. P.; Scott, R. C. Pig ear skin as an in-vitro model for human skin permeability. *J Pharm Pharmacol* **1992**, *44*, 640–645, doi:10.1111/j.2042-7158.1992.tb05485.x.

55. Singh, S.; Zhao, K.; Singh, J. In vitro permeability and binding of hydrocarbons in pig ear and human abdominal skin. *Drug Chem. Toxicol.* **2002**, *25*, 83–92, doi:10.1081/DCT-100108474.

56. Sato, K.; Sugibayashi, K.; Morimoto, Y. Species differences in percutaneous absorption of nicorandil. *J. Pharm. Sci.* **1991**, *80*, 104–107, doi:10.1002/jps.2600800203.

57. Landmann, L. The epidermal permeability barrier. Comparison between in vivo and in vitro lipid structures. *Eur. J. Cell Biol.* **1984**, *33*, 258–264.

58. Ghonaim, H. M.; Periasamy, N.; Noro, M. G.; Anwar, J. Towards a simplified model membrane of skin lipids: Preparation and characterisation of a ternary lipid mixture. *Int. J. Pharm. Pharm. Sci.* **2014**, *6*, 148–152.

59. Haq, A.; Dorrani, M.; Goodyear, B.; Joshi, V.; Michniak-Kohn, B. Membrane properties for permeability testing: Skin versus synthetic membranes. *Int. J. Pharm.* **2018**, *539*, 58–64, doi:10.1016/j.ijpharm.2018.01.029.

60. Ottaviani, G.; Martel, S.; Carrupt, P.-A. Parallel artificial membrane permeability assay: a new membrane for the fast prediction of passive human skin permeability. *J. Med. Chem.* **2006**, *49*, 3948–3954, doi:10.1021/jm060230+.

61. Mensch, J.; Melis, A.; Mackie, C.; Verreck, G.; Brewster, M. E.; Augustijns, P. Evaluation of various PAMPA models to identify the most discriminating method for the prediction of BBB permeability. *Eur. J. Pharm. Biopharm.* **2010**, *74*, 495–502, doi:10.1016/j.ejpb.2010.01.003.

62. Markovic, B. D.; Vladimirov, S. M.; Cudina, O. a.; Odovic, J. V.; Karljikovic-Rajic, K. D. A PAMPA assay as fast predictive model of passive human skin permeability of new synthesized corticosteroid C-21 esters. *Molecules* **2012**, *17*, 480–491, doi:10.3390/molecules17010480.

63. Chen, M. L.; Shah, V.; Patnaik, R.; Adams, W.; Hussain, A.; Conner, D.; Mehta, M.; Malinowski, H.;

Lazor, J.; Huang, S. M.; Hare, D.; Lesko, L.; Sporn, D.; Williams, R. Bioavailability and bioequivalence: An FDA regulatory overview. *Pharm. Res.* 2001, *18*, 1645–1650.

64. Raney, S. G.; Franz, T. J.; Lehman, P. A.; Lionberger, R.; Chen, M. L. Pharmacokinetics-Based Approaches for Bioequivalence Evaluation of Topical Dermatological Drug Products. *Clin. Pharmacokinet.* 2015, *54*, 1095–1106.

65. Pershing, L. K.; Silver, B. S.; Krueger, G. G.; Shah, V. P.; Skelley, J. P. Feasibility of Measuring the Bioavailability of Topical Betamethasone Dipropionate in Commercial Formulations Using Drug Content in Skin and a Skin Blanching Bioassay. *Pharm. Res. An Off. J. Am. Assoc. Pharm. Sci.* **1992**, *9*, 45–51, doi:10.1023/A:1018975626210.

66. Pershing, L. K.; Corlett, J.; Jorgensen, C. In vivo pharmacokinetics and pharmacodynamics of topical ketoconazole and miconazole in human stratum corneum. *Antimicrob Agents Chemother* **1994**, *38*, 90–95.

67. Pershing, L. K.; Bakhtian, S.; Poncelet, C. E.; Corlett, J. L.; Shah, V. P. Comparison of skin stripping, in vitro release, and skin blanching response methods to measure dose response and similarity of triamcinolone acetonide cream strengths from two manufactured sources. *J. Pharm. Sci.* **2002**, *91*, 1312–1323, doi:10.1002/jps.10147.

68. Au, W. L.; Skinner, M.; Kanfer, I. Comparison of tape stripping with the human skin blanching assay for the bioequivalence assessment of topical clobetasol propionate formulations. *J. Pharm. Pharm. Sci.* **2010**, *13*, 11–20.

69. Swain, R. J.; Stevens, M. M. Raman microspectroscopy for non-invasive biochemical analysis of single cells. *Biochem. Soc. Trans.* **2007**, *35*, 544–549, doi:10.1042/BST0350544.

70. Ellis, D. I.; Goodacre, R. Metabolic fingerprinting in disease diagnosis: biomedical applications of infrared and Raman spectroscopy. *Analyst* **2006**, *131*, 875, doi:10.1039/b602376m.

71. Krafft, C.; Sergo, V. Biomedical applications of Raman and infrared spectroscopy to diagnose tissues. *Spectroscopy* **2006**, *20*, 195–218, doi:10.1155/2006/738186.

72. Sulé-Suso, J.; Forsyth, N. R.; Untereiner, V.; Sockalingum, G. D. Vibrational spectroscopy in stem cell characterisation: Is there a niche? *Trends Biotechnol.* 2014, *32*, 254–262.

73. Falcone, D.; Uzunbajakava, N. E.; Varghese, B.; De Aquino Santos, G. R.; Richters, R. J. H.; Van De Kerkhof, P. C. M.; Van Erp, P. E. J. Microspectroscopic Confocal Raman and Macroscopic Biophysical Measurements in the in vivo Assessment of the Skin Barrier: Perspective for Dermatology and Cosmetic Sciences. *Skin Pharmacol. Physiol.* 2015, *28*, 307–317.

74. Dumas, P.; Miller, L. The use of synchrotron infrared microspectroscopy in biological and biomedical investigations. In *Vibrational Spectroscopy*; 2003; Vol. 32, pp. 3–21.

75. Cotte, M.; Dumas, P.; Besnard, M.; Tchoreloff, P.; Walter, P. Synchrotron FT-IR microscopic study of chemical enhancers in transdermal drug delivery: Example of fatty acids. *J. Control. Release* **2004**, *97*, 269–281, doi:10.1016/j.jconrel.2004.03.014.

76. Vyumvuhore, R.; Tfayli, A.; Manfait, M.; Baillet-Guffroy, A. Vibrational spectroscopy coupled to classical least square analysis, a new approach for determination of skin moisturizing agents' mechanisms. *Ski. Res. Technol.* **2014**, *20*, 282–292, doi:10.1111/srt.12117.

77. Jaumot, J.; de Juan, A.; Tauler, R. MCR-ALS GUI 2.0: New features and applications. *Chemom. Intell. Lab. Syst.* **2015**, *140*, 1–12, doi:10.1016/j.chemolab.2014.10.003.

78. Felten, J.; Hall, H.; Jaumot, J.; Tauler, R.; De Juan, A.; Gorzsás, A. Vibrational spectroscopic image

analysis of biological material using multivariate curve resolution-alternating least squares (MCR-ALS). *Nat. Protoc.* **2015**, *10*, 217–240, doi:10.1038/nprot.2015.008.

79. Bonnist, E. Y. M.; Gorce, J. P.; MacKay, C.; Pendlington, R. U.; Pudney, P. D. A. Measuring the penetration of a skin sensitizer and its delivery vehicles simultaneously with confocal raman spectroscopy. *Skin Pharmacol. Physiol.* **2011**, *24*, 274–283, doi:10.1159/000328729.

80. Tres, F.; Treacher, K.; Booth, J.; Hughes, L. P.; Wren, S. A. C.; Aylott, J. W.; Burley, J. C. Real time Raman imaging to understand dissolution performance of amorphous solid dispersions. *J. Control. Release* **2014**, *188*, 53–60, doi:10.1016/j.jconrel.2014.05.061.

81. Veselinović, A. M.; Nikolić, R. S.; Nikolić, G. M. Application of multivariate curve resolution-alternating least squares (MCR-ALS) for resolving pyrogallol autoxidation in weakly alkaline aqueous solutions. *Cent. Eur. J. Chem.* **2012**, *10*, 1942–1948, doi:10.2478/s11532-012-0125-z.

82. Ando, M.; Hamaguchi, H. Molecular component distribution imaging of living cells by multivariate curve resolution analysis of space-resolved Raman spectra. *J. Biomed. Opt.* **2013**, *19*, 11016, doi:10.1117/1.JBO.19.1.011016.

83. Noothalapati, H.; Sasaki, T.; Kaino, T.; Kawamukai, M.; Ando, M.; Hamaguchi, H.; Yamamoto, T. Label-free Chemical Imaging of Fungal Spore Walls by Raman Microscopy and Multivariate Curve Resolution Analysis. *Nat. Publ. Gr.* **2016**, *6*, 27789, doi:10.1038/srep27789.

84. Oecd Guidance document for the conduct of skin absorption studies. *Env / Jm / Mono* **2004**, 1–31, doi:10.1787/9789264078796-en.

85. European Commission THE SCCS NOTES OF GUIDANCE FOR THE TESTING OF COSMETIC INGREDIENTS. *SCCS* **2016**, *1564*, 151, doi:10.2772/47128.

86. Schaefer, H.; Redelmeier, T. E.; Schaefer, H.; Redelmeier, T. E. *Skin barrier: Principles of percutaneous absorption*; 1996; ISBN 3-8055-6326-4.

87. Bronaugh, R. L.; Stewart, R. F.; Congdon, E. R. Methods for in vitro percutaneous absorption studies II. Animal models for human skin. *Toxicol. Appl. Pharmacol.* **1982**, *62*, 481–488, doi:10.1016/0041-008X(82)90149-1.

88. Wooldryscouring (WDS) - Eco-Efficient Dry Wool Scouring with total by-products recovery Available online: http://ec.europa.eu/environment/life/project/Projects/index.cfm?fuseaction=search.dspPage&n_proj_id=4254#RM.

89. Pullmannová, P.; Pavlíková, L.; Kováčik, A.; Sochorová, M.; Školová, B.; Slepička, P.; Maixner, J.; Zbytovská, J.; Vávrová, K. Permeability and microstructure of model stratum corneum lipid membranes containing ceramides with long (C16) and very long (C24) acyl chains. *Biophys. Chem.* **2017**, *224*, 20–31, doi:10.1016/j.bpc.2017.03.004.

90. GOLDSMITH, L. A.; KATZ, S. I.; GILCHREST, B. A.; PALLER, A. S.; LEFFELL, D. J.; WOLFF, K. Fitzpatrick's Dermatology in General Medicine Eighth Edition. *McGraw-Hill* **2012**, *150*, 22, doi:10.1017/CBO9781107415324.004.

91. Rougier, A.; Dupuis, D.; Lotte, C.; Roguet, R.; Schaefer, H. In vivo correlation between stratum corneum reservoir function and percutaneous absorption. *J. Invest. Dermatol.* **1983**, *81*, 275–278, doi:10.1111/1523-1747.ep12518298.

92. Lademann, J.; Jacobi, U.; Surber, C.; Weigmann, H.-J.; Fluhr, J. W. The tape stripping procedure – evaluation of some critical parameters. *Eur. J. Pharm. Biopharm.* **2009**, *72*, 317–323, doi:10.1016/j.ejpb.2008.08.008.

93. Ich ICH Topic Q2 (R1) Validation of Analytical Procedures : Text and Methodology. *Int. Conf. Harmon.* **2005**, *1994*, 17, doi:http://www.ich.org/fileadmin/Public_Web_Site/ICH_Products/Guidelines/Quality/Q2_R1/Step4/Q2_R1__Guideline.pdf.

94. Franzen, L.; Windbergs, M. Applications of Raman spectroscopy in skin research - From skin physiology and diagnosis up to risk assessment and dermal drug delivery. *Adv. Drug Deliv. Rev.* 2015, *89*, 91–104.

95. Franzen, L.; Mathes, C.; Hansen, S.; Windbergs, M. Advanced chemical imaging and comparison of human and porcine hair follicles for drug delivery by confocal Raman microscopy. *J. Biomed. Opt.* **2013**, *18*, 61210, doi:10.1117/1.JBO.18.6.061210.

96. Jaumot, J.; Gargallo, R.; De Juan, A.; Tauler, R. A graphical user-friendly interface for MCR-ALS: A new tool for multivariate curve resolution in MATLAB. *Chemom. Intell. Lab. Syst.* **2005**, *76*, 101–110, doi:10.1016/j.chemolab.2004.12.007.

97. Vajna, B.; Patyi, G.; Nagy, Z.; Bódis, A.; Farkas, A.; Marosi, G. Comparison of chemometric methods in the analysis of pharmaceuticals with hyperspectral Raman imaging. *J. Raman Spectrosc.* **2011**, *42*, 1977–1986, doi:10.1002/jrs.2943.

98. Benseny-Cases, N.; Álvarez-Marimon, E.; Castillo-Michel, H.; Cotte, M.; Falcon, C.; Cladera, J. Synchrotron-Based Fourier Transform Infrared Microspectroscopy (μFTIR) Study on the Effect of Alzheimer's Aβ Amorphous and Fibrillar Aggregates on PC12 Cells. *Anal. Chem.* **2018**, *90*, 2772–2779, doi:10.1021/acs.analchem.7b04818.

99. Menter, A. Pharmacokinetics and safety of tazarotene. *J. Am. Acad. Dermatol.* **2000**, *43*, S31–S35, doi:10.1067/mjd.2000.108321.

100. Lazar, A.; Lenkey, N.; Pesti, K.; Fodor, L.; Mike, A. Different pH-sensitivity patterns of 30 sodium channel inhibitors suggest chemically different pools along the access pathway. *Front. Pharmacol.* **2015**, *6*, doi:10.3389/fphar.2015.00210.

101. Williams, A. C.; Barry, B. W. Penetration enhancers. *Adv. Drug Deliv. Rev.* **2012**, *64*, 128–137, doi:10.1016/j.addr.2012.09.032.

102. Tsakovska, I.; Pajeva, I.; Al Sharif, M.; Alov, P.; Fioravanzo, E.; Kovarich, S.; Worth, A. P.; Richarz, A. N.; Yang, C.; Mostrag-Szlichtyng, A.; Cronin, M. T. D. Quantitative structure-skin permeability relationships. *Toxicology* **2017**, *387*, 27–42, doi:10.1016/j.tox.2017.06.008.

103. Ponec, M.; Polano, M. K. Penetration of various corticosteroids through epidermis in vitro. *Arch. Dermatol. Res.* **1979**, *265*, 101–104, doi:10.1007/BF00412706.

104. Korting, H. C.; Kerscher, M. J.; Schafer-Korting, M. Topical glucocorticoids with improved benefit/risk ratio: do they exist? *J. Am. Acad. Dermatol.* **1992**, *27*, 87–92, doi:10.2165/00002018-199614060-00003.

105. Ponec, M.; Kempenaar, J. A. Biphasic entry of glucocorticoids into cultured human skin keratinocytes and fibroblasts. *Arch. Dermatol. Res.* **1983**, *275*, 334–344.

106. Cross, S. E.; Magnusson, B. M.; Winckle, G.; Anissimov, Y.; Roberts, M. S. Determination of the effect of lipophilicity on the in vitro permeability and tissue reservoir characteristics of topically applied solutes in human skin layers. *J. Invest. Dermatol.* **2003**, *120*, 759–764, doi:10.1046/j.1523-1747.2003.12131.x.

107. Caron, D.; Queille-Roussel, C.; Shah, V. P.; Schaefer, H. Correlation between the drug penetration and the blanching effect of topically applied hydrocortisone creams in human beings. *J. Am. Acad.*

Dermatol. **1990**, *23*, 458–462, doi:10.1016/0190-9622(90)70240-I.

108. Stoughton, R. B. Are generic formulations equivalent to trade name topical glucocorticoids? *Arch. Dermatol.* **1987**, *123*, 1312–4, doi:10.1001/archderm.1987.01660340074023.

109. Noon, J. P.; Evans, C. E.; Haynes, W. G.; Webb, D. J.; Walker, B. R. A comparison of techniques to assess skin blanching following the topical application of glucocorticoids. *Br. J. Dermatol.* **1996**, *134*, 837–42, doi:10.1046/j.1365-2133.1996.114849.x.

110. Mitra, A.; Wu, Y. Topical delivery for the treatment of psoriasis. *Expert Opin. Drug Deliv.* **2010**, *7*, 977–992, doi:10.1517/17425247.2010.503953.

111. Moser, K.; Kriwet, K.; Naik, A.; Kalia, Y. N.; Guy, R. H. Passive skin penetration enhancement and its quantification in vitro. *Eur. J. Pharm. Biopharm.* 2001, *52*, 103–112.

112. Ponec, M.; Kempenaar, A.; De Kloet, E. R. Corticoids and cultured human epidermal keratinocytes: Specific intracellular binding and clinical efficacy. *J. Invest. Dermatol.* **1981**, *76*, 211–214, doi:10.1111/1523-1747.ep12525761.

113. Katz, M.; Gans, E. H. Topical corticosteroids, structure-activity and the glucocorticoid receptor: Discovery and development - A process of planned serendipity. *J. Pharm. Sci.* 2008, *97*, 2936–2947.

114. Merck Sharp & Dohme de España, S. . Diproderm 0,5 mg/g crema Summary of Product Characteristics 1–7.

115. Industrial farmacéutica Cantabria, S. . *Clovate 0,5 mg/g crema Summary of Product Characteristics*;

116. Pharmaceuticals, A. *Cordran ® SP Cream and Cordran ® Ointment Summary of Product Characteristics*;

117. Teofarma Srl *Decloban 500 microgramos/g pomada Summary of Product Characteristics*;

118. Wiedersberg, S.; Leopold, C. S.; Guy, R. H. Bioavailability and bioequivalence of topical glucocorticoids. *Eur. J. Pharm. Biopharm.* 2008, *68*, 453–466.

119. Pflugshaupt, C. [Basic principles in local dermatologic therapy]. *Ther. Umsch.* **1998**, *55*, 470–477.

120. Jackson, M.; Mantsch, H. H. The Use and Misuse of FTIR Spectroscopy in the Determination of Protein Structure. *Crit. Rev. Biochem. Mol. Biol.* **1995**, *30*, 95–120, doi:10.3109/10409239509085140.

121. Golden, G. M.; Guzek, D. B.; Harris, R. R.; McKie, J. E.; Potts, R. O. Lipid thermotropic transitions in human stratum corneum. *J. Invest. Dermatol.* **1986**, *86*, 255–259, doi:10.1111/1523-1747.ep12285373.

122. Olsztyńska-Janus, S.; Pietruszka, A.; Kiełbowicz, Z.; Czarnecki, M. A. ATR-IR study of skin components: Lipids, proteins and water. Part I: Temperature effect. *Spectrochim. Acta - Part A Mol. Biomol. Spectrosc.* **2018**, *188*, 37–49, doi:10.1016/j.saa.2017.07.001.

123. Moghadam, S. H.; Saliaj, E.; Wettig, S. D.; Dong, C.; Ivanova, M. V.; Huzil, J. T.; Foldvari, M. Effect of chemical permeation enhancers on stratum corneum barrier lipid organizational structure and interferon alpha permeability. *Mol. Pharm.* **2013**, *10*, 2248–2260, doi:10.1021/mp300441c.

124. Goodman, M.; Barry, B. W. Action of penetration enhancers on human skin as assessed by the permeation of model drugs 5-fluorouracil and estradiol. I. Infinite dose technique. *J. Invest. Dermatol.* **1988**, *91*, 323–327, doi:10.1111/1523-1747.ep12475655.

125. López-Mesas, M.; Christoe, J.; Carrillo, F.; Crespi, M. Supercritical fluid extraction with cosolvents of wool wax from wool scour wastes. *J. Supercrit. Fluids* **2005**, *35*, 235–239, doi:10.1016/j.supflu.2005.01.008.

126. Boncheva, M.; Damien, F.; Normand, V. Molecular organization of the lipid matrix in intact Stratum corneum using ATR-FTIR spectroscopy. *Biochim. Biophys. Acta - Biomembr.* **2008**, *1778*, 1344–1355, doi:10.1016/j.bbamem.2008.01.022.

127. Coderch, L.; Fonollosa, J.; Marti, M.; Parra, J. Ceramides from wool wax. *J. Am. Oil Chem.* **2004**, *81*, 897–898, doi:10.1007/s11746-004-0998-0.

128. Elias, P. M.; Mao-Qiang, M.; Feingold, K. R. *The Epidermal Barrier: Effects of Physiologic and Non-physiological. The lanolin Book*; Hoppe, U., Ed.; Beiersdorf, 1999;

129. Barba, C.; Carrer, V.; Marti, M.; Iglesias, J.; Coderch, L. Solvent-extracted wool wax: thermotropic properties and skin efficacy. *Ski. Pharmacol. Press.*

130. Hafeez, F.; Chiang, A.; Hui, X.; Zhu, H.; Kamili, F.; Maibach, H. I. Stratum corneum reservoir as a predictive method for in vitro percutaneous absorption. *J. Appl. Toxicol.* **2016**, *36*, 1003–1010, doi:10.1002/jat.3262.

131. Alonso, C.; Rubio, L.; Touriño, S.; Martí, M.; Barba, C.; Fernández-Campos, F.; Coderch, L.; Luís Parra, J. Antioxidative effects and percutaneous absorption of five polyphenols. *Free Radic. Biol. Med.* **2014**, *75*, 149–155, doi:10.1016/j.freeradbiomed.2014.07.014.

132. Shah, V. P.; Flynn, G. L.; Yacobi, A.; Maibach, H. I.; Bon, C.; Fleischer, N. M.; Franz, T. J.; Kaplan, S. A.; Kawamoto, J.; Lesko, L. J.; Marty, J. P.; Pershing, L. K.; Schaefer, H.; Sequeira, J. A.; Shrivastava, S. P.; Wilkin, J.; Williams, R. L. Bioequivalence of topical dermatological dosage forms - Methods of evaluation of bioequivalence. In *Pharmaceutical Research*; 1998; Vol. 15, pp. 167–171.

133. Ya-Xian, Z.; Suetake, T.; Tagami, H. Number of cell layers of the stratum corneum in normal skin - relationship to the anatomical location on the body, age, sex and physical parameters. *Arch. Dermatol. Res.* **1999**, *291*, 555–559, doi:10.1007/s004030050453.

134. Schwindt, D. A.; Wilhelm, K. P.; Maibach, H. I. Water diffusion characteristics of human stratum corneum at different anatomical sites in vivo. *J. Invest. Dermatol.* **1998**, *111*, 385–389, doi:10.1046/j.1523-1747.1998.00321.x.

135. Löffler, H.; Dreher, F.; Maibach, H. I. Stratum corneum adhesive tape stripping: Influence of anatomical site, application pressure, duration and removal. *Br. J. Dermatol.* **2004**, *151*, 746–752, doi:10.1111/j.1365-2133.2004.06084.x.

136. Baur, J. A.; Sinclair, D. A. Therapeutic potential of resveratrol: The in vivo evidence. *Nat. Rev. Drug Discov.* 2006, *5*, 493–506.

137. Hung, C.-F.; Lin, Y.-K.; Huang, Z.-R.; Fang, J.-Y. Delivery of Resveratrol, a Red Wine Polyphenol, from Solutions and Hydrogels <i>via</i> the Skin. *Biol. Pharm. Bull.* **2008**, *31*, 955–962, doi:10.1248/bpb.31.955.

138. Caspers, P. J.; Lucassen, G. W.; Carter, E. A.; Bruining, H. a; Puppels, G. J.; Caspers; Lucassen; Carter; Bruining; Puppels In vivo confocal Raman microspectroscopy of the skin: noninvasive determination of molecular concentration profiles. *J. Invest. Dermatol.* **2001**, *116*, 434–42, doi:10.1046/j.1523-1747.2001.01258.x.

139. Tfaili, S.; Josse, G.; Angiboust, J. F.; Manfait, M.; Piot, O. Monitoring caffeine and resveratrol cutaneous permeation by confocal Raman microspectroscopy. *J Biophotonics* **2013**, doi:10.1002/jbio.201300011.

140. Rubio, L.; Alonso, C.; López, O.; Rodríguez, G.; Coderch, L.; Notario, J.; de la Maza, A.; Parra, J. L. Barrier function of intact and impaired skin: percutaneous penetration of caffeine and salicylic acid. *Int. J. Dermatol.* **2011**, *50*, 881–889, doi:10.1111/j.1365-4632.2010.04819.x.

141. Rubio, L.; Alonso, C.; Coderch, L.; Parra, J. L.; Martí, M.; Cebrián, J.; Navarro, J. A.; Lis, M.; Valldeperas, J. Skin Delivery of Caffeine Contained in Biofunctional Textiles. *Text. Res. J.* **2010**, *80*, 1214–1221, doi:10.1177/0040517509358798.

142. Tfaili, S.; Josse, G.; Angiboust, J. F.; Manfait, M.; Piot, O. Monitoring caffeine and resveratrol cutaneous permeation by confocal Raman microspectroscopy. *J. Biophotonics* 2014, *7*, 676–681.

143. Franzen, L.; Anderski, J.; Windbergs, M. Quantitative detection of caffeine in human skin by confocal Raman spectroscopy - A systematic in vitro validation study. *Eur. J. Pharm. Biopharm.* **2015**, *95*, 110–116, doi:10.1016/j.ejpb.2015.03.026.

144. Tfayli, A.; Piot, O.; Pitre, F.; Manfait, M. Follow-up of drug permeation through excised human skin with confocal Raman microspectroscopy. *Eur. Biophys. J.* **2007**, *36*, 1049–1058, doi:10.1007/s00249-007-0191-x.

145. Williams, A. C.; Edwards, H. G. M.; Barry, B. W. Raman spectra of human keratotic biopolymers: Skin, callus, hair and nail. *J. Raman Spectrosc.* **1994**, *25*, 95–98, doi:10.1002/jrs.1250250113.

146. Stone, N.; Kendall, C.; Smith, J.; Crow, P.; Barr, H. Raman spectroscopy for identification of epithelial cancers. *Faraday Discuss.* **2004**, *126*, 141, doi:10.1039/b304992b.

147. Frushour, B. G.; Koenig, J. L. Raman spectroscopic study of mechanically deformed poly-L-alanine. *Biopolymers* **1974**, *13*, 455–474, doi:10.1002/bip.1974.360130303.

148. Silveira, L.; Silveira, F. L.; Bodanese, B.; Zângaro, R. A.; Pacheco, M. T. T. Discriminating model for diagnosis of basal cell carcinoma and melanoma *in vitro* based on the Raman spectra of selected biochemicals. *J. Biomed. Opt.* **2012**, *17*, 77003, doi:10.1117/1.JBO.17.7.077003.

149. Baranska, M.; Proniewicz, L. M. Raman mapping of caffeine alkaloid. *Vib. Spectrosc.* **2008**, *48*, 153–157, doi:10.1016/j.vibspec.2007.12.016.

ANNEX

ANNEX

Annex 1. In vitro penetration through the skin layers of topically applied glucocorticoids

Received: 4 January 2018 | Revised: 26 April 2018 | Accepted: 14 May 2018
DOI: 10.1002/dta.2412

RESEARCH ARTICLE

WILEY

In vitro penetration through the skin layers of topically applied glucocorticoids

Victor Carrer | Cristina Alonso | Marc Adrià Oliver | Luisa Coderch

Advanced Chemical Institute of Catalonia (IQAC-CSIC), Barcelona, Spain

Correspondence
Victor Carrer, IQAC, Jordi Girona 18-26, 08034 Barcelona, Spain.
Email: victor.carrer@iqac.csic.es

Funding information
Spanish Ministry of Economy and Competitiveness, Grant/Award Number: RTC-2014-1901-1

Abstract

Corticoids are actives widely used in the treatment of skin diseases. This work aims to study the penetration of 3 corticoids (betamethasone, clobetasol, and flurandrenolide), their relationship with their Log D values and the effects of the vehicles. The 3 compounds were applied on a Franz-type diffusion cell in propylene glycol solution and their respective commercial creams and ointments. The active amounts found in the stratum corneum, epidermal, and dermal layers of the skin were investigated. Their diffusions were greatly affected by the formulation; moreover higher amounts of substance in the epidermis and dermis were detected in ointments than in creams. The enhancement effect of propylene glycol was also observed. The differences between the 3 substances could be related to their lipophilicity, molecular structure, and molecular weight. The more hydrophobic compounds (clobetasol and betamethasone) are present in higher amounts in the epidermis and dermis, while the hydrophilic compound (flurandrenolide) is mostly present in the receptor fluid.

KEYWORDS

clobetasol, corticosteroids, flurandrenolide, percutaneous absorption, propylene glycol

1 | INTRODUCTION

Inflammatory skin diseases are extremely common dermatological problems that are present in a variety of forms, from occasional rashes accompanied by skin itching and redness to more chronic conditions such as atopic dermatitis or psoriasis. A frequently prescribed treatment is a topical glucocorticoid (GC).

The absorption of topically applied drugs through the skin is a complex process. Once GCs are released from the formulation, permeation/diffusion through the stratum corneum occurs. Keratinocytes and fibroblasts present in the epidermis are the known target cells of the GC effects. Moreover, skin contains other types of cells involved in the immune response (phagocytes, eosinophils, mast cells, NK cells, dendritic cells, Langerhans, and dendritic cells) that are also cell targets of GCs.[1]

Anti-inflammatory properties of GCs are due to lots of different mechanisms such as the gene regulation,[2] the responsiveness modulation of skin immune cells,[3] or the immunosuppression.[4]

The efficacies of topical GCs are linked to their availability to reach their receptors. The affinity between the receptor and the steroid as well as its cellular uptake and residence time determines the clinical effect.[5-7] All of the previously detailed processes are highly influenced by the physicochemical properties of the drug as well as the vehicle.[8]

Glucocorticoids are a family of chemical compounds derived from cortisol. Different chemical changes are made to optimize its anti-inflammatory and immunosuppressive properties. Overall, the lipophilicity of topical corticosteroids has been shown to correlate with the steroid receptor affinity.[9] Moreover the lipophilicity of a substance affects its diffusion of across the lipidic matrix and corneocytes from the stratum corneum, which is considered the rate-limiting step for skin absorption.[10]

The potencies of steroids can also differ depending on the vehicle, so they are available in lots of different preparations.[11] The efficacies between them are roughly comparable[12] so the selected formula has to consider many aspects, such as the disease severity or the affected

region. Bioassays comparing vehicles have demonstrated that ointments are the most effective, followed by creams and lotions. Ointments are anhydrous preparations of a fairly firm consistency, are usually greasy, and have a water-insoluble base. They provide more lubrication and occlusion than other preparations, and they are the most useful for treating dry or thick hyperkeratotic lesions. Their occlusive nature also improves steroid absorption.

Creams are essentially emulsions of oil in water (usually a 1:2 ratio). They have good lubricating qualities, and their ability to vanish into the skin makes them cosmetically appealing. Creams are generally less potent than ointments of the same medication. Creams are also useful in intertriginous areas where ointments may not be used. However, creams do not provide the occlusive effects that ointments provide.

One specific ingredient often used to increase the bioavailability is propylene glycol (PG), which behaves as a percutaneous absorption enhancer[13] in many chemical agents. This substance has been selected as a common solvent for the 3 GCs that are often used in topical preparations due to its humectant properties. PG is a solvent, and it is used especially for drugs unstable or insoluble in water (like GCs). Previous studies have investigated the interactions of PG with the stratum corneum and hypothesized that PG could interact with the polar head group regions of the intercellular lipids, solvate the alpha-keratin structures in SC after the thermodynamic activity and have a solvent drag effect when PG diffuses across the skin.[14,15] In addition, PG readily permeates the skin and may carry the drug with it, as shown by in vitro correlations between the permeation of both PG and the drug.[16,17]

Considerable efforts has been channeled toward the development and validation of approaches to demonstrate the bioequivalence of topical and transdermal products. One way to determine topical steroid potency is the vasoconstrictor assay, which classifies steroids based on the extent to which the agent causes cutaneous vasoconstriction ("blanching effect") in normal healthy people. The blanching intensity has also been shown to correlate directly to the clinical efficacy in patients with plaque psoriasis.[18,19] This assay, which measures the vasoconstrictor effect to measure the corticoid activity, is recognized by the Food and Drug Administration (FDA) as a bioequivalent method.[20,21] Nevertheless, the FDA identifies in vitro studies as interesting surrogates with regard to topical bioequivalence.[22] Franz et al[23] reported the use of excised skin to specifically demonstrate the bioequivalence of topical products using the finite dose method. In the specific case of glucocorticoids, the authors showed that there was a good correlation between the in vitro diffusion method and the blanching effect.[24] *In* vitro diffusion studies are a useful assay to screen formulations, select drug candidates, study permeation enhancers, or demonstrate post-approval equivalence of products.[25,26]

Vertical diffusion Franz cells is one of the most widely used systems for in vitro skin permeation studies. The excised skin is mounted between donor and receptor chambers. Test formulations are applied to the skin facing the donor chamber, and receptor fluid samples are collected and analyzed for their drug content. Moreover the different skin compartments (SC, E, and D) can be collected to determine the drug concentration, and then, the amount of drug that gets localized in each compartment over a period of time can be compared against bioequivalent generics.

The aim of this work is to study the relationship between the skin absorption, the substance lipophilicity and the effect of the vehicle of glucocorticoids. Therefore, a study is presented using the static diffusion cells of betamethasone dipropionate (Bet), clobetasol propionate (Clo) and flurandrenolide (Fra). Three different vehicles are assayed including commercial creams, their respective ointments and propylene glycol solutions. This article compares 3 different corticoids formulated in different vehicles and tries to stablish a relation between their demonstrated and known activity/efficacy and their ability to reach the target site of action (epidermis and dermis). Then, permeation effects of formulations would help to design new drugs and to demonstrate bioequivalence of products.

2 | MATERIALS AND METHODS

The 3 studied glucocorticoids (Figure 1) were betamethasone dipropionate (Bet) (CAS: 5593–20-4, Sigma, San Louis Missouri USA), clobetasol propionate (Clo) (CAS: 25122–46-7, AK Scientific, San Francisco, California USA), and flurandrenolide (Fra) (CAS: 1524–88-5, Sigma, San Louis, Missouri USA).

2.1 | Distribution coefficient determination

These 3 substances were employed to establish their Log D values (Bet, Clo, and Fra), which were determined following the procedure for highly lipophilic compounds detailed by Andrés et al.[27] This procedure was proposed to avoid the formation of precipitate of hydrophobic compounds during the experiment and was successfully employed with Log D ranges between −1.5 and 3.5 showing a high correlation with other published data. In brief, every compound was diluted to 10 mM in dimethyl sulfoxide (Sigma, San Louis, Missouri USA) and diluted 1/100 in a 5.5 and 7.4 pH phosphate buffered saline solutions (Sigma, Steinheim, Germany). These pHs were selected considering the acidic pH of the skin of 5.5 and the physiological pH of 7.4. The solutions pH were determined using a Crison 5014 combined electrode, connected to a GLP 22 potentiometer (Crison, Alella, Spain) with an accuracy of ±0.002 in pH units. Partitions were shaken for one hour with octanol

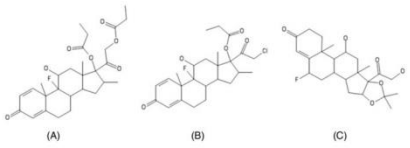

FIGURE 1 Chemical structure of (a) betamethasone dipropionate, (b) clobetasol dipropionate, and (c) flurandrenolide

(Sigma, San Louis, Missouri USA) at room temperature. Both phases of each partition are determined in triplicate by ultra-performance liquid chromatography–tandem mass spectrometry (UPLC–MS/MS) following the analytical conditions described in Section 2.3.

2.2 | Franz cell assay

Table 1 summarizes the formulas and the respective abbreviations of the 3 compounds studied in the Franz cell assay. All of the compounds actives were prepared in propylene glycol solutions (PG, Sigma Aldrich, St Louis, MO, USA) at the same concentration as in the commercial formulations.

Static vertical diffusion Franz cells (Lara-Spiral, Courtenon, France) were employed. Dermatomed pig skin was used in these investigations since the morphological and permeability characteristics of the skin of pigs are similar to those of humans,[28] and therefore, it is an accepted model for the skin penetration assessment of cosmetic ingredients.[29] The nominal surface area was 1.86 cm^2, and the receiver compartment capacity was approximately 3 mL. Six replicates/formulation were performed. The OECD Guidelines[30] and the published opinions of the Scientific Committee on Cosmetic Products and Non-Food Products (SCCNFP) were closely adhered to during this study. The accepted mass balance value was set at 100 ± 15.

In accordance with an approved Institutional Animal Care and Use Committee protocol (OECD guideline no. 428 [2004a]), unboiled porcine skin was obtained from the dorsal area of 3 different weanling female white/Landrace pigs weighing 30–40 kg. The skin was provided by the Department of Cardiology from the Clinic Hospital of Barcelona. Animal handling was approved by the Institutional Review Board and Ethics Committee of Institut d'Investigacions Biomèdiques August Pi i Sunyer (IDIBAPS) and the management of the animals conforms to the Guide for the Care and Use of Laboratory Animals.[31] The method of euthanasia was an overdose of an anesthetic. Following euthanasia, the bristles were removed carefully with an animal clipper and subsequently washed with water. The hair-clipped skin was dermatomed with a Dermatome GA630 (Aesculap, Germany) to a thickness in the range of 500 ± 50 μm, cut into appropriate pieces (2.5 cm inner diameter) and then stored at −20°C until their use.

The skin was thawed and mounted with the SC side facing the donor compartment. The receptor chamber was filled with receptor fluid. The receptor fluid was formulated considering the directives from the OECD.[30] Its composition was Dulbecco's phosphate-buffered saline (Sigma Aldrich, St Louis MO, USA) in MilliQ water, 0.04% (w/v) gentamicin sulphate salt (Sigma Aldrich, St Louis MO, USA) and 5% (w/v) bovine serum albumin (Sigma, Aldrich, St Louis MO, USA). Air bubbles were carefully removed between the skin and the RF. The RF was agitated with a magnetic stir bar.

The assembled Franz-type cell was placed in a thermostatically-controlled water bath maintained at 37°C containing a magnetic stirring device, and the skin surface temperature at approximately 32°C. In order to eliminate the damaged skin, the transepidermal water loss value (TEWL) was measured with a Tewameter TM210 (Courage & Khazaka, Cologne, Germany) at the moment of the application of the formulation, considering TEWL values under 15 $g/m^2/h$ to be acceptable.

Having reached this point, the 20 μL of formulation applied to the skin and left during 24 h. This amount was calculated considering finite dose conditions[30] and the skin surface delimited by the upper cell (1.86 cm^2). An additional cell applied with pure propylene glycol was also mounted to be used as a control. At 24 h, the skin surface was washed and wiped with a cotton bud to remove any remaining formulation. Then the different skin layers were sepparated. First 8 strippings were carried out on the surface horny layers of stratum corneum with adhesive tape (D-Squame, Cuderm Corporation, Dallas, USA) applied under controlled pressure. Lastly, the epidermis was separated from the dermis after heating the skin at 80°C for several seconds. The receptor fluid (FR) was transferred to a 5 mL volumetric flask and stored at −20°C. The different samples were extracted with ACN-TFA: a solution of 0.5% trifluoroacetic acid (Alfa Aesar, Germany) in acetonitrile 99% for HPLC (Fisher, UK). The wash and cotton bud were extracted into 10 mL of 0.5% ACN-TFA. The strips (SC or stratum corneum) were extracted into 2 mL of extractor solution. The epidermis (E) and dermis (D) in 1 mL.

Receptor fluid (RF) sample levels were determined by UPLC-MS/MS after protein precipitation with a ACN-TFA, centrifugation at 4000 rpm from 10 min (4°C) and 1:3 (v/v) dilution of the supernatant with water. Wash, D-Squame tapes, epidermis and dermis samples were diluted 1:3 (v/v) with water before analysis by UPLC-MS/MS.

2.3 | Analytical conditions

All the analyses were validated following the ICH methodology [32] and carried out by UPLC-MS/MS. The employed UPLC model was a UPLC Waters I-class (Waters Corporation, USA) attached to a MS detector Waters XEVO TQS (Waters Corporation, USA). The column used was a Waters Acquity UPLCTM BEH C18 (1.7 μm, 2.1 × 50 mm) at 40°C. The sample injection volume was set at 10 μL, electrospray inoization (ESI) was employed and positive ion mode was applied. Nitrogen (Praxair, Spain) was used as desolvatation and nebulizing

TABLE 1 Formulations, concentrations, manufacturers and abbreviations used in the Franz cell assay.

	Formulation	Concentration	Formulation manufacturer	Abreviation
Bet	Betamethasone dipropionate PG Sol.	0.5 mg/g	Self-prepared	Bet-PG
	Diproderm® cream	0.5 mg/g	MSD	Bet-cre
	Diproderm® ointment	0.5 mg/g	MSD	Bet-oin
Clo	Clobetasol PG Sol.	0.5 mg/g	Self-prepared	Clo-PG
	Clovate® cream	0.5 mg/g	IFC	Clo-cre
	Declobán® ointment	0.5 mg/g	Teofarma	Clo-oin
Fra	Flurandrenolide PG	0.5 mg/g	Self-prepared	Fra-PG
	Cordran® SP Cream	0.5 mg/g	Oclassen Pharmaceuticals Inc	Fra-cre
	Cordran® SP ointment	0.5 mg/g	Oclassen Pharmaceuticals Inc	Fra-oin

gas. The desolvatation gas flow was set at 1000 L/h. Argon (Praxair, Spain) was used as a collision gas. The autosampler temperature was 8°C. Mobile phase A contained 0.05% HCOOH +2.5 mM NH_3 (pH = 3) and mobile phase B was acetonitrile (ACN). The flow remained stable at 0.400 µL/min for all of the compounds. The UPLC analytical conditions and the non-isocratic method for all substances are detailed in Table 2.

For each active, three solutions with a concentration between the upper limit of the range curve and the LOQ were analyzed in sextuplicate in 4 different days. The R.S.D was calculated inter- and intraday, showing good repeatability (R.S.D < 0.50%). In order to avoid possible interferences samples from a cell treated PG (Blank) and a non-treated skin were also analyzed.

2.4 | Statistical analysis

Six cells/formulation were studied using Franz cells. UPLC results were evaluated using the MassLynx spectrometry software (Waters, USA). Dixon's test was applied with IBM SPSS statistics software (IMB corp., USA) and used for detecting outliers, which were excluded from the results. The results are presented as a mean value and its standard deviation in µg. The mass balance was obtained for every cell considering the amount of applied drug divided by the total amount founded in all the layers and hence demonstrating that no interactions occur between the active and the tissue/sample. Additionally, the normalized amounts of substance in each sample were calculated. All the data is compiled in Table 4.

3 | RESULTS AND DISCUSSION

The molecular weights and the obtained Log D values at pH values of 5.5 and 7.4 are listed in Table 3. As it could be expected due to the neutral nature of the actives, no remarkable differences at any of the tested pH values were detected for any drug. Bet showed the highest Log D values, which was probably because of the esterification of C-17 and C-21, which increases the lipophilicity of corticoids.[33,34] Clo and Fra have similar molecular weights; however, substantial differences can be observed regarding their Log D values. Different molecular changes may explain these differences (see inure 1). Fra, unlike Bet and Clo, does not have fluorination at C9, and the original hydroxylation at C21 from cortisol is maintained. The esterification at C17 of Clo that is not present in Fra is a specific chemical change that provides a higher lipophilicity to the active molecule.[33]

TABLE 3 Physico-chemical properties: molecular weight (MW) and octanol–water distribution coefficients (Log D) at pH values of 5.5 and 7.4.

Name	MW (g/mol)	Log D (pH 5.5)	Log D (pH 7.4)
Bet	504.59	4.30	4.33
Clo	466.97	4.02	4.04
Fra	436.51	2.15	2.07

The target of a drug is commonly referred to as a receptor. The interaction between a drug and its receptor is affected by the chemical structure of the actives. In the case of corticosteroids it has been largely demonstrated that molecule lipophillicity is intrinsingly related to their glucocorticoid effect.[35-37] Fra is the least potent of the selected drugs, which is in accordance with its low Log D value. In the cases of Bet and Clo, it has to be considered that betamethasone dipropionate and clobetasol propionate are prodrugs of the free forms.[38,39] After topical administration, the drugs can be hydrolysed by esterase enzymes primarily in the skin.[40,41] Then, the lipophillicity of the free form has to be kept in mind to relate the LogD and the active activity. In our subset of actives, clobetasol propionate is generally classified as the most potent corticoid even if betamethasone dipropionate has a higher lipophillicity. This is probably due because the free form of betamethasone dipropionate has a lower Log D than the free form of clobetasol propionate because of the hydrolysis of the propionate group.[42]

The Franz diffusion cell is used to determine the distribution on the skin of three actives (Bet, Clo and Fra) formulated in PG solution and in the following commercial formulations: for Bet, Diproderm® ointment and Diproderm® cream; for Clo, Decloban® ointment and Clovate® cream; and for Fra, Cordran® ointment and Cordran® cream. The concentration of all of the PG and commercial formulations is 0.5 mg/g (Table 1). However, it should be noted that although each formulation has the same concentration of the active ingredient, each formulation will have a different degree of saturation in each vehicle, which highly influences the absorption of substances through the skin.[43]

TABLE 2 Analytical UPLC conditions. Employed abbreviations: limit of detection (LOD); limit of quantification (LOQ); time 0 (i); cone voltage (CV) in V; collision energy in eV (EC); no signal (NS); excitation wavelength (λ) in nanometers; retention time (Tr) in minutes.

	Betamethasone	Clobetasol	Flurandrenolide
Method range (ng/mL)	0.2–5000	2–2000	0.5–5000
LOQ (ng/mL)	0.2	2	0.5
LOD (ng/mL)	0.1	1.2	0.3
% Phase A (time)	55 *(i)*- 5 (1 min)- 55 (1.70 min)	20 *(i)*- 5 (1 min)- 1.70 (20 min)	62(i)- 45 (0.70 min)- 5 (1.10 min)- 62 (1.20 min)
Precursor ion (m/z)	505.25	467.19	437.3
Product ion (m/z)	279.1	278.0	361
CV	20	50	5
EC	20	25	15
λ	254	246	NS
Tr	1.05	1.07	0.6

For each formulation, 6 cells were studied. Moreover, additional penetration cells applying the vehicle as blank control and a non-treated skin have been processed, in order to detect possible interferences in the drug analysis during the percutaneous absorption experiments. The compounds were recovered from the skin surface, stratum corneum, epidermis (E), dermis (D) and receptor fluid (RF). In the cases of the blank controls, the different compartments obtained from the cell were analysed and the results indicated that compounds were not detected in any sample and no interferences were appreciated. Table 4 and Figure 2 show the distribution of each compound in the different compartments investigated. In all cases, the obtained mass balance (total recovery) was acceptable (100 ± 15). The concentrations retained by the SC are not absorbed by the skin and do not contribute to the systemic dose. However, the concentrations found in the epidermis and dermis can be absorbed and reach the systemic level.[44] Besides the affinity of a substance for its receptor, the efficacy of a topically applied substance is linked to its availability to contact the target/receptor. Glucocorticoid receptors are known to be located in epidermal and dermal cells.[5,45] Therefore, in Table 4, in addition to the compound distribution in the different layers, the amount of compound in E + D and the percutaneous absorption (E + D + RF) are also described.

It is important to bear in mind the limitations of the Franz diffusion cell methodology performed with dermatomed porcine skin, which gives results with high standard deviations[46]. However, in general, all of the compounds in all of the formulations have a common penetration profile, in which the amount of substance found in each layer decreased when increasing in depth (SC > E > D). Only Clo-oin and Clo-cre have similar amounts in all three skin strata. The amount found in the receptor fluid is clearly dependent not only on the substance but also on the vehicle.

For Bet, when it is applied in PG solution, the amount found in the receptor fluid is quite significant, whereas in the cream and ointment, the amount decreases. This is probably due to the enhancement effect of PG. Therefore, higher amounts of both E + D and E + D + RF for Bet are obtained for the PG formulation.

Clo has a similar lipophilicity to that of Bet but a lower MW, and it is the most retained compound in the E and D as well as in the E + D + RF in all of the employed formulations. This higher accumulation of the substance agrees with the higher potency of Clo compared

TABLE 4 Distribution of compounds in pig skin expressed in μg and % for each sample: surface excess, stratum corneum, epidermis, dermis, receptor fluid, and the total amount in μg. Sum of epidermis and dermis (E + D) and epidermis, dermis and receptor fluid (E + D + RF) are also presented

	Bet- PG		Clo-PG		Fra-PG	
PG Solutions	**(μg)**	**(%)**	**(μg)**		**(μg)**	**(%)**
Surface excess	6.00 ± 1.58	88.85	10.49 ± 0.87	88.12	8.80 ± 0.91	89.99
Stratum corneum	0.35 ± 0.14	5.21	0.59 ± 0.31	4.94	0.42 ± 0.22	4.25
Epidermis	0.26 ± 0.09	3.78	0.46 ± 0.22	3.84	0.19 ± 0.06	1.94
Dermis	0.03 ± 0.02	0.48	0.28 ± 0.20	2.37	0.12 ± 0.16	1.33
Receptor Fluid	0.12 ± 0.06	1.75	0.08 ± 0.05	0.70	0.15 ± 0.21	1.64
Total	6.76	100	11.9	100	9.68	100
E + D	0.29	4.26	0.74	6.21	0.31	3.27
E + D + RF	0.41	6.01	0.82	6.91	0.46	4.91
	Bet-oin Diproderm®		**Clo-oin Decloban®**		**Fra-oin Cordran®**	
Ointments	**(μg)**	**(%)**	**(μg)**	**(%)**	**(μg)**	**(%)**
Surface excess	4.90 ± 0.31	96.32	7.51 ± 1.72	89.72	5.12 ± 0.34	93.08
Stratum corneum	0.10 ± 0.02	2.06	0.21 ± 0.21	2.53	0.09 ± 0.12	1.69
Epidermis	0.05 ± 0.02	0.94	0.18 ± 0.04	2.12	0.08 ± 0.04	1.45
Dermis	0.02 ± 0.01	0.49	0.22 ± 0.14	2.65	0.04 ± 0.03	0.80
Receptor Fluid	0.01 ± 0.01	0.18	0.25 ± 0.19	3.03	0.07 ± 0.01	1.28
Total	5.08	100	8.37	100	5.4	100
E + D	0.07	1.43	0.4	4.77	0.12	2.25
E + D + RF	0.08	1.61	0.65	7.8	0.19	3.53
	Bet-cre Diproderm®		**Clo-cre Clovate®**		**Fra-cre Cordran®**	
Creams and Gels	**(μg)**	**(%)**	**(μg)**	**(%)**	**(μg)**	**(%)**
Surface excess	5.95 ± 1.75	97.30	8.33 ± 1.18	95.91	5.62 ± 0.40	91
Stratum corneum	0.09 ± 0.06	1.43	0.09 ± 0.14	0.99	0.11 ± 0.03	1.76
Epidermis	0.05 ± 0.03	0.87	0.07 ± 0.08	0.86	0.05 ± 0.02	0.77
Dermis	0.02 ± 0.01	0.33	0.10 ± 0.15	1.17	0.04 ± 0.02	0.69
Receptor Fluid	0.01 ± 0.01	0.13	0.01 ± 0.00	0.07	0.36 ± 0.22	5.79
Total	6.12	100	8.6	100	6.18	100
E + D	0.07	1.2	0.17	2.03	0.09	1.46
E + D + RF	0.08	1.33	0.18	2.1	0.45	7.25

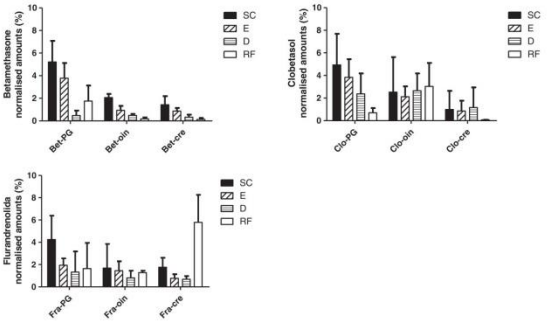

FIGURE 2 Normalized amounts in stratum corneum (SC), epidermis (E), dermis (D) and receptor fluid (RF) of betamethasone (Bet), clobetasol (Clo), and flurandrenolide (Fra) applied in propylene glycol solutions (PG), ointments (oin) and creams (cre).

to Fra and Bet. The glucocorticoid receptors are located in the E and D, and hence, high amounts of Clo in both tissues can lead to a higher efficacy of this corticoid.

Fra is the most hydrophilic compound and showed less affinity for the E and D. For example, the three formulations of Fra show higher amounts of the substance in the RF than in the upper layer, the D. This is clearly more marked for Fra-cre. This special behaviour is consistent in the three formulations and can be explained by the presence of the acetonide group in the D ring, which enhances the penetrability and the percutaneous absorption of this type of corticoid.[47] In summary, in Clo, Bet and Fra, the retention in the tissue (E + D) is always greater when PG is employed. Fra-cre contains a high amount of analyte in the RF, which leads to high absorption (E + D + RF) with higher systemic exposure.

Therefore, comparing the drug penetration profiles of PG solutions and their physico-chemical properties, it can be concluded that the more hydrophobic compounds (Clo and Bet) are present in higher amounts in the E + D, while the hydrophilic compound (Fra) is mostly present in the receptor fluid, which leads to higher percutaneous absorption.

Additionally, it is important to note the effect of the vehicle. The three compounds showed great differences when they were applied in the different formulations, proving that the vehicle is critical in regards to percutaneous absorption. Surveying the data sheet of the commercial formulations, the main components are water, cetostearyl alcohol and other oily components for creams and paraffin along with waxes without any water content for ointments. Besides, it could be mentioned that Clo-cre, Clo-oin and Fra-cre also contain an unknown amount of PG.

Higher amounts of the substance are obtained in the epidermis and dermis when ointments are employed compared to creams. This is consistent with the general rule that the highest glucocorticoid efficacy is fulfilled with ointments compared to creams.[48] This fact is also related to the absence of water content and the presence of the waxes and petrolatum of ointments, which is believed to enhance the penetration of the substance due to the occlusive effect.[49] In view that oily formulations enhance the GC effect/penetration, ointments are mostly used in cases of severe dermal diseases and/or on areas with a large stratum corneum (such as the palms of the hands or soles of the feet).

On the other hand the enhancement effect of propylene glycol can be discerned. For the three PG solutions, the distribution patterns are similar. The SC retains the highest amount of substance (about 5%); moreover, the amounts found in the E were also higher than with the other vehicles. This is not so clear for the amount in the dermis. It could be noted that the PG solutions show the highest amounts of corticoid in the E + D when compared with creams and ointments, mainly due to the important amount in the E. However, the influence that the degree of saturation may induce in the percutaneous absorption of the different vehicles, which has not been considered in this work, should be investigated.

Summarizing the effects of the vehicles, the influence of PG on the maximum amounts of the analyte in the SC and E and similar amounts of the analyte in the D for PG and ointments, with level being much lower for creams, should be pointed out. The penetration enhancement for Clo-oin and for Fra-cre in the receptor fluid is also observed. This could be due to the presence of PG in these vehicles.

Since the aim of these glucocorticoids is to act at the E and D, this study confirms the higher corticoid efficacy of Clo due to its higher presence in the skin layers. Additionally, propylene glycol and the ointments applied induced a higher penetration into these layers than the corresponding creams.

It is important to underline that future steps should be carried out to study the effect of the substance saturation grade within the vehicle and its percutaneous absorption. Moreover, our study considered only an exposure time of 24 h, and a kinetic study comparing the formulations would be highly valuable. Then, the obtained fluxes could be correlated with other *in vivo* data. This will help to screen formulations, select drug candidates, study the permeation effects of enhancers or demonstrate the bioequivalence of products.

4 | CONCLUSIONS

The lipophilicities (distribution coefficients) and skin distributions of three different corticoids (flurandrenolide, clobetasol and betamethasone) in different formulations were studied. The molecular structure could be related to the differences in lipophilicity of the three substances. The fluorination and esterification increased the lipophilicity at both pH values studied, despite the intrinsic variablity of the Franz cell assay, the higher lipophillicities of Bet and Clo could be related to their higher retention in the epidermis and dermis. For Fra, the higher hydrophilicity could be linked to the higher amounts in the receptor fluid. When comparing the different formulations PG solutions showed a high retention in the stratum corneum and epidermis demonstrating the known effect of propylene glycol. When the different ointments are applied, higher amounts in the epidermis or dermis are found compared to creams, and this data agrees with the higher efficacy of ointments compared to creams. The most potent corticoid studied (Clo) has a higher presence in the epidermis and dermis in the three employed formulations investigated. This can be related to the higher efficacy of this substance since the glucocorticoid receptors are mostly found in the epidermis and dermis. Summarizing, clobetasol (the most potent corticoid) and ointments (the formulation with the highest corticoid activity) are retained to a greater extent in the epidermis and dermis, where the corticoid receptors are located.

ACKNOWLEDGEMENTS

The present work could not be done without the important collaboration and contributions of Miriam Zanuy, Sonia Espinosa, Mònica Córdoba, Mercè Pont and M. Jose Domínguez from Almirall, S.A. The authors are also grateful to Montserrat Rigol Muxart and Núria Solanes Batlló from the Department of Cardiology (Institut d'Investigacions Biomèdiques August Pi i Sunyer (IDIBAPS) Hospital Clínic, Universitat de Barcelona, Spain) for supplying the porcine skin biopsies. This work was partially funded by Spanish Ministry of Economy and Competitiveness, project code RTC-2014-1901-1.

ORCID

Victor Carrer http://orcid.org/0000-0003-0498-6754

REFERENCES

1. Cato ACB, Nestl A, Mink S. Rapid actions of steroid receptors in cellular signaling pathways. *Sci. STKE*. 2002;2002:re9.
2. Barnes PJ. Anti-inflammatory Actions of Glucocorticoids: Molecular Mechanisms. *Clin. Sci.* 1998;94:557-572.
3. Hafezi-Moghadam A, Simoncini T, Yang Z, et al. Acute cardiovascular protective effects of corticosteroids are mediated by non-transcriptional activation of endothelial nitric oxide synthase. *Nat. Med.* 2002;8:473-479.
4. Uva L, Miguel D, Pinheiro C, et al. Mechanisms of action of topical corticosteroids in psoriasis. *Int. J. Endocrinol.* 2012;2012. https://doi.org/10.1155/2012/561018
5. Ponec M, Polano MK. Penetration of various corticosteroids through epidermis in vitro. *Arch. Dermatol. Res.* 1979;265:101-104.
6. Korting HC, Kerscher MJ, Schafer-Korting M. Topical glucocorticoids with improved benefit/risk ratio: do they exist? *J. Am. Acad. Dermatol.* 1992;27:87-92.
7. Ponec M, Kempenaar JA. Biphasic entry of glucocorticoids into cultured human skin keratinocytes and fibroblasts. *Arch. Dermatol. Res.* 1983;275:334-344.
8. Cross SE, Magnusson BM, Winckle G, Anissimov Y, Roberts MS. Determination of the effect of lipophilicity on the in vitro permeability and tissue reservoir characteristics of topically applied solutes in human skin layers. *J. Invest. Dermatol.* 2003;120:759-764.
9. Derendorf H, Meltzer EO. Molecular and clinical pharmacology of intranasal corticosteroids: Clinical and therapeutic implications. *Allergy Eur. J. Allergy Clin. Immunol.* 2008;63:1292-1300.
10. Hadgraft J, Lane ME. Skin permeation: the years of enlightenment. *Int. J. Pharm.* 2005;305:2-12.
11. Mitra A, Wu Y. Topical delivery for the treatment of psoriasis. *Expert Opin. Drug Deliv.* 2010;7:977-992.
12. Warino L, Balkrishnan R, Feldman SR. Clobetasol propionate for psoriasis: are ointments really more potent? *J. Drugs Dermatol.* 2006;5:527-532.
13. Van De Kerkhof PCM, Kragballe K, Segaert S, Lebwohl M. Factors impacting the combination of topical corticosteroid therapies for psoriasis: Perspectives from the international psoriasis council. *J. Eur. Acad. Dermatology Venereol.* 2011;25:1130-1139.
14. Barry BW. Mode of action of penetration enhancers in human skin. *J. Control. Release*. 1987;6:85-97.
15. Watkinson RM, Guy RH, Hadgraft J, Lane ME. Optimisation of cosolvent concentration for topical drug delivery - II: Influence of propylene glycol on ibuprofen permeation. *Skin Pharmacol. Physiol.* 2009;22:225-230.
16. Squillante E, Needham T, Maniar A, Kislalioglu S, Zia H. Codiffusion of propylene glycol and dimethyl isosorbide in hairless mouse skin. *Eur. J. Pharm. Biopharm.* 1998;46:265-271.
17. Trottet L, Merly C, Mirza M, Hadgraft J, Davis AF. Effect of finite doses of propylene glycol on enhancement of in vitro percutaneous permeation of loperamide hydrochloride. *Int. J. Pharm.* 2004;274:213-219.
18. Gibson JR, Kirsch JM, Darley CR, Harvey SG, Burke CA, Hanson ME. An assessment of the relationship between vasoconstrictor assay findings, clinical efficacy and skin thinning effects of a variety of undiluted and diluted corticosteroid preparations. *Br. J. Dermatol.* 1984;111:204-212.
19. Cornell RC, Stoughton RB. Correlation of the vasoconstriction assay and clinical activity in psoriasis. *Arch. Dermatol.* 1985;121:63-67.
20. Stoughton RB. Are generic formulations equivalent to trade name topical glucocorticoids? *Arch. Dermatol.* 1987;123:1312-1314.
21. E. Benfeldt. Chapter 10: Application of Microdialysis in Assessing Cutaneous Bioavailability, 2014.
22. Lionberger RA. FDA Critical Path Initiatives: Opportunities for Generic Drug Development. *AAPS J.* 2008;10:103-109.
23. Franz TJ, Lehman PA, Raney SG. Use of excised human skin to assess the bioequivalence of topical products. *Skin Pharmacol. Physiol.* 2009;22:276-286.
24. Feldmann RJ, Maibach HI. Absorption of some organic compounds through the skin in man. *J. Invest. Dermatol.* 1970;54:399-404.
25. Sapra B, Jain S, Tiwary AK. Percutaneous Permeation Enhancement by Terpenes: Mechanistic View. *AAPS J.* 2008;10:120-132.
26. Zhou X, Liu D, Liu H, et al. Effect of low molecular weight chitosans on drug permeation through mouse skin: 1. Transdermal delivery of baicalin. *J. Pharm. Sci.* 2010;99:2991-2998.
27. Andrés A, Rosés M, Ràfols C, et al. Setup and validation of shake-flask procedures for the determination of partition coefficients (logD) from low drug amounts. *Eur. J. Pharm. Sci.* 2015;76:181-191.
28. Dick IP, Scott RC. Pig ear skin as an in-vitro model for human skin permeability. *J Pharm Pharmacol.* 1992;44:640-645.

29. Scientific Committee on Consumer Safety. Basic criteria for the in vitro assessment of dermal absorption of cosmetic ingredients. *Eur. Comm.* 2010, SCCS/1358;1-14.
30. Oecd. Guidance document for the conduct of skin absorption studies. *Env/Jm/Mono*. 2004;1-31.
31. Institute for Laboratory Animal Research. *Guide for the Care and Use of Laboratory Animals*. 8th ed. :2011.
32. Ich. ICH Topic Q2 (R1) Validation of Analytical Procedures: Text and Methodology. *Int. Conf. Harmon.* 2005;1994:17.
33. Mori M, Pimpinelli N, Giannotti B. Topical corticosteroids and unwanted local effects. Improving the benefit/risk ratio. *Drug Saf*. 1994;10:406-412.
34. Schackert C, Korting HC, Schäfer-Korting M. Qualitative and quantitative assessment of the benefit-risk ratio of medium potency topical corticosteroids in vitro and in vivo: characterisation of drugs with an increased benefit-risk ratio. *BioDrugs*. 2000;13:267-277.
35. Brazzini B, Pimpinelli N. New and established topical corticosteroids in dermatology: clinical pharmacology and therapeutic use. *Am. J. Clin. Dermatol.* 2002;3:47-58.
36. Ponec M, Kempenaar J, Shroot B, Caron J-C. Glucocorticoids: Binding affinity and lipophilicity. *J. Pharm. Sci.* 1986;75:973-975.
37. Johnson M. Pharmacodynamics and pharmacokinetics of inhaled glucocorticoids. *J. Allergy Clin. Immunol.* 1996;97:169-176.
38. Ahmad I, Usmanghani K, Khattak SUR, Sheikh D. Kinetics of thermal degradation of betamethasone valerate and betamethasone dipropionate in different media. *Indian J. Pharm. Sci.* 2012;74:133.
39. Hajnal K, Gabriel H, Aura R, Erzsébet V, Blanka SS. Prodrug Strategy in Drug Development. *Acta Medica Marisiensis*. 2016;62. https://doi.org/10.1515/amma-2016-0032
40. Mitriaikina S, Müller-Goymann CC. Comparative permeation studies of nondiluted and diluted betamethasone-17-valerate semisolid formulations through isolated human stratum corneum and artificial skin construct. *Skin Pharmacol. Physiol.* 2009;22:142-150.
41. Cheung YW, Li Wan Po A, Irwin WJ. Cutaneous biotransformation as a parameter in the modulation of the activity of topical corticosteroids. *Int. J. Pharm.* 1985;26:175-189.
42. Kwatra G, Mukhopadhyay S. Topical corticosteroids: Pharmacology. In: *A Treatise Top. Corticosteroids Dermatology Use, Misuse Abus*; 2017:11-22.
43. Moser K, Kriwet K, Naik A, Kalia YN, Guy RH. Passive skin penetration enhancement and its quantification in vitro. *Eur. J. Pharm. Biopharm.* 2001;52:103-112.
44. Epa. Dermal Exposure Assessment: Principles and applications. 1992, 1–388.
45. Ponec M, Kempenaar A, De Kloet ER. Corticoids and cultured human epidermal keratinocytes: Specific intracellular binding and clinical efficacy. *J. Invest. Dermatol.* 1981;76:211-214.
46. Akomeah FK, Martin GP, Brown MB. Variability in human skin permeability in vitro: Comparing penetrants with different physicochemical properties. *J. Pharm. Sci.* 2007;96:824-834.
47. Katz M, Gans EH. Topical corticosteroids, structure-activity and the glucocorticoid receptor: Discovery and development - A process of planned serendipity. *J. Pharm. Sci.* 2008;97:2936-2947.
48. Wiedersberg S, Leopold CS, Guy RH. Bioavailability and bioequivalence of topical glucocorticoids. *Eur. J. Pharm. Biopharm.* 2008;68:453-466.
49. Pflugshaupt C. Basic principles in local dermatologic therapy. *Ther. Umsch.* 1998;55:470-477.

How to cite this article: Carrer V, Alonso C, Oliver MA, Coderch L. In vitro penetration through the skin layers of topically applied glucocorticoids. *Drug Test Anal.* 2018;1-8. https://doi.org/10.1002/dta.2412

Annex 2. Solvent-Extracted Wool Wax Thermotropic Properties and Skin Efficacy

Original Paper

Skin Pharmacology and Physiology

Skin Pharmacol Physiol 2018;31:198–205
DOI: 10.1159/000488247

Received: November 17, 2017
Accepted after revision: March 6, 2018
Published online: May 9, 2018

Solvent-Extracted Wool Wax: Thermotropic Properties and Skin Efficacy

Clara Barba Albanell[a] Victor Carrer[a] Meritxell Marti[a] Jordi Iglesias[b] Joan Iglesias[c] Luisa Coderch[a]

[a]Department of Chemicals and Surfactant Technology, IQAC-CSIC, Barcelona, Spain; [b]RMT, Santa Eulàlia de Ronçana, Barcelona, Spain; [c]Dos-I Solutions SL, Palau Solità i Plegamans, Barcelona, Spain

Keywords
Wool wax · Thermotropic properties · Skin efficacy · Skin barrier · Skin physiology/structure

Abstract
Background/Aims: Wool wax is a soft, yellow, waxy substance that is secreted by the sebaceous glands of sheep. The purpose of wool wax is to waterproof and protect the wool. Chemically, wool wax is a complex mixture of esters, fatty acids, and alcohols. Wool waxes with different properties can be obtained by following different extraction methodologies. ***Methods:*** Two differently extracted wool waxes are compared in this study. Their effectiveness in mimicking the properties of skin lipids is evaluated. In addition, the lipid compositions and thermotropic behaviours of the 2 differently extracted wool waxes were evaluated. ***Results:*** The solvent-extracted wool wax was found to have a significantly higher polar lipid content than that of the water-extracted wool wax. This increase in the polar character of the solvent-extracted wool wax was also demonstrated by increased values of transition and degradation temperatures in the differential scanning calorimetry and thermogravimetric analyses, respectively. In addition, solvent-extracted wool wax demonstrated the ability to reinforce stratum corneum lipids, which led to improved skin barrier function. ***Conclusions:*** The suitability of the solvent-extracted wool wax for application in the preparation of cosmetics and dermatological products was demonstrated.

Introduction

Wool is a natural fibre that is obtained from sheep and is subject to global supply and demand.

Sheep wool is protected by a very special combination of lipids, called lanolin. Lanolin is a smelly, pale-yellow, natural oil that can be described as the wax obtained from the wool of sheep during the scouring process [1]. Wool wax is secreted from the skin of sheep and accumulates in the wool fibres as they grow. The natural role of lanolin is to protect wool from climate and the environment. Furthermore, lanolin protects the animal against getting wet and also seems to play a role in skin hygiene.

KARGER

E-Mail karger@karger.com
www.karger.com/spp

Clara Barba Albanell
IQAC-CSIC
Jordi Girona 18–26
ES–08034 Barcelona (Spain)
E-Mail cbaesl@iqac.csic.es

The lipid composition of wool wax comprises a mixture of esters, diesters, and hydroxy esters of high molecular weight as well as free fatty alcohols and free fatty acids (FFA) [2–4]. More polar compounds, such as ceramides and phospholipids, can also be found in wool wax. Wool wax is known to share chemical and physical similarities with human skin lipids, particularly with stratum corneum (SC) lipids. The skin barrier is located in the SC, where the SC cells (corneocytes) are embedded in a continuous, lipid-enriched, extracellular matrix. These lipids mediate cutaneous barrier function. Wool wax shares important features with SC lipids: wool wax contains cholesterol (Chol), fatty acids and ceramides, essential constituents of SC lipids; moreover, wool wax and SC lipids can coexist as solids and liquids at physiological temperatures [5–7]. Lipids in the SC play an important role in the properties of the skin barrier. As the continuous phase in the SC, intercellular lipids are the major route of transport through the skin, and the barrier function is highly dependent on the lipid structure of the SC [8, 9]. Understanding the structure of the lipid matrix structure and the molecular interactions dictating this structure is crucial for understanding and controlling the penetration of substances through the skin.

Industrially, the wool-scouring processes are carried out in a series of aqueous solutions with surfactants and a builder. Wool wax is recovered from the scouring liquor by centrifugation [1]. In addition to lipids, wool wax contains detergents and suint [10], a water-soluble substance that is obtained from washing fleece. A recently developed LIFE project – eco-efficient dry wool scouring with total by-product recovery (WDS) – was based on a new technology for washing wool with organic solvents with full recovery of by-products [11]. In comparison to conventional aqueous scouring, the WDS project uses a mixed washing process with a solvent-based wool extraction followed by an aqueous scouring process. The WDS procedure achieves the recovery of by-products, with a decrease in the contaminant load of the waste effluents generated. Of particular interest is the extraction of wool wax, which is more effectively recovered following the WDS procedure.

The goal of this work is to compare different extracted wool waxes and determine their effectiveness as SC lipid mimics. For this, the lipid composition and thermotropic behaviour of the solvent-extracted (SE) wool wax will be determined and compared with those of the wool wax obtained from the conventional aqueous scouring process. Furthermore, an in vivo assay will be performed to test the efficacies of the wool waxes when applied on skin.

Materials and Methods

Materials

Cholesteryl stearate (Chol S) (>96%), Chol (>92%), and palmitic acid (>99%) were all obtained from Sigma-Aldrich (St. Louis, MO, USA). Ceramide NP was obtained from ITEQSA (Sabadell, Spain). The SE wool wax was provided by RMT SA (Santa Eulàlia de Ronçana, Spain), and the water-extracted (WE) wool wax by Textil Manuel Tavares SA (Portugal).

Wool Wax Extraction

Wool waxes obtained from 2 different extraction procedures were studied. The wool from which the waxes were extracted came from the same breed of sheep: Spanish merino.

In the traditional procedure, wool scouring is carried out in a complex countercurrent aqueous washing train (manufactured by ANDAR, New Zealand, which has a line of scouring technologies) with 6 baths containing water, soap, and soda ash or a similar alkali. The wool wax was separated in the second bath by centrifugation (WE wool wax).

The WDS process consisted of a solvent degreasing phase followed by rinsing in water to remove any remaining dust impurities by a batch method (SE wool wax); the solvent used was hexane. A pilot plant was designed consisting of a closed reactor with an internal hydraulic piston, which, through a sequential discontinuous process, allows the recovery of wool grease and dust and the reduction of water and chemical consumption. The wool wax was recovered from the hexane washes by distillation.

Lipid Analyses

Lipid analyses of the differently obtained wool waxes were performed by thin-layer chromatography (TLC) coupled to an automated flame ionization detector (FID) (Iatroscan MK-5, Iatron, Tokyo, Japan). This technique enables the rapid separation and precise quantification of different classes of lipids; furthermore, sample pretreatment is not required for this method [12]. The lipid samples (10 µg/mL) and standards (2 µg/mL) were dissolved in chloroform/methanol (2/1, v/v) and spotted (0.6–2 µL) on silica gel S-III Chromarods using an SES (Nieder-Olm, Germany) 3202/15-01 sample spotter. The lipid content and composition were determined using an optimized TLC-FID protocol [13].

A general lipid analysis (1 scan) was performed by eluting the rods 4 times, consecutively, using the following mobile phases: the rods were eluted twice to a distance of 2.5 cm with chloroform/methanol/water (57/12/0.6, v/v/v) to separate apolar lipids from more polar lipids, such as ceramides. Then, a third elution with hexane/diethyl ether/formic acid (50/20/0.3, v/v/v) up to 8 cm and a fourth elution with hexane/benzene (35/35, v/v) up to 10 cm were performed to separate the different apolar lipids. Each bath was prepared 30 min before development. To obtain a good vapour saturation of the development tank, a filter paper was placed along one side of the tank and wetted with the solvent system. After each elution, the rods were heated for 5 min at 60 °C to dry the remaining solvent and left for 10 min in a conditioned flask before elution.

The experimental conditions were as follows: an air flow of 2,000 mL/min, a hydrogen flow of 160–180 mL/min, and a scanning speed of 2–3 mm/s. Data were processed with PeakSimple v. 388 software. These procedures were applied to the following standard compounds to determine the corresponding calibration curves for the quantification of each compound: Chol S, Chol, pal-

Skin Pharmacol Physiol 2018;31:198–205
DOI: 10.1159/000488247

mitic acid, and ceramide NP. Lipid analyses were performed in triplicate for each wool wax. The analysis followed is able to separate the following lipid families: apolar lipids (mainly cholesteryl esters), FFA, sterols (mainlyChol) and polar lipids (mainly ceramide but also Chol S).

Differential Scanning Calorimetry

A differential scanning calorimeter, DSC-821 (Mettler Toledo, Columbus, OH, USA), was used to determine the transition temperatures of the wool waxes. Samples (5–10 mg) were placed in a hermetically sealed aluminium pan (40 µL) and cooled under a stream of nitrogen from 25 to –100 °C at a cooling rate of 10 °C/min and then immediately heated from –100 to 100 °C at a heating rate of 10 °C/min and purged with nitrogen gas at 50 mL/min.

Thermogravimetric Analyses

Thermogravimetric analyses (TGA) were performed with a TGA instrument (model TGA/SDTA 851^e, Mettler Toledo, Spain). Approximately 5 mg of wool wax was packed into a pierced aluminium pan (100 µL) and heated, under a nitrogen stream, from 25 °C to 600 °C at a heating rate of 10 °C/min

Sample Preparation for in vivo Studies

Wool wax creams were prepared by dissolving the 2 wool waxes into a commercial base cream (Base Beeler sens®, Acofarma, Spain), which is based on an anionic oil-in-water emulsion that contains water (>50%), cetyl alcohol, propylene glycol, white wax and sodium lauryl sulphate as its main ingredients, that was previously heated to 50 °C; 15% wool wax creams were obtained by this method. To facilitate the incorporation of the lipid mixture into the base cream, a temperature of 70 °C was maintained.

In vivo Studies

Biophysical skin parameters were measured in order to evaluate the effects of the wool wax creams on skin in vivo. Six healthy Caucasian volunteers (all female, phototypes III–IV, mean age 31 ± 6 years, age range 26–43 years) participated in the studies. Written informed consent was obtained from all participants. Four different skin areas (4 cm^2) on the left forearm were delimited, corresponding to the following treatments: untreated (control), treated with the placebo cream, and one zone each for the different extracted wool wax creams. These areas were randomized on each volunteer. The participants were advised to avoid topical drugs or moisturizers on the tested zones for 48 h before the experiments and during the experiments. To obtain reliable measurements, the participants were acclimatized for 15 min in an air-conditioned room (23 °C, 50% relative humidity) before the experiments. Samples were applied (20 µL) onto the marked area using a micropipette Microman® M25 (Gilson, France). The application of the formulations was repeated once a day for 8 days (not including the weekend days) for a total of 8 applications, and the parameters (transepidermal water loss, TEWL, and skin capacitance) were measured each day before application (24 h after cream application).

A Tewameter TM 210 (Courage and Khazaka, Cologne, Germany), which evaluates TEWL in grams per square metre per hour, was used to monitor the barrier function of skin. Skin hydration was determined using a Corneometer CM 85 (Courage and Khazaka), which measures skin capacitance in arbitrary units. Both parameters were recorded in accordance with established guidelines [14, 15].

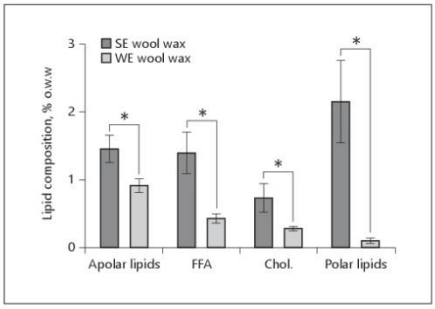

Fig. 1. Mean values (±SD) of wool wax lipid composition in percent over wool weight (o.w.w.) obtained in triplicate by TLC-FID (apolar lipids, free fatty acids [FFA], cholesterol [Chol.], and polar lipids). * $p < 0.05$.

Data Treatment

Statistical analyses were performed with StatGraphics software (version 5.0). Differences were tested for statistical significance using non-parametric tests (Kruskal-Wallis); $p < 0.05$ was considered significant.

Results

Wool waxes were obtained, as described in the Materials and Methods section, following 2 different scouring processes. The wool waxes obtained (WE and SE wool wax) were analysed to determine the differences in their lipid compositions. TLC-FID analyses enabled us to quantify the most important lipid compounds. Lipid analyses were performed in triplicate for each wool wax. The results show the solvent extraction procedure recovered almost all of the wool wax (12%, compared to the initial 14% of the wool weight), whereas the conventional water process only recovered 4.5% of the wool wax. Different lipid families were identified by the analysis performed in this investigation: apolar lipids, FFAs, sterols and polar lipids. The differently extracted wool waxes showed different lipid distributions (Fig. 1). When the wool wax is extracted with solvents, a greater amount of all the analysed lipids was found. In particular, the SE wool wax was found to contain a significantly higher polar lipid content than the WE wool wax. By the conventional water extraction procedure, polar lipids might have

Skin Pharmacol Physiol 2018;31:198–205
DOI: 10.1159/000488247

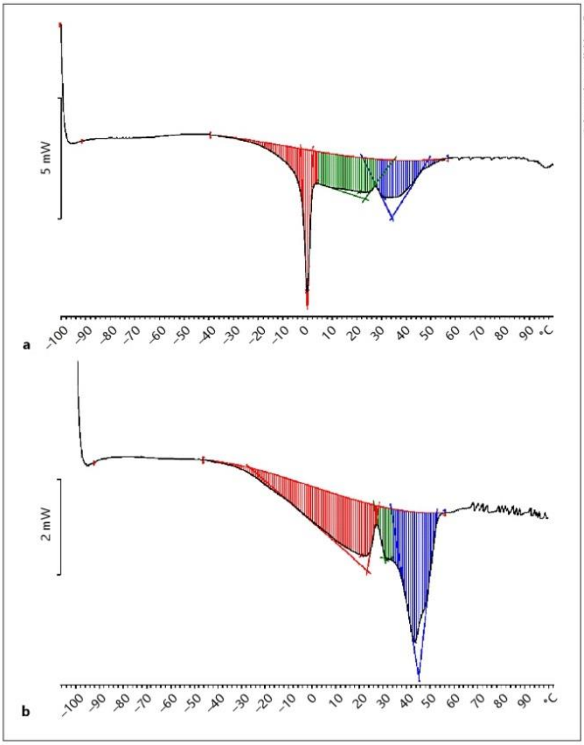

Fig. 2. DSC thermographs obtained at 10 °C/min under a stream of nitrogen (50 mL/min) in a hermetically sealed aluminium pan of WE wool wax (**a**) and SE wool wax (**b**).

been retained in the water waste. In this case, the WE wool wax was found to be rich in apolar lipids.

Several studies have demonstrated the primary role that SC lipids play in the function of the skin barrier [16, 17]. The compositions of SC lipids are crucial for their contribution to the epidermal barrier. In a previous study, TLC-FID analyses of SC lipids identified 3 main lipid families: polar lipids (mainly ceramides), Chol, and FFA; in addition, some apolar lipids were also detected [18]. As mentioned earlier, the lipids of the WE wool wax exhibited a different pattern, primarily consisting of apolar lipids and, in descending order, FFA, Chol, and polar lipids (Fig. 1). However, when a solvent scouring procedure is followed, the resultant SE wool wax has higher amounts of lipids and is enriched in polar lipids. Skin barrier disruption in different skin pathologies has been attributed to decreased levels of polar lipids, particularly ceramides, in skin [19–21]. It has been shown that deficits in SC polar lipids significantly impair cutaneous permeability [22]. Therefore, the SE wool wax studied in this work, with its high content of polar lipids, might be appropriate not only for cosmetic applications, where wool wax is extensively used, but also in dermatology as a modulator of skin barrier function for different skin disorders.

The thermotropic behaviour of the lipids of the different wool waxes was studied by DSC (Fig. 2). The obtained

Skin Pharmacol Physiol 2018;31:198–205
DOI: 10.1159/000488247

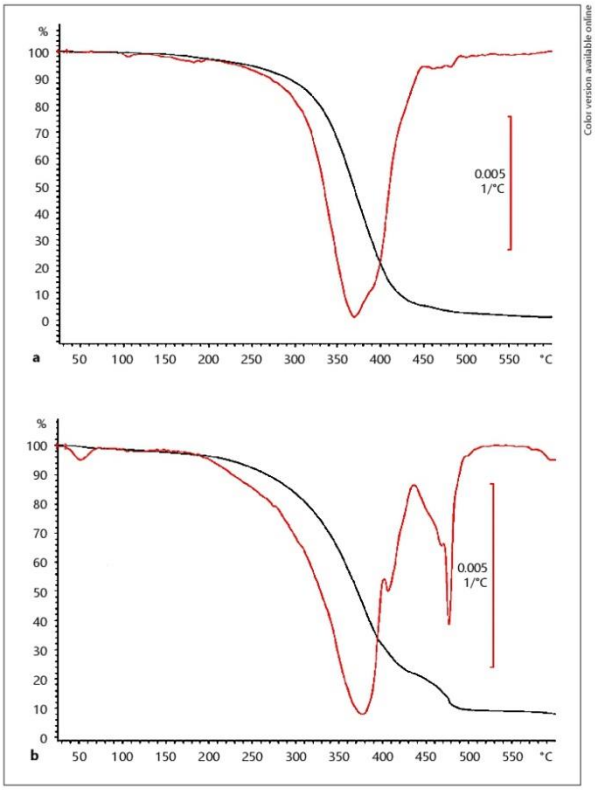

Fig. 3. Thermogravimetric curves (TGA) obtained at 10 °C/min under a nitrogen stream (50 mL/min), from 25 to 600 °C, of WE wool wax (**a**) and SE wool wax (**b**).

results indicate that when analysing the WE wool wax, the main endothermic transition (31.3 J/g) occurs at 0 °C with 2 smaller ones at 22 and 35 °C (9 and 8 J/g, respectively). The 2 latter peaks are in agreement with other DSC studies of lanolins, which showed 2 endothermic transitions at 22 and 38 °C. Both temperatures are in agreement with the Cryo-SEM findings and indicate that lanolin, such as human SC lipids, can coexist in both liquid and solid phases at physiological temperatures [6]. DSC experiments for the SE wool wax also showed 2 main endothermic transitions (25.1 and 19.6 J/g) at higher temperatures, 23 and 43 °C. This increase in the values of the transition temperatures and in the enthalpies for the SE wool wax could be associated with the increase in the polar character of the SE wool wax lipid composition. Another lanolin fraction, known as lanolin oil, which contains a higher concentration of lower-molecular-weight esters and branched-chain and hydroxyl compounds than the anhydrous lanolin wax, presents a similar DSC pattern with 2 transition temperatures, 23 and 42 °C. The higher polarity of this fraction is in agreement with the higher polarity of SE wool wax. Lanolin oil has been demonstrated to

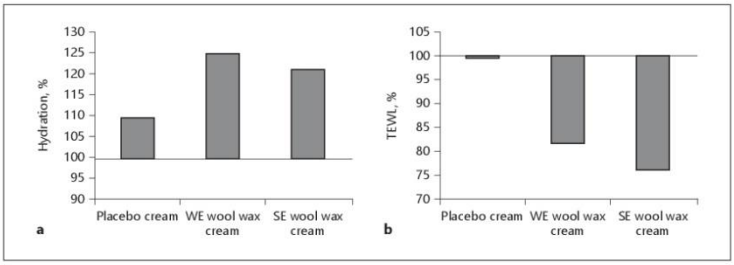

Fig. 4. Final percentages of skin hydration (**a**) and TEWL (**b**). Changes were doubly evaluated versus basal and control values.

Table 1. Skin hydration and TEWL before and after the in vivo treatment period with the different wool wax creams

		Control (untreated)	Placebo cream	WE wool wax cream	SE wool wax cream
Hydration	Initial	29.83 (28.17; 30.25)	28.83 (27.84; 29.59)	29.00 (27.17; 31.09)	28.33 (27.09; 30.09)
	Final	32.33 (31.17; 33.25)	36.83 (33.08; 41.58)	37.67 (34.67; 39.42)	40.00 (36.83; 42.92)
TEWL	Initial	10.48 (9.23; 13.06)	11.93 (10.35; 12.83)	11.93 (10.87; 13.02)	11.31 (10.64; 13.32)
	Final	11.09 (9.85; 13.99)	11.67 (8.80; 13.61)	11.32 (9.48; 13.83)	10.93 (9.53; 12.57)

Results are expressed as medians with 25th and 75th percentiles in parentheses.

be a carrier for soluble bacteriostats, to soothe stinging eyes and to increase the tensile strength of hair [23]. The similarities between SE wool wax and lanolin oil could be beneficial for hair-related applications due to the chemical and physical similarities between lanolin oil and the cell membrane complex of hair.

TGA were performed to follow the weight loss of the lipid samples with the increase in temperature (Fig. 3). A main degradation step of 92% was obtained for the WE wool wax at approximately 366 °C. A similar degradation step was obtained for the SE wool wax: 69% at 357 °C. However, additional steps at higher temperatures – 9, 13, and 7% at 416, 469, and 648 °C, respectively – were also found. When the wool wax is solvent extracted, approximately 30% of the resultant lipid mixture degrades at temperatures above 400 °C. Again, the TGA results demonstrate that when solvent-based scouring is performed, the resultant wool wax (SE wool wax) composition is enriched with compounds that degrade at higher temperatures.

To estimate the effects of the differently extracted wool waxes on skin, non-invasive biophysical studies were performed in vivo on 6 healthy volunteers. The skin hydration and TEWL, an indicator of the barrier function integrity, were tested. On 4 test areas on the left volar forearm of the volunteers, placebo cream, SE wool wax cream, WE wool wax cream, and control (untreated) were applied; the application areas were randomized for each subject. A total of 8 applications of the different tested samples were performed, and the skin parameters were measured each day before application. Table 1 shows the median values for skin hydration and TEWL before and after the treatment period. Variations of skin hydration and TEWL were doubly evaluated as a percentage of modification with respect to the basal (initial) value and after as a percentage of modification with respect to the control zone at the same time for each volunteer at the end of the in vivo treatment; the median values are represented in Figure 4.

This investigation showed that, although no statistically significant differences were obtained, consecutive application of the wool wax creams considerably increased the skin hydration, in both samples, by more than 20%; this effect was more pronounced for the WE wool

wax cream, which showed a 25% increase in this parameter (Fig. 4a). These results are in agreement with previous studies where corneometry was used to follow the increase in skin hydration produced by lanolin. In addition, both wool wax creams led to the reinforcement of skin barrier function, as shown by the distinct decrease in the TEWL values by more than 18% (Fig. 4b). In this case, the cream containing the SE wool wax promoted a higher skin barrier reinforcement, with a TEWL decrease of approximately 23%.

Additional in vivo studies have also been performed, where the protective and reparative capacities of the SE wool wax cream has been tested. The ability of this new polar wool wax to protect the skin barrier and accelerate the skin barrier repair, both of which were adversely affected by the conventional water scouring process, has been demonstrated, with results clearly comparable to those obtained previously with either conventional lanolin or a ceramide-enriched lanolin fraction [24].

Skin barrier function and water retention are the most important functions of the SC [25]. Both skin properties are dependent on the adequate functioning of SC lipids. The optimal composition and structure of SC lipids are required. The absorption of lanolin into human SC was demonstrated by previous studies [26]. Because it is highly compatible with SC lipids, topically applied lanolin appeared to be incorporated into intercellular lipid bilayers [27]. Similar results were demonstrated in an earlier work where the penetration of petrolatum into the SC layers was also suggested. Petrolatum, composed of a mixture of long-chain aliphatic hydrocarbons, was shown to be incorporated within the bilayer structure of the SC providing an improvement of the skin barrier function [28]. The topical application of the differently extracted wool wax creams demonstrated the beneficial effect of the topical application of exogenous lipids, with an improvement of the skin barrier integrity and increased skin hydration. SE wool wax, with a more polar composition, demonstrated the ability to reinforce the SC lipids, leading to improved skin barrier function. These properties are similar to those conferred by lanolins that are currently used in cosmetics, rendering this SE wool wax suitable for application in the preparation of cosmetics and dermatological products.

Conclusions

The lipid compositions and thermotropic behaviours of 2 differently extracted wool waxes have been evaluated. A higher amount of all the analysed lipids was found when the wool wax was extracted with solvents. In addition, the SE wool wax was found to have a significantly higher polar lipid content than the WE wool wax. This increase in the polar character of the SE wool wax was also demonstrated by the increased transition temperatures in the DSC analysis. TGA results showed that when the wool wax was solvent extracted more than 30% of the resultant lipid mixture degraded at temperatures above 400 °C, demonstrating that when a solvent-based scouring is performed the resultant wool wax composition is enriched with compounds that degrade at higher temperatures.

The beneficial effects of the topical application of the differently extracted wool wax creams were demonstrated, with an improvement of the skin barrier integrity and increased skin hydration. In addition, SE wool wax, with its more polar composition, demonstrated the ability to reinforce SC lipids, leading to improved skin barrier function. The results demonstrated the suitability of the SE wool wax for application in the preparation of cosmetics and dermatological products.

Acknowledgements

The authors wish to thank the LIFE program for financial support of the WDS "Eco-efficient dry wool scouring with total by-products recovery" LIFE 11 ENV/ES/588 and the Textile Manuel Tavares for providing the WE wool wax.

Statement of Ethics

All the procedures performed involving human participants were in accordance with the ethical standards of the institutional research committee and with the 1964 Helsinki Declaration and its later amendments or comparable ethical standards. Informed consent was obtained from all the individual participants included in the study.

Disclosure Statement

The authors do not have any conflicts of interests.

References

1 Datyner A: Surfactants in Textile Processing. Surfactant Science Series. New York, Dekker, 1983, vol 14, p 55.
2 Domínguez C, Jover E, Bayona JM, Erra P: Effect of the carbon dioxide modifier on the lipid composition of wool wax extracted from raw wool. Anal Chim Acta 2003;477:233–242.
3 Clark EW: The history and evolution of lanolin; in Hoppe U (ed): The Lanolin Book. Hamburg, Beiersdorf, 1999, pp 17–49.
4 Coderch L, Fonollosa J, Martí M, Parra JL: Ceramides from wool wax. JAOCS 2004;81:897–898.
5 Loden M, Maibach H: Dry Skin and Moisturizers. Boca Raton, CRC Press, 2000, p 259.
6 White SH, Mirejovsky D, King GI: Structure of lamellar lipid domains and corneocyte envelopes of murine stratum corneum. An X-ray diffraction study. Biochemistry 1988;27: 3725–3732.
7 Clark EW, Steel I: Investigations into biomechanisms of the moisturizing function of lanolin. J Soc Cosmet Chem 1993;44:181–195.
8 Mao G, Van Wyck D, Xiao X, Mack Correa C, Gunn E, Flach CR, Mendelsohn R, Walters RM: Oleic acid disorders stratum corneum lipids in Langmuir monolayers. Langmuir 2013;29:4857–4865.
9 Talreja P, Kasting G, Kleene N, Pickens W, Wang TF: Visualization of the lipid barrier and measurement of lipid path length in human stratum corneum. AAPS Pharm Sci 2001;3:48–56.
10 Stewart RG: Wool Scouring and Allied Technology, ed 3. Christchurch, Wool Research Organisation of New Zealand, 1988.
11 Iglesias S, Martí M: Eco-efficient dry wool scouring with total by-products recovery. Rev Quím Indust Text 2016;217:16–21.
12 Ackman RG, McLeod CA, Banerjee AK: An overview of analysis by Chromarod-Iatroscan TLC-FID. J Planar Chromatogr 1990;3:450–462.
13 Coderch L, Fonollosa J, Martí M, Garde F, de la Maza A, Parra JL: Extraction and Analysis of Ceramides from Internal Wool Lipids. J Am Oil Chem Soc 2002;79:1215–1220.
14 Berardesca E; European Group for Efficacy Measurements on Cosmetics and Other Topical Products: EEMCO guidance for the assessment of stratum corneum hydration: electrical methods. Skin Res Technol 1997;3:126–132.
15 Berardesca E, Maibach HI: Transepidermal water loss and skin surface hydration in the noninvasive assessment of stratum corneum function. Derm Beruf Umwelt 1990;38:50–53.
16 Jungersted JM, Hellgren LI, Jemec GRB, Agner T: Lipids and skin barrier function – a clinical perspective. Contact Dermatitis 2008; 58:255–262.
17 Van Smeden J, Hoppel L, van der Heijden R, Hankemeier T, Vreeken RJ, Bouwstra JA: LC/MS analysis of stratum corneum lipids: ceramide profiling and discovery. J Lipid Res 2011;52:1211–1221.
18 Barba C, Alonso C, Martí M, Manich A, Coderch L: Skin barrier modification with organic solvents. Biochim Biophys Acta 2016; 1858:1935–1943.
19 Imokawa G, Abe A, Jin K, Higaki Y, Kawashima M, Hidano A: Decreased level of ceramides in stratum corneum of atopic dermatitis: an etiologic factor in atopic dry skin? J Invest Dermatol 1991;96:523–526.
20 Arikawa J, Ishibashi M, Kawashima M, Takagi Y, Ichikawa Y, Imokawa G: Decreased levels of sphingosine, a natural anti-microbial agent, may be associated with vulnerability of the stratum corneum from patients with atopic dermatitis to colonization by *Staphylococcus aureus*. J Invest Dermatol 2002;119:433–439.
21 Jungersted JM, Scheer H, Mempel M, Baurecht H, Cifuentes L, Høgh JK, Hellgren LI, Jemec GB, Agner T, Weidinger S: Stratum corneum lipids, skin barrier function and filaggrin mutations in patients with atopic eczema. Allergy 2010;65:911–918.
22 Imokawa G, Ishida K: Role of ceramide in the barrier function of the stratum corneum: implications for the pathogenesis of atopic dermatitis. J Clin Exp Dermatol Res 2014;5:1.
23 Barnett G: Lanolin and derivatives. Cosmet Toiletr 1986;101:21–44.
24 De Pera M, Coderch L, Fonollosa J, de la Maza A, Parra JL: Effect of internal wool lipid liposomes on skin repair. Skin Pharmacol Appl Skin Physiol 2000;13:188–195.
25 Coderch L, Fonollosa J, de Pera M, Martí M, de la Maza A, Parra JL: Ceramide-rich lanolin fractions and compositions and use thereof in the preparation of products for skin care and treatment. Patent No ES 2178960. 2002.
26 Clark EW: Short-term penetration of lanolin into human stratum corneum. J Soc Cosmet Chemists 1992;43:219–227.
27 Clark EW, Steel I: Investigations into biomechanisms of the moisturizing function of lanolin. J Soc Cosmet Chemists 1993;44:181–193.
28 Ghadially R, Halkier-Sorensen L, Elias PM: Effects of petrolatum on stratum corneum structure and function. J Am Acad Dermatol 1992;26:387–396.

Skin Pharmacol Physiol 2018;31:198–205
DOI: 10.1159/000488247

Annex 3. Lanolin-Based Synthetic Membranes as Percutaneous Absorption Models for Transdermal Drug Delivery

pharmaceutics

MDPI

Article

Lanolin-Based Synthetic Membranes as Percutaneous Absorption Models for Transdermal Drug Delivery

Victor Carrer *, Beatriz Guzmán, Meritxell Martí, Cristina Alonso and Luisa Coderch

Department of Chemical and Surfactants Technology, Institute of Advanced Chemistry of Catalonia (IQAC-CSIC), 08304 Barcelona, Spain; bgmtqt@cid.csic.es (B.G.); mmgesl@cid.csic.es (M.M.); cristina.alonso@iqac.csic.es (C.A.); lcnesl@cid.csic.es (L.C.)

* Correspondence: victorcarrer@gmail.com; Tel.: +34-93-400-6100 (ext. 2328)

Received: 8 May 2018; Accepted: 13 June 2018; Published: 21 June 2018

check for updates

Abstract: Background: The major in vitro permeation studies are currently performed in Franz-type diffusion cells because of their simplicity, cost effectiveness and because the experimental conditions can be easily controlled. Apart from the skin, Franz-type diffusion cells can be used with synthetic membranes. Nevertheless, they do not emulate the nature of the lipidic matrix, which is responsible for the topical barrier function. Objective: This paper offers two new approaches combining different synthetic membranes (Strat-M® and Nucleopore®) with lanolin, which provides lipidic components similar to the lipidic matrix. Methods: The molecular structure of lanolin was studied in membranes by attenuated total reflectance infrared spectroscopy (ATR-IR). The water permeability and absorption of lidocaine, diclofenac sodium and betamethasone dipropionate were also studied and compared against free-lanolin membranes and skin. Results: The results showed an increasing barrier function after lanolin application in both membranes, resulting in a decrease in water permeability. Observing the IR spectra, the lateral packaging of the lipid in the synthetic membranes seems to emulate the orthorhombic disposition from the stratum corneum. Moreover, the three substances applied to the lanolin-containing membranes have a similar absorption to that of the skin. Conclusions: In conclusion, combining synthetic membranes with lanolin may be a useful approach to mimic topical actives' absorption.

Keywords: synthetic membranes; lanolin; skin absorption; Franz cell; topical exposure

1. Introduction

The primary barrier to dermal drug delivery is the stratum corneum (SC), which forms the outermost layer of the epidermis [1]. The SC consists of several layers of partially-overlapping corneocytes, which are surrounded by the cell envelope and are imbedded in a lipid matrix. Only a limited number of drugs can cross the SC. Drug permeation across the SC depends on the interaction between the skin, the drug and the components in the formulation vehicle [2,3]. Due to the highly impermeable character of the cornified envelope of corneocytes, the SC lipid matrix provides the actual barrier to diffusion of the substance through the skin [4–6].

Percutaneous penetration warrants in vivo experiments in humans. These experiments are often morally undesirable, expensive and time consuming. Additionally, high inter- and intra-individual variability is found in the data [7]. Therefore, alternatives to in vivo studies in humans are sought. The suitability of the different in vitro permeability models using excised skin (human or animal) to mimic the in vivo studies has been widely reviewed [8], but obtaining a sufficient supply of excised human and animal skin is often a challenge and tends to be costly.

There have also been attempts to create synthetic membranes that may be used as human skin models to investigate the transdermal diffusion properties of pharmaceutical and cosmetic compounds

and formulations [9]. The FDA has encouraged the use of porous synthetic membranes to evaluate the performance of topical products because they act as a support without posing a rate-limiting barrier [10]. Unlike skin, these membranes are inert and do not introduce biological variations. Moreover, the variability subjected to the anatomical site, age, race of the skin donor and skin-biopsy preparation and storage can be overtaken. Such synthetic membranes are composed of a thin sheet of polymeric macromolecules that can control the passage of components through them. They may be composed of synthetic polymers (e.g., polysulfone, polycarbonate) or semi-synthetic cellulose polymers (e.g., cellulose acetate, cellulose nitrate). Despite these synthetic models, more efforts should be carried out to emulate the complex composition of the SC lipidic structure [11].

The lipid lamellae are oriented approximately parallel to the surface of the corneocytes, and they are mainly composed of cholesterol, ceramides and free fatty acids [12,13]. The skin contains at least six ceramide families, which are believed to play a different role in skin properties [14]. Moreover, the free fatty acids cause the skin barrier to have a pH of 5.5, which affects the ionization state of the topically-applied substances. Skin barrier disruption due to topical treatment with surfactants or organic solvents is attributed to a selective/integral depletion or lipidic alteration [15]. The first efforts to study lipidic synthetic membranes and compare to skin absorption were carried out by Landmann in 1984 [16]. More recently, Anwar and colleagues [17] developed a simplified model that should serve to a bridge the gap between the more realistic, but complex model systems and the simple models. The challenge here is to develop models that lend themselves to both molecular-level experiments and simulations.

The structure of lanolin, which mimics the lipidic matrix of the SC by having a similar chemical composition and properties, may offer a suitable strategy to achieve accurate modeling of the skin barrier properties by combination with synthetic membranes. It has been demonstrated that wool wax shares important features with SC lipids: wool wax contains cholesterol, an essential constituent of SC lipids. Cholesterol and its derivatives, ceramides or some free fatty acids have been found in lanolin [18–20]. Moreover, wool wax and SC lipids can coexist as solids and liquids at physiological temperatures [21–23]. In this study, lanolin was obtained with a closed-loop process to scouring wool fibers designed in a pilot plant called the wool dry scouring process (WDS) [24]. It is important to note that with the WDS process, the resulting lanolin has more polar lipids and hence a more human resemblance [25].

The present study focuses on whether the addition of lanolin to synthetic membranes (Nucleopore® and Strat-M®) improves the membrane barrier and emulates porcine skin. Dermatomed pig skin is used in these investigations because pig skin morphology and permeability are similar to those of humans [26], and therefore, it is an accepted model for the skin penetration assessment of cosmetic ingredients [2]. Nucleopore® is a 10-µm-thick filter in which a 0.05-nm pore size is created in a polyethylene terephthalate membrane 25 mm in diameter [27], whereas Strat-M® is an ultrafiltration membrane composed of polyethylene sulfone that is predictive of diffusion in human skin [28].

The water permeability is an indicator of the membrane integrity/barrier function and will be evaluated by measuring the transepidermal water loss (TEWL). Additionally, the lipid structure of the lanolin models is evaluated by attenuated total reflection Fourier transform infrared (ATR-IR) spectroscopy to be compared against the porcine SC lipidic spectra. A highly lipidic order (orthorhombic and hexagonal) has been found in isolated SC [29] and in model mixtures of SC lipids [30,31]. This is strongly related to the SC lipid barrier function considering that numerous studies have shown that the permeability of water and small molecules in healthy skin differs considerably depending on the lipidic order [31,32].

The absorption of three substances widely employed in dermatology with different molecular weights and hydrophilic/hydrophobic balances such as lidocaine, diclofenac sodium and betamethasone dipropionate were compared. Considering that the lipophilicity of the substance is a crucial parameter on its skin absorption, the octanol/water distribution coefficient (LogD) of the three actives is also determined at pH 7.4 (physiological pH) and pH 5.5 (skin surface pH) and is discussed together with the permeation results.

Next, the main aim of this work was to obtain lanolin-based synthetic membranes to be used in skin permeation studies as models of mammalian skin. Lipid structural IR evaluation and water

permeation and penetration assays of three topical actives will be performed to determine the effect of lanolin on the membrane skin models.

2. Methodology

2.1. Materials

The Institutional Review Board and Animal Ethics Committee of the University of Barcelona, Barcelona, Spain, approved the protocol (28 January 2013). Animal handling was approved by our Institutional Review Board and Ethics Committee (approval reference number: DMAH 5605). The management of the animals used in this study conforms to the Guide for the Care and Use of Laboratory Animals published by the United States National Institutes of Health [33] Unboiled porcine skin was obtained from the dorsal area of weanling female white/landrace pigs weighing 30–40 kg. Following euthanasia, the bristles were removed carefully with an animal clipper and were subsequently washed with water. The hair-clipped skin was dermatomed using a Dermatome GA630 system (Aesculap, Tuttlingen, Germany) to a thickness of 500 ± 50 µm, cut into pieces (2.5-cm inner diameter) and then stored at −20 °C until their use.

Two synthetic membranes were studied, as well as the matrix from which the lanolin-containing models originated. StratM® (Merck Millipore, Darmstadt, Germany) and Nucleopore® (Sigma Aldrich, St. Louis, MO, USA) synthetic membranes were purchased. Both membranes were cut into discs that overlapped with the edges of the Franz cell compartment to prevent leakage.

The lanolins that were applied to the synthetic membranes were extracted from Spanish merino sheep using the WDS process from the European Union's funding program LIFE 11 (project ENV/ES/588 [24]). Briefly, the wool was scoured with hexane to remove dust impurities, then the hexane solution was centrifuged, and the lanolin was recovered from the hexane with distillation at 35 °C. Finally, lanolin was desiccated to remove the residual water.

To study the potential of the membranes to mimic the skin absorption, they were tested with three actives: lidocaine (Sigma Aldrich, St. Louis, MO, USA), diclofenac sodium (Sigma Aldrich, St. Louis, MO, USA) and betamethasone 17,21-dipropionate (Sigma Aldrich, St. Louis, MO, USA).

2.2. Membrane Formation

2.2.1. Strat-M-Lanolin

The addition of lanolin to the Strat-M® membranes was carried out following the next protocol: 100 µL of lanolin (see Section 2.1) 5% in a hexane (Merck, Darmstadt, Germany), ethanol 96% (Merck, Darmstadt, Germany) 2:1 solution were applied three times on the top of the Strat-M® membranes under nitrogen flow (Carburos metalicos, Aranjuez, Spain). Next, these Strat-M-lanolin membranes were stored at 85 °C for 10 min to fix the lipids and dry the membrane.

2.2.2. Nucleopore-Lanolin

Lanolin was added to the Nucleopore® membranes following the more complex procedure for lipid fixation previously detailed by Pullmannová et al. [34], wherein the membranes were hydrated in hexane:ethanol 96% (2:1) and then dried at room temperature. Under nitrogen, 100 µL of lanolin 5% in hexane:ethanol 96% (2:1) were applied on the top. The membranes are stored at 2–6 °C in a vacuum desiccator for 24 h. Finally, the membranes were placed at 85 °C for 10 min, and after 3 h at room temperature, the membranes were ready to use.

2.3. Lipidic Conformation Analysis by ATR-IR

The lipidic conformation for pure lanolin, porcine skin, Nucleopore-lanolin and Strat-M-lanolin was studied using ATR-IR spectroscopy. The infrared spectra were obtained using the 360-FTIR spectrophotometer Nicolet Avatar (Nicolet Instruments, Inc., Madison, WI, USA) equipped with

an attenuated total reflection (ATR) accessory that used a diamond with an angle of incidence of 45° in a horizontal orientation.

Before analysis, the samples were placed with the SC/lanolin side facing the ATR diamond. To ensure reproducible contact between the sample and crystal, a pressure of 10 kPa was applied to the samples. All analyzed spectra represented an average of 32 scans obtained with a resolution of 4 cm^{-1}, and the wavenumber range used was 4000–700 cm^{-1}. The peak positions were determined with the aid of OMNIC software Version 7.3 (Nicolet, Madison, WI, USA) using a Gaussian–Lorentzian peak fitting and baselined spectra. Two different peaks were studied: 2850 and 2920 cm^{-1}, which are assigned to the CH_2 symmetric and asymmetric stretching vibration, respectively. Analysis of every sample was made in triplicate.

2.4. Water Permeability by TEWL

The commercial synthetic membranes (Strat-M® and Nucleopore®), lanolin-containing membranes (Strat-M-lanolin and Nucleopore-lanolin) and excised pig skin were mounted in a static Franz diffusion cell with the SC/lanolin side facing the donor compartment.

The nominal surface area was 1.86 cm^2, and the receptor chamber capacity was approximately 3 mL. The receptor chamber was filled with receptor fluid. The receptor fluid (RF) was Dulbecco's phosphate-buffered saline at pH 7.4 (Sigma Aldrich, St. Louis, MO, USA) in Milli-Q water with the addition of 0.04% (*w*/*v*) gentamicin sulfate salt (Sigma Aldrich, St. Louis, MO, USA) and 5% (*w*/*v*) bovine serum albumin (Sigma Aldrich, St. Louis, MO, USA). Air bubbles were carefully removed between the skin and RF with a syringe. Finally, the assembled Franz-type cells were placed in a temperature-regulated water bath on top of a water-resistant magnetic stirring plate and stirred at 400 rpm to maintain receptor fluid homogeneity. The water bath was maintained at 37 °C to obtain a membrane surface temperature of 32 ± 1 °C.

Once the skin and membranes were stabilized in the water bath, the integrity and permeability of all the studied membranes were studied with the transepidermal water loss value (TEWL). This was measured for 2 min using a Tewameter TM300 system (Courage & Khazaka, Cologne, Germany) in every replicate before the beginning of the penetration assay. Nine replicates for every model were evaluated. Once the results were obtained, the Kruskal–Wallis test was applied to detect significant differences between the different models. The Statgraphics plus 5 software (Statgraphics.Net, Madrid, Spain) was used for statistical analyses. Significant differences in the mean values were evaluated by the F test. A *p*-value below 0.1 was considered significant.

2.5. Penetration Assay on Static Diffusion Franz-Cell Assembly

Lidocaine, diclofenac sodium and betamethasone dipropionate were selected considering that they are commonly employed in topical formulations. Their respective distribution coefficient (LogD) at pH 7.4 and 5.5, as well as their molecular weight were calculated in silico using the Pipeline Pilot software (Accelrys, San Diego, CA, USA).

To avoid the permeability differences caused by the formulation, the three actives were formulated in propylene glycol. Propylene glycol (PG) (Sigma Aldrich, St. Louis, MO, USA) was added to lidocaine, diclofenac sodium and betamethasone dipropionate at 2%, 0.5% and 1%, respectively (same concentration of commercial topical formulations), and then solicited for 10 min to assure the complete solubility of each active in PG.

Having reached this point, 20 µL of each PG solution were applied to the surface delimited by the donor compartment. PG formulations were studied in triplicate in every membrane. After 24 h, the receptor fluid of all the membranes were collected, extracted and analyzed by high-performance liquid chromatography (HPLC) (see the following section). The extractor solvents of each active are established in Table 1.

Table 1. HPLC analytical conditions for lidocaine (Lid), diclofenac sodium (Dic) and betamethasone dipropionate (Bet).

Compound	Lidocaine	Diclofenac Sodium	Betamethasone Dipropionate
Extractor solvent	ACN-TFA 0.5%	Methanol	Methanol
Column	LiChrocart® 125-4 Lichrosphere® 100RP-18 5 µm	LiChrocart® 250-4 Lichrosphere® 100RP-18 5 µm	LiChrocart® 250-4 Lichrosphere® 100RP-18 5 µm
Wavelength (nm)	205	254	239
Injection volume (µL)	20	20	20
Mobil phase	70% buffer phosphate pH 7.4 30% acetonitrile	66% methanol 34% phosphoric acid 0.7%	73% methanol 27% water
Linear regression equation (R^2)	$A = 414,046\,[Lid] - 68,532$ (0.9999)	$A = 80,050\,[Dic] - 2484$ (0.9997)	$A = 1,811,416[Bet] + 47,781$ (0.9999)

In the case of the skin, the different skin layers were separated and analyzed following the ensuing procedure. The skin surface was washed and wiped with a cotton swab to remove any remaining formulation and was extracted into 10 mL of extractor solvent (W). Next, 8 strip preparations were carried out on the surface horny layers of the stratum corneum with adhesive tape (D-Squame, Cuderm Corporation, Dallas, TX, USA) applied under controlled pressure (80 g/cm^2) using a metallic bar for 5 s. The 8 strips were extracted into 2 mL of extractor solvent (S). Finally, the epidermis (E) was separated from the dermis (D) after heating the skin at 80 °C for several seconds. Both tissues were extracted with 1 mL of extractor solvent. All the skin extracts remained overnight with the extractor solvent and then were shaken for 30 min and subsequently sonicated for 15 min. Before the HPLC analysis, all the extracts were filtered with a 0.45-nm nylon filter (Cameo, Perrysburg, OH, USA). The employed reagents were: acetonitrile (Sigma Aldrich, St. Louis, MO, USA), methanol (Merck, Darmstadt, Germany), buffer phosphate (pH 7) (Merck, Darmstadt, Germany), phosphoric acid (Merck, Kenilworth, NJ, USA) and trifluoroacetic acid (Alfa Aesar, Karlsruhe, Germany).

The amount of the active in the samples was determined by the HPLC methodology validated according to the International Conference on Harmonisation Q2 (R1) guidelines in terms of linearity, accuracy and precision [35]. The HPLC system consisted of a VWR-Hitachi HPLC apparatus with a CM5430 DAD detector, L-2130 Pump, L-2200 Autosampler and an interface device. The flow rate was 1 mL/min under isocratic conditions; the injection volume was 20 µL; and all the analyses were performed under room temperature. The columns, wavelengths and mobile phases for every active are compiled in Table 1.

The results are presented as normalized amounts (%) of permeated substance with its standard deviation. The permeated amount in the case of skin is considered the sum of the epidermis, dermis and receptor fluid. For the rest of the membranes, the amounts were found to be equivalent to those in the receptor fluid. Permeability differences between porcine skin and lanolin membranes were sought with the Kruskal–Wallis test previously described in Section 2.4.

3. Results and Discussion

3.1. Evaluation of the Lipid Conformation of Membranes by ATR-FTIR

The lipidic order of lanolin, Strat-M-lanolin, Nucleopore-lanolin and pig skin was studied using ATR-FTIR. This technique is a non-invasive technique with a depth penetration of 1 µm that makes it suitable to investigate lanolin or SC without isolation from other layers. For this study, of particular interest were the bands associated with the alkyl chain of the lipids. Information about the conformational order-disorder of the skin lipids can be extracted by the analysis of the 2920 and 2850 cm^{-1} stretching bands. In the case of symmetric CH_2 stretching, vibrations of 2849 cm^{-1}, 2850 cm^{-1} and 2852 cm^{-1} indicate orthorhombic, hexagonal and liquid crystalline, respectively.

An increase in the vibrational frequency generally indicates an increase in the disorder. A similar behavior was observed for the asymmetric CH_2 stretching at 2920 cm^{-1}, although the symmetric stretching is more sensitive to the conformation changes.

In our case, the peak position in all the replicates was determined, and their average and standard deviation were calculated (Table 2). All the analyzed samples have a vibrational frequency of approximately 2849 cm^{-1} or less corresponding in all cases to orthorhombic conformations. Low standard deviations were obtained in all the samples. These values agree with the ones corresponding to the natural lipidic packaging of healthy pig skin. Therefore, the two proposed synthetic models present a highly ordered lipidic structure that could emulate the lipidic package of the stratum corneum.

Table 2. ATR-FTIR of CH_2 symmetric and asymmetric stretching modes of pure lanolin, Nucleopore-lanolin, Strat-M-lanolin and pig skin.

	Lanolin	Nucleopore-Lanolin	Strat-M-Lanolin	Pig Skin
λCH2 St. Sym	2848.5 ± 0.01	2848.5 ± 0.10	2848.5 ± 0.03	2849.4 ± 0.03
λCH2 St. Asym	2917.9 ± 0.07	2917.9 ± 0.19	2916.3 ± 0.03	2916.9 ± 0.08

λCH2 St. Sym: CH2 symmetric stretching; λCH2 St. Asym: CH2 asymmetric stretching.

3.2. Water Permeability of Membranes

Transepidermal water loss (TEWL) is commonly used to measure membrane/skin barrier function permeability and integrity. The loss of water across the membrane is a valuable clue to determine whether a membrane is suitable to test the skin absorption. In this work, the TEWL values and their respective standard deviation have been calculated for each membrane (n = 9) before topical application (Figure 1).

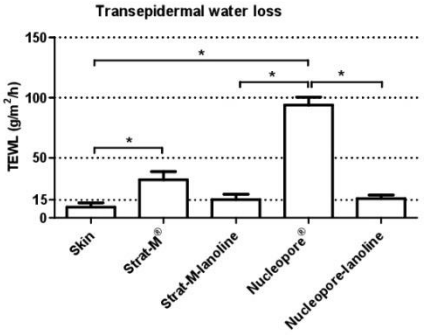

Figure 1. Transepidermal water loss (TEWL) measured on skin, Strat-M®, Strat-M-lanolin, Nucleopore® and Nucleopore-lanolin. * indicates a p-value ≤ 0.1 from the Kruskal–Wallis test.

A low standard deviation was obtained in all the different membranes, including the skin. This is an important detail considering that it may imply homogeneity and stability not only of the skin biopsy but also of the commercial membranes (Strat-M® and Nucleopore®) and the presented lanolin-containing membranes from this work (Strat-M-lanolin and Nucleopore-lanolin).

The skin biopsies were appropriate to test because the values were equal to or below 15 $g/m^2/h$ [36]. Observing the values obtained from the commercial models, the TEWL values for Strat-M® were lower than those for Nucleopore®, indicating a better barrier function for Strat-M®. However, their permeability was far away from the maximum accepted for the Organisation for Economic Co-operation and Development (OECD) guidelines. The TEWL results of Strat-M-lanolin and Nucleopore-lanolin indicated that the addition of lanolin brings an important reduction of the TEWL values, making the values comparable to those from the skin. The addition of the lanolin layer on Strat-M® and Nucleopore® sought the empowerment of the barrier function in both membranes, overcoming one of the main problems when mimicking the skin barrier with artificial membranes: the high permeability compared with that of the skin [37]. By adding lanolin to the original synthetic membrane, a significant reduction was observed ($p \leq 0.1$) when the Kruskal–Wallis test was performed, implying an increase in barrier function.

In summary, the lanolin layer on Strat-M® and Nucleopore® reduced the TEWL values. No significant differences were found between the skin and the two membranes with lanolin after performing the Kruskal–Wallis test ($p > 0.1$). This means there was a similarity between the skin and the lanolin membranes on water permeability.

3.3. Physico-Chemical Properties of Actives

Lidocaine, diclofenac sodium and betamethasone dipropionate were selected considering that they are commonly employed in topical formulations and because they have a different chemical nature (basic, acid and neutral, respectively) and a wide range of lipophilicity. Their respective distribution coefficients (LogD) at pH 7.4 and 5.5, as well as their molecular weights were calculated in silico using Pipeline Pilot software (Accelrys, San Diego, CA, USA).

LogD was determined at pH 5.5 because it is the pH of the skin surface, and LogD was determined at pH 7.4 because it is the pH of the receptor fluid and blood. As shown in Table 3, betamethasone dipropionate, as a neutral active, showed no changes in LogD at the different pH values. By contrast, lidocaine (base) and diclofenac sodium (acid) showed opposite behaviors. At lower pH, the increase in the ionized form of the lidocaine caused a decrease in LogD, resulting in higher hydrophilicity. In the opposite case, the LogD at pH 5.5 for diclofenac sodium was higher than that at pH 7.4 because the non-ionized form was predominant at acidic pH. This implied that, at pH 5.5, the LogD range was, from highest to lowest, betamethasone dipropionate > diclofenac sodium > lidocaine, with lidocaine the most hydrophilic compound. However, at pH 7.4, the LogD range was betamethasone dipropionate > lidocaine > diclofenac sodium, with diclofenac sodium the most hydrophilic compound. This could be important to predict or explain the permeation of these actives through the different membranes.

Table 3. Molecular weight (MW) and octanol water distribution coefficients (LogD) at pH 5.5 and 7.4 obtained from the ChemAxon platform.

Active (Acidic Nature)	LogD at pH 5.5	LogD at pH 7.4	MW (g/mol)
Lidocaine (basic)	0.61	2.33	234.34
Diclofenac sodium (acid)	2.75	1.1	318.14
Betamethasone 17,21-dipropionate (neutral)	3.96	3.96	504.59

3.4. Penetration Assay of Actives through Membranes

As described in the methodology, lidocaine, diclofenac sodium and betamethasone dipropionate solubilized in PG were applied via Franz-cells onto pig skin biopsies, lanolin-free synthetic membranes (Strat-M® and Nucleopore®) and lanolin synthetic membranes (Strat-M-lanolin and Nucleopore-lanolin).

When pig skin biopsies were used, the amount of actives was evaluated in the stratum corneum (S), epidermis (E), dermis (D) and receptor fluid (RF). Skin permeation (Perm) was considered the summed amounts from the epidermis, dermis and receptor fluid (Table 4).

Table 4. Normalized amounts (%) found in the stratum corneum (SC), epidermis (E) dermis (D) and receptor fluid (RF). In the case of artificial membranes, skin permeation (Perm) belongs to the amounts found in the receptor fluid.

Normalized Amounts (%)		Lidocaine 2%	Diclofenac Sodium 0.5%	Betamethasone Dipropionate 1%
Skin	S	5.02 ± 4.56	9.70 ± 4.25	13.60 ± 3.37
	E	4.61 ± 3.63	7.34 ± 2.22	4.30 ± 1.58
	D	2.94 ± 0.96	1.84 ± 1.53	0.00 ± 0.01
	RF	50.02 ± 10.05	11.68 ± 6.17	0.00 ± 0.00
	Perm	57.58 ± 7.63	20.86 ± 9.24	4.30 ± 1.57
Strat-M®	Perm	26.48 ± 8.14	49.19 ± 4.23	0.78 ± 1.36
Strat-M-lanolin	Perm	68.40 ± 6.50	45.22 ± 9.36	4.03 ± 0.59
Nucleopore®	Perm	98.37 ± 2.10	94.56 ± 0.45	8.69 ± 2.16
Nucleopore-lanolin	Perm	90.81 ± 2.84	29.58 ± 9.78	10.54 ± 0.99

When the actives were applied on the skin, lidocaine showed the highest permeation rates followed by diclofenac sodium. Betamethasone dipropionate was the less absorbed compound. As explained previously, LogD was an important parameter when studying diffusion across membranes. In the case of skin, LogD at pH 5.5 must be considered because this is the physiological pH in this tissue. When observing the LogD at pH 5.5 and molecular weight for the three actives, the absorption through the skin seemed to be promoted by low molecular weights and low LogD values. Lidocaine (highly absorbed) was small and the most hydrophilic compound, followed by diclofenac sodium with a medium value of LogD and molecular weight. Betamethasone dipropionate was a lipophilic and heavy molecule poorly absorbed across the skin (Figure 2 and Table 4).

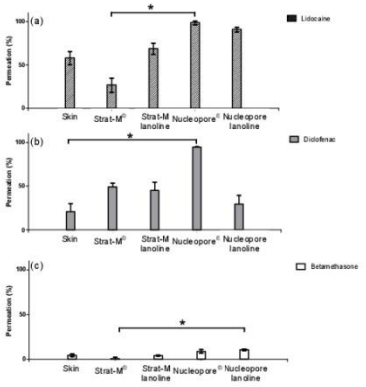

Figure 2. Normalized absorbed amounts (%) in skin, Strat-M®, Strat-M-lanolin, Nucleopore®, Nucleopore-lanolin for lidocaine (**a**), diclofenac sodium (**b**) and betamethasone dipropionate (**c**). * indicates a p-value ≤ 0.1 from the Kruskal–Wallis test.

The permeation obtained using the commercial membranes confirms the deductions made when observing the TEWL values. We observed higher values of TEWL on Nucleopore® than in Strat-M® that could imply higher permeation on Nucleopore®. Hence, the three different actives permeated more

into Nucleopore® rather than into Strat-M®. These differences were hardly seen on betamethasone dipropionate because the lack of solubility in the acceptor fluid limited its diffusion through the membrane (Figure 2). For the three compounds, the Kruskal–Wallis test could not detect any significant difference ($p > 0.1$) between the skin permeability and the lanolin surrogates.

When observing the actives' absorption rank on Strat-M®, unlike on skin, diclofenac sodium permeated more than lidocaine. Similar results could be deduced for Nucleopore, but its low barrier (demonstrated observing the TEWL values) did not allow the differentiation between lidocaine and diclofenac sodium. These permeability changes between diclofenac sodium and lidocaine could be explained by observing their respective LogD. As discussed previously, the pH of the skin is 5.5, whereas the pH of the commercial membranes was that of the receptor fluid, pH 7.4. Observing their respective LogD, diclofenac sodium was demonstrated to be more hydrophilic than lidocaine at pH 7.4. Therefore, the same deduction observed when the actives were applied on the skin could be extracted: the most hydrophilic compound, which, in this case was diclofenac sodium, permeated more than lidocaine. Betamethasone dipropionate with the highest LogD remained the least permeated compound.

In summary, the lanolin layer was added to Strat-M® and Nucleopore® synthetic membranes. Comparing their TEWL values against those from the lanolin-containing membranes, an increment of the barrier function as a result of the addition of lanolin was observed. The permeation results obtained for the three actives showed this barrier enhancement. The addition of lanolin promoted the reduction in the absorption of the three substances. Moreover, the rank in which the actives were absorbed, lidocaine > diclofenac sodium > betamethasone dipropionate, was identical to that for the lanolin-containing membranes and pig skin one (Figure 2). As stated in the Introduction section, lanolin has a similar composition and pH as the skin lipidic matrix. Therefore, the LogD value that must be considered is 5.5. At this pH, lidocaine was the most hydrophilic active followed by diclofenac sodium and betamethasone dipropionate.

Lanolin addition to the artificial membranes caused a reduction of TEWL and a modulation of the permeation of the three different compounds, leading to results very similar to those obtained with the skin. Lanolin previously demonstrated its ability to reinforce SC lipids, leading to improved skin barrier function in in vivo topical studies [25]. This work confirms its suitability regarding its use as an artificial membrane for permeation or percutaneous absorption models.

4. Conclusions

This study demonstrated the potential utility of lanolin addition to artificial membranes Strat-M® and Nucleopore® as a model for the absorption of topical actives. Both membranes were mounted in a vertical diffusion cell, and the transepidermal water loss and percutaneous absorption of three topical actives (lidocaine, diclofenac sodium and betamethasone dipropionate) were compared against the membranes without lanolin and porcine skin. To better understand the permeability changes of the actives in the different models, the active lipophilicities were determined in silico at pH 5.5 and 7.4, corresponding to the skin surface and systemic environment, respectively.

Results have shown that the addition of lanolin to synthetic membranes significantly reduces the TEWL values, similar to the porcine skin levels. The lipid conformation and structure studied by ATR-IR indicate a high lipidic order and orthorhombic structure for lanolin synthetic membranes, similar to the lipidic structure of the skin. The Franz-cell absorption study showed that the hydrophilicities of the actives were closely related to their diffusion through the membranes. Lanolin addition to the artificial membranes caused a reduction of TEWL and modulation of the permeation of the three different compounds, leading to results very similar to those obtained with the skin. Either in the TEWL or the penetration results, no significant differences were observed between the skin and the lanolin-membranes. In conclusion, combining synthetic membranes with lanolin may be a useful approach to mimic the absorption of topical actives. Future steps should include other

studies of membrane integrity such as transepithelial resistance and the percutaneous absorption of other formulations and actives.

Author Contributions: L.C. and M.M. conceived and designed the experiments; B.G. performed the experiments; C.A. and V.C. analyzed the data; V.C. and L.C. wrote the paper.

Funding: The authors have no funding to report.

Acknowledgments: The authors are grateful to Montserrat Rigol Muxart and Núria Solanes Batlló from the Department of Cardiology (Institut d'Investigacions Biomèdiques August Pi i Sunyer (IDIBAPS) Hospital Clínic, Universitat de Barcelona, Spain) for supplying porcine skin biopsies. The authors acknowledge also the Life program for financial support of the WDS "Eco-Efficient dry wool scouring with the total by-products recovery" LIFE 11 ENV/ES/588, Recuperación de Materiales Textiles (RMT) and Textile Manuel Tavares for providing the lanolins.

Conflicts of Interest: The authors have no conflict of interest to declare.

References

1. Vandervoort, J.; Ludwig, A. Microneedles for transdermal drug delivery: A minireview. *Front. Biosci.* **2008**, *13*, 1711–1715. [CrossRef] [PubMed]
2. Barbero, A.M.; Frasch, H.F. Pig and guinea pig skin as surrogates for human in vitro penetration studies: A quantitative review. *Toxicol. Vitr.* **2009**, *23*, 1–13. [CrossRef] [PubMed]
3. El Maghraby, G.M.; Barry, B.W.; Williams, A.C. Liposomes and skin: From drug delivery to model membranes. *Eur. J. Pharm. Sci.* **2008**, *34*, 203–222. [CrossRef] [PubMed]
4. Boddé, H.E.; van den Brink, I.; Koerten, H.K.; de Haan, F.H.N. Visualization of in vitro percutaneous penetration of mercuric chloride; transport through intercellular space versus cellular uptake through desmosomes. *J. Control. Release* **1991**, *15*, 227–236. [CrossRef]
5. Meuwissen, M.E.; Janssen, J.; Cullander, C.; Junginger, H.E.; Bouwstra, J.A. A cross-section device to improve visualization of fluorescent probe penetration into the skin by confocal laser scanning microscopy. *Pharm. Res.* **1998**, *15*, 352–356. [CrossRef] [PubMed]
6. Johnson, M.E.; Blankschtein, D.; Langer, R. Evaluation of solute permeation through the stratum corneum: Lateral bilayer diffusion as the primary transport mechanism. *J. Pharm. Sci.* **1997**, *86*, 1162–1172. [CrossRef] [PubMed]
7. Leal, L.B.; Cordery, S.F.; Delgado-Charro, M.B.; Bunge, A.L.; Guy, R.H. Bioequivalence Methodologies for Topical Drug Products: In Vitro and Ex Vivo Studies with a Corticosteroid and an Anti-Fungal Drug. *Pharm. Res.* **2017**, *34*, 730–737. [CrossRef] [PubMed]
8. Waters, L.J. Recent developments in skin mimic systems to predict transdermal permeation. *Curr. Pharm. Des.* **2015**, *21*, 2725–2732. [CrossRef] [PubMed]
9. Haq, A.; Dorrani, M.; Goodyear, B.; Joshi, V.; Michniak-Kohn, B. Membrane properties for permeability testing: Skin versus synthetic membranes. *Int. J. Pharm.* **2018**, *539*, 58–64. [CrossRef] [PubMed]
10. CDER Semisolid Dosage Forms Scale-Up and Postapproval Changes: Chemistry, Manufacturing, and Controls; In Vitro Release Testing and In Vivo Bioequivalence Documentation. Available online: https://www.fda.gov/downloads/drugs/guidances/ucm070930.pdf (accessed on 1 June 2018).
11. Abd, E.; Yousef, S.A.; Pastore, M.N.; Telaprolu, K.; Mohammed, Y.H.; Namjoshi, S.; Grice, J.E.; Roberts, M.S. Skin models for the testing of transdermal drugs. *Clin. Pharmacol. Adv. Appl.* **2016**, *8*, 163–176. [CrossRef] [PubMed]
12. Madison, K.C.; Swartzendruber, D.C.; Wertz, P.W.; Downing, D.T. Presence of Intact Intercellular Lipid Lamellae in the Upper Layers of the Stratum Corneum. *J. Investig. Dermatol.* **1987**, *88*, 714–718. [CrossRef] [PubMed]
13. Swartzendruber, D.C.; Wertz, P.W.; Kitko, D.J.; Madison, K.C.; Downing, D.T. Molecular models of the Intercellular Lipid Lamellae in Mammalian Stratum Corneum. *J. Investig. Dermatol.* **1989**, *92*, 251–257. [CrossRef] [PubMed]
14. Kessner, D.; Ruettinger, A.; Kiselev, M.A.; Wartewig, S.; Neubert, R.H.H. Properties of ceramides and their impact on the stratum corneum structure: A review—Part 2: Stratum corneum lipid model systems. *Skin Pharmacol. Physiol.* **2008**, *21*, 58–74. [CrossRef] [PubMed]
15. Yang, L.; Mao-Qiang, M.; Taljebini, M.; Elias, P.M.; Feingold, K.R. Topical stratum corneum lipids accelerate barrier repair after tape stripping, solvent treatment and some but not all types of detergent treatment. *Br. J. Dermatol.* **1995**, *133*, 679–685. [CrossRef] [PubMed]

16. Landmann, L. The epidermal permeability barrier. Comparison between in vivo and in vitro lipid structures. *Eur. J. Cell Biol.* **1984**, *33*, 258–264. [PubMed]
17. Ghonaim, H.M.; Periasamy, N.; Noro, M.G.; Anwar, J. Towards a simplified model membrane of skin lipids: Preparation and characterisation of a ternary lipid mixture. *Int. J. Pharm. Pharm. Sci.* **2014**, *6*, 148–152.
18. López-Mesas, M.; Christoe, J.; Carrillo, F.; Crespi, M. Supercritical fluid extraction with cosolvents of wool wax from wool scour wastes. *J. Supercrit. Fluids* **2005**, *35*, 235–239. [CrossRef]
19. Boncheva, M.; Damien, F.; Normand, V. Molecular organization of the lipid matrix in intact Stratum corneum using ATR-FTIR spectroscopy. *Biochim. Biophys. Acta Biomembr.* **2008**, *1778*, 1344–1355. [CrossRef] [PubMed]
20. Coderch, L.; Fonollosa, J.; Marti, M.; Parra, J. Ceramides from wool wax. *J. Am. Oil Chem.* **2004**, *81*, 897–898. [CrossRef]
21. Clark, E.W.; Steel, I.; Company, L.; Yorkshire, W. Investigations into biomechanisms of the moisturizing function of lanolin. *J. Soc. Cosmet. Chem.* **1993**, *44*, 181–195.
22. Flynn, T.C.; Petros, J.; Clark, R.E.; Viehman, G.E. Dry skin and moisturizers. *Clin. Dermatol.* **2001**, *19*, 387–392. [CrossRef]
23. White, S.H.; Mirejovsky, D.; King, G.I. Structure of Lamellar Lipid Domains and Corneocyte Envelopes of Murine Stratum Corneum. *An X-ray Diffraction Study. Biochemistry* **1988**, *27*, 3725–3732. [CrossRef] [PubMed]
24. Wooldryscouring (WDS)—Eco-Efficient Dry Wool Scouring with Total by-Products Recovery. Available online: http://ec.europa.eu/environment/life/project/Projects/index.cfm?fuseaction=search.dspPage&n_proj_id=4254#RM (accessed on 8 June 2018).
25. Barba, C.; Carrer, V.; Marti, M.; Iglesias, J.; Coderch, L. Solvent-extracted wool wax: Thermotropic properties and skin efficacy. *Ski. Pharmacol. Press.* **2018**, *31*, 198–205.
26. DICK, I.P.; SCOTT, R.C. Pig Ear Skin as an In-vitro Model for Human Skin Permeability. *J. Pharm. Pharmacol.* **1992**, *44*, 640–645. [CrossRef] [PubMed]
27. *Whatman Filter Papers and Membranes*; Whatman Filters: Kent, UK, 2013; pp. 1–68.
28. Joshi, V.; Brewster, D.; Colonero, P. In vitro diffusion studies in transdermal research: A synthetic membrane model in place of human skin. *Drug Dev. Deliv.* **2012**, *12*, 40–42.
29. Babita, K.; Kumar, V.; Rana, V.; Jain, S.; Tiwary, A.K. Thermotropic and spectroscopic behavior of skin: Relationship with percutaneous permeation enhancement. *Curr. Drug Deliv.* **2006**, *3*, 95–113. [CrossRef] [PubMed]
30. Arseneault, M.; Lafleur, M. Cholesterol sulfate and Ca^{2+} modulate the mixing properties of lipids in stratum corneum model mixtures. *Biophys. J.* **2007**, *92*, 99–114. [CrossRef] [PubMed]
31. Potts, R.O.; Francoeur, M.L. Lipid biophysics of water loss through the skin. *Proc. Natl. Acad. Sci. USA* **1990**, *87*, 3871–3873. [CrossRef] [PubMed]
32. Rawlings, A.V.; Matts, P.J. Stratum Corneum Moisturization at the Molecular Level: An update in relation to the dry skin cycle. *J. Investig. Dermatol.* **2005**, *124*, 1099–1110. [CrossRef] [PubMed]
33. Committee for the Update of the Guide for the Care and Use of Laboratory Animals. *Guide for the Care and Use of Laboratory Animals*; National Academies Press (US): Washington, DC, USA, 2011; ISBN 978-0-309-15400-0.
34. Pullmannová, P.; Pavlíková, L.; Kováčik, A.; Sochorová, M.; Školová, B.; Slepička, P.; Maixner, J.; Zbytovská, J.; Vávrová, K. Permeability and microstructure of model stratum corneum lipid membranes containing ceramides with long (C16) and very long (C24) acyl chains. *Biophys. Chem.* **2017**, *224*, 20–31. [CrossRef] [PubMed]
35. Ich ICH Topic Q2 (R1) Validation of Analytical Procedures: Text and Methodology. *Int. Conf. Harmon.* **2005**, *1994*, 17. Available online: http://www.ich.org/fileadmin/Public_Web_Site/ICH_Products/Guidelines/Quality/Q2_R1/Step4/Q2_R1__Guideline.pdf (accessed on 13 June 2018).
36. Hafeez, F.; Chiang, A.; Hui, X.; Zhu, H.; Kamili, F.; Maibach, H.I. Stratum corneum reservoir as a predictive method for in vitro percutaneous absorption. *J. Appl. Toxicol.* **2016**, *36*, 1003–1010. [CrossRef] [PubMed]
37. Ng, S.F.; Rouse, J.; Sanderson, D.; Eccleston, G. A Comparative study of transmembrane diffusion and permeation of ibuprofen across synthetic membranes using franz diffusion cells. *Pharmaceutics* **2010**, *2*, 209–223. [CrossRef] [PubMed]

Annex 4. Patent of lanolin-based synthetic membranes as a skin model.

Justificante de presentación electrónica de solicitud de patente

Este documento es un justificante de que se ha recibido una solicitud española de patente por vía electrónica utilizando la conexión segura de la O.E.P.M. De acuerdo con lo dispuesto en el art. 16.1 del Reglamento de ejecución de la Ley 24/2015 de Patentes, se han asignado a su solicitud un número de expediente y una fecha de recepción de forma automática. La fecha de presentación de la solicitud a la que se refiere el art. 24 de la Ley le será comunicada posteriormente.

Número de solicitud:	P201830343	
Fecha de recepción:	06 abril 2018, 11:04 (CEST)	
Oficina receptora:	OEPM Madrid	
Su referencia:	ES1641.1355	
Solicitante:	CONSEJO SUPERIOR DE INVESTIGACIONES CIENTÍFICAS (CSIC)	
Número de solicitantes:	1	
País:	ES	
Título:	MODELOS DE PIEL BASADOS EN MEMBRANAS ARTIFICIALES CON LANOLINA	
Documentos enviados:	Descripcion.pdf (22 p.) Reivindicaciones-1.pdf (1 p.) Dibujos-1.pdf (4 p.) Resumen-1.pdf (1 p.) OLF-ARCHIVE.zip FEERCPT-1.pdf (1 p.) FEERCPT-2.pdf (1 p.)	package-data.xml es-request.xml application-body.xml es-fee-sheet.xml feesheet.pdf request.pdf
Enviados por:	C=ES,O=PONS PATENTES Y MARCAS INTERNACIONAL SL,2.5.4.97=#0C0F56415445532D423834393231373039,CN=50534279 J ANGEL PONS (R: B84921709),SN=PONS ARIÑO,givenName=ANGEL,serialNumber=IDCES-50534279J,descriptio n=Ref:AEAT/AEAT0297/PUESTO 1/40639/05102016093524	
Fecha y hora de recepción:	06 abril 2018, 11:04 (CEST)	
Codificación del envío:	7C:22:A5:93:83:1B:44:71:9A:A9:27:F0:4E:27:BE:54:D0:C4:7B:1E	

AVISO IMPORTANTE
Las tasas pagaderas al solicitar y durante la tramitación de una patente o un modelo de utilidad son las que se recogen en el Apartado "Tasas y precios públicos" de la página web de la OEPM (http://www.oepm.es/es/propiedad_industrial/tasas/). Consecuentemente, si recibe una comunicación informándole de la necesidad de hacer un pago por la inscripción de su patente o su modelo de utilidad en un "registro central" o en un "registro de internet" posiblemente se trate de un fraude.
La anotación en este tipo de autodenominados "registros" no despliega ningún tipo de eficacia jurídica ni tiene carácter oficial.
En estos casos le aconsejamos que se ponga en contacto con la Oficina Española de Patentes y Marcas en el correo electrónico informacion@oepm.es.

ADVERTENCIA: POR DISPOSICIÓN LEGAL LOS DATOS CONTENIDOS EN ESTA SOLICITUD PODRÁN SER PUBLICADOS EN EL BOLETÍN OFICIAL DE LA PROPIEDAD INDUSTRIAL E INSCRITOS EN EL REGISTRO DE PATENTES DE LA OEPM, SIENDO AMBAS BASES DE DATOS DE CARÁCTER PÚBLICO Y ACCESIBLES VÍA REDES MUNDIALES DE INFORMÁTICA.
Para cualquier aclaración puede contactar con la O.E.P.M.

/Madrid, Oficina Receptora/

MINISTERIO
DE INDUSTRIA, ENERGÍA
Y TURISMO

Oficina Española
de Patentes y Marcas

(1) MODALIDAD:	
PATENTE DE INVENCIÓN	[✓]
MODELO DE UTILIDAD	[ ]
(2) FORMULARIO 5101. TIPO DE SOLICITUD:	
PRIMERA PRESENTACIÓN	[✓]
SOLICITUD DIVISIONAL	[ ]
CAMBIO DE MODALIDAD	[ ]
TRANSFORMACIÓN SOLICITUD PATENTE EUROPEA	[ ]
PCT: ENTRADA FASE NACIONAL	[ ]
(3) EXP. PRINCIPAL O DE ORIGEN:	
MODALIDAD:	
N.º SOLICITUD:	
FECHA SOLICITUD:	
4) LUGAR DE PRESENTACIÓN:	OEPM, Presentación Electrónica
(5-1) SOLICITANTE 1:	
DENOMINACIÓN SOCIAL:	CONSEJO SUPERIOR DE INVESTIGACIONES CIENTÍFICAS (CSIC)
UNIVERSIDAD PÚBLICA	[ ]
NACIONALIDAD:	España
CÓDIGO PAÍS:	ES
NIF/NIE/PASAPORTE:	Q2818002D
CNAE:	
PYME:	
DOMICILIO:	C/ Serrano, nº 117
LOCALIDAD:	Madrid
PROVINCIA:	28 Madrid
CÓDIGO POSTAL:	28006
PAÍS RESIDENCIA:	España
CÓDIGO PAÍS:	ES
TELÉFONO:	
FAX:	
CORREO ELECTRÓNICO:	
EMPRENDEDOR:	[ ]
PERSONA DE CONTACTO:	
MODO DE OBTENCIÓN DEL DERECHO:	
INVENCIÓN LABORAL:	[✓]
CONTRATO:	[ ]
SUCESIÓN:	[ ]
PORCENTAJE DE TITULARIDAD:	100,00 %
(6-1) INVENTOR 1:	
APELLIDOS:	ALONSO MERINO
NOMBRE:	CRISTINA
NACIONALIDAD:	España
CÓDIGO PAÍS:	ES
NIF/NIE/PASAPORTE:	46059320-A
DOMICILIO:	IQAC. C/ Jorge Girona Salgado, 18-26
LOCALIDAD:	Barcelona
PROVINCIA:	08 Barcelona
CÓDIGO POSTAL:	08034
PAÍS RESIDENCIA:	España

CÓDIGO PAÍS:	ES
TELÉFONO:	
FAX:	
CORREO ELECTRÓNICO:	
EL INVENTOR RENUNCIA A SER MENCIONADO:	[ ]
(6-2) INVENTOR 2:	
APELLIDOS:	CARRER VIVES
NOMBRE:	VICTOR
NACIONALIDAD:	España
CÓDIGO PAÍS:	ES
NIF/NIE/PASAPORTE:	47100847-K
DOMICILIO:	IQAC. C/ Jorge Girona Salgado, 18-26
LOCALIDAD:	Barcelona
PROVINCIA:	08 Barcelona
CÓDIGO POSTAL:	08034
PAÍS RESIDENCIA:	España
CÓDIGO PAÍS:	ES
TELÉFONO:	
FAX:	
CORREO ELECTRÓNICO:	
EL INVENTOR RENUNCIA A SER MENCIONADO:	[ ]
(6-3) INVENTOR 3:	
APELLIDOS:	MARTI GELABERT
NOMBRE:	MERITXELL
NACIONALIDAD:	España
CÓDIGO PAÍS:	ES
NIF/NIE/PASAPORTE:	43688381-L
DOMICILIO:	IQAC. C/ Jorge Girona Salgado, 18-26
LOCALIDAD:	Barcelona
PROVINCIA:	08 Barcelona
CÓDIGO POSTAL:	08034
PAÍS RESIDENCIA:	España
CÓDIGO PAÍS:	ES
TELÉFONO:	
FAX:	
CORREO ELECTRÓNICO:	
EL INVENTOR RENUNCIA A SER MENCIONADO:	[ ]
(6-4) INVENTOR 4:	
APELLIDOS:	CODERCH NEGRA
NOMBRE:	Mª LUISA
NACIONALIDAD:	España
CÓDIGO PAÍS:	ES
NIF/NIE/PASAPORTE:	46111247-L
DOMICILIO:	IQAC. C/ Jorge Girona Salgado, 18-26
LOCALIDAD:	Barcelona
PROVINCIA:	08 Barcelona
CÓDIGO POSTAL:	08034
PAÍS RESIDENCIA:	España
CÓDIGO PAÍS:	ES
TELÉFONO:	
FAX:	
CORREO ELECTRÓNICO:	
EL INVENTOR RENUNCIA A SER MENCIONADO:	[ ]
(7) TÍTULO DE LA INVENCIÓN:	MODELOS DE PIEL BASADOS EN MEMBRANAS ARTIFICIALES CON LANOLINA
(8) NÚMERO DE INFORME TECNOLÓGICO DE PATENTES (ITP):	

(9) SOLICITA LA INCLUSIÓN EN EL PROCEDIMIENTO ACELERADO DE CONCESIÓN	
SI	[ ]
NO	[✓]
(10) EFECTUADO DEPÓSITO DE MATERÍA BIOLÓGICA:	
SI	[ ]
NO	[✓]
(11) DEPÓSITO:	
REFERENCIA DE IDENTIFICACIÓN:	
INSTITUCIÓN DE DEPÓSITO:	
NÚMERO DE DEPÓSITO:	
ORÍGEN BIOLÓGICO:	
(12) RECURSO GENÉTICO:	
NÚMERO DE REGISTRO:	
NÚMERO DE CERTIFICADO DE ACCESO AL RECURSO:	
UTILIZACIÓN DEL RECURSO GENÉTICO:	
CONOCIMIENTO TRADICIONAL ASOCIADO A UN RECURSO GENÉTICO:	
(13) DECLARACIONES RELATIVAS A LA LISTA DE SECUENCIAS:	
LA LISTA DE SECUENCIAS NO VA MÁS ALLÁ DEL CONTENIDO DE LA SOLICITUD	[ ]
LA LISTA DE SECUENCIAS EN FORMATO PDF Y ASCII SON IDENTICOS	[ ]
(14) EXPOSICIONES OFICIALES:	
NOMBRE:	
LUGAR:	
FECHA:	
(15) DECLARACIONES DE PRIORIDAD:	
PAÍS DE ORIGEN:	
CÓDIGO PAÍS:	
NÚMERO:	
FECHA:	
(16) REMISIÓN A UNA SOLICITUD ANTERIOR:	
PAÍS DE ORIGEN:	
CÓDIGO PAÍS:	
NÚMERO:	
FECHA:	
(17) AGENTE DE PROPIEDAD INDUSTRIAL:	
APELLIDOS:	PONS ARIÑO
NOMBRE:	ÁNGEL
CÓDIGO DE AGENTE:	0499/5
NÚMERO DE PODER:	20081765
(18) DIRECCIÓN A EFECTOS DE COMUNICACIONES: DIRECCIÓN ASOCIADA AL PRIMER SOLICITANTE	
DOMICILIO:	
LOCALIDAD:	
PROVINCIA:	
CÓDIGO POSTAL:	
PAÍS RESIDENCIA:	
CÓDIGO PAÍS:	
TELÉFONO:	
FAX:	
CORREO ELECTRÓNICO:	
MEDIO PREFERENTE DE COMUNICACIÓN	
(19) RELACIÓN DE DOCUMENTOS QUE SE ACOMPAÑAN:	
DESCRIPCIÓN:	[✓] N.º de páginas: 22
REIVINDICACIONES:	[✓] N.º reivindicaciones: 11
DIBUJOS:	[✓] N.º de dibujos: 7
RESUMEN:	[✓] N.º de páginas: 1
FIGURA(S) A PUBLICAR CON EL RESUMEN:	[✓] N.º de figura(s):
ARCHIVO DE PRECONVERSION:	[✓]
DOCUMENTO DE REPRESENTACIÓN:	[ ] N.º de páginas:

JUSTIFICANTE DE PAGO (1):	[✓] N.º de páginas: 1
JUSTIFICANTE DE PAGO (2):	[✓] N.º de páginas: 1
LISTA DE SECUENCIAS PDF:	[ ] N.º de páginas:
ARCHIVO PARA LA BUSQUEDA DE LS:	[ ]
OTROS (Aparecerán detallados):	
(20) EL SOLICITANTE SE ACOGE A LA REDUCCIÓN DE TASAS PARA EMPRENDEDORES PREVISTA EN EL ART. 186 DE LA LEY 24/2015 DE PATENTES Y, A TAL EFECTO, APORTA LA SIGUIENTE DOCUMENTACIÓN ADJUNTA:	[ ]
(21) NOTAS:	
(22) FIRMA:	
FIRMA DEL SOLICITANTE O REPRESENTANTE:	50534279J ANGEL PONS (R: B84921709)
LUGAR DE FIRMA:	MADRID
FECHA DE FIRMA:	06 Abril 2018

Annex 5. Skin permeation and antioxidant efficacy of topically applied resveratrol

Arch Dermatol Res (2017) 309:423–431
DOI 10.1007/s00403-017-1740-5

ORIGINAL PAPER

Skin permeation and antioxidant efficacy of topically applied resveratrol

Cristina Alonso[1] · M. Martí[1] · C. Barba[1] · V. Carrer[1] · L. Rubio[1] · L. Coderch[1]

Received: 13 December 2016 / Revised: 14 March 2017 / Accepted: 4 April 2017 / Published online: 7 April 2017

Abstract The permeation of resveratrol was assessed by in vitro and in vivo experiments 24 h after topical administration. The in vitro profile of resveratrol was assessed by Raman spectroscopy. Human skin permeation was analysed in vivo by the tape stripping method with the progressive removal of the stratum corneum layers using adhesive tape strips. Moreover, the free radical scavenging activity of resveratrol after its topical application was determined using the DPPH assay. The Raman spectra indicated that the topically applied resveratrol penetrates deep into the skin. The results showed high amounts of resveratrol in the different stratum corneum layers close to the surface and a constant lower amount in the upper layers of the viable epidermis. The concentration of resveratrol present in the outermost stratum corneum layers was obtained by tape stripping after in vivo application. The results demonstrated that resveratrol mainly remained in the human stratum corneum layers. After topical application, resveratrol maintained its antiradical activity. The antioxidant efficacy of the compound was higher in the inner layers of the stratum corneum. As these results have demonstrated, topically applied resveratrol reinforces the antioxidant system of the stratum corneum and provides an efficient means of increasing the tissue levels of antioxidants in the human epidermis.

Keywords Resveratrol · Percutaneous absorption · In vivo · In vitro · Antiradical activity

✉ Cristina Alonso
cristina.alonso@iqac.csic.es

[1] Department of Chemicals and Surfactants Technology, Advanced Chemical Institute of Catalonia (IQAC-CSIC), Jordi Girona 18-26, 08034 Barcelona, Spain

Introduction

Resveratrol (trans-3,4′,5-trihydroxystilbene, MW 228.24) (Fig. 1) is a polyphenolic compound with biological activity that is found in a variety of plants, and is notable for its antioxidant properties [11]. Polyphenolic compounds act as antioxidants because of their ability to donate hydrogen to neutralize free radical species generated by conditions of oxidative stress, such as lipoperoxidation caused by UV radiation, or by biologically mediated processes. Resveratrol may play the role of a primary antioxidant in the form of a scavenger that reacts with free radicals and transforms them into products [1, 12, 21] or a secondary antioxidant with a preventive function, e.g., it can decrease oxidation via enzyme inhibition. Resveratrol has been demonstrated to regulate the levels of cyclooxygenase, lipoxygenase and xanthine oxidase, thereby inhibiting their activities and preventing a variety of diseases [1, 6]. It also has beneficial effects on the neurological, hepatic and cardiovascular systems [5, 7]. Moreover, the potential chemopreventive function of resveratrol in cancer has been explored, and it has been shown to block the process of cancerogenesis at different stages [6, 18, 32]. A wide variety of in vitro methodologies have been developed to measure the free radical scavenging ability of compounds [23]. One of them involves assessing the degree of reduction of the free radical 1,10-diphenyl-2-picrylhydrazyl (DPPH) in the presence of the compound. This method is quick, simple, and a routine assay used in both in vitro and in vivo studies to determine the antioxidant activity of compounds.

Resveratrol is included in many cosmetic and dermopharmaceutical preparations as a chemopreventive and an antioxidative agent due to its medical properties [15, 17, 19]. Exogeneous antioxidants may decrease the

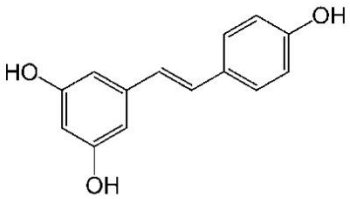

Fig. 1 Chemical structure of resveratrol

action of free radicals in a similar manner as endogenous antioxidants [36, 37]. However, the metabolism of resveratrol is immediate when it is present at systemic levels [5] after oral consumption. Therefore, its topical administration could be an efficient way for it to reach its target by avoiding systemic circulation.

Traditional in vitro and in vivo methodologies are used to evaluate the permeation of exogenous compounds that are topically applied on the skin. One common method is an in vitro assay using Franz static diffusion cells, which consist of an upper donor and a lower receptor chamber (containing receptor fluid) separated by a membrane (e.g., skin). The receptor fluid is in permanent contact with part of the dermis, and it can extract skin components or produce some of the physiological modifications of the skin. Normally, HPLC is used to quantify the penetration of the compound into the skin and receptor fluid samples. Some detection problems can exist as a consequence of a potential degradation of the applied compound caused by the skin enzymes [4, 25, 27].

Tape stripping of the outermost layers of the skin, i.e., the stratum corneum (SC), is another commonly used technique [26, 28]. This is a minimally invasive method that can yield the concentration profiles of topically applied compounds in vivo by analysis of the tape strips with HPLC.

A linear relationship has been found between the permeation fluxes of lipophilic compounds into the human skin using Franz cells with the amount of drug retained in the SC by the stripping technique [38]. These two methodologies provide predictive results for the skin absorption profile. However, these techniques can modify the skin structure and expose the skin to similar physiological conditions. The confocal Raman microscopy (CRM) is an innovative optical method for studying the delivery of pro-drugs and drugs. CRM is a promising technique that enables the non-destructive measurement of the molecular composition of skin layers, without extrinsic markers. Raman microscopy has facilitated studies of the penetration of active compounds through the skin layers and their interactions with endogenous skin components that can cause potential structural modifications. Until now, several studies have been conducted for the determination of molecular penetration into the skin [35, 41].

The objective of the present work was to examine and compare the skin penetration of resveratrol using different methodologies. CRM was employed to study the penetration of this antioxidant. The in vivo percutaneous permeation of resveratrol through the human SC was also determined using the stripping assay. Previously, the in vitro percutaneous penetration had been evaluated to assess compound delivery into the different layers of the skin (SC, epidermis and dermis) as well as into the receptor fluid when the compound was applied topically on porcine skin [3]. Moreover, DPPH was used to assess the antiradical activity of resveratrol after topical application to test for possible modifications of its antioxidant capacity due to its metabolism in the skin, especially after in vivo application.

Materials and methods

Chemicals and formulations

Resveratrol (Rs) [PubChem CID 445154(501-36-0)] was purchased from Sigma (St. Louis, MO, USA), and ethanol was purchased from Merck (Darmstadt, Germany).

The formulation composition was 5% resveratrol (w/v) in ethanol/water (70:30 v/v). The formulation was prepared by stirring the compound at 20 °C. The concentration of resveratrol was quantified by HPLC (see section "Extraction and analysis of resveratrol in the tape strips") after adequate dilution. Three replicates were performed.

Sample preparation for CRM

The porcine skin used in these experiments was obtained from the unboiled backs of freshly killed domestic pigs (Landrace Large White). The in vitro porcine skin permeation experiments were conducted as reported previously using vertical glass Franz diffusion cells (1.86 cm^2, Lara-Spiral, Courtenon, France) [2]. A 10 $\mu L/cm^2$ sample of resveratrol solution (537 µg of resveratrol/cm^2) was applied to the total surface of the skin, delimited within the upper cell compartment. At the end of the exposure time (24 h), excess formulation on the skin surface was removed by five iterations of tape stripping.

Raman data acquisitions

Raman spectra were obtained with a Renishaw (Gloucestershire, UK) Model inVia confocal Raman microscope. Excitation (approximately 100 mW at the sample) was

performed with a 532 nm diode laser. The excitation laser radiation was coupled into the microscope through a wavelength-specific mode optical fibre. The incident laser emission was collimated via a lens and passed through a holographic band-pass filter before being focused onto the sample through the objective lens of the microscope. A Leica 50×/0.75 NA objective was used in this study. Spectra were obtained using 10 s exposure time, 1 accumulation and 1800 line/mm grating. Slices at depths of 0–49 µm below the surface of the skin were examined in increments of 7 µm. The spectral resolution was approximately 1 cm^{-1}, and the spectral window ranged from 300 to 3200 cm^{-1}.

In vivo experimental procedure

Six volunteers (all women) with no history of dermatological disease participated in this study, which was approved by the Ethics Committee (IQAC-CSIC, Barcelona, Spain). Specific information of the study was given to the participants, and their written consents were obtained. The median age of the volunteers was 33 years, ranging between 25 and 42 years, and phototypes II, III and IV were included [14]. The treated sites (2 × 1 cm) were the non-hairy areas of the ventral forearm surface. The administration involved application of 10 µL/cm^2 of resveratrol solution, according to reported guidelines [24]. This amount represents 500 µg of the total amount of resveratrol per area (cm^2). The application was non-occlusive.

SC sampling procedure

The resveratrol permeation profile across the SC was determined with the stripping method [20, 28]. After an application time of 24 h, a sequential removal of the outer skin layers from each volunteer was carried out by tape stripping (D-Squame™ tapes, ø = 22 mm, CuDerm, Dallas, USA). Each tape was fixed to the skin surface using a specific device that exerted a constant pressure of 80 g/cm^2 for 5 s, and the tape was removed from the test area with a gentle movement. For each repeated strip, the tear-off direction was varied to obtain homogeneous removal of the SC cell layers. A total of ten tape strips were used on all the treated sites.

Extraction and analysis of resveratrol in the tape strips

The tape strips from the treated and untreated SC were placed in vials. Resveratrol was extracted with methanol (Merck, Darmstadt, Germany) and analysed by HPLC using a reverse phase C18 column (LiChroCART 250-4/LiChrosorb RP-18, 5 µm) (Merck, Darmstadt, Germany) and a L-4250 UV–Vis detector from Hitachi-Merck (Darmstadt, Germany) at 303 nm. The isocratic mobile phase was 5% acetic acid in methanol/water 52:48 (v/v). The retention of resveratrol was approximately 5 min at a flow rate of 1.2 mL/min at room temperature. A standard curve was obtained using the median data of the triplicate determinations in the concentration range of 0.022–140 µg/mL. The linear regression equation for the experimental dates was given by ABS=52321·[RS]-21132, $R^2 = 0.9998$. The reproducibility and repeatability of the analytical procedure were established using the absorbance of a resveratrol standard sample. The dates for each determination indicated good repeatability and intra- and inter-day precision with an adequate R.S.D. (<0.50%).

Antioxidant activity measurement

The antioxidant efficacy of resveratrol in the samples was determined using the 1,1-diphenyl-2-picrylhydrazyl free radical (DPPH) (Aldrich, Gillingham-Dorset, UK) assay [30]. When an antioxidant compound is in contact with DPPH, the free electron of DPPH is converted into a pair and the colour changes from purple to yellow. This change is determined as a decrease in the absorbance at 517 nm. The amount of DPPH was obtained for each extracted SC sample as described elsewhere [3]. Briefly, the resveratrol present in the SC was extracted with methanol (Merck, Darmstadt, Germany). An 500 µL aliquot of the SC sample was mixed with 500 µL DPPH to form a solution. Methanol extractions from untreated SC samples were used as controls. The mixture was vortexed and incubated in the dark for 1 h at room temperature. An aliquot (20 µL) of the sample was examined by HPLC [10]. Resveratrol concentration was obtained using an external calibration curve for the absorbance at 517 nm using standard solutions of DPPH at different concentrations obtained with HPLC. The calibration equation was $A_{517} = 20702[\text{DPPH}] - 59877$ ($R^2 = 0.9987$) as determined by linear regression. The percentage of inhibition of antioxidant activity (% inhibition of DPPH) for resveratrol in SC samples was obtained as the balance in the decrease of DPPH peak area measured at 517 nm between the control and the resveratrol samples. The antioxidant efficacy of the compound was determined from the dates of the antioxidant activity of resveratrol in the skin layer divided by the amount of compound found in the corresponding skin layer after the permeation assay and HPLC quantification.

Statistical analyses

Standard deviations were determined for all the mean values. The Kruskal–Wallis test was applied for group

comparisons. The STATGRAPHICS plus 5 software was used for statistical analyses. Significant differences in the mean values were evaluated by the F test. A p value below 0.05 was considered significant.

Results and discussion

In the present investigation, the CRM technique was applied to obtain the profile of resveratrol penetration into the skin. CRM is a non-destructive and relatively easy technique that provides information about biochemical compounds that are both extrinsic and intrinsic to the skin. Porcine skin was used in this experimental assay. Porcine skin is a representative tissue for percutaneous penetration because it has permeation characteristics analogous to the human skin [2]. In addition, the density of hair follicles in the porcine skin is comparable to that of the human skin [8].

The Raman spectrum of the untreated porcine skin obtained at the skin surface and the spectrum for resveratrol in the 100–3200 cm^{-1} region are shown in Fig. 2a, b, respectively.

The spectrum of the porcine membrane shows different bands that are distinctive for the lipids and proteins of SC layer, for example, the ring-breathing mode in Phe is shown at 1004 cm^{-1}, Amide I at 1650 cm^{-1}, lipids at 2820 cm^{-1} and protein (keratin) at 2940 cm^{-1}. In Fig. 1b, the band at 995 cm^{-1}, and the overlapped 1610/1640 cm^{-1} pair detected in the spectrum of resveratrol, can be used to follow resveratrol permeation into the skin. The other peaks from resveratrol, such as the ones in the 1003 cm^{-1} region, are as a result of the aromatic ring-breathing mode, and the ones in the 1610 cm^{-1} region are due to conjugated C=C bonds and ring-stretching modes.

The resveratrol solution was topically applied to the pigskin. After 24 h of exposure, five tape strips were used to remove the excess compound from the skin surface. Afterwards, successive confocal Raman spectra from the applied skin were obtained every 7 µm to a final depth of 49 µm in the 600–2300 cm^{-1} region. The spectral series are shown in Fig. 3.

The spectral signals from both the skin and the applied resveratrol compound are shown. The perception of the peaks in the 1610/1640 cm^{-1} region from the SC surface to a depth of ~49 µm demonstrated the penetration of resveratrol to 49 µm into the skin. Modifications in the C=C peak regions and amplitudes are noted with the depth, as shown in Fig. 3. The results show the presence of resveratrol in the SC compartment and in the viable epidermis. Relative resveratrol concentrations were obtained from the Raman profiles, following the method described by Caspers et al. [9]. To rectify the variability of the absolute Raman intensity, which diminishes at the deeper levels of the skin, the corresponding coefficients were normalized to the Raman keratin signal (~2940 cm^{-1}). Normalization to the Raman Phe ring peak from the SC layer (~1004 cm^{-1}) was not considered because the intensity of this band increases due to the contribution of the vibration of resveratrol at 995 cm^{-1} giving a signal that is superimposed with the skin Phe ring breathing [34]. The normalization approach revealed the amount of resveratrol in the SC and viable epidermis relative to the amount of keratin. The depth concentration profiles of resveratrol are presented in Fig. 4. The highest concentration of the compound was obtained near the skin surface. The concentration decreased at a depth of approximately 20 µm. It can be observed that the resveratrol concentration was constant between the depths of 20–49 µm, corresponding to the viable epidermis.

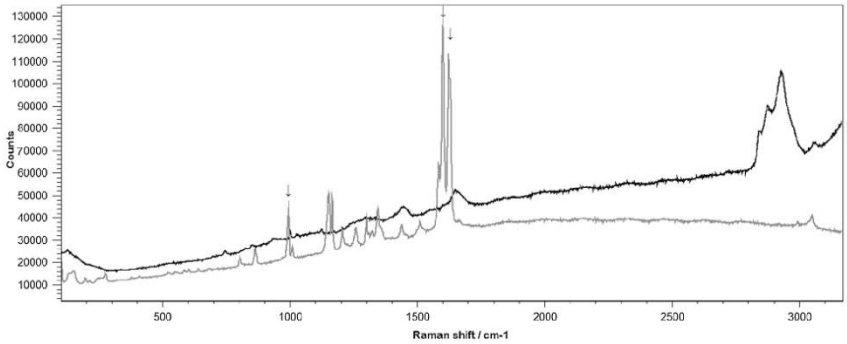

Fig. 2 Confocal Raman spectra (100–3200 cm^{-1}) of untreated pigskin acquired at the skin surface (**a**) and resveratrol (**b**)

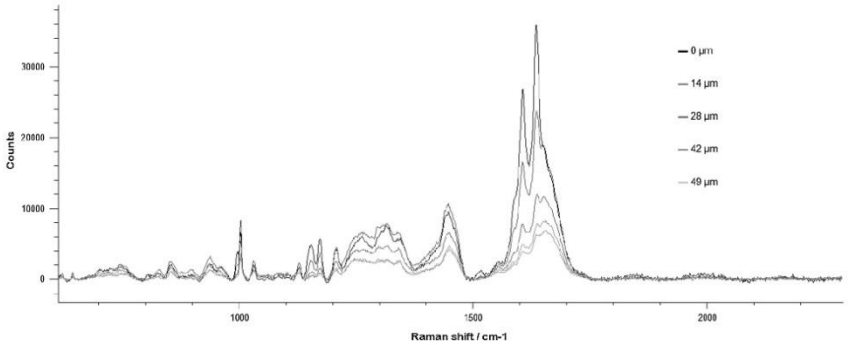

Fig. 3 Illustration of spectral changes obtained from the pigskin following the application of resveratrol, at different depths. The *top* spectrum was collected at the surface of the skin, while the *bottom* one was collected 49 µm below the surface

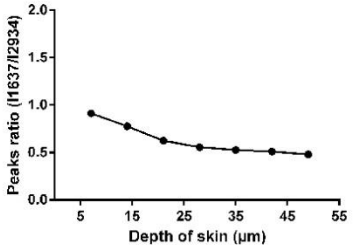

Fig. 4 Representative distribution profiles of resveratrol in the porcine skin from 7 to 49 µm

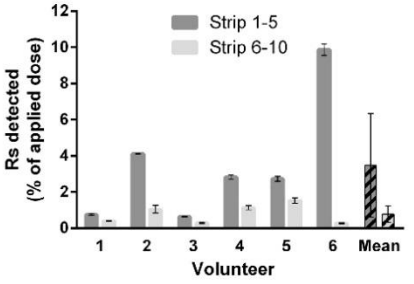

Fig. 5 Concentration profiles of resveratrol (RS) from strips 1 to 5 and 6 to 10 in the SC in vivo, expressed as a percentage of the applied dose detected

In this work, the percutaneous penetration of resveratrol was also determined in vivo on human skin. For these experiments, the same aqueous-ethanolic solution was selected as the simple application vehicle to dissolve the compound to be used at the same concentration. The in vivo penetration of resveratrol into the human skin was obtained using the stripping methodology, based on the successive extraction of the SC layers by consecutive stripping with adhesive tapes [13, 33].

The content of resveratrol removed with the tape strips was quantified by triplicate HPLC measurements after methanol extraction of the combined groups of strips from 1–5 and 6–10 strips. The concentration of resveratrol obtained in the combined tapes, as a function of the strip number, is shown in Fig. 5 and Table 1, along with the mean values.

Taking into account the differences observed among the volunteers from Fig. 5, the mean resveratrol recovery was 4.27 ± 3.35%, and the majority was present on strips 1–5. The lack of total recovery could be due to the penetration of the product into the inner layer of skin and to the horizontal spreading of the product, which was caused by the non-occlusive topical application. The amount of resveratrol detected in the combined tapes for each volunteer, expressed in µg/cm^2 is detailed in Table 1.

The amount of SC extracted by the adhesive tape strips was dependent on a variety of factors [20, 29], such as the anatomical site, subject age, and time of year. The quantity of cells in the layers [40] and the thickness of the SC [31] change with the anatomical zone, corresponding to the changes in the composition and amount of lipids. External factors can also influence the quantity of the SC extracted by the stripping method. The mode of extraction from the skin, the pressure time on the forearm skin and the presence of

Table 1 Amount of resveratrol detected in the combined tapes for each volunteer, expressed in μg/cm²

Volunteer	1	2	3	4	5	6	Mean ± SD
Strips 1–5	3.99	12.17	1.89	8.61	8.24	19.72	9.10 ± 6.35
Strips 6–10	1.06	3.11	0.83	3.45	3.63	0.83	2.15 ± 1.38
Total amount (μg/cm²)	5.05	15.28	2.72	12.06	11.86	20.55	11.25 ± 6.56

topically applied substances are external factors [22] to take into account. In this work, efforts were made to control the intrinsic variability by carrying out the assays during the same time of year (over 2 days) for the group of volunteers and by using only the same area of the arm (the volar forearm). To take the external factors into consideration, the adhesive strips were attached to the skin surface with constant pressure and all the assays were carried out by the same technician. Despite considering the above factors, the amount of RS obtained showed a high variability.

Moreover, the major amount (77%) of the penetrated resveratrol was localized to the upper layer of the SC (strips 1–5), and the compound detection decreased with the SC-depth because smaller amounts of resveratrol were extracted and less SC tissue were removed by the tape strips from the deeper layers.

After the in vivo assay, the antiradical activity of resveratrol towards DPPH was evaluated with an optimized methodology [3]. The same resveratrol extracts from the volunteer SC samples were assayed against DPPH and measured at 517 nm 1 h later. The experiment was conducted using an excess of DPPH radicals to measure the antiradical capacity of the SC extracts. The DPPH radicals remaining after contact with the resveratrol SC samples was compared with untreated SC samples (control) yielding a percentage of the antiradical activity or inhibition. The inhibition percentage for each volunteer as well as the mean value of the inhibition percentage of DPPH, are represented in Fig. 6. The results demonstrated that resveratrol conserved its antioxidant activity after penetrating the SC layer, as showed by the increase of percentage of DPPH inhibition.

Antioxidant activity was associated with the antioxidant power and the amount of the compound detected in the skin layer. Resveratrol is a potent antioxidant with an effective dose (ED50) of 0.25 μmol/μmol DPPH [3]. The antioxidant activity was higher in the upper SC (strips 1–5) than in the inner SC (strips 6–10) (Fig. 6). This can be easily correlated with the higher amounts of the antioxidant on the SC surface (Fig. 5). The mean values of 17.91 ± 14.16 and 10.15 ± 4.55% inhibition were obtained for the upper SC and inner SC, respectively, yielding a total DPPH inhibition percentage of 28.06 ± 17.90% for the total SC removed by stripping (Fig. 6). In the in vivo percutaneous study, resveratrol was found in large amounts in the volunteers 2 and 6; therefore, a higher DPPH inhibition was observed in these samples. In general, the DPPH inhibition results obtained showed variability due to the differences in the intrinsic skin antioxidant capacities of each individual.

The antioxidant efficacy of resveratrol was obtained from the in vivo permeation assay and the antiradical activity data in the SC layer. The antioxidant efficacy determined in the SC compartment, expressed by the amount of antioxidant per area (inhibition DPPH/nmol/cm²), is shown in Fig. 7. The data shown in Fig. 7 was obtained from the values of antioxidant activity of

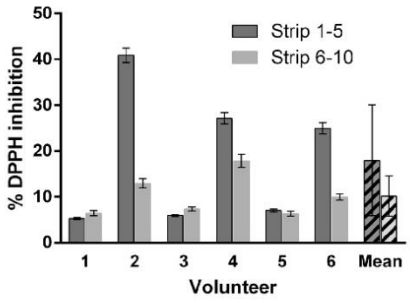

Fig. 6 Percentage of DPPH inhibition in the resveratrol-treated SC samples for each volunteer

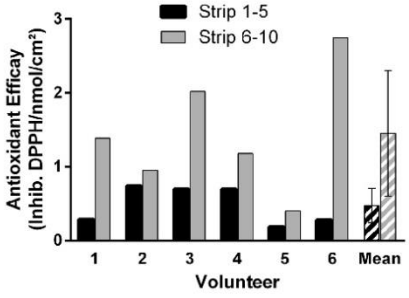

Fig. 7 Antioxidant efficacy (inhibition DPPH/nmol/cm²) obtained in vivo for resveratrol in the SC layer. The antioxidant activity values were divided by the amount of the compound detected in the SC layer after the in vivo stripping assay

resveratrol in the SC layer divided by the amount of the compound found in the SC removed from each volunteer by the in vivo stripping assay. The antioxidant efficacy is more notable in the inner SC. The mean value of the antioxidant efficacy, considering the total SC layer, was 1.93 ± 0.86 inhibition DPPH/nmol/cm^2.

The SC is the principal barrier of the skin in its function as a multipurpose defence system, and it is the protective part of the epidermis. Topical application of lipophilic antioxidants, such as resveratrol, can cause modifications in the physicochemical properties of the SC keratins by hindering their oxidation [36]. Thus, resveratrol applied in vivo might act as a supplement to the antioxidant network of the SC.

In vivo studies are essential assays for a more realistic evaluation of the skin permeation of topical applications. However, the usage of skin biopsies ex vivo with Franz cells is an alternative to in vivo methods. This in vitro method represents a practical and easy model for the estimation of percutaneous penetration in humans. In a previous study, a specific in vitro percutaneous absorption was carried out to obtain the percutaneous profile of resveratrol in the porcine skin [3]. Figure 8 shows the comparison of the mean values from the in vivo study with the percutaneous absorption in vitro, expressed as a percentage of the applied amount recovered (%).

The results indicated that resveratrol was located mainly in the SC layer and the viable epidermal layer. Resveratrol is immediately metabolized in the body [5]; thus, a topical administration could be an efficient option for its application to benefit the skin while avoiding the systemic presence of the compound. Other authors had established the permeation data of resveratrol using different topical formulations [16]. The results obtained also indicated higher amounts of the compound in the skin than are observed from delivery at the systemic level. Therefore, the low capacity of percutaneous penetration observed for resveratrol (0.6% skin absorbed [3]) may confirm its use as an ingredient in cosmetic products.

The results obtained in vivo demonstrate that resveratrol penetrates the SC layers, corroborating the results obtained in vitro. The percentage of resveratrol obtained in the SC layer from the in vivo permeation (4.27 ± 3.35% of the applied dose) was similar to (not significantly different) that in vitro (3.36 ± 2.51% of the applied dose) (Fig. 8).

The antiradical activity of resveratrol remaining in each skin layer after in vitro topical application was assessed. The comparison between the DPPH radical remaining in each skin compartment from the samples treated with the antioxidant and the control samples demonstrated the radical scavenging capacity as a relative antioxidant activity (% inhibition). Figure 9 shows the DPPH inhibition in the skin layers after in vitro and in vivo applications of resveratrol. As shown in the figure, the inhibition results from the in vivo (28.06 ± 17.90% inhibition) and the in vitro assays, considering only the SC layer (23.86 ± 3.09% inhibition), were similar. The antioxidant capacity is directly related to the compound concentration. The amount of the compound detected in the SC layer was similar in both methods, as shown. Therefore, it was not surprising that the inhibitions obtained by the two methods were not very different, even after considering the variability of the stripping results with the in vivo antioxidant system.

Likewise, similar results were obtained when the antioxidant efficacies were calculated in the SC layer using the in vitro and in vivo methods (Fig. 9).

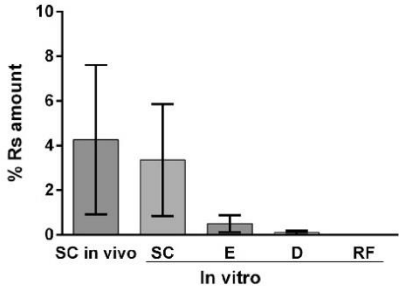

Fig. 8 Percutaneous absorption of resveratrol in vitro expressed as a percentage of the amount detected in the different skin layers [stratum corneum (SC), epidermis (E), dermis (D)] and the receptor fluid (RF). The results were compared to the mean value obtained from the SC layer by the stripping method

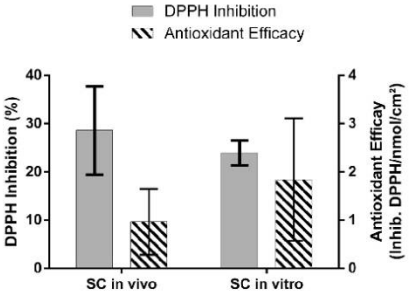

Fig. 9 Percentage of DPPH inhibition and antioxidant efficacy obtained after the in vitro percutaneous absorption. Mean result from stripping and the mean value obtained from the SC layers in vivo

The SC is the most important protective layer of the epidermis, absorbing major fractions of UVB and UVC and reflecting approximately 5% of the incident light. The horny layer might especially profit from an increased antioxidant activity from topical administration of antioxidants. There is scientific evidence that the protective function of the skin should be improved with antioxidant approaches to prevent impairment of the SC lipids and proteins.

The percutaneous absorption of resveratrol was assessed by in vivo and in vitro methodologies. The potential diffusion of a specific compound is determined by the polarity of the horny layer (Log Ko/w of 0.8 [39]) and the vehicle (in our case ethanol, Log Ko/w, −3.2). Therefore, resveratrol (with Log Ko/w, 3) can be expected to diffuse into the SC from the formulation, thus establishing a penetration capacity, as SC permeation studies have indicated. Compared to the in vivo results, the in vitro results indicated an analogous amount of resveratrol in the SC layer after 4 h exposure. Therefore, the in vitro method can be sufficient to evaluate the permeation of the lipophilic compound of resveratrol.

Retention of compounds with antioxidant activity in the skin after topical application may represent an effective mechanism to decrease free radical exposure. Topical administration can diminish the possible degradation of the active compound due to the low degree of its metabolism in the skin, leading to a prolonged half-life and radical scavenging activity. Here, the antiradical activity of resveratrol present in the SC layers after in vivo topical application was demonstrated, along with its antiradical capacity in the SC, epidermis and dermis, after in vitro application.

Conclusions

In this work, different in vitro and in vivo methodologies were used to assess the skin permeation of the antioxidant resveratrol after topical application. A depth concentration profile of resveratrol was obtained by CRM. The presence of bands in the 1610 cm^{-1} zone indicated that resveratrol permeated to a minimum of 50 μm.

The results demonstrated that the percentage of resveratrol obtained from the in vivo permeation assay was similar to that obtained in vitro using the Franz cell system. The antioxidant efficacies in the SC were also similar for the in vitro and in vivo methods. The decreasing amount of resveratrol in the inner skin layers correlated with DPPH inhibition, which indicated the antioxidant efficacy of this compound in the epidermis and dermis compared to the SC.

The findings reported in the present study indicate the suitability of Raman microscopy and in vitro/in vivo percutaneous absorption procedures for the evaluation of resveratrol skin permeation. The active compound retained within the skin, especially in the SC, after topical administration may be an effective treatment for the mitigation of free radical exposure.

Acknowledgements The authors are grateful to Montserrat Rigol Muxart and Núria Solanes Batlló from the Department of Cardiology (Institut d'Investigacions Biomèdiques August Pi i Sunyer (IDIBAPS) Hospital Clínic, Universitat de Barcelona, Spain) for supplying the porcine skin biopsies.

Compliance with ethical standards

Conflict of interest The authors declare that they have no conflict of interest.

Funding The authors wish to thank the Ministerio de Educación y Ciencia (Spanish National Project CTQ2013-44998-P) and the 2009 SGR 1212 (AGAUR) for providing financial support.

Ethical approval All procedures performed in the study involving human participants were in accordance with the ethical standards of the institutional research committee and with the 1964 Helsinki Declaration and its later amendments or comparable ethical standards. Animal handling was approved by the Institutional Review Board and Ethics Committee of Institut d'Investigacions Biomèdiques August Pi i Sunyer (IDIBAPS) Hospital Clínic, Universitat de Barcelona, Barcelona, Spain. The management of the Landrace Large White pigs used in this study conforms to the Guide for the Care and Use of Laboratory Animals published by the United States National Institutes of Health (Eighth Edition. Washington, DC: The National Academies Press, 2011).

Informed consent Informed consent was obtained from all the individual participants included in the study.

References

1. Acquaviva R, Russo A, Campisi A, Sorrenti V, Di Giacomo C, Barcellona ML, Avitabile M, Vanella A (2002) Antioxidant activity and protective effect on DNA cleavage of resveratrol. J Food Sci 67:137–141. doi:10.1111/j.1365-2621.2002.tb11373.x
2. Alonso C, Ramon E, Lozano C, Parra JL, Torres JL, Coderch L (2004) Percutaneous absorption of flavan-3-ol conjugates from plant procyanidins. Drug Exp Clin Res 30:1–10
3. Alonso C, Rubio L, Touriño S, Martí M, Barba C, Fernández-Campos F, Coderch L, Luís Parra J (2014) Antioxidative effects and percutaneous absorption of five polyphenols. Free Radical Biol Med 75:149–155. doi:10.1016/j.freeradbiomed.2014.07.014
4. Amr S, Brown MB, Martin GP, Forbes B (2001) Activation of clindamycin phosphate by human skin. J Appl Microbiol 90:550–554. doi:10.1046/j.1365-2672.2001.01282.x
5. Baur JA, Sinclair DA (2006) Therapeutic potential of resveratrol: the in vivo evidence. Nat Rev Drug Discov 5:493–506. doi:10.1038/nrd2060
6. Bhat KP, Pezzuto JM (2002) Cancer chemopreventive activity of resveratrol. Ann NY Acad Sci 957:210–229. doi:10.1111/j.1749-6632.2002.tb02918.x
7. Bradamante S, Barenghi L, Villa A (2004) Cardiovascular protective effects of resveratrol. Cardiovasc Drug Rev 22:169–188. doi:10.1111/j.1527-3466.2004.tb00139.x
8. Bronaugh RL, Stewart RF, Congdon ER (1982) Methods for in vitro percutaneous absorption studies. II. Animal models for

human skin. Toxicol Appl Pharm 62:481–488. doi:10.1016/0041-008X(82)90149-1
9. Caspers PJ, Lucassen GW, Carter EA, Bruining HA, Puppels GJ (2001) In vivo confocal Raman microspectroscopy of the skin: noninvasive determination of molecular concentration profiles. J Invest Dermatol 116:434–442. doi:10.1046/j.1523-1747.2001.01258.x
10. Chandrasekar D, Madhusudhana K, Ramakrishna S, Diwan PV (2006) Determination of DPPH free radical scavenging activity by reversed-phase HPLC: a sensitive screening method for polyherbal formulations. J Pharm Biomed Anal 40:460–464. doi:10.1016/j.jpba.2005.07.042
11. Deostri JE (2000) Antioxidant polyphenols in tea, cocoa and wine. Nutrition 16:692–694. doi:10.1016/S0899-9007(00)00304-X
12. Fauconneau B, Waffo-Teguo P, Huguet F, Barrier L, Decendit A, Merillon JM (1997) Comparative study of radical scavenger and antioxidant properties of phenolic compounds from *Vitis vinifera* cell cultures using in vitro tests. Life Sci 61:2103–2110. doi:10.1016/S0024-3205(97)00883-7
13. Fernandez C, Nielloud F, Fortune R, Vian L, Marti-Mestres G (2002) Benzophenone-3: rapid prediction and evaluation using non-invasive methods of in vivo human penetration. J Pharm Biomed Anal 28:57–63. doi:10.1016/S0731-7085(01)00630-6
14. Fitzpatrick TB, Eisen AZ, Wolff K, Freedberg IM (1993) Dermatology in general medicine. McGraw-Hill, New York
15. Frémont L (2000) Biological effects of resveratrol. Life Sci 66:663–673. doi:10.1016/S0024-3205(99)00410-5
16. Hung CF, Lin YK, Huang ZR, Fang JY (2008) Delivery of resveratrol, a red wine polyphenol, from solutions and hydrogels via the skin. Biol Pharm Bull 31:955–962. doi:10.1248/bpb.31.955
17. Iacopini P, Baldi M, Storchi P, Sebastiani L (2008) Catechin, epicatechin, quercetin, rutin and resveratrol in red grape: content, in vitro antioxidant activity and interactions. J Food Compos Anal 21:589–598. doi:10.1016/j.jfca.2008.03.011
18. Jang M, Cai L, Udeani GO, Slowing KV, Thomas CF, Beecher CWW, Fong HHS, Farnsworth NR, Kinghorn AD, Mehta RG, Moon RC, Pezzuto JM (1997) Cancer chemopreventive activity of resveratrol, a natural product derived from grapes. Science 275:218–220. doi:10.1126/science.275.5297.218
19. King RE, Bomser JA, Min DB (2006) Bioactivity of resveratrol. Compr Rev Food Sci Food Saf 5:65–70. doi:10.1111/j.1541-4337.2006.00001.x
20. Lademann J, Jacobi U, Surber C, Weigmann HJ, Fluhr JW (2009) The tape stripping procedure—evaluation of some critical parameters. Eur J Pharm Biopharm 72:317–323. doi:10.1016/j.ejpb.2008.08.008
21. Li ZD, Ma QY, Wang CA (2006) Effect of resveratrol on pancreatic oxygen free radicals in rats with severe acute pancreatitis. World J Gastroenterol 12:137–140. doi:10.3748/WJG.v12.i1.137
22. Löffler H, Dreher F, Maibach HI (2004) Stratum corneum adhesive tape stripping: influence of anatomical site, application pressure, duration and removal. Brit J Dermatol 151:746–752. doi:10.1111/j.1365-2133.2004.06084.x
23. Niki E (2010) Assessment of antioxidant capacity in vitro and in vivo. Free Radic Biol Med 49:503–515. doi:10.1016/j.freeradbiomed.2010.04.016
24. OECD No. 28 (2004) Guidance document for the conduct of skin absorption studies. OECD Series on Testing and Assessment No. 28. OECD Publishing, Paris
25. Prusakiewicz JJ, Ackermann C, Voorman R (2006) Comparison of skin esterase activities from different species. Pharm Res 23:1517–1524. doi:10.1007/s11095-006-0273-y
26. Ramon E, Alonso C, Coderch L, De la Maza A, Lopez O, Parra JL, Notario I (2005) Liposomes as alternative vehicles for sun filter formulations. Drug Deliv 12:83–88. doi:10.1080/10717540490446080
27. Redoules D, Perie J, Viode C, Mavon A, Fournier D, Daunes S, Casas C, Lougarre A, De Viguerie N (2005) Slow internal release of bioactive compounds under the effect of skin enzymes. J Invest Dermatol 125:270–277. doi:10.1111/j.0022-202X.2005.23785.x
28. Rougier A, Dupuis D, Lotte C, Rouguet R, Shaefer H (1983) In vivo correlation between stratum corneum reservoir function and percutaneous absorption. J Invest Dermatol 81:275–278. doi:10.1111/1523-1747.ep12518298
29. Rougier A, Lotte C, Maibach HI (1987) In vivo percutaneous penetration of some organic compounds related to anatomic site in humans: predictive assessment by the stripping method. J Pharm Sci 76:451–454. doi:10.1002/jps.2600760608
30. Sánchez- Moreno C, Larrauri JA, Saura-Calixto F (1998) A procedure to measure the antiradical efficiency of polyphenols. J Sci Food Agric 76:270–276. doi:10.1002/(SICI)1097-0010(199802)76:2<270:AID-JSFA945>3.0.CO;2-9
31. Schwindt DA, Wilhelm KP, Maibach HI (1998) Water diffusion characteristics of human stratum corneum at different anatomical sites in vivo. J Invest Dermatol 111:385–389. doi:10.1046/j.1523-1747.1998.00321.x
32. Sengottuvelan M, Viswanathan P, Nalini N (2006) Chemopreventive effect of trans-resveratrol—a phytoalexin against colonic aberrant crypt foci and cell proliferation in 1,2-dimethylhydrazine induced colon carcinogenesis. Carcinogenesis 27:1038–1046. doi:10.1093/carcin/bgi286
33. Shah VP, Flynn GL, Yacobi A, Maibach HI, Bon C, Fleischer NM, Franz TJ, Kaplan SA, Kawamoto J, Lesko LJ, Marty JP, Pershing LK, Schaefer H, Sequeira JA, Shrivastava SP, Wilkin J, Williams RL (1998) Bioequivalence of topical dermatological dosage forms—methods of evaluation of bioequivalence. Pharm Res 15:167–171
34. Tfaili S, Josse G, Angiboust JF, Manfait M, Piot O (2014) Monitoring caffeine and resveratrol cutaneous permeation by confocal Raman microspectroscopy. J Biophotonics 7:676–681. doi:10.1002/jbio.201300011
35. Tfayli A, Piot O, Manfait M (2008) Confocal Raman microspectroscopy on excised human skin: uncertainties in depth profiling and mathematical correction applied to dermatological drug permeation. J Biophotonics 1:140–153. doi:10.1002/jbio.200710004
36. Thiele JJ, Dreher F, Packer L (2000) Antioxidant defense systems in skin. In: Elsner P, Maibach H (eds) Drugs vs. cosmetics: cosmeceutical?. Dekker, New York, pp 145–187
37. Ting WW, Vest CD, Sontheimer R (2003) Practical and experimental consideration of sun protection in dermatology. Int J Dermatol 42:505–513. doi:10.1046/j.1365-4362.2003.01867.x
38. Wagner H, Kostka KH, Lehr CM, Schaefer UF (2001) Interrelation of permeation and penetration parameters obtained from in vitro experiments with human skin and skin equivalents. J Control Release 75:283–295. doi:10.1016/S0168-3659(01)00396-0
39. Wiechers JW, Kelly CL, Blease TG, Dederen JC (2004) Formulating for efficacy. Int J Cosmetic Sci 26:173–182. doi:10.1111/j.1467-2494.2004.00211.x
40. Ya-Xian Z, Suetake T, Tagami H (1999) Number of cell layers of the stratum corneum in normal skin—relationship to the anatomical location on the body, age, sex and physical parameters. Arch Dermatol Res 291:555–559. doi:10.1007/s004030050453
41. Zhang G, Moore DJ, Sloan KB, Flach CR, Mendelsohn R (2007) Imaging the prodrug-to-drug transformation of a 5-fluorouracil derivative in skin by confocal raman microscopy. J Invest Dermatol 127:1205–1209. doi:10.1038/sj.jid.5700690

Annex 6. Surface determination of 3D confocal Raman microscopy imaging of the skin

IOP Publishing | Astro Ltd
Laser Physics Letters
Laser Phys. Lett. 00 (2017) 000000 (8pp)
UNCORRECTED PROOF

Letter

Surface determination of 3D confocal Raman microscopy imaging of the skin

J Schleusener[1], V Carrer[2], A Patzelt[1], J Lademann[1] and M E Darvin[1]

[1] Department of Dermatology, Venerology and Allergology, Center of Experimental and Applied Cutaneous Physiology, Charité—Universitätsmedizin Berlin, corporate member of Freie Universität Berlin, Humboldt-Universität zu Berlin, and Berlin Institute of Health, Charitéplatz 1, 10117 Berlin, Germany
[2] Department of Chemical and Surfactants Technology, Advanced Chemical Institute of Catalonia
AQ1 (IQAC-CSIC), Jordi Girona 18-26, 08034 Barcelona, Spain

E-mail: johannes.schleusener@charite.de

Received 11 August 2017
Accepted for publication 10 September 2017
Published

Abstract

A surface determination method for the application of 3D confocal Raman microscopy on inhomogeneous skin sections has been presented, which is based on depth profiles of the keratin contribution of the acquired Raman spectra. The method was compared to two similar auto-focusing methods that are based on the intensity of the reflected excitation light and Raman spectra, respectively.

The measurements were performed on hair follicles containing skin sections of porcine ears *ex vivo*. The surface determination on such samples is especially challenging due to their different molecular composition and surface inhomogeneity.

AQ2 An advantage of this method is molecular sensitivity, whereby only the surface of the sample will be detected and not the substrate of the microscope slide, in the case of disruptions during the processing of samples. A disadvantage of the method is the increased overall acquisition time if only the surface spectra are to be applied for 2D mapping.

Keywords: optical microscopy, confocal microscopy in biophysics, Raman spectroscopy in biophysics, depth profiling, laser imaging, medical, medical imaging

AQ3 (Some figures may appear in colour only in the online journal)

1. Introduction

Confocal Raman microscopy (CRM) is a useful tool for the analysis of biologic tissues and skin and has been used for various purposes [1–5]. The advantages of CRM are molecular specificity and a high spatial resolution of $\leqslant 5$ μm. The spatial resolution is achieved because the out-of-focus light is rejected by the incorporated pinhole. This advantage can also be challenging, as the measurements are more sensitive towards microscopic shifts of the sample compared to measurement conditions where a signal is acquired from an integral measurement volume.

For CRM mapping measurements, the laser focus is translated across the sample, resulting in a spectrum for every measured coordinate. Doing so can enable Raman imaging of either single band intensities, or of contributions (scores) calculated by a multivariate data analysis method. If the Raman spectra of pure components (loadings) are known, a spectral unmixing method such as classical least squares regression can be performed [6]. As this is, for example, the case for pharmaceutical mixtures, Raman imaging has been used to determine the distribution of pure substances in pharmaceutical tablets [7, 8]. Similar measurements for the distribution of different molecular components of skin and tissues, such as lipids, proteins, water and carotenoids [9–15] or of single cells have also been accomplished [16–18]. Due to the complex composition of biologic materials, more sophisticated

multivariate statistical methods such as, for example, hierarchical cluster analysis or multivariate curve resolution, were used to differentiate between the cell components in these studies. Similar approaches have also been applied in CRM imaging of different components of the hair [19]. A further application of CRM is the analysis of the diffusion of drugs into the skin [13, 20–22].

For determining drug penetration into the skin, hair follicles are of particular interest, because follicular penetration has recently been investigated as an important drug penetration route [23–26]. An investigation of hair follicles containing sections is important for determining drug penetration through the hair follicles, which cannot be realized *in vivo* and should be performed *ex vivo* on thin sections. The surface determination of skin sections containing hair follicles is especially difficult, because the gradient of skin surface inhomogeneity is very high in these cases.

For a surface mapping of thin slices, the laser focus will be translated in an *XY* direction at a constant *Z*-distance. However, if the surface is not homogeneous, which mostly reflects real situations, the *Z*-position will vary, entailing a signal decrease in the case of focus positions outside, or due to absorption and scattering deeper inside the sample. Because of the confocal nature of this method with typical focus dimensions in the range of several few micrometers, surface inhomogeneity in this range will result in severe changes of the acquired spectra.

Several auto-focusing methods have been applied in order to compensate surface inhomogeneity and readjust the *Z*-position of the focus for every *XY* position.

One method is to perform a quick *Z*-scan for every *XY* position to determine the position of maximum intensity of the reflected signal. This approach can be troublesome, if the detected signal is not of constant intensity. Due to the effects of fluorescence photobleaching (for example) [27], the signal intensity can decrease over time for measurements on the biologic tissue. In the case of transparent samples, the position of maximum intensity is not necessarily the sample surface.

Another approach is the illumination with white light through the microscope objective. Due to the wavelength dependent focal distance of the objective, the surface position can then be determined based on the wavelength of the detected reflected light [28, 29]. This approach is challenging in the case of surfaces that are not perpendicular to the optical axis if no signal is reflected back along the optical axis.

Also, different image analysis methods of a microscopic overview image can be used for auto focusing [30, 31]. In this case, the surface ~~is (for example),~~ determined at the position with the highest contrast of recorded sample structures and the out-of-focus images are detected by a lower amount of high frequency content in the image data. For methods that take advantage of the visual microscopic overview image, it is highly essential that the laser- and visual focus are in the same plane. Due to the wavelength dependent focal plane position there may be a significant shift if the excitation is e.g. provided in the UV range due to chromatic aberration of the microscope objective. In transparent samples, the application of such methods might be restricted.

Most of the described methods have been implemented into spectroscopy software packages by manufacturers of microscopes and are successfully used depending on the kind of sample to be analyzed. Several other methods exist [25], such as skin surface topography determination, which was used to determine age-dependent skin roughness [32]. This method can reach a high axial resolution, but it was not combined with CRM.

For the surface determination of skin using CRM, a method has been established taking into account the depth profile of keratin, which is the main component in the stratum corneum (SC), the outermost horny layer of the skin [13]. Since keratin is homogeneously distributed inside the keratinocytes and keratinocytes constitute most of the volume within the SC, its spectral profile is also often used to compensate the depth dependent signal attenuation [33].

When the laser focus is moved from above into the skin, the intensity of the keratin profile will increase to the position where the laser focus is just about inside the skin. Due to absorption and scattering based signal attenuation, the intensity of the keratin will decrease with increasing depths from this position. The skin surface has been defined to be the position where 50% of the maximal intensity of the keratin profile from outside the skin occurs [22, 34]. At this position, the laser focus is approximately halfway inside the skin. In other studies, the maximum of the keratin profile has also been defined as the skin surface, where the whole laser focus is inside the skin [15, 35].

In this study, a method based on the surface determination by the position of 50% of the maximal intensity is applied for CRM imaging by recording depth dependent keratin profiles for every measured *XY* position of the surface of vertical sections of porcine ear skin containing hair follicles *ex vivo*. Porcine ear skin was used because it has been proven to be morphologically similar to human skin [36, 37] and is a suitable model for penetration studies to human skin [38, 39].

Raman imaging of hair follicles has successfully been shown using different optical profilometry methods for surface determination [28]. The surface determination on hair follicles is of great interest due to the composition of the different molecular constituents, and the hair is often not sectioned in the same plane as the follicle. Depending on the body site, the SC is ≈10–20 μm thick [12, 38, 40, 41], but can be ≈100 μm e.g. on the palm [42], while the viable epidermis has a thickness of ≈40–100 μm [38, 43]. The SC is mostly composed of highly keratinized dead squamous cells [43], which are continuously desquamated [44]. Although the keratin distribution in the deeper skin layers below the SC is lower and possibly not as homogenous, the method can also be used in these areas and also on the hairs, which are rich in keratin [45].

2. Materials and methods

2.1. Sample preparation

Measurements were performed *ex vivo* on sections of hair follicles of porcine ear skin samples. The porcine ears have been obtained from a local abattoir and were processed on

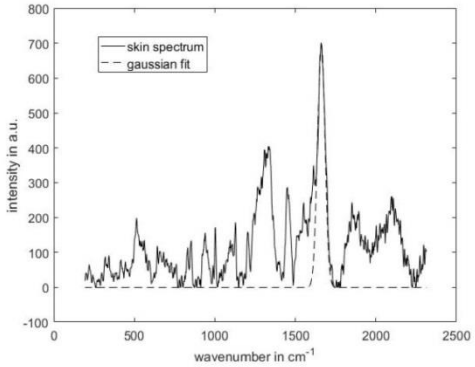

Figure 1. Pre-processed Raman spectrum of a porcine ear skin section in the fingerprint region (solid line) and fitted Gaussian function of the keratin-related band centered around 1655 cm^{-1} by non-linear regression (dashed line).

the same day of slaughter. The skin was cleaned under cold running water and hair was carefully removed using scissors without damaging the SC. The skin was embedded in a tissue freezing medium (Leica Biosystems Nussloch GmbH, Nussloch, Germany) and thin slices of 30 μm thickness were prepared by cryo-sectioning using a Cryostat Microm HM 560 (Microm International GmbH, Walldorf, Germany). The sections were then stored at −20 °C before the measurements. The experiments were performed under standard ambient conditions at ≈+20 °C.

2.2. Data acquisition

The skin sections were measured using a LabRAM HR Evolution CRM (Horiba Jobin Yvon, Longjumeau, Cedex, France) using 473 nm excitation with 6.1 mW laser power on the sample surface. A 600 g mm^{-1} grating, a ⌀100 μm pinhole and a 100× MPlanN objective with NA = 0.9 (Olympus, Tokyo, Japan) was used for the experiments, which were performed in the biologic fingerprint region (200–2300 cm^{1}). For the visual microscopic overview images, a 10× MPlanN objective with NA = 0.25 (Olympus, Tokyo, Japan) was used. A point mapping approach was used, where the laser focus was moved across the sample in an *X*- and *Y*-direction. Increments of 2 μm were applied in the *Z*-direction. The depth range for the profiles was set 10 μm below the lowest position and 10 μm above the highest position (usually on the hair) of the visual focus of the microscopic overview image of the section. The acquisition time for a single spectrum was 5 s.

2.3. Data analysis

Labspec 6 (Horiba Jobin Yvon, Longjumeau, Cedex, France) was used for the control of data acquisition and pre-processing. For all spectra, cosmic spikes were manually removed, and the fluorescence background was removed by subtracting a fifth order polynomial, iteratively fitted by linear least squares regression, in order to retain the baseline steadily just below the spectrum [46].

Further data analysis was performed in self-programmed software based on Matlab R2016a (The MathWorks, Inc., Natick, Massachusetts). For every pre-processed spectrum, a Gaussian function was fitted to the keratin-related Amide I Raman band around 1655 cm^{-1} [47] by non-linear regression with non-negativity constraints, shown in figure 1. For every *XY* position, the depth profile of the determined 1655 cm^{-1} peak height as a function of depth was approached using a seventh order polynomial by linear regression, which resulted in sufficient fitting for further analysis. With respect to the given depth resolution, the best fit could be achieved using a seventh order polynomial. The derivative of this polynomial is used to determine the extrema of the depth profile. The skin surface is defined to be at the *Z*-position with 50% of the difference between maximum and minimum intensity from the outside of the skin sample, as defined in equation (1).

$$I_{\min} + \frac{I_{\max} - I_{\min}}{2}. \quad (1)$$

Here, $I_{\max}$ is the maximum intensity of the profile and $I_{\min}$ is the minimum in the direction outside of the sample from the maximum. In the case of fitting errors, the sample surface was assigned to be not a number (NaN). A typical example of a *Z*-profile is shown in figure 2(a), which represents a profile where no surface could be determined. This could likely occur in the case of artifacts such as very thin sample positions, holes in the thin skin slices or at *XY*-positions on the glass substrate beside the sample. The surface position was determined by interpolation.

For the following Raman imaging, the surface spectra were selected, which were recorded at the closest *Z*-depth of the sample surface. A spectral data cube was reconstructed, where

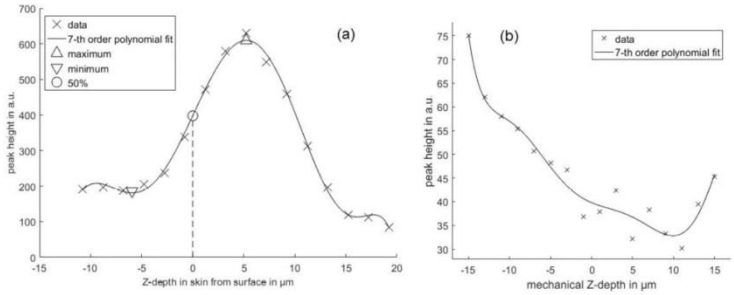

Figure 2. Z-profiles of the keratin-related 1655 cm^{-1} peak intensity. The surface is defined as the position with the mean of maximum and minimum intensity from the outside of the skin (negative Z-values). The Z-values in (a) have been adjusted to set the surface as origin with negative values above the skin. In a profile where no surface could be defined, the Z-values relate to the initial acquisition settings and are shown as mechanical depth (b). The surface position of such profiles was denoted as NaN. In this case the origin relates to the initially set visual focus.

the surface spectra ($Z = 0$) and subsequent spectra from the depth of the sample were organized accordingly, as schematically shown in figure 3. Spectra from above the sample surface were discarded.

For comparison of the 'peak fit' (described here) with established auto-focusing methods, two methods that were integrated in the Labspec 6 spectroscopy software package were additionally used. The 'reflection' method determines the sample surface based on the maximum intensity of the reflected excitation signal of a Z-scan, while for the 'spectral' method, the surface is determined based on the maximum intensity of Raman spectra of 5 s acquisition time recorded for every *XY* position. For every measured sample, the 'peak fit' method was applied first, followed by the 'reflection' and finally the 'spectral' method; each method was applied on the same *XY* positions.

3. Results and discussion

Figure 4 shows two examples of microscopic overview images of thin sections of porcine skin containing hair follicles that were used for *XYZ* Raman mapping and surface determination. The marked frames determine the areas in which 10×10 Z-profiles were acquired. The distance between measurement points was 33 μm in *X* and 22 μm in *Y* direction. The marked positions in figure 4 determine points where no surface determination was possible based on the acquired depth profile, as shown in figure 2(b). This can occur at artefactual spectra, where the non-linear regression of the Gaussian function to the 1655 cm^{-1} Raman band leads to an insufficient fit. A likely explanation could be that these profiles were acquired at defective regions within the section. Although the sections were cut with a thickness of 30 μm to allow a sufficient profile resolution with the applied Z-increments of 2 μm, the sections are inhomogeneous and can be significantly thinner especially on the borders or close to the hair. In fact, the artefacts of the section shown in figure 4(a) occur exclusively in the region directly in the follicle beside the hair. It is assumed that this region represents a cut in the section, showing the glass substrate below the sample. The section shown in figure 4(b) only shows a few artefacts, which are distributed across the hair, epidermis and dermis. In this section, the hair follicle is considerably thinner, and the glass substrate is barely visible between the hair and the follicle.

The determined surface positions of the 'peak fit' method were compared with the 'reflection' and 'spectral' auto-focusing method provided by the Labspec6 software package. Of all the measured *XY* positions, the surface of the section determined by the 'peak fit' method was on average 12 ± 1 μm below the position (inside the section) determined as the surface by the 'reflection' method, and 13 ± 2 μm below the position determined as the sample surface by the 'spectral' method. The difference between the 'reflection' and the 'spectral' method was only 1 ± 3 μm. A possible explanation could AQ4 be the definition of the skin surface at the position with 50% of the maximal signal of the defined Raman intensity from above the skin section, where the laser focus is already partly inside the sample. However, the shift between this position and the position of maximal intensity is only in the range of ≈ 5 μm, which is shown in figure 2(b), and can therefore only account for part of the shift between the methods.

The mean of all surface positions determined by the 'peak fit' method was 1 ± 5 μm, while it was 14 ± 7 μm for the 'reflection' and 15 ± 8 μm for the 'spectral' method. The calculation of the mean surface positions supports the assumption of a mainly systematic difference between the 'peak fit' method on one side and the 'reflection' and 'spectral' methods on the other side, due to the comparable standard deviation in all methods. This is further supported by comparing the determined surface positions of the two samples using these different methods, as shown in figure 5. All methods detect the

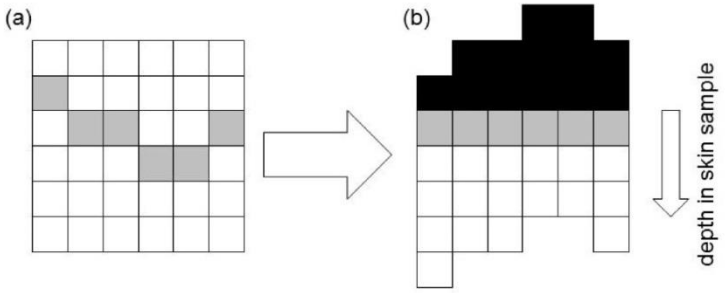

Figure 3. Schematic *XZ*-illustration of the rearrangement of the surface spectra. The spectra that were acquired closest to the determined skin surface in (a) are shaded in grey. In the reconstructed data matrix in (b), spectral *Z*-profiles are reorganized to achieve equal surface position. Spectra that were acquired above the skin sample were discarded (black).

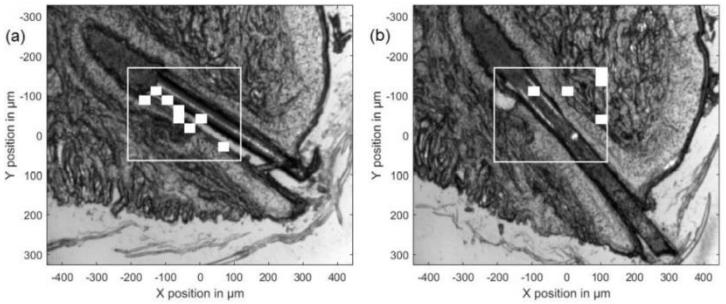

Figure 4. Microscopic overview images of 2 skin sections containing hair follicles. The marked frame determines the area where the measurements for the surface determination have been performed. The positions marked in white represent *Z*-scans, where a surface determination was not possible.

surface of the hairs in the follicles of the two samples at the highest *Z*-position compared to the position of the surrounding follicular skin.

The measurements for the three auto-focusing methods were subsequently taken on the identical samples at the same positions without moving the samples in between measurements. Although no long-term sample movement, such as for example, due to drying, was examined in the timeframe of the measurements, it remains possible that the focal positions of the subsequent measurements were not taken at the exact identical positions on the microscopic scale. The 'peak fit' method was applied first, followed by the 'reflectance' and the 'spectral' method. It would appear reasonable that the samples dried during the application of the 'peak fit' method and consequently were reduced in thickness, entailing a lower surface for the subsequent methods. However, if this were the case, increased surface inhomogeneity during the relatively long acquisition of the first method would be expected. The surface inhomogeneity of the three methods was not considerably different, as shown in figure 5. For the sample shown in figure 4(a), the total acquisition time was 133, 8 and 142 min, respectively for the three methods. For the sample shown in figure 4(b), the total acquisition time was 83, 8 and 92 min, respectively.

Therefore, a disadvantage of the 'peak fit' method is the long acquisition time for 3D mapping. This however, only applies to circumstances where only a 2D mapping is desired, for 3D mapping, i.e. depth dependent Raman imaging, the extended acquisition time is unavoidable. In the presented results, the acquisition time of the 'spectral' method was longer than that of the 'peak fit' method, although only spectra from the surface were available for further analysis after the acquisition. However, the acquisition time of the initial surface determination in the 'spectral' method could be reduced, since a high signal-to-noise ratio is only important for the final acquisition of a spectrum from the surface position. In this study, a point mapping approach was applied. The acquisition time could be further accelerated for line mapping or global

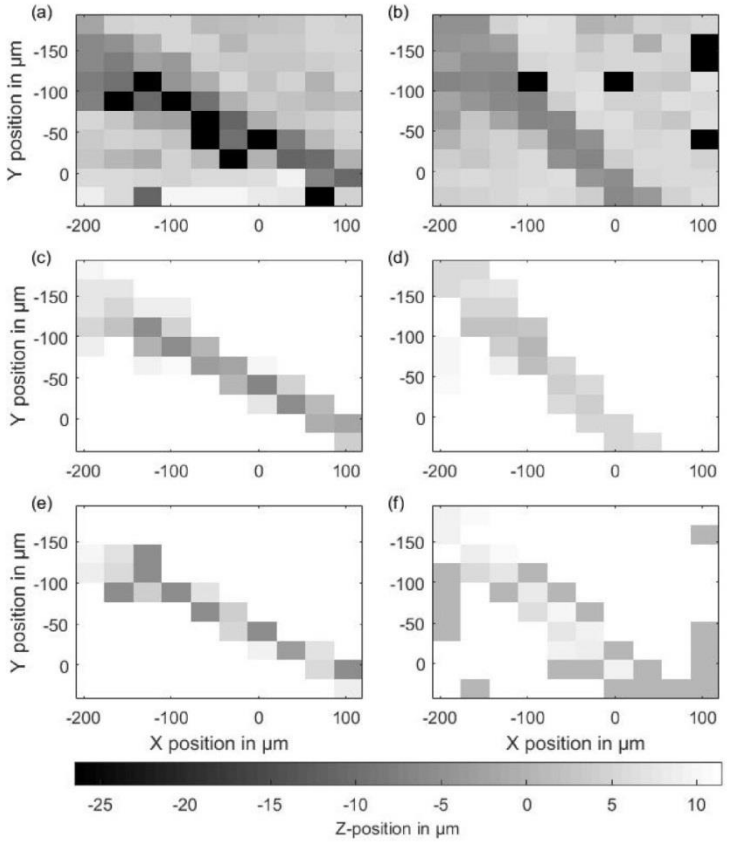

Figure 5. Intensity images of the determined *Z*-positions from the two skin sections shown in figure 4(a) ((a), (c) and (e)) and figure 4(b) ((b), (d) and (f)). The *Z*-positions were determined by the 'peak fit' ((a) and (b)), the 'reflection' ((c) and (d)) and the 'spectral' method ((e) and (f)). All images are scaled from the maximal position of all images (dark) to the minimal position of all images (bright). The scaling of the *Z*-position is in relation to the initially set visual focus (0 μm). The values increase in the direction inside the skin section, with negative values determining positions outside the sample. Positions where the surface could not be determined were set as NaN and are shown in black.

Raman-imaging approaches, where confocal scanning is not necessary [48, 49]. These methods are, however, not particularly suitable for the purpose of 3D mapping as discussed here. For line mapping, the laser focus is extended to a line shape in the *X*-direction, which is moved across the sample in the *Y*-direction. This enables the simultaneous detection of the Raman signal of all *X*-positions by the CCD pixel rows perpendicular to the spectrometer entrance slit. However, the laser focus extension results in decreased signal excitation power that could be compensated by higher laser power or extended acquisition times. For global Raman-imaging, the laser focus is extended to the whole sample surface and the detected signal can be simultaneously detected. This method usually entails a decreased spectral resolution, or only intensities of single Raman bands are detected. A fiber bundle based Raman imaging approach has been presented, in which

each pixel is imaged on one fiber in a fiber array, which are reshaped in a vertical orientation in front of the spectrometer entrance slit [50]. Using a very laborious experimental setup, this approach allowed the simultaneous acquisition of 400 spectra, but a confocal characteristic was not reached at the current stage.

4. Conclusion

A comparison of the available methods for the surface determination of skin sections for 3D confocal Raman microscopic imaging that are based on the depth profiles of keratin-related Raman band intensities 'peak fit', as well as on the intensity of the reflected excitation intensity 'reflection' and the intensity of the detected Raman spectrum 'spectral' was presented. Unlike visual image analysis, these methods are independent of the wavelength dependent focal length of the objective. Since the 'peak fit' method is based on the Raman intensity, it is insensitive to the effect of tissue fluorescence photobleaching and will detect the profile of the determined molecular constituent. The maximum of the reflected signal, which is used in the 'reflection' method, might not necessarily occur at the sample surface.

A further advantage of the 'peak fit' method is the detection of the sample surface only. At positions that are defined in the *XY* grid, but where the sample is not present, the 'reflection' and the 'spectral' methods incorrectly determine the substrate surface as the sample surface. The proposed method will only determine the skin surface based on the keratin profile and result in NaN in the case of measurements beside or holes in the sample. Since the surface determination is based on spectral depth profiles, a disadvantage of the method compared to the 'reflection' method is the increased acquisition time, if only surface spectra are to be collected. For application of the analysis of hair follicles containing skin sections in cases where the acquisition time is not critical, the 'peak fit' method shown has proven to be suitable for surface determination using 3D CRM.

AQ5 ## Acknowledgment

This study was supported by the Foundation for Skin Physiology of the Donor Association for German Science and Humanities.

Declaration of interest

The authors report no conflict of interest.

AQ6 ## References

[1] Richters R J, Falcone D, Uzunbajakava N E, Varghese B, Caspers P J, Puppels G J, van Erp P E and van de Kerkhof P C 2017 Sensitive skin: assessment of the skin barrier using confocal Raman microspectroscopy *Skin Pharmacol. Physiol.* **30** 1–12

[2] Chen W W, Li Z F, Yu Y, Lin D, Huang H and Shi H 2016 Houttuynia cordata Thunb extract induces cytotoxicity in human nasopharyngeal carcinoma cells: Raman spectroscopic studies *Laser Phys. Lett.* **13** AQ7

[3] Cao G *et al* 2015 A potential method for non-invasive acute myocardial infarction detection based on saliva Raman spectroscopy and multivariate analysis *Laser Phys. Lett.* **12**

[4] Caspers P J, Lucassen G W and Puppels G J 2003 Combined *in vivo* confocal Raman spectroscopy and confocal microscopy of human skin *Biophys. J.* **85** 572–80

[5] Eklouh-Molinier C, Gaydou V, Froigneux E, Barlier P, Couturaud V, Manfait M and Piot O 2015 *In vivo* confocal Raman microspectroscopy of the human skin: highlighting of spectral markers associated to aging via a research of correlation between Raman and biometric mechanical measurements *Anal. Bioanal. Chem.* **407** 8363–72

[6] Zhou Y and Cao H 2013 An augmented classical least squares method for quantitative Raman spectral analysis against component information loss *Sci. World J.* **6**

[7] Zhang L, Henson M J and Sekulic S S 2005 Multivariate data analysis for Raman imaging of a model pharmaceutical tablet *Anal. Chim. Acta* **545** 262–78

[8] Vajna B, Farkas I, Szabo A, Zsigmond Z and Marosi G 2010 Raman microscopic evaluation of technology dependent structural differences in tablets containing imipramine model drug *J. Pharm. Biomed. Anal.* **51** 30–8

[9] Choe C, Lademann J and Darvin M E 2016 A depth-dependent profile of the lipid conformation and lateral packing order of the stratum corneum *in vivo* measured using Raman microscopy *Analyst* **141** 1981–7

[10] Schie I W, Krafft C and Popp J 2015 Applications of coherent Raman scattering microscopies to clinical and biological studies *Analyst* **140** 3897–909

[11] Lademann J, Caspers P J, van der Pol A, Richter H, Patzelt A, Zastrow L, Darvin M, Sterry W and Fluhr J W 2009 *In vivo* Raman spectroscopy detects increased epidermal antioxidative potential with topically applied carotenoids *Laser Phys. Lett.* **6** 76–9

[12] Ashtikar M, Matthaus C, Schmitt M, Krafft C, Fahr A and Popp J 2013 Non-invasive depth profile imaging of the stratum corneum using confocal Raman microscopy: first insights into the method *Eur. J. Pharm. Sci.* **50** 601–8

[13] Mujica Ascencio S, Choe C, Meinke M C, Muller R H, Maksimov G V, Wigger-Alberti W, Lademann J and Darvin M E 2016 Confocal Raman microscopy and multivariate statistical analysis for determination of different penetration abilities of caffeine and propylene glycol applied simultaneously in a mixture on porcine skin *ex vivo Eur. J. Pharm. Biopharm.* **104** 51–8

[14] Choe C, Lademann J and Darvin M E 2016 Depth profiles of hydrogen bound water molecule types and their relation to lipid and protein interaction in the human stratum corneum *in vivo Analyst* **141** 6329–37

[15] Quatela A, Miloudi L, Tfayli A and Baillet-Guffroy A 2016 *In vivo* Raman microspectroscopy: intra- and intersubject variability of stratum corneum spectral markers *Skin Pharmacol. Physiol.* **29** 102–9

[16] Draux F, Jeannesson P, Beljebbar A, Tfayli A, Fourre N, Manfait M, Sule-Suso J and Sockalingum G D 2009 Raman spectral imaging of single living cancer cells: a preliminary study *Analyst* **134** 542–8

[17] Ando M and Hamaguchi H O 2014 Molecular component distribution imaging of living cells by multivariate curve resolution analysis of space-resolved Raman spectra *J. Biomed. Opt.* **19** 011016

[18] Hamada K, Fujita K, Smith N I, Kobayashi M, Inouye Y and Kawata S 2008 Raman microscopy for dynamic molecular imaging of living cells *J. Biomed. Opt.* **13**

[19] Pudney P D, Bonnist E Y, Mutch K J, Nicholls R, Rieley H and Stanfield S 2013 Confocal Raman spectroscopy of whole hairs *Appl. Spectrosc.* **67** 1408–16

[20] Zhu Y, Choe C S, Ahlberg S, Meinke M C, Alexiev U, Lademann J and Darvin M E 2015 Penetration of silver nanoparticles into porcine skin *ex vivo* using fluorescence lifetime imaging microscopy, Raman microscopy, and surface-enhanced Raman scattering microscopy *J. Biomed. Opt.* **20** 051006

[21] Lunter D J 2016 How confocal is confocal Raman microspectroscopy on the skin? Impact of microscope configuration and sample preparation on penetration depth profiles *Skin Pharmacol. Physiol.* **29** 92–101

[22] Bonnist E Y M, Gorce J P, Mackay C, Pendlington R U and Pudney P D A 2011 Measuring the penetration of a skin sensitizer and its delivery vehicles simultaneously with confocal Raman spectroscopy *Skin Pharmacol. Physiol.* **24** 274–83

AQ8

[23] Knorr F, Patzelt A, Darvin M E, Lehr C M, Schafer U, Gruber A D, Ostrowski A and Lademann J 2016 Penetration of topically applied nanocarriers into the hair follicles of dog and rat dorsal skin and porcine ear skin *Vet. Dermatol.* **27** 256–e60

[24] Tran N, Knorr F, Mak W C, Cheung K Y, Richter H, Meinke M, Lademann J and Patzelt A 2017 Gradient-dependent release of the model drug TRITC-dextran from FITC-labeled BSA hydrogel nanocarriers in the hair follicles of porcine ear skin *Eur. J. Pharm. Biopharm.* **116** 12–6

[25] Otberg N, Shapiro J, Lui H, Wu W Y, Alzolibani A, Kang H, Richter H and Lademann J 2017 Scalp imaging techniques *Laser Phys. Lett.* **14** 11

[26] Abd E, Roberts M S and Grice J E 2016 A comparison of the penetration and permeation of caffeine into and through human epidermis after application in various vesicle formulations *Skin Pharmacol. Physiol.* **29** 24–30

[27] Schleusener J, Lademann J and Darvin M E 2017 Depth-dependent autofluorescence photobleaching using 325, 473, 633, and 785 nm of porcine ear skin *ex vivo J. Biomed. Opt.* **22** 091503

[28] Franzen L, Mathes C, Hansen S and Windbergs M 2013 Advanced chemical imaging and comparison of human and porcine hair follicles for drug delivery by confocal Raman microscopy *J. Biomed. Opt.* **18** 061210

[29] Tiziani H J and Uhde H M 1994 Three-dimensional image sensing by chromatic confocal microscopy *Appl. Opt.* **33** 1838–43

[30] Shen F, Hodgson L and Hahn K 2006 *Methods in Enzymology* ed I James (New York: Academic) pp 620–32

[31] Qiu Y, Chen X, Li Y, Chen W R, Zheng B, Li S and Liu H 2013 Evaluations of auto-focusing methods under a microscopic imaging modality for metaphase chromosome image analysis *Anal. Cell. Pathol.* **36**

[32] Korn V, Surber C and Imanidis G 2016 Skin surface topography and texture analysis of sun-exposed body sites in view of sunscreen application *Skin Pharmacol. Physiol.* **29** 291–9

[33] Caspers P J, Lucassen G W, Carter E A, Bruining H A and Puppels G J 2001 *In vivo* confocal Raman microspectroscopy of the skin: noninvasive determination of molecular concentration profiles *J. Invest. Dermatol.* **116** 434–42

[34] Caspers P J, Lucassen G W, Bruining H A and Puppels G J 2000 Automated depth-scanning confocal Raman microspectrometer for rapid *in vivo* determination of water concentration profiles in human skin *J. Raman Spectrosc.* **31** 813–8

[35] Franzen L, Anderski J and Windbergs M 2015 Quantitative detection of caffeine in human skin by confocal Raman spectroscopy—a systematic *in vitro* validation study *Eur. J. Pharm. Biopharm.* **95** 110–6

[36] Darvin M E, Richter H, Zhu Y J, Meinke M C, Knorr F, Gonchukov S A, Koenig K and Lademann J 2014 Comparison of *in vivo* and *ex vivo* laser scanning microscopy and multiphoton tomography application for human and porcine skin imaging *Quantum Electron.* **44** 646

[37] Sohn M, Korn V and Imanidis G 2015 Porcine ear skin as a biological substrate for *in vitro* testing of sunscreen performance *Skin Pharmacol. Physiol.* **28** 31–41

[38] Jacobi U, Kaiser M, Toll R, Mangelsdorf S, Audring H, Otberg N, Sterry W and Lademann J 2007 Porcine ear skin: an *in vitro* model for human skin *Skin Res. Technol.* **13** 19–24

[39] Choe C, Lademann J and Darvin M E 2015 Analysis of human and porcine skin *in vivo*/*ex vivo* for penetration of selected oils by confocal Raman microscopy *Skin Pharmacol. Physiol.* **28** 318–30

[40] König K, Ehlers A, Stracke F and Riemann I 2006 *In vivo* drug screening in human skin using femtosecond laser multiphoton tomography *Skin Pharmacol. Physiol.* **19** 78–88

[41] Falcone D, Uzunbajakava N E, Varghese B, de Aquino Santos G R, Richters R J H, van de Kerkhof P C M and van Erp P E J 2015 Microspectroscopic confocal Raman and macroscopic biophysical measurements in the *in vivo* assessment of the skin barrier: perspective for dermatology and cosmetic sciences *Skin Pharmacol. Physiol.* **28** 307–17

[42] Egawa M, Hirao T and Takahashi M 2007 *In vivo* estimation of stratum corneum thickness from water concentration profiles obtained with Raman spectroscopy *Acta Derm. Venereol.* **87** 4–8

[43] Bashkatov A N, Genina E A, Kochubey V I and Tuchin V V 2005 Optical properties of human skin subcutaneous and mucous tissues in the wavelength range from 400 to 2000 nm *J. Phys. D: Appl. Phys.* **38** 2543

[44] Voloshina O V, Shirshin E A, Lademann J, Fadeev V V and Darvin M E 2017 Fluorescence detection of protein content in house dust: the possible role of keratin *Indoor Air* **27** 377–85

[45] Williams A C, Edwards H G M and Barry B W 1994 Raman spectra of human keratotic biopolymers: skin, callus, hair and nail *J. Raman Spectrosc.* **25** 95–8

[46] Lieber C A and Mahadevan-Jansen A 2003 Automated method for subtraction of fluorescence from biological Raman spectra *Appl. Spectrosc.* **57** 1363–7

[47] Darvin M E, Lademann J and Brandt N N 2016 Comment on 'Dengue viral infection monitoring from diagnostic to recovery using Raman spectroscopy' *Laser Phys. Lett.* **13**

[48] Schlücker S, Schaeberle M D, Huffman S W and Levin I W 2003 Raman microspectroscopy: a comparison of point, line, and wide-field imaging methodologies *Anal. Chem.* **75** 4312–8

[49] Stewart S, Priore R J, Nelson M P and Treado P J 2012 Raman imaging *Annu. Rev. Anal. Chem.* **5** 337–60

[50] Schmälzlin E, Moralejo B, Bodenmüller D, Darvin M E, Thiede G and Roth M M 2016 Ultrafast imaging Raman spectroscopy of large-area samples without stepwise scanning *J. Sens. Sens. Syst.* **5** 261–71